TIME DEPENDENT DEFORMATION AND STRESS DIFFUSION IN THE LITHOSPHERE

by

Mai Yang

B.S., National Taiwan University, Taipei, Taiwan (1970)

M.A., Washington University, St. Louis, Missourri (1973)

SUBMITTED IN PARTIAL FULFILMENT

OF THE REQUIREMENTS FOR THE

DEGREE OF

DOCTOR OF PHILOSOPHY

at the

MASSACHUSETTS INSTITUTE OF TECHNOLOGY

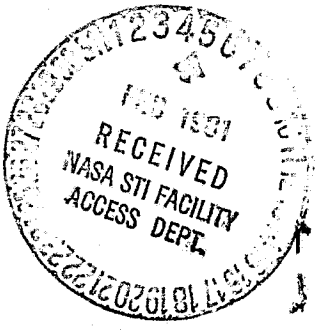

December 1980

Signature of Author.....
Department of Earth and Planetary Sciences
December 1980

Certified by.....
Thesis Supervisor

Accepted by.....
Chairman, Department Committee on Graduate Students

TIME DEPENDENT DEFORMATION AND STRESS DIFFUSION IN THE LITHOSPHERE

by

Mai Yang

Submitted to the
Department of Earth and Planetary Sciences
in December 1980 in partial fulfillment
of the requirements for the degree of
Doctor of Philosophy

ABSTRACT

The transient deformations and stresses due to earthquakes are studied using time dependent finite element models. Efficient computer programs incorporating frontal solution and time stepping procedure are developed for the modelling of geodynamic problems. This scheme allows us to investigate the quasi-static phenomena including the effects of the complex rheological structure of a tectonically active region.

From three dimensional models of strike slip earthquakes, it is found that lateral variation of viscosity affects the characteristics of surface deformations. The vertical deformation is especially informative about the viscosity structure in a strike slip fault zone. The subsiding region near the fault in a layered model can become an uplift region with a laterally heterogeneous model. For an earthquake with a fault length of 350 km and maximum slip of 5 m, the post-seismic uplift can reach 15 cm in 25 years if the low viscosity zone beneath the fault extends to 20 km deep. In such a model, the shear stress in the region adjacent to the fault tip along the strike direction increases with time rapidly for about two decades following the event, and reaches a constant value about 30 years after the event. The time dependent stress due to post-seismic relaxation can be larger than the stress due to the elastic response. This accelerated stress accumulation may have caused the observed earthquake migration along the North Anatolian fault zone.

Fine grid two dimensional models are used to study the time dependent deformation following a thrust event in a subduction zone. In particular, results from a series of models with different viscosity structures are compared with the uplift data along a leveling route from Whittier to Anchorage following the 1964 Alaskan earthquake. It is found that a simple layered model does not explain the data, but a model including a descending slab and a low viscosity wedge

above the wedge can produce the observed features.

Three dimensional viscoelastic model of a thrust earthquake indicates that the transient disturbance on plate velocity due to a great plate boundary earthquake is significant at intermediate distances, but becomes barely measurable 1000 km away from the source. The accelerated stress accumulation along the strike direction following a model thrust earthquake is consistent with the observation of earthquake migration along the subduction zones.

Thesis Supervisor: M. Nafi Toksoz
Professor of Geophysics

ACKNOWLEDGEMENTS

I wish to express my sincere gratitude to my advisor, Professor Nafi Toksoz, for his guidance throughout the course of my work at M.I.T. Nafi's broad knowledge and deep insights in geophysics are invaluable to this study. I also benefited from conversations with Professors Sean Solomon and Keiiti Aki during my years at M.I.T. Professor Albert Smith introduced the field of finite element analysis to me; his work has great influence on this study.

Free computation was avilable to me on the PDP-11 in the Applied Seismology Group of Lincoln Laboratory. I am grateful to the generous help from the members of the Applied Seismology Group. I appreciate the discussions with Dr. Mike Chinnery, whose information and comments are gratefully acknowleged. I owe special thanks to Ken Anderson and Ken Schroder for their helps in programming.

I wish to thank Drs. S.W.Lee, Oscar Orringer and H.C.Wang of the Aeronautics and Areospace Engineering Department of M.I.T. for their help in developing the finite element programs. The FRAP subroutines of Dr. Orringer provided the basic computational framework in this thesis. Lynn Hall, Jay Pulli, Mike Shield, Ken Tubman and Jim Wingo read the manuscript of this work; their suggestions greatly improved this thesis. I sincerely thank them for their help. Discussions with Paul Huang about

Alaska and information about Japan from Kei Ikeda are gratefully acknowledged. I also appreciate the interaction with Howard Patton, Tony Shakal, and Jim Scheimer during my years at M.I.T.

This work was supproted by the NASA grant NAG5-41 and NAG5-44.

TABLE OF CONTENTS

		Page
Abstract		2
Acknowlegement		4
Chapter 1.	Introduction	8
Chapter 2.	Computational Methods for Time Dependent Problems in Geodynamics	13
2.1	Analytical Models of Crustal Movements Associated with Earthquakes	13
2.2	Remarks on Available Numerical Solutions	20
2.3	Finite Element Solutions of Geodynamic Problems	25
2.4	Frontal Solution Technique and Time Dependent Calculation	27
2.4.1	The Principles of Frontal Solution and Time Stepping Scheme	27
2.4.2	Test Examples	32
2.5	Discussion of Non-linear Problems	36
Figures		40
Chapter 3.	Time Dependent Deformation and Stress Relaxation after Strike Slip Earthquakes	52
3.1	Introduction	53
3.2	Model Descriptions	55
3.3	Model Results	63
3.4	Discussion	71
Figures		76
Chapter 4.	Two Dimensional Analysis of Time Dependent Movements Associated with Dip Slip Earthquakes	99

4.1 Introduction 99

4.2 Brief Review of Deformation Data in Subduction Regions 102

4.3 Effects of Layered Structure on Postseismic Deformation 120

4.4 The Interaction of Deep Aseismic Slip and a Shallow Earthquake 128

4.5 Modelling of the 1964 Alaskan Earthquake 134

4.6 Discussion 147

Figures 155

Chapter 5 Three Dimensional Analysis of Dip Slip Earthquakes 232

5.1 Introduction 232

5.2 Model Description 235

5.3 Model Results 237

5.4 Discussion 242

Figures 248

Chapter 6 Conclusions 269

References 273

CHAPTER 1

INTRODUCTION

In this thesis, we will consider the problem of modelling the time dependent deformations and stresses associated with earthquakes and aseismic slips. Two and three dimensional time dependent finite element schemes have been implemented to do the calculations. The purposes of this study are to understand the physical processes underlying the observed time dependent phenomena of crustal movements and seismicity, to develop a scheme of modelling that can be used to interpret the data from modern geodetic techniques, and to study the rheological structure of the earth.

One of the clearest expressions of current plate motions are the great earthquakes that occur at plate boundaries. Investigating these events may provide us with information about the geodynamic processes in the earth. Elastic and viscoelastic motions associated with these events are also valuable in probing the rheological structure of the earth. Plate tectonics theory has provided the basic framework for the interpretations of earthquake mechanisms. Stresses build up as the plates are pulled apart, converge together, or slide past each other. Earthquakes are simply the fractures to relieve these stresses. However, knowledge about many important phases in the earthquake mechanisms is still far from complete.

In particular, the important problem of the accumulation, release, and relaxation of the stresses associated with earthquakes is still not fully understood. This problem must be considered within the context of the tectonics of the region containing the earthquake fault zone. A very useful tool for studying this problem is the time dependent crustal movements associated with an earthquake. These movements result from the interaction of the asthenosphere and the lithosphere and provide information about the physical processes of stress accumulation and relaxation. However, the data are still fragmentary; the fault region is usually complex; the interpretations of these data are difficult and the possibilities of the application to practical problems like earthquake prediction have not been fully exploited.

At the present time, there are intensive surveying activities in various seismically active areas in the world. There are also efforts to use space technologies for geodetic measurements to a precision never before achieved. Precise and frequent geodetic measurements covering large areas may be available in the near future. The interpretation and modelling of these high quality data will require considerable efforts.

In this thesis we use the finite element method to study the time dependent deformations and stress diffusions

associated with earthquakes and aseismic slips. An earthquake is modelled as an abrupt (step function in time) slip and an aseismic slip event is modelled as a prescribed time dependent slip. The faulting interacts with the viscoelasticity of a region and causes time dependent deformations and stresses, and these effects are evaluated in the models. When data are available, the model results are compared with geodetic and seismicity observations to obtain constraints on viscosity structure. The finite element scheme is capable of realistically modeling a complex region like the subduction zone. Both linear and nonlinear rheologies can be used. The models are constructed from our knowledge of the regional tectonics, and the viscosity distribution in a region is modelled in a realistic way. Fine grid two dimensional models are constructed to study the effects of vertical and lateral variations of viscosity in detail. In particular, two dimensional models have been used to study the post-seismic uplift of the 1964 Alaskan earthquake. When two dimensional models are not adequate to describe the problem, three dimensional models are utilized, and the effects particular to three dimensional models are evaluated. These include the stress diffusions associated with finite strike slip and dip slip events, the effects of lateral heterogeneities across a strike slip fault zone, and the time dependent movements off the symmetry plane of a dip slip event. We

have adopted the frontal solution technique into the time dependent finite element solution, which greatly reduces the amount of computer memory needed. The programs can be implemented on a moderate size computer while providing efficienct calculation speed.

Chapter 2 discusses the numerical scheme used in this thesis. Its merits and shortcomings are compared with other solution techniques. The principles underlying the frontal solution technique and the extension to time depenedent solutions are presented. Test examples are given, and the model results using linear and nonlinear flow laws are compared.

In chapter 3 we discuss the time dependent deformation and stress relaxation after strike slip earthquakes. Three dimensional models with lateral heterogeneities are used. It is found that the lateral heterogeneities can alter the characteristics of the time dependent deformations in a distinctive way. The possible relation of time dependent stress and earthquake migration along transform fault zone are also discussed.

Chapter 4 is concerned with the modelling of dip slip earthquakes using two dimensional plane strain models. The effects of the layered structure, the descending lithosphere, and the low viscosities on the crustal movements are discussed. In section 4.5, a model of the

great 1964 Alaskan earthquake is constructed. The model results are compared with the repeated leveling data collected after the earthquake. Discussion on the results in chapter 4 are given in section 4.6. In particular, the various possible mechanisms to explain the observed crustal movements after the 1964 Alaskan earthquake are discussed. Three dimensional effects of dip slip events are discussed in chapter 5, where we consider the perturbation on plate motion at far distances by a great dip slip event. Stress diffusion phenomenon and its relation to seismicity in subduction zones are also discussed. Chapter 6 summarizes the principal results and conclusions of this thesis.

Chapter 2

COMPUTATIONAL METHODS FOR TIME DEPENDENT PROBLEMS IN GEODYNAMICS

2.1 Analytical models of crustal movements of earthquakes

In solving simple problems, analytical methods are usually available and desirable, since they give exact solutions, are usually simple in form, and the physical meaning of each term in the solution can be identified. However, in the calculation of time dependent stress and deformation in the lithosphere, we soon realize that analytical methods are of limited use. Too many simplifications must be imposed and a realistic solution is usually impossible. Some previous work will be briefly reviewed in this section, as they provide a physical picture for the process going on in time dependent phenomena, and provide check of the validity of numerical solutions.

The simplest model for an earthquake fault is a dislocation in a half space. A strike slip fault is represented by a screw dislocation while a dip slip is modelled by an edge dislocation. Analytical solutions for dislocations in continuum have long been of interest in engineering and solid state physics. Steketee (1958a,b) first applied general Volterra dislocations to the problem of faulting. This formulation has been further pursued by Chinnery (1961,1963,1966), Maruyama (1963,1964,1966) and

Press (1965). Static dislocation models in a half space have been generalized to three dimensions by Mansinha and Smylie (1971), and to the spherical earth problem by Ben-Menahem et al (1969) and Singh and Ben-Menahem (1969). These models have also been generalized to layered media (Singh 1970, Sato 1971, Sato and Matsu'ura 1973, Javanovich et al 1974ab, Brown 1975), and to general polygonal dislocations (Brown 1975). Static dislocations have also been extensively used to fit observed geodetic deformation by earthquakes (Chinnery 1961, Press 1965, Savage and Hastie 1966, Hastie and Savage 1970, Fitch and Scholz 1971, Canitez and Toksoz 1972, Thatcher 1975ab, Ando 1975, Freund and Barnett 1976, Savage 1979). A review of dislocations in seismology was given by Savage (1979).

When repeated survey data are compared with models, time dependent effects should be included in the modelling. Although the elastic properties of the earth are slowly varying functions of space and a simple analytic solution in a homogeneous medium may be adequate, the viscosity structure of the earth changes by orders of magnitude with space. This should be taken into account when modelling the time dependent phenomena.

For a model of a two dimensional homogeneous viscoelastic half space, there is no time dependent deformation associated with either a screw or an edge

dislocation. This can be seen directly from the elastic half space solution and the elastic-viscoelastic correspondence principle. Briefly stated, the elastic-viscoelastic correspondence principle says that if the solution of an elastic problem is known, then the Laplace transform of the solution to the corresponding viscoelastic problem can be found by replacing the elastic constants by some quotient of operator polynomials, and the actual loads by their Laplace transforms. The time domain solution can then be obtained through inverse Laplace transform (Christensen 1971). For example, the vertical displacement U on free surface for a vertically dipping fault is

$$U = \frac{U_o}{\pi}\left(\frac{x^2}{x^2 + d^2} - \frac{x^2}{x^2 + D^2}\right) \qquad (2.1.1)$$

where U_o is the fault offset, x is the horizontal coordinate, and D and d are the lower and upper limits of the fault depth respectively. The surface deformation depends only on the geometry of the fault, not on the elastic constants. From the elastic-viscoelastic correspondence principle, the solutions are thus identical for both elastic and viscoelastic solutions. In general, surface deformation from a two dimensional dislocation in a homogeneous half space does not depend on the elastic constants (Savage and Prescott 1978b). Inhomogeneities are required to introduce time dependent behavior in two

dimensional problems. Singh and Rosenman (1974) showed that the identitiy of elastic and viscoelastc displacement solutions persists for a vertical dip slip fault in a homogeneous three dimensional half space. However, three dimensional strike slip earthquakes in general have time dependent deformation.

Elsasser (1969) first proposed a one dimensional scheme to model the stress diffusion in the lithosphere caused by an earthquake. The model is an elastic beam overlying a layer of Newtonian fluid, where the elastic beam simulates the lithosphere and the viscous fluid simulates the asthenosphere. A sudden (step function) push or pull on the edge of the elastic plate simulates an earthquake. The equation governing the displacement in space and time can be reduced to a diffusion equation, and the solution for a step function input to such a system is the complementary error function. Similar one dimensional models have been further discussed by Bott and Dean (1973) and Anderson (1975). Melosh (1976) extended this linear one dimensional model from Newtonian fluid to power law behavior and applied it to the study of the aftershock sequence of the Rat Island earthquake of 1965. The common feature of these elastic plate over viscous fluid systems is that they have a rather prominent stress diffusion effect. The stress at a point far away from the source increases rather rapidly with time as the stress propagates through the point. Savage and

Prescott (1978b) pointed out that this system of elastic plate and viscous fluid substratum is not a suitable model for studying transient phenomenon. In such a system, viscous fluid cannot be deformed instantaneously by shear, and the deformation at the time of the earthquake at any place other than the source is zero. Because of this, the stress caused by the disturbance at any place has a rather sharp rise time. This system has been extended to viscoelastic media by Ho and Smith (1979).

Rosenman and Singh (1973ab) obtained the time dependent stress and deformation due to three dimensional strike slip earthquakes in a homogeneous viscoelastic half space by using the correspondence principle and the known elastic solution for a strike slip fault. Nur and Mavko (1974) first found a solution to large time dependent deformation associated with a dislocation in a vertically inhomogeneous medium. The model is an elastic layer overlying a viscoelastic half space. They used the method of images to obtain an approximate solution of a two dimensional dislocation in an elastic layer over an elastic half space with different elastic constants. The time dependent solution of a linear viscoelastic medium can be obtained from elastic-viscoelastic correspondence principle. Nur and Mavko pointed out that a large thrust type earthquake may provide a tool for exploring the rheology of the earth's upper mantle. Barker (1976) used Haskell's

(1953) method of propagator matrix to obtain a solution of a screw dislocation in a layered elastic medium; then he obtained the time dependent solution of a viscoelastic medium by using the elastic-viscoelastic correspondence principle. Rundle and Jackson (1977ab) and Rundle (1978) obtained solutions for a strike slip fault in an elastic layer overlying a viscoelastic half space. They used the method of images to obtain the elastic solution; then they used the elastic-viscoelastic correspondence principle to obtain the time dependent solutions. Thatcher and Rundle (1979) also obtained a solution for a two dimensional edge dislocation in an elastic layer over a viscoelastic half space. However, their solution does not agree with that of Nur and Mavko. Smith (1974) pointed out that Nur and Mavko's solution for an edge dislocation involves some gross approximations. Thatcher and Rundle (1979) also pointed out that Nur and Mavko's solution for an edge dislocation cannot be reduced to the corresponding elastic solution at the time immediately after the earthquake. Savage and Prescott (1978b) extended the Nur and Mavko solution for a screw dislocation to the study of the earthquake cycle for strike slip faults. Spence and Turcotte (1979) obtained the response of an infinite sequence of step-wise offsets on a two dimensional strike slip fault. Cohen (1980ab) extended Rundle's solution of a three dimensional strike slip earthquake to a standard linear solid medium.

The analytical solutions for time dependent calculations usually use the elastic-viscoelastic correspondence principle. The medium property is thus restricted to linear viscoelastic materials. At the present time, most solutions are restricted to a flat layer over half space models. This may be adequate in modelling general effects at large distance from a zone of complicated tectonics where the earthquake occurs (if three dimensional models are available). But it certainly has limitations in applying the layered solution to a complex region like subduction zone. Furthermore, the inverse Laplace transformation must often be done in approximation, thus the exactness of analytical solutions, their other advantage, is also lost.

To model the earth realistically, including complications due to structure and materials, we decided to take a numerical approach. When the geometry is complicated, the numerical approach is not only more versatile than the analytic solutions, but is also more convenient to use. Once the programs are set up, they can be used to compute different solutions; only some input parameters have to be changed. A brief discussion on numerical methods used in this thesis is given in the following sections.

2.2 Remarks on available numerical schemes

There are several well developed numerical methods to calculate stresses and strains. The most commonly used numerical techniques for solving partial differential equations are probably the finite difference method (FDM), the finite element method (FEM), and the boundary integral equation method (BIE). Historically, the developement of each of these three methods has its own origin and physical basis. However, as each method developed, the definition of each method became more general and the techniques became more involved, and the distinction among these three methods became less clear. For example, some finite element worker interpreted BIE as a kind of finite element process with a special form of trial function (Zienkiewicz 1977). There are also finite difference equations derived via finite elements (Wempner 1971). If we disregard these artifacts due to definitions and consider the basic form of the method, each method does have its own merits and shortcomings. The choice of the numerical method depends very much on the problems to be solved.

FDM has been used longer than the other two methods. The basic essence of this technique is to replace the govering differential equations and boundary conditions by a set of algebraic equations using finite difference approximations. If the boundaries in the problem can be described easily with some mathematical formulation, FDM can

provide a very efficient solution. In such cases the length of the program code and computational time are often shorter than those of the corresponding FEM solutions. On the other hand, it is awkward to use FDM if the boundaries in the problem have complex geometric shapes. FDM does not have to use regular mesh points, but the advantage of simplicity is lost when irregular mesh points are used.

FEM is often (but not always) derived from the governing variational principle and Rayleigh-Ritz principle. The governing differential equations do not appear in the formulation. Each element can be considered as a physical element. The behavior of the element depends only on its material properties and nodal values. The solution region can be built up with finite elements as if the actual object is built up by pieces of structural elements. There is great freedom in choosing the element type and size to suit the actual problem. Complicated geometry of boundaries and material inhomogeneities can be handled with ease. In particular, the grid space can be designed so that high resolution is obtained where it is needed, and coarse grid spacing can be used in regions of little interest. On the other hand, there are lengthy bookkeeping jobs in finite element programs. The computational costs are often higher than those of finite difference solutions (if FDM can also do the job). Nowadays, both FDM and FEM are standard tools in engineering analysis and there are excellent textbooks

covering these subjects (e.g. Hildebrand 1968, Zienkiewicz 1977).

The boundary integral solutions are obtained by transforming the differential equations governing the behavior inside and on the boundary of the domain to integral equations over the boundaries. There was no general way to solve these integral equations before the advent of computers. The use of boundary integrals was, to a great extent, limited to theoretical investigations of the existence and uniqueness of the solutions. The developement of BIE as a real tool for problem solving using computers is relatively new, but in recent years it has gained growing attention (e.g., Massonet 1965, Mendelson 1973, Lachat and Watson 1976, Zienkiewicz et al 1977, Cruse 1977, Cole et al 1978). There are a number of advantages for BIE to make a scheme competitive with FEM and FDM. The most obvious one is that it reduces the dimensionality of the problem by one. The numerical solution of the integral equations involves the modelling of boundary data rather than volume data. For three dimensional problems the numerical analysis is performed on the two dimensional boundary surface; thus the size of the problem is greatly reduced. The procedure can be used to calculate the solution at any interior point, unlike FEM or FDM which allows calculation only at nodal points. Sometimes it also has advantages in problems with infinite region or singularities. However, the matrice

involved in BIE are not banded or symmetric. This may well offset the reduction of problem size, as efficient algorithms exist for solving symmetric and banded matrix equations. The solutions are limited to problems which have suitable Green's functions, thus its use in non-linear material or highly heterogeneous bodies is limited. BIE can sometimes be coupled to FEM to combine the advantages of both methods (Zienkiewicz et al 1977)

In this thesis, we will use the finite element method exclusively. The main reason for this choice of numerical scheme is that we would like to have a versatile method. Among the above three methods, FEM takes the most effort to program, and the computational cost is the highest. But it is also the most versatile. The realistic earth is far from a homogeneous body, and the regions where earthquakes occur are usully more complicated than other regions. If we are interested in modelling the time dependent movements associated with earthquakes, we must be prepared to use the solution method under various conditions. For an earthquake in subduction regions, there are descending slabs dipping at various angles and low viscosity wedges above the descending slabs. In transform fault regions, the shear heating may produce lateral heterogeneities. It is essential that our approach can handle these features. We also desire a method which can handle a wide varieties of material properties. For this reason, we choose the more involved but more

versatile finite element method as our numerical method.

2.3 Finite element solutions of geodynamic problems

Since FEM is suitable for modelling the heterogeneous medium, it has been applied to the study in geophysics by many investigators. It has been applied to study geological folds using a viscous fluid model (Dieterich 1969, Parish et al 1976, Cobbold 1977, Woidt and Neugebauer 1980), to the studies of regional stress fields and tectonics using either creep or static models (Jungels and Frazier 1973, Shimazaki 1974ab, Luo 1974, Smith 1974, Bischke 1974, Neugebauer and Breitmeyer 1975, Kusznir and Bott 1977, Bird 1978, Neugebauer and Sophon 1978, Melosh and Raefsky 1978,1979, Slade et al 1979, Kasahara 1978, Kosloff 1978, Richardson 1978ab, Richardson and Bergman 1979, Kato 1979), and to studies of seismic wave propagation (Lysmer and Drake 1972, McCowan et al 1977, Smith 1975, Smith and Bolt 1976, Archuleta and Frazier 1978, Schlue 1979). In addition, there is a large amount of literature using the finite element method for studies in soil mechanics and rock mechanics. The first study of earthquake deformation using the finite element method is probably by Jungels and Frazier (1973). They used two dimensional static models to study the deformation of the 1972 San Fernando earthquake. Smith (1974) extended the analysis to a viscoelastic medium and time dependent behaviors using two dimensional plane strain models. Two dimensional plane strain models has also been used by Bischke (1974) , Melosh and Raefsky (1979) and Slade et al (1979).

The computational scheme used in this thesis have been influenced by the work of Smith (1974). We adopted his treatment of the fault model and boundary conditions, however, we designed a scheme with wider applicability. Smith used the elastic-viscoelastic correspondence principle and solved a set of static solutions in Laplace domain using finite elements. The time dependence was obtained by using numerical Laplace transform (Schapery 1961, Adey and Brebbia 1973). Smith (1974) was mainly interested in two dimensional plane strain models and linear materials. An in core finite element solver (FEABL) was used. Later Smith (1979) extended his programs to three dimensional viscoelastic models. However, some out of core solver must be designed to take care of the storage problem for three dimensional applications. We wanted to extend the two dimensional analysis to three dimensions, and to cover a wider class of material properties and modes of fault displacements. To achieve these goals, we developed a scheme combining the time stepping approach (Zienkiewicz and Cormeau 1974) and frontal solution technique (Irons 1970). These will be discussed in the next section.

2.4 Frontal solution technique and time dependent calculation

2.4.1 The principles of frontal solution and time stepping scheme

The basic finite element method has been covered in many textbooks (e.g. Cook 1974, Zienkiewicz 1977), so it will not be repeated here. In finite element models of time dependent behaviors associated with earthquakes, we have to deal with two practical problems: The first is the large size (number of degrees of freedom, storage requirement, and computational cost) of the problem, and the second is the extension to time dependent calculations. We followed the time stepping approach of Zienkiewicz and Cormeau (1974) for time dependent calculations, and combined the frontal solution technique (Irons 1970) to the time stepping approach for an efficient solution scheme and great savings in computer memory requirements.

In the time stepping approach for time-dependent calculations, the total strain {e} is divided into three parts:

$$\{e\} = \{e\}^{el} + \{e\}^{cp} + \{e\}^{o} \qquad (2.4.1)$$

where $\{e\}^{el}$ is the elastic strain, $\{e\}^{o}$ is the initial strain, and $\{e\}^{cp}$ is the creep strain. Engineering stress and strain are used. We use curly brackets to denote

vectors and square brackets to denote matrice. Quite generally the constitutive law for creep strain rate and stress can be put into the form

$$\{\dot{\varepsilon}\}^{cp} = [\Gamma]\{\sigma\} \tag{2.4.2}$$

where dot indicates time rate of change, $[\Gamma]$ is a symmetric matrix (may depend on stress) and $\{\sigma\}$ is the stress.

The virtual work principle is:

$$\int_V \delta\{e\}^T\{\sigma\}dV - \int_V \delta\{u\}^T\{b\}dV - \int_S \delta\{u\}^T\{t\}dS = 0 \tag{2.4.3}$$

where $\{b\}$ is the prescribed body force, $\{t\}$ is the prescribed boundary traction, and $\{u\}$ is the displacement. δ indicates variation and T indicates transpose. Integration is over the volume V and traction boundary S respectively.

Let

$$\{e\} = [L]\{u\} \tag{2.4.4}$$

$$\{u\} = [N]\{a\} \tag{2.4.5}$$

where $[L]$ is the operator relating strain and displacement, $[N]$ is the interpolation function, and $\{a\}$ is the nodal displacement. Then equation (2.4.3) becomes

$$\delta\{a\}^T\Big[\int_V [N]^T[L]^T\{\sigma\}\,dV - \int_V [N]^T\{b\}\,dV - \int_S [N]^T\{t\}\,dS\Big] = 0 \qquad (2.4.6)$$

or

$$\int_V [B]^T\{\sigma\}dV - \{F\} = 0 \qquad (2.4.7)$$

where $[B] = [L][N]$, $\{F\} = \int_V [N]^T\{b\}dV + \int_S [N]^T\{t\}dS$

Substituting $\{\sigma\} = [D]\{e\}^{el} = [D](\{e\}-\{e\}^{cp}-\{e\}^{o})$, equation (2.4.7) can be put into the standard form:

$$[K]\{a\} = \{R\} \qquad (2.4.8)$$

where

$$[K] = \int_V [B]^T[D][B]dV$$

$$\{R\} = \{F\} + \int_V [B]^T[D]\{e\}^{o}dV + \int_V [B]^T[D]\{e\}^{cp}dV$$

Equation (2.4.8) is the set of linear equations to be solved using the frontal solution. $\{e\}^{cp}$ is obtained in a time stepping fashion using the equation $\{\dot{e}\}^{cp} = [\Gamma]\{\sigma\}$. It can be shown that this procedure can be applied to the general visco-plastic problems (Zienkiewicz and Cormeau, 1974), including plasticity and creep problem as two extreme cases. The scheme handles a nonlinear creep material in the same way as a linear material.

In equation 2.4.8, the vectors {a} and {R} have the dimension of the degrees of freedom N in the problem, and the stiffness matrix {K} has the dimension of N x N. In three dimensional problems, it is very common to have thousands of degrees of freedom in a model. The problem of computer storage then becomes very serious, so it is imperative to fully exploit the banded property of the stiffness matrix. We have chosen the frontal solution approach (Irons 1970, Orringer 1974) to minimize the in core storage requirement. In this approach, the familiar Gaussian elimination method is still the central process, however the assembly and elimination processes are not seperated. We accumulate the contribution to the stiffness matrix and consistent nodal force vector element by element until one diagonal element K_{nn} of the stiffness matrix has received all the contributions from the elements connected to it. Then the global force-displacement relation associated with K_{nn}

$$\sum_{j=0}^{N} K_{nj} a_j = R_n \qquad (2.4.9)$$

is eliminated. The coefficients in this equation are moved to outside storage, and their previous locations in core are cleared for storing other coefficients. The remaining equations are updated according to

$$K^{*}_{ij} = K_{ij} - \frac{K_{in}K_{jn}}{K_{nn}} \qquad (2.4.10)$$

$$R^{*}_{i} = R_{i} - \frac{K_{in}R_{n}}{K_{nn}} \qquad (2.4.11)$$

Since each degree of freedom accepts contributions only from elements connected to it, the in core storage is usually greatly reduced (if the elements are numbered properly). At the end of the elimination process, the last equation will be in the form of:

$$K^{**\ldots*}_{NN} \; a_N = R^{**\ldots*}_{N} \qquad (2.4.12)$$

which can be readily solved for the displacement a_N. a_N is then back substituted into the penultimate equation which contains only two degrees of freedom. This back-substitution process continues in the order exactly opposite to that of the assembly process until all the nodal displacements are solved.

Notice in equation 2.4.8, the stiffness matrix [K] is the same for each time step. Only the force vector {R} is different. So we do not have to perform assembly and elimination for each time step; once the reduced stiffness matrix elements have been saved on outside storage, all we have to do is to update the force vector {R} and back substitute. This constitutes tremendous savings when the

size of the problem is large. For the three dimensional problems we described in chapter 3 and 5, the c.p.u time for each subsequent time step was about 5 to 10 percent of the first step (which did the assembly and elimination). Because of this huge saving of computation time, we have refrained from using implicit time stepping schemes (e.g. Hughes and Taylor 1978), which may be more stable but requires assembly and elimination for each time step.

2.4.2 Test examples

Several examples were used to test the finite element programs. First we tested the static deformations of a vertical dip slip earthquake. The finite element grid for this example is given in figure 2.4.1. The model region is 1600 km long and 800 km deep. The fault lies on the center line of the region and has a constant slip 5 m from surface to 75 km deep and tapers off to zero at 80 km deep. We have used the treatment of Smith (1974) to model the fault. There are double nodes along the fault zone. The fault offset is prescribed as relative displacement between the double nodes, but the absolute locations of the double nodes are allowed to move in response to the stress field. In this example, we have assumed that the bottom and sides of the region, which are far away from the fault, are rigid. Since the earthquake is very far from the external boundaries, this assumption has little effect on the result.

The resulting vertical displacement on the free surface of the finite element model is given in figure 2.4.2. The analytical solution of the vertical displacement on the free surface for a vertically dipping fault with uniform slip in an infinite homogeneous half space was given in equation 2.1.1. The resulting analytical solution of vertical displacement on free surface for a vertically dipping fault from surface to 80 km deep with a uniform slip 5 m is superimposed on the finite element solution in figure 2.4.2. The difference between the numerical and analytical solutions is insignificant.

The second test example is a fault dipping 45 degrees, with a 5 m offset from the surface to 75 km depth, and tapers off to zero at 80 km depth. The finite element grid is given in figure 2.4.3. The model region is 2560 km long and 1160 km deep. The resulting vertical displacement on the free surface of the finite element model is given in figure 2.4.4. The analytical solution for vertical displacement on the ree surface for a 45 degree dipping fault with uniform slip is (Jungels and Frazier 1973)

$$U = -\frac{U_o}{11.3\pi}\left[\frac{2(2D-x)^2 + 4x(2D-x) + 6x^2}{(2D-x)^2 + x^2}\right. \qquad (2.4.13)$$

$$\left. + 4\tan^{-1}\left(\frac{2D-x}{x}\right) + 2 + \pi\right]$$

where U_o is the fault offset, D and d are the lower and upper limits of the fault depth, x is the horizontal coordinate, and the fault intercepts the free surface at x = 0. The resulting analytical solution of the vertical displacement on the free surface for a 45 degree dipping fault from surface to 80 km deep with a uniform slip 5 m is superimposed on the finite element solution in figure 2.4.4. Again the agreement between the analytical and numerical solutions is very good.

To test the time stepping procedure, we calculated the creep of a cylinder under internal pressure. The material of the cylinder is elastic in bulk and Maxwellian in distortion with bulk modulus 1 unit, shear modulus 1 unit, and viscosity 1 unit. The outer boundary of the cylinder is rigidly fixed. The internal pressure is 10 units. The inside radius of the cylinder is 1 unit and the outside radius is 2 units. A schematic diagram of the problem and the finite element grid are given in figure 2.4.5. Only a section of the cylinder is needed because of the symmetry in this problem. The finite element grid has 48 elements and 130 degrees of freedom. The analytical solution for the radial stress S_r and hoop stress S_h as functions of radial distance r and time t are (Flugge 1967):

$$S_r = -P \left[1 - \frac{\lambda q a^2 (r^2 - b^2)}{2Kb^2 r^2} e^{-\lambda t} \right] \qquad (2.4.14)$$

$$S_h = -P \left[1 - \frac{\lambda q a^2 (r^2 + b^2)}{2Kb^2 r^2} e^{-\lambda t} \right] \qquad (2.4.15)$$

with

$$\lambda = \frac{6Kb^2}{6Kfb^2 + q(3a^2 + b^2)}$$

$$f = \frac{\mathcal{V}}{g}$$

$$q = 2\mathcal{V}$$

where P is the pressure, K is the bulk modulus, g is the shear modulus, $\mathcal{V}$ is the viscosity, and a and b are the outer and inner radii.

Figure 2.4.6 gives the finite element result of the hoop stress superimposed on the analytical solution, and figure 2.4.7 gives the results of radial stress. The very good fit between the analytical and numerical results confirms that the time dependent finite element procedure we adopted works well.

2.5 Discussion of non-linear problems

The flow property of the earth is vitally relevent to many fundamental phenomena in geodynamics. For example, the mantle convection and the driving force in plate tectonics, the strength and the stress state of the lithosphere, and the accumulation of strain in a fault zone all depend on the flow properties of rocks. Despite great advances in recent years in both experimental and observational works, some controversy still exists. Inferred from the experimental work (Weertman 1970, Carter and Ave'Lallemant 1970, Stocker and Ashby 1973, Kohlstedt and Goetze 1974, Weertman and Weertman 1975, Carter 1976, Weertman 1978, Goetze 1978, Ashby and Verall 1978), the probable creep law under mantle conditions should be a non-linear power law creep. However, it is difficult to achieve the small strain rate of geological processes in the laboratory. Inference on the long term behavior of rocks is largely obtained from extrapolation. On the other hand, analysis of glacial rebound data suggests that the flow law in the mantle may be Newtonian (Walcott 1973, Cathles 1975, Peltier and Andrews 1975, Peltier 1976). If the time dependent crustal movements associated with earthquakes behave distinctively different for linear and non-linear rheologies, then we can infer the flow law through the modelling of crustal movements with linear and nonlinear models. In section 2.4 we mentioned that our finite element scheme is suitable for both linear and nonlinear models,

however available observation may not be sensitive to the form of the creep law (Turcotte et al 1973, Parmentier et al 1976). We conducted a numerical experiment on the behavior of postseismic deformations for linear and nonlinear rheologies. Model 2A and model 2B have the same elastic response, grid structure, and fault configuration, except that model 2A follows power law creep and model 2B follows Newtonian creep behavior. The fault model is a uniform slip of 3 m from surface to 40 km deep and tapers off to zero at 80 km deep, with a fault dip of 60 degrees. Both models have elastic lithospheres, each 80 km thick. Below this depth the creep law for model 2A is assumed to be

$$\dot{e} = \frac{gbA}{kT} \left(\frac{\sigma}{g} \right)^3 \exp\left(- \frac{Q_{cr} + PV}{kT} \right) \qquad (2.5.1)$$

where $\dot{e}$ is the shear strain rate, σ is the shear stress, g is the shear modulus, b is the Buerger vector, k is the Boltzman constant, T is the absolute temperature, Q_{cr} is the activation energy, P is the pressure and V is the activation volume. We also assumed that the lattice parameters and elastic moduli are related to temperature and pressure as given by equations (2.1) to (2.5) of Ashby and Verall (1978). We assume the temperature and pressure are related to depth by the relations

$$P = 3.2 \times 10^4 D \qquad (2.5.2)$$

$$T = 300 + 1579 \times [\ 1 - \exp(\ -7.6\times10^{-6}D\ )\ ] \qquad (2.5.3)$$

where D is depth in meters. The relations and the constants are taken from Ashby and Verall (1978) for the flow properties of dry olivine. All the quantities involved are in MKS units. The result of vertical displacement changes on the free surface at 0.0, 8.0, 25.8 and 114 years after the event is given in figure 2.5.1.

We would like to see if a linear model can also produce such a result. Model 2B assumes a Newtonian flow law. The viscosity is assumed to have a layered structure, where the lithosphere is again elastic and 80 km thick. From 80 to 180 km deep the viscosity is 1×10^{23} poise; from 180 to 360 km deep it is 2×10^{21} poise; from 360 to 600 km deep it is 0.8×10^{20} poise and below 600 km deep it is 2.2×10^{21} poise. Figure 2.5.2 gives the plot for the vertical displacement changes at the same times as in figure 2.5.1. The results are very similar to model 2A. The difference is probably too subtle to be detected by geodetic data at the present time. This numerical experiment demonstrates that the crustal deformations are not uniquely determined by the form of creep law (although they are in general sensitive to the values of viscosity, as we will see in later chapters). As far as the time dependent deformation following an earthquake is concerned, linear models contain the essential elements of time dependent behavior. In the absence of

exact information about the material composition, viscosity structure, and flow law in different regions, we choose to use linear models to study the relaxation effects of viscoelsatic materials in the following chapters.

Figure Captions - Chapter 2

Figure 2.4.1 The finite element grid for computing the deformation of a vertically dipping fault. The model fault intercepts the surface at coordinate (0,0). The fault extends from 0 to 80 km deep. The grid has 1050 d.o.f and 496 elements. The model region is 1600 km long and 800 km deep.

Figure 2.4.2 Solution for the vertical displacement of the vertical dipping fault. Solid curve is the analytical solution from Jungels and Frazier (1973). The symbols are the finite element solution using the grid in figure 2.4.1. The fault in the analytic solution has uniform fault slip 5 m from surface to 80 km deep. The fault in the finite element solution has a 5 m fault slip from the surface to 75 km deep and tapers off to zero at 80 km deep.

Figure 2.4.3 The finite element grid for computing the deformation of a 45 degrees dipping fault. The model fault intercepts the surface at coordinate (0,0). The fault extends from 0 to 80 km deep. The grid has 1050 d.o.f and 496 elements. The model region is 2560 km long and 1160 km deep.

Figure 2.4.4 Solution for the vertical displacement of the 45 degrees dipping fault. Solid curve is the analytical solution from Jungels and Frazier (1973).

The symbols are the finite element solution from the grid in figure 2.4.3. The fault in the analytic solution has a uniform fault slip 5 m from surface to 80 km deep. The fault in the finite element solution has a 5 m fault slip from surface to 75 km deep and tapers off to zero at 80 km deep.

Figure 2.4.5 (a) The test problem of cylinder creep under internal pressure. The cylinder is elastic in bulk and Maxwellian viscoelastic in distortion. The outer boundary is rigidly fixed and the inner boundary is under 10 unit of pressure. (b) The finite element grid used to calculate the time dependent stress in the cylinder creep problem. Because of symmetry, only a small section of the cyliner is used in actual computation. The finite element grid has 48 elements and 130 degrees of freedom.

Figure 2.4.6 Hoop stress as a function of distance in the cylinder creep problem. Curves 1, 2, 3 and 4 are analytical solutions at times = 0.0, 1.0, 3.0 and 12 relaxation times. Symbols are the corresponding finite element solutions.

Figure 2.4.7 Radial stress of the cylinder creep problem. Curves 1, 2, 3 and 4 are analytical solutions at times = 0.0, 1.0, 3.0 and 12 relaxation times. Symbols are the finite element solutions.

Figure 2.5.1 Postseismic vertical displacement change on the free surface due to the relaxation for model 2A, which assumes a power law creep behavior. The curves 1, 2, 3, and 4 are at time 0.0, 8.0, 25.8 and 114 years after the event.

Figure 2.5.2 Postseismic vertical displacement change on the free surface due to the relaxation for model 2B, which assumes a Newtonian creep behavior. The curves 1, 2, 3, and 4 are at time 0.0, 8.0, 25.8 and 114 years after the event.

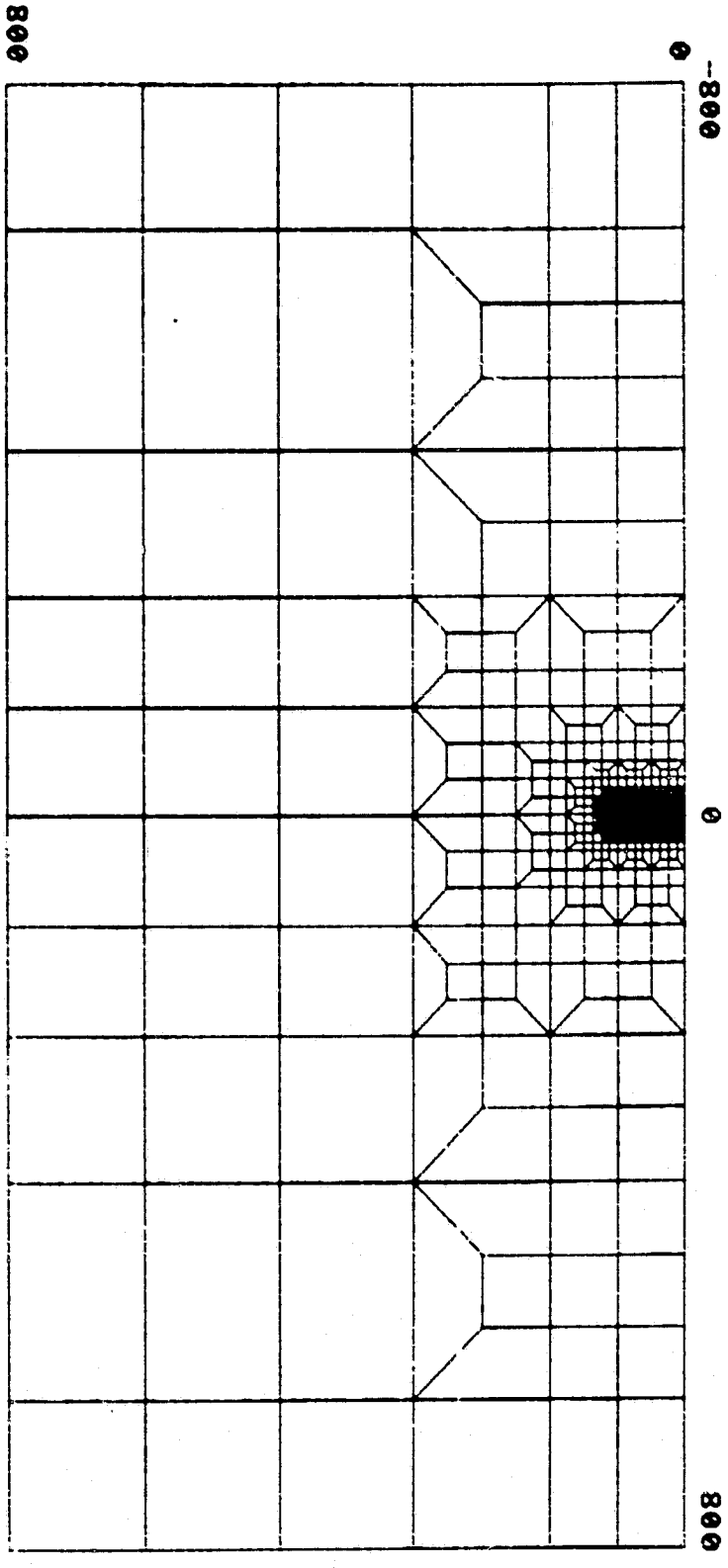

Fig. 2.4.1

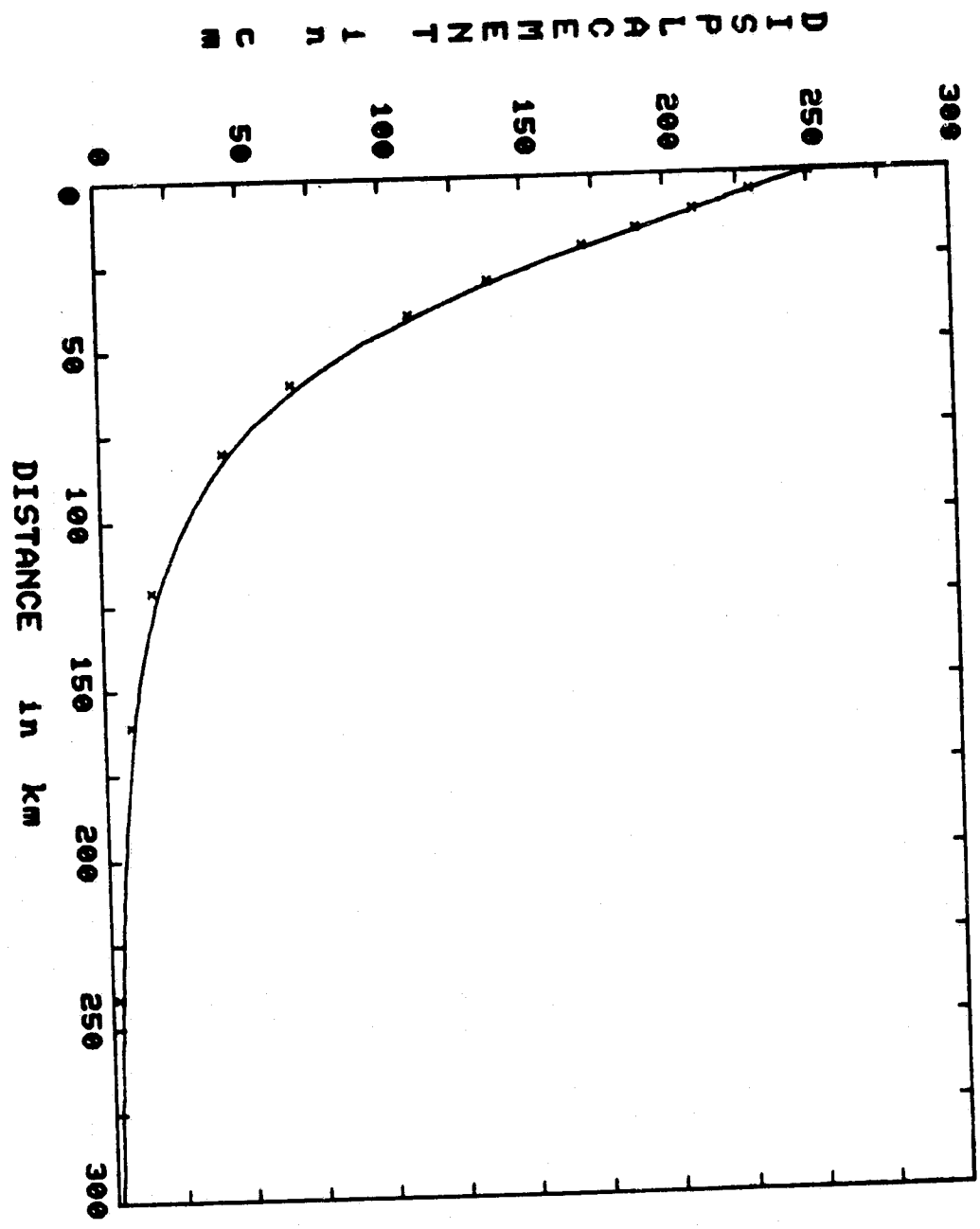
DISPLACEMENT in cm
0
50
100
150
200
250
300
DISTANCE in km
0
50
100
150
200
250
300

Fig. 2.4.2

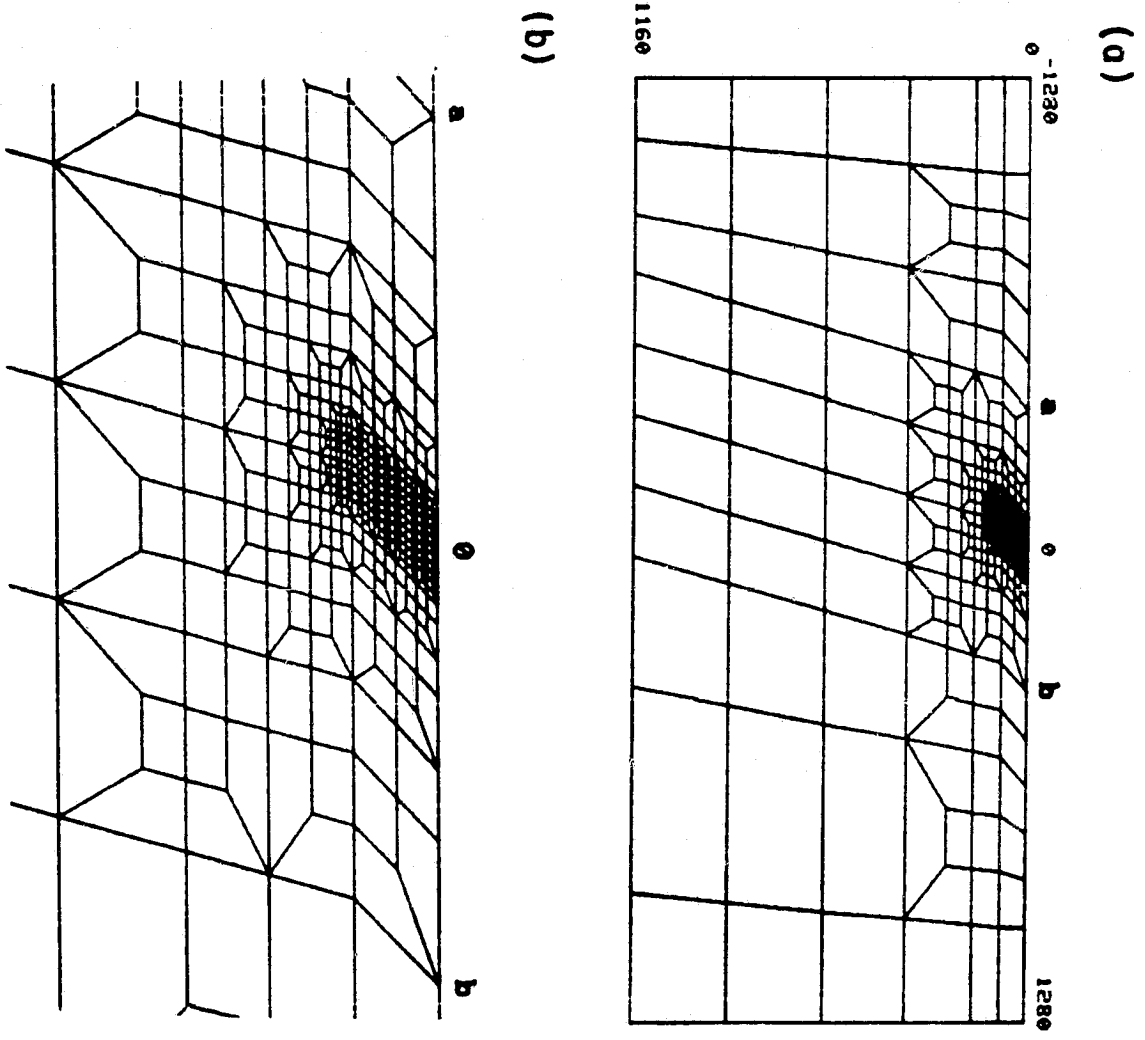

Fig 2.4.3

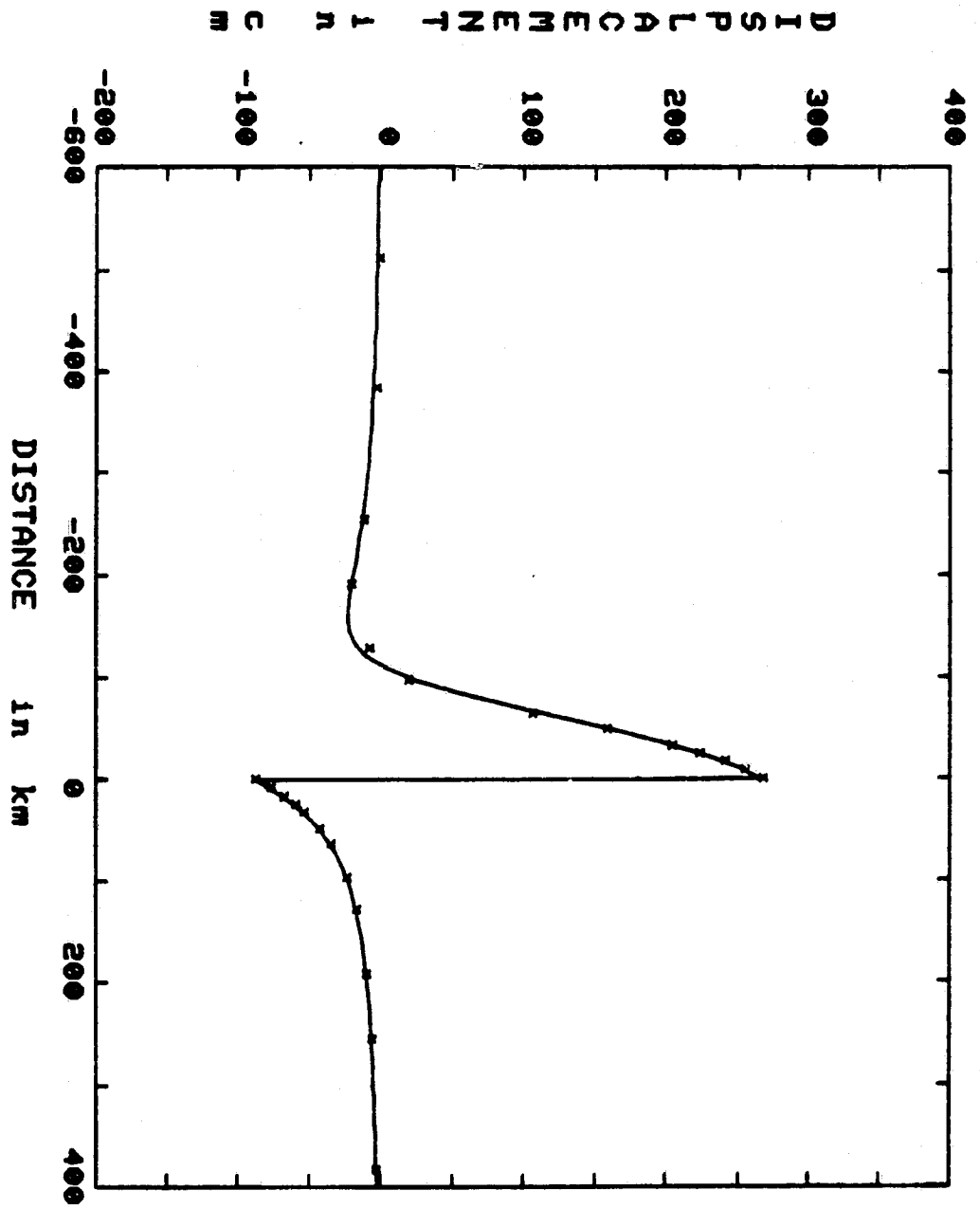
DISPLACEMENT in cm
-200
-100
0
100
200
300
400
-600
-400
-200
0
200
400
DISTANCE in km

Fig. 2.4.4

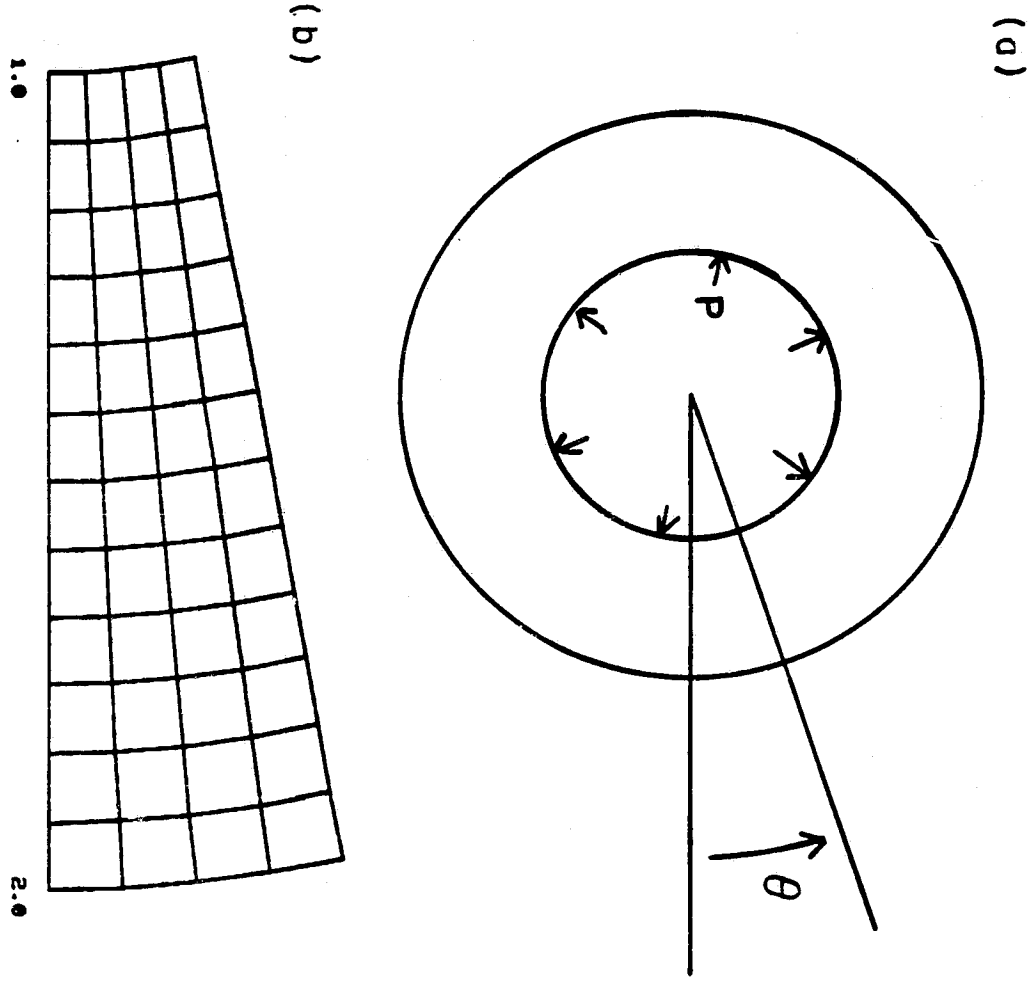

Fig. 2.4.5

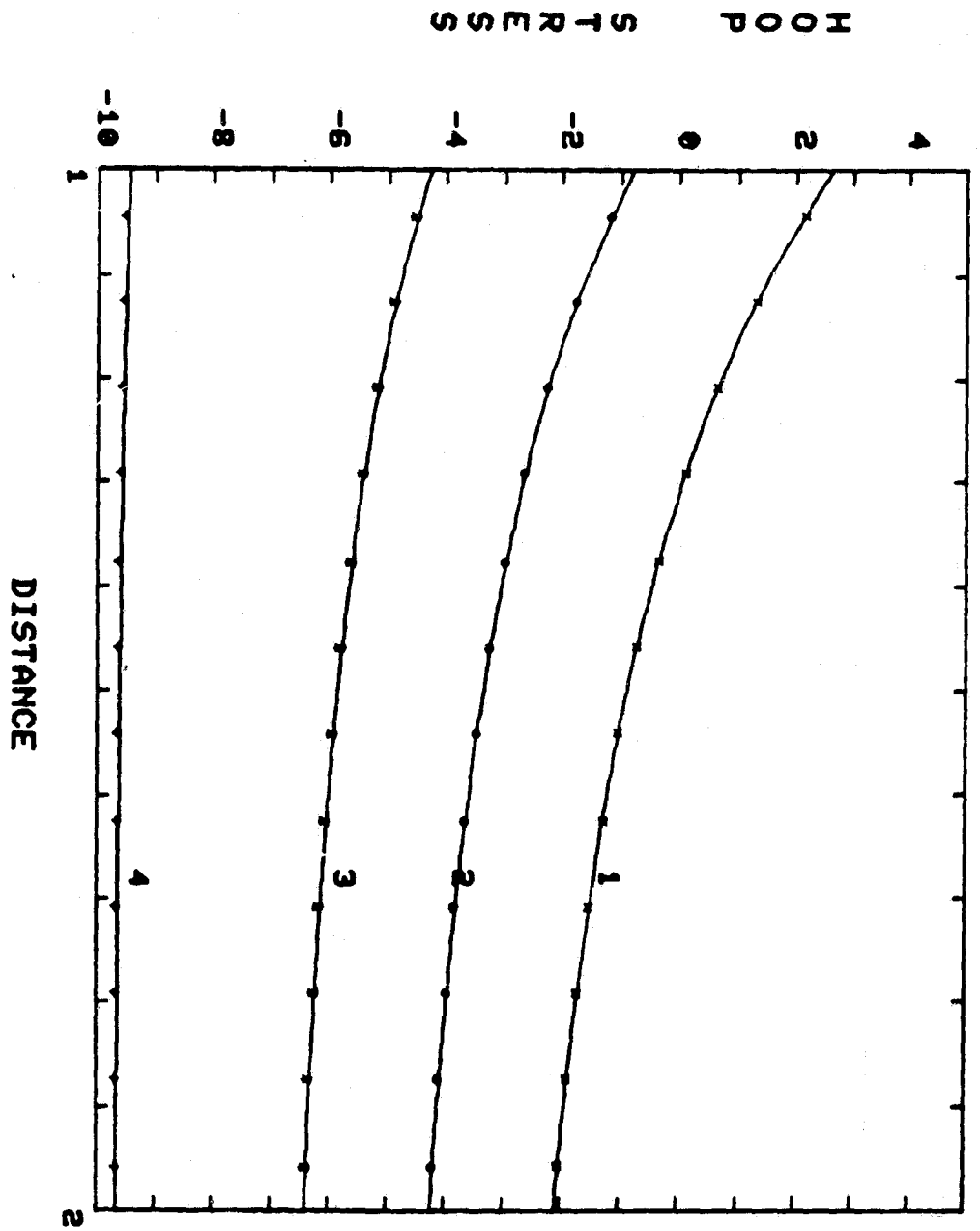

Fig. 2.4 6

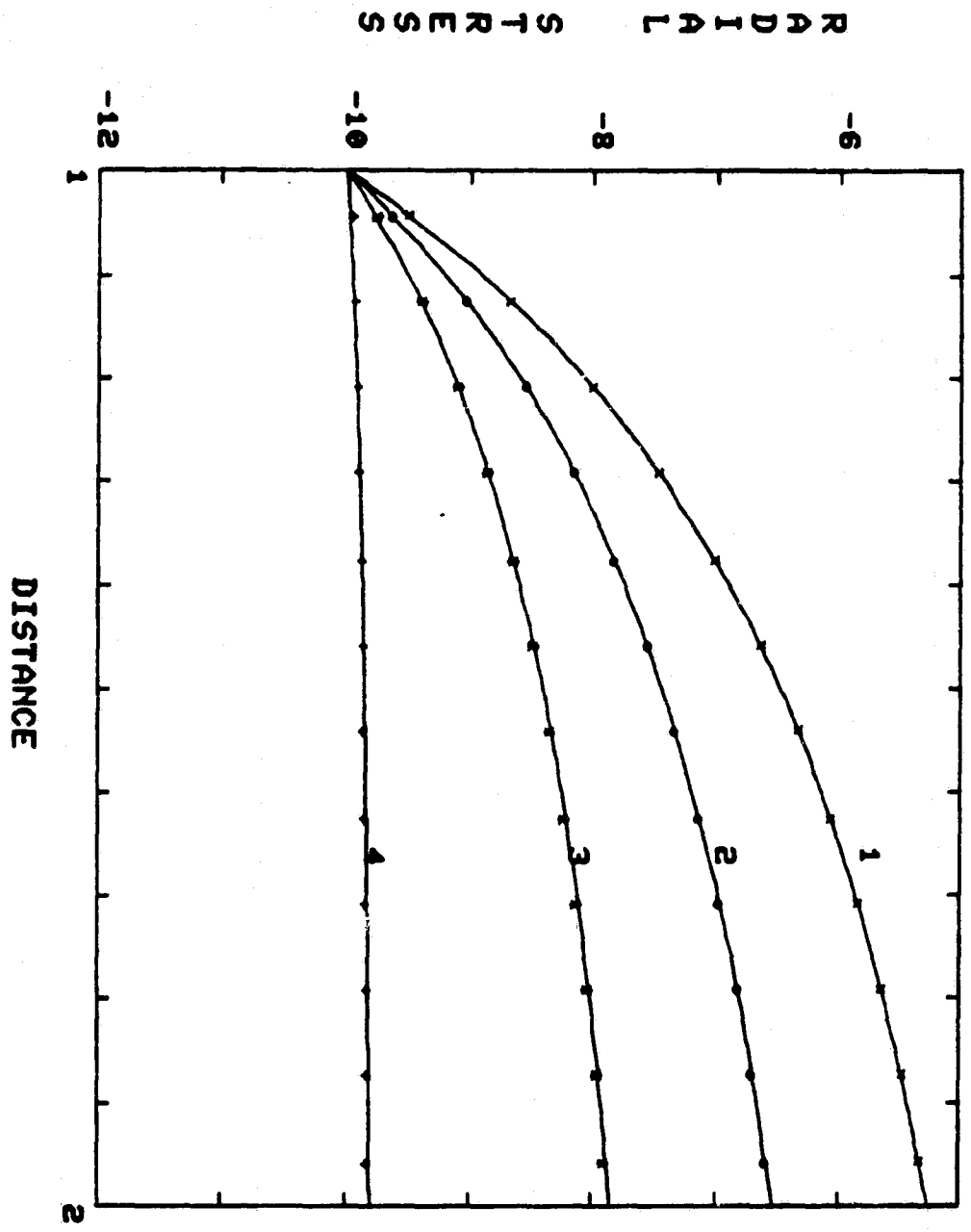

Fig. 2.4.7

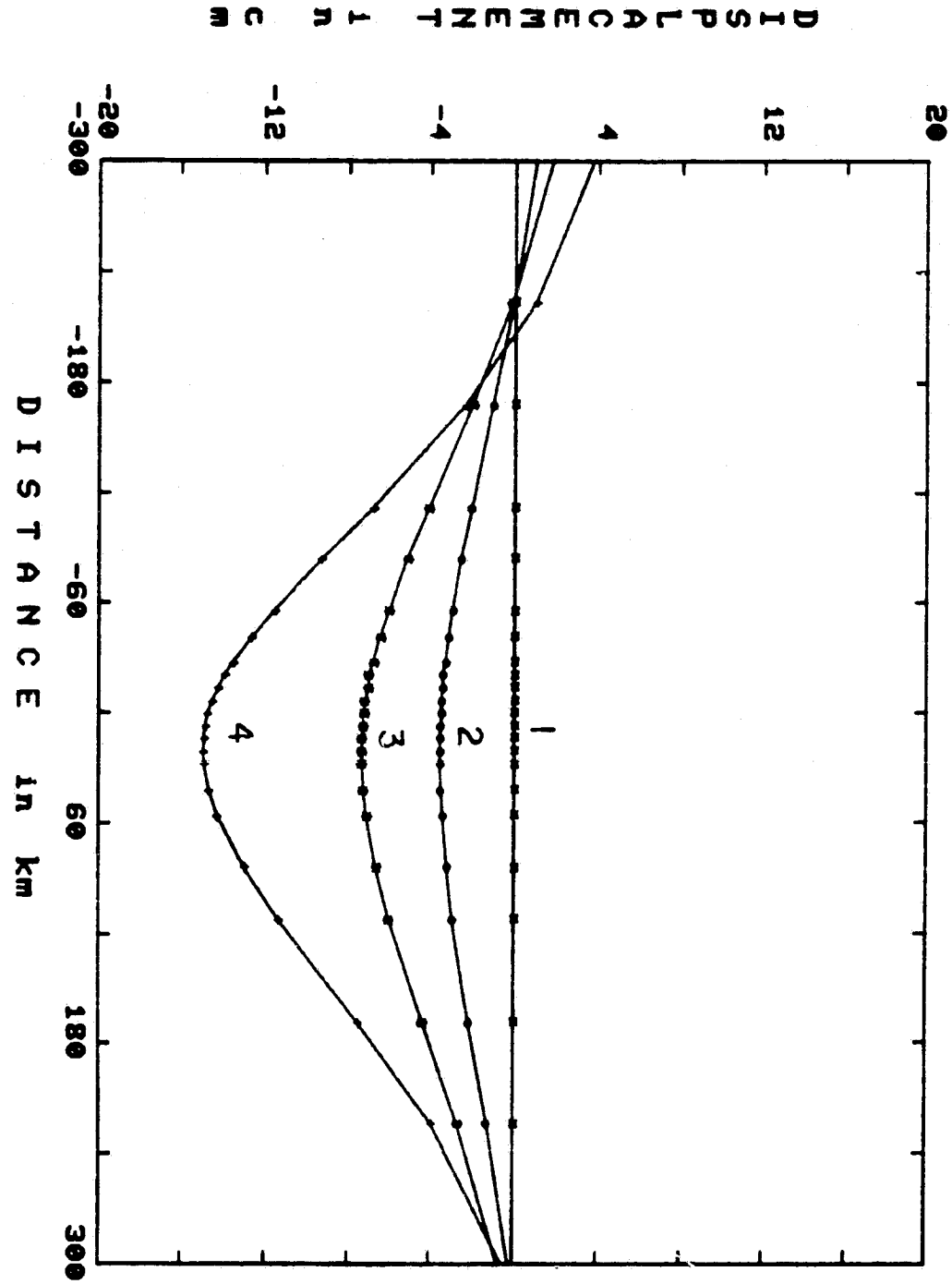
DISPLACEMENT in cm
20
12
4
-4
-12
-20
300
180
60
-60
-180
-300
DISTANCE in km
1
2
3
4

Fig. 2.5.1

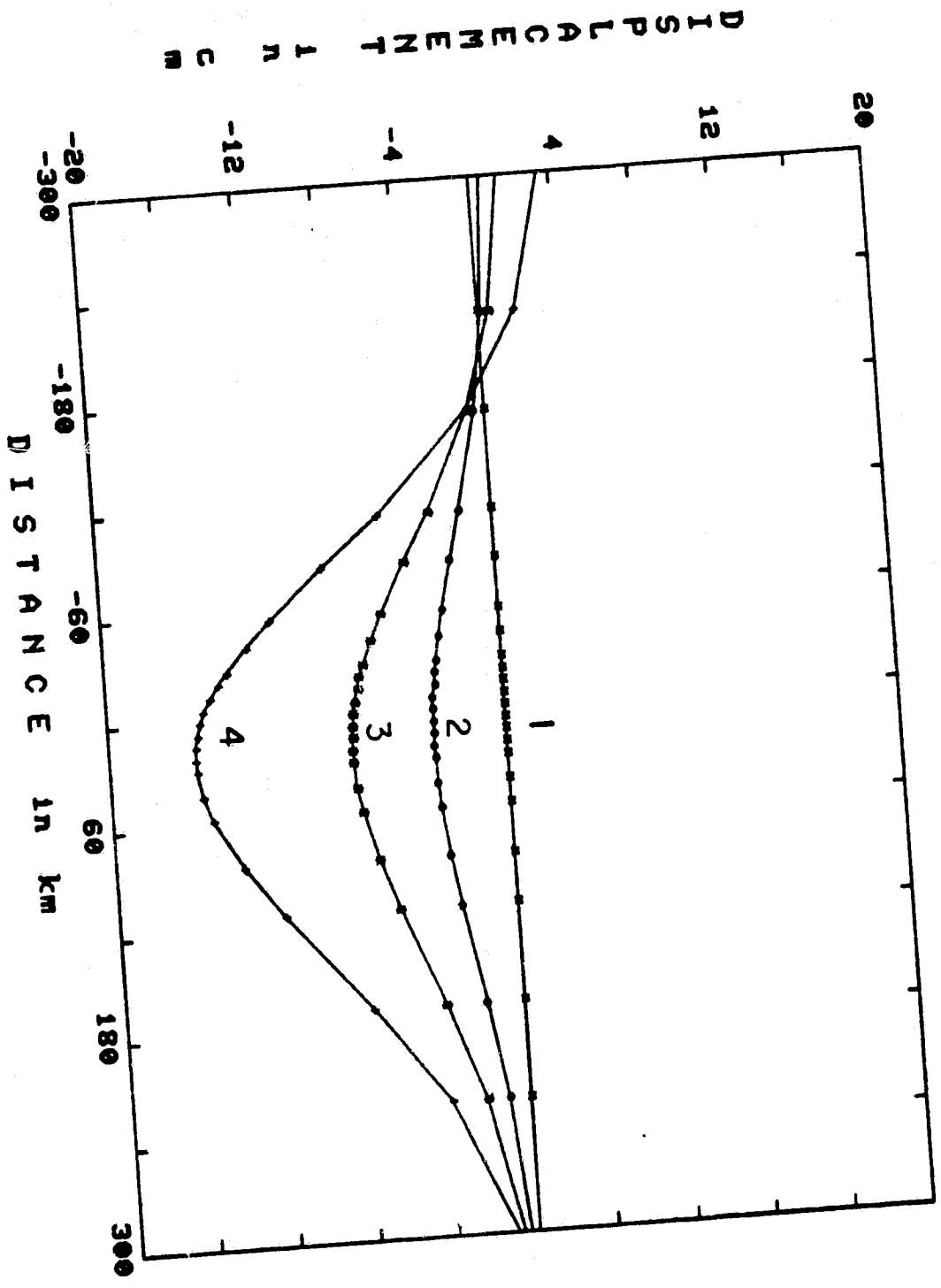
DISPLACEMENT in cm
-20
-12
-4
4
12
20
-300
-180
-60
60
180
300
DISTANCE in km
1
2
3
4

Fig. 2.5.2

CHAPTER 3

TIME DEPENDENT DEFORMATION AND STRESS RELAXATION AFTER STRIKE SLIP EARTHQUAKES

Mai Yang and M. Nafi Toksöz

Department of Earth and Planetary Sciences
Massachusetts Institute of Technology
Cambridge, Massachusetts 02139

1. INTRODUCTION

Great damage has been caused by shallow strike slip earthquakes that occur along plate boundaries in various parts of the world. The mechanism of these earthquakes has long interested seismologists. The study of geodetic measurements of the 1906 San Francisco earthquake led to the formulation of elastic rebound theory (Reid, 1910), and this theory has remained a basic tenet of the earthquake mechanism. The continuous study of accumulation, release and relaxation of stresses near the fault zone has provided a more detailed mechanism of strike slip earthquakes (e.g. Chinnery, 1961; Scholz and Fitch, 1969; Turcotte and Spence, 1974; Savage, 1975; Thatcher, 1975a,b; Budiansky and Amazigo, 1976; Rundle and Jackson, 1977a,b; Savage and Prescott, 1978; Savage, 1979; Thatcher, 1979; Turcotte et al., 1979). Much of the study used geodetic measurements near the fault zone. In particular, static elasticity and dislocation theory have often been used to study the stress and displacement field caused by strike slip earthquakes.

Stress accumulation, release and relaxation are time dependent phenomena. This is evident from geodetic data, and follows from the migration behavior of earthquakes and asthenospheric viscosity. In recent years, there have been intensive geodetic and creep measurements in the San Andreas fault zone, and ultra precise space technology has been applied to geodetic measurements (e.g., Niell et al., 1979;

Smith et al., 1979). Accurate data will be available in the near future on the time dependence of crustal deformation. A detailed, three-dimensional time dependent model may be necessary for the interpretation of such data. On the other hand, earthquake migration phenomenon have been observed along plate boundaries, most noticeably along the North Anatolian fault (e.g. Mogi, 1968; Allen, 1969; Dewey, 1976; Toksöz et al., 1979). Explaining this time dependent phenomenon also requires time dependent models.

We calculated the long term time dependent response of a set of models of strike slip events. The effect of relaxation is isolated in these calculations. Most of the previous attempts to model time dependent tectonic phenomonon after earthquakes used two-dimensional models (e.g., Nur and Mavko, 1974; Bischke, 1974; Smith, 1974; Savage and Prescott, 1978; Thatcher and Rundle, 1979; Melosh and Raefsky, 1979) or simple layer and half space solutions (Rosenman and Singh, 1973a,b; Barker, 1976; Rundle and Jackson, 1977a,b,; Cohen, 1980a,b; Lehner et al., 1979).
Two-dimensional models assume an infinite long fault, and the effects in the region beyond the fault tip cannot be described. However, in this paper we show that there are significant effects in the region beyond the fault tip for strike slip events. Laterally homogeneous models that assume no lateral heterogeneities across the fault zone oversimplify the

near-source problem. Most data indicate the presence of lateral heterogeneities near the fault (e.g. Sass and Lachenbruch 1973, Zandt, 1978).

In this paper, we present time dependent calculations for finite strike-slip faults in laterally heterogeneous media. We use the three-dimensional finite element method to model strike slip events. The forward problem is set up to predict time dependent deformation and stress for years and tens of years following a modelled earthquake. The models are representative earthquakes to show the characteristic time dependent features of strike slip events. The boundaries of inhomogeneities in the models are kept geometrically simple. The model results indicate that geodetic measurements after an event may provide information on rheological properties near the fault zone which are vitally related to earthquake occurrence.

II. MODEL DESCRIPTIONS

Fault Models

We present the computation for two classes of models, one for a great earthquake, and the other for a moderate size earthquake. Due to uncertainty in the viscosity structure, several sets of viscosity values for the same fault model are used to show a range of possible results. We are interested in the general behavior of relaxation following the model earthquake. No attempt is made to model a specific region in detail. However, the fault displacement and

dimension for great earthquake models (G1, G2 and G3) are comparable to those of the 1906 San Francisco earthquake or the 1939 North Anatolian earthquake. The dimension for fault models M1 and M2 are appropriate for a magnitude 5.5-6.0 earthquake such as the Coyote Lake earthquake of 1979 (M = 5.7) (Lee et al. 1979).

We model the strike slip earthquake as a sudden slip on two sides of a rectangular vertical fault surface. The offset values are prescribed, and the subsequent displacements and relaxation are computed (details given in the section on computational scheme and Chapter 2). We assume that the slip on fault stops after the step function slip. This probably will happen if deviatoric tectonic stresses are relieved near the fault zone and friction again takes over, and the region deforms in a coherent manner. However, there may be cases where this condition is violated. Slow afterslip is sometimes observed after an earthquake (e.g., Burford, 1972; Bucknam et al., 1977; Coppersmith et al., 1979). If afterslip does not last long relative to relaxation time (years) the long term effect will be similar to a step function.

The model region for models G1, G2 and G3 is 2740 km long, 2320 km wide and 700 km deep. The fault is a rectangular region 350 km long and extends vertically from 0 to 40 km depth. The relative fault offset is 5 meters strike slip, except that near the edges of the fault area

it tapers off. The offset tapers off linearly from 5 meters at 20 km depth to zero at 40 km depth, and it tapers off linearly to zero at 35 km from the tips along the strike direction as shown in Figure 1.

The model region for models M1 and M2 is 196 km long, 169 km wide and 80 km deep. The fault is a vertical rectangular region 20 km long and 12 km deep. The model earthquake has no surface rupture. It has relative offset of 30 cm from 3 to 9 km depth, and the offset tapers off linearly to zero from 9 to 12 km depth and 3 to 0 km depth. It also tapers off linearly to zero at 2.5 km from tips along the strike direction (Figure 2).

Material Properties

There is controversy over the laws governing the creep behavior of earth materials (Weertman, 1978). Linear Newtonian behavior of the mantle fits the post-glacial rebound data (e.g., Cathles, 1975; Peltier and Andrews, 1976), but laboratory rock mechanics experiments exhibit non-linear creep behavior. For calculation of perturbation caused by the earthquake, we choose the linear viscoelastic model, simply because visco-elastic materials contain the essential elements of the time dependent relaxation phenomena. Furthermore the assumption of linearity greatly simplifies the physical picture, as we can separate the effect of perturbations caused by the earthquake. We concentrate on the calculation of the relaxation effect following strike-slip events; other effects can be superimposed due to linearity.

The material in the model is assumed to be elastic in bulk and Maxwellian viscoelastic in distortion. The short term elastic constants of earth vary slowly in space (Hadden and Bullen, 1969). On the other hand, the viscosity value changes by orders of magnitude from the lithosphere to asthenosphere (Cathles, 1975; Peltier and Andrews, 1976). The contribution to viscoelastic relaxation due to changes in elastic parameters is therefore relatively unimportant. In order that we do not unnecessarily complicate the physical picture, we assume all the models have the same instantaneous response (elastic) properties of bulk modulus 1.3×10^{12} dyne/cm^2 and Poisson's ratio 0.25, which are about the average values for crust and upper mantle from seismic studies. The different model results will be due to different viscosity structures in the models.

The viscosity of the earth is not a well constrained quantity, especially near a tectonically active zone such as a transform fault. The lithosphere in general can withstand deviatoric stresses for a million years or longer. The thickness of the elastic lithosphere in continental regions is probably greater than 50 km. The asthenosphere has a viscosity value orders of magnitude smaller than the lithosphere. From analyses of post-glacial rebound data, the low viscosity layer beneath the lithosphere is probably on the order of 10^{20} poise (Cathles, 1975; Peltier and

Andrews, 1976). This magnitude of viscosity implies that deviatoric stresses cannot be sustained there for a time scale larger than several years to decades.

Near an active transform fault, where only shallow earthquakes are observed suggests lateral heterogeneities may exist. For example, in the San Andreas fault zone earthquakes are usually shallower than 10 to 15 km, indicating that stress below this depth is being relieved continuously below this depth. This thickness of the "seismo-genic" layer is simply too small compared to the generally accepted lithospheric thickness, suggesting the existence of low viscosity zone, plastic yield or slow slip at depth below. Lachenbruch and Sass (1973, 1979) found that the San Andreas fault system is contained in a broad zone of high heat flow anomaly. They concluded that the thin seismo-genic layer is more brittle than the layer beneath it, implying the possibility of a shallow low viscosity zone there. Theoretically, the shearing motion should also cause temperature and viscosity structure to vary laterally (Yuan et al., 1978). Three dimensional inhomogeneities in elastic parameters are also observed in tectonically active regions (Zandt, 1978) although it is difficult to estimate viscosity structures from elastic parameters.

There is little information on the viscosity of a

fault zone. Budiansky and Amazigo (1976) estimate the "effective viscosity" of lithosphere to be 10^{21} poise in California. Nur and Mavko (1974) and Smith (1974) analyzed the vertical deformation of the 1946 Nankaido earthquake and conclude the viscosity value below the elastic lithosphere is on the order of 10^{19} to 10^{20} poise. Thatcher and Rundle (1979) found that a viscosity value of about 5×10^{20} poise in the asthenosphere beneath Japan fits geodetic measurements. It is plausible that the shearing motion and higher temperature in the fault zone make the viscosity lower than in its adjacent regions. We will carry out calculations for a range of viscosity values.

Great earthquakes model G1 is the control model; a layered structure is assumed. The lithosphere extends to 80 km depth; it is given a viscosity value of 10^{25} poise from 0 to 40 km, and 10^{24} poise from 40 to 80 km depth. A low viscosity layer extends from 80 to 180 km depth, with a viscosity value of 10^{20} poise. Below 180 km, the mantle viscosity is assumed to be 10^{22} poise as shown in Figure 3.

More realistic models incorporate lateral heterogeneities across the fault. If a shallow low viscosity zone exists beneath a fault, we may assume it extends to the bottom of the seismogenic layer; however, its width is not known. If the width is much larger than the fault length, the

effects of such a zone will be similar to that of a low viscosity layer. We use rather wide low viscosity zones. A very narrow low viscosity zone may produce different results, probably similar to that of an elastic layer. In model G2, a low viscosity zone rising to 20 km below the surface and extending 140 km on each side of the fault is assumed. The viscosity value is assumed to be 10^{20} poise, the same as in the low viscosity asthenosphere extending from 80 to 180 km depth. Calculations show that differences in resulting time dependent deformation and stress relaxation between model G1 and G2 are significant. Model G3 has properties intermediate between model 1 and 2, with the low viscosity layer extending to 40 km depth. For moderate earthquake models M1 and M2 we assume that under the fault the low viscosity zone extends to shallower depths. Far away from the fault, the lithosphere is 80 km thick. Both models assume that from 12 km to 46 km depth there is a low viscosity zone 40 km wide on each side of the fault; from 46 km to 80 km depth, it is 70 km wide as shown in Figure 4. Fast relaxation time is assumed for model M1 (viscosity 10^{19} poise) to establish the maximum possible effect of relaxation. Model M2 assumes the low viscosity value to be 10^{20} poise.

Computational Scheme

We use three-dimensional time dependent finite element models to calculate time dependent motions following a modeled earthquake. We combine the frontal solution technique (Irons, 1970) to the unified time stepping approach (Zienkiewicz and Cormeau, 1974) for a versatile and efficient solution scheme. The calculation scheme is described in Chapter 2.

Due to symmetry of a vertical strike slip earthquake, only a quarter of the region is needed to be modelled in the numerical scheme. All the models in this study use 720 elements and 2982 degrees of freedom. The grid structure of the moderate earthquake models is a scaled grid of great earthquake models. Figure 5 is the top view of the grid structure of both classes of models. The three-dimensonal model is made up of seven identical grid surfaces. The element is in 8 node, 24 degrees of freedom hexahedron with 8 gaussian integration stations. Elements with 27 integration stations have been used on some models. The results are nearly identical with those of 8 integration stations.

Since only a quarter of the region is used in the numerical scheme, the boundary conditions must simulate those of the complete strike slip fault. The fault area is contained in the boundary plane $x = 0$ (Figure 5). The

boundary plane y = 0 is a symmetry surface bisecting the physical fault model. On plane y = 0, the displacement in x direction is set to zero; on plane x = 0, on the fault surface the y displacement is set to half the fault offset value and on the rest of the x = o plane the y displacements are set to zero. The other external boundaries are far away from the fault zone. The effect caused by the event decreases with distance from the fault. We choose a region large enough such that boundaries far away from fault zone have little influence on the behavior of the region we are interested in. We used rigid and free boundary conditions on the sides far away from the fault zone. We present results only for those elements where resulting stresses differ by less than a few per cent for these two extreme cases. The lower boundary of the region is prescribed to be rigid. We used 12 time steps for models G1, G2 and G3 to calculate time dependent values for up to 49 years after the event. For thin lithosphere and fast relaxing models M1 and M2, we used 14 time steps for 9.5 years after the event.

III. Model Results

Great Earthquake Models

The results of time dependent deformation and stress from different models are presented and compared in this section. Model G1 is the control model with a laterally

homogeneous layered structure. The horizontal displacements on free surface at selected locations for model G1 are shown in Figure 6a. The four figures give the horizontal displacements at time = 0, 9.5, 25 and 49 years after event, respectively. The initial (time = 0) pattern is typical of a strike slip fault in elastic media (cf. Chinnery, 1961). Afterwards the displacement increases with time although the displacement rate decreases. The initial displacements decrease very fast with distance from the fault. The relaxation process spreads the deformation outward from the fault zone.

In contrast with model G1, model G2 has a low viscosity zone extending to shallow depth near fault. The horizontal displacements on the free surface at selected locations for model G2 are given in Figure 6b. The instantaneous response is the same as model G1, since they have the same elastic parameters. However, the magnitude of time dependent displacement is much larger and concentrated near the fault zone (where the low viscosity zone is shallow). The time dependent effects can be seen more clearly in Figures 7a and 7b, where the displacements along the line perpendicular to the center of fault (x axis in Figure 1) are shown. Near the fault zone the time dependent deformation is in general small compared to the instantaneous response for model G1, while the shallow low viscosity zone in model G2 significantly increases

the magnitude of time dependent displacement.

The contours of vertical displacement on free surface immediately after the event are shown in Figure 8a. Also shown (Fig. 8b) are the shear stress contours. The results are what we expect from a shallow strike slip event. In the vertical displacement figure there is subsidence in a broad area in the upper right quadrant, except near the fault tip. Our grid resolution cannot resolve the very small uplift zone near the fault tip, but the overall pattern is very similar to that of the analytic half space solution of Chinnery (1961). Subsequent time dependences show characteristic differences between layered and lateral inhomogeneous models. The contours of vertical displacement change after the event (total displacement minus instantaneous response) at 5 and 25 years after the event for model G1 and are given in Figures 9a and 9b. The results of model G2 are given in Figures 10a and 10b. On the upper right quadrant, for model G1 the time dependent vertical movement is continuous subsidence near the fault zone, and uplift away from it. This result is expected provided that the horizontal displacement is spreading out from the near fault region. The magnitude of this vertical movement is on the order of several centimeters. In contrast, the results for model G2 is continuous uplift throughout the upper right quadrant. The physical reason

for this difference can be seen from the horizontal displacement plots (Figures 6a and 6b). In the upper right quadrant in the figure, the "flow pattern" of the strike slip event is such that material enters the near fault zone parallel to the strike direction, but leaves the fault zone in the direction 45 degrees from the strike direction at large distances. The low viscosity channel near the fault zone makes it easier for material to enter the fault zone; the thicker lithosphere beyond the low viscosity channel forms a barrier for material to fan out, thus material piles up near the fault zone and a bulge results. The uplift in model G2 is about 15 cm in 25 years. This effect is measureable by geodetic means, and could serve as a tool for investigating the viscosity structure of the fault zone.

Another interesting phenomenon is the time dependent character of the stress relaxation for these two different models. The instantaneous perturbation of horizontal shear stress component σ_{xy} at 10 km depth caused by the strike slip event is shown in Figure 8b, and σ_{xy} at 25 years later is shown in Figures 11a and 11b for models G1 and G2 respectively. Before an event, due to relative plate motion the stress component σ_{xy} should be positive near the fault zone for a left lateral strike slip fault as in the models. The earthquake relieves the prestress along the fault, but reinforces the prestress in front of the fault

tip. More detailed time dependency can be seen in Figures 12a and 12b, where σ_{xy} vs. time at selected positions is shown. It can be seen that along the side of the fault, σ_{xy} is negative, implying the prestress is relieved. However, viscoelastic relaxation in general accelerates the stress recovery. In front of the fault tip, σ_{xy} is positive, and the prestress is reinforced. This result of reinforcement of prestress has been considered to be the cause of secondary faulting (Chinnery, 1966) or creep and aftershocks in front of fault tip (Scholz et al., 1969). The earthquake may in time trigger subsequent events along the same fault. However, for the uniform thick lithosphere model G1, the time dependent stress is small compared to the instantaneous response, in this case subsequent earthquakes should happen immediately after the event rather than being delayed for years. Aftershocks located at the end of the main shock fit this picture, however, the short time delay of the aftershock is most likely due to local inhomogeneities, time dependent friction and creep type relaxation rather than large scale mantle relaxation (Dieterich, 1972; Mikumo and Miyatake, 1979, Yamashita, 1979). On the other hand, for the laterally inhomogeneous model G2, a significant portion of the perturbing stress in front of the fault tip is accumulated years after the event. The perturbing stress levels off a few decades after the event. This accelerated stress accumulation in front of the region of a strike slip

fault makes the chance of earthquake happening greater during the several decades after the event. Triggered events can then happen years after the triggering event, as long as the stress diffusion is reinforcing the prestress. The earthquake sequence after the 1939 North Anatolian event (Toksöz et al., 1979) is consistent with this stress diffusion mechanism. It is a general result that the relaxation effect near surface becomes more important as the thickness of the lithosphere becomes thinner (Rundle and Jackson 1977a,b; Savage and Prescott 1978; Cohen, 1980a,b; Lehner et al., 1979). Rundle and Jackson (1977b) and Lehner et al. (1979) also pointed out that stress in front of the fault tip increases with time after a strike slip event for layered models.

It has been reported (Thatcher 1975a) that the strain accumulation accelerates near the fault after the 1906 San Francisco event, the average strain rate parallel to the fault was about 2.5×10^{-6} per year for about 25 years after the event, and 0.6×10^{-6} per year afterwards. For model G1, the strain at a point 18 km away from the fault accumulates at an average rate of about 0.1×10^{-6} per year, much less than the observed value. This simple model does not explain the 1906 data. For the laterally inhomogeneous model G2, the average strain rate at 18 km away from the fault is about 1.0×10^{-6} per year, which is of the same order of magnitude as the observed values of the 1906 San Francisco

earthquake. The model is not a model of the San Francisco earthquake in detail, however, the results indicate that if the low viscosity extends to shallow depth under the fault, viscoelastic relaxation may contribute significantly to the time dependent deformation.

Model G3 has the low viscosity channel to 40 km depth instead of 20 km in model G2. The results are intermediate between G1 and G2. Figure 13 compares the contours of vertical displacement change at 25 years after the event for model G2 and G3. The result for model G3 in the upper right quadrant is a broad region of uplift, and a small region of slight subsidence near the fault tip. This indicates that time dependent vertical displacement is sensitive to the viscosity structure. Figure 14 compares the shear stress σ_{xy} at selected positions vs. time for models G2 and G3. There is accelerated strain rate a few decades after the event for model G3, but the magnitude is smaller than that of model G2.

Moderate Size Strike Slip Earthquake Models

Models M_1 and M_2 are models of moderate size earthquakes with buried faults. Model M1 is the fast relaxation model, with viscosity 10^{19} poise in the low viscosity zone, while model M_2 uses viscosity 10^{20} poise instead. The horizontal displacements at selected locations on free surface are

shown in Figures 15a and 15b. The results are generally a gradual increase in magnitude of the displacements. Figure 16 shows the instantaneous response of vertical deformation on free surface. In the upper right quadrant, there is a relatively broad region of uplift near the fault, and subsidence far away. This is expected for a fault with large fault depth to length ratio (0.6 in this case). The vertical deformation changes at 9.5 years later are given in Figures 17a and 17b. For both models M1 and M2, in the upper right quadrant, the vertical deformation is subsidence near the fault zone and uplift far away from the fault, similar to that of the layered medium case. This is probably because the width of the low viscosity channel is relatively large compared to the earthquake fault dimension. The magnitude of time dependent vertical deformation is small, generally less than 1 cm.

Figure 18 gives the time dependence of shear stress σ_{xy} at selected locations at 7.5 km depth. We again see the stress is relieved along the fault, and reinforced in front of the fault. The time dependence is quite different for the two models: significant changes are completed within 5 years after the event for model M1, while the relaxation is linear in model M2 for the first decades. Though the magnitudes of quantities involved in those moderate earthquakes are of marginal use with the

precision of present day available geodetic data, in the future when more precise and frequent geodetic measurements are available, the models may be used to study the detailed structure near a fault zone.

IV. Discussion

In this study, we calculated the time-dependent stress relaxation and deformation for large and moderate size earthquakes using different models. To compare these to observations we look at space-time migration of seismicity and to geodetic data. Migration of seismicity along plate boundaries has been observed in South America (Kelleher, 1972), the West Pacific (Mogi, 1968), Alaska-Aleutian (Kelleher, 1970), the San Andreas Fault zone (e.g. Wood and Allen, 1973; Lee et al., 1979), and the North Anatolian fault zone (e.g. Richter, 1958; Mogi, 1968; Savage, 1971; Dewey, 1976; Toksöz et al., 1979). In the case of the North Anatolian faults there was a relatively quiescent period in seismicity prior to 1939. A bi-directional trend of seismic migration followed the great earthquake of 1939 (Toksöz et al., 1979). Savage (1971) proposed a dislocation wave theory to explain the earthquake migration phenomenon. The occurrence of a sequence of events in rapid succession can also be due to an accelerated stress accumulation process. In all the model results in section III, there is an accelerated stress accumulation process in the region in front of the fault tip. The

magnitude of this accelerated stress accumulation is significant if a low viscosity zone under the fault extends to a depth of 40 km or less below the surface. It is important to clarify that other processes (such as change of material properties due to stress level change, slip at depth) may contribute to accelerated strain accumulation and earthquake migration. These have not been investigated in detail.

A possible scenario for the occurrence of a sequence of earthquake follows. The initial earthquake happens when stress accumulation exceeds the strength of the fault zone. After this event, the stress accumulation accelerates in the region in front of the fault tip. The next earthquake happens when the combination of diffused stress and initial stress exceeds the strength; in turn this "triggered" earthquake triggers the next event in an adjacent region. The process continues until the stress along the whole fault zone is relieved. This episode is then followed by a slow stress accumulation stage and relative quiescence in seismicity. Aftershocks that immediately follow the earthquake are probably due to local stress adjustments. Creep resulting from stress changes at the immediate vicinity of the source may result in relatively rapid stress adjustments in the source area. Migration of earthquakes in time may be related to viscoelastic

relaxation and stress diffusion. However, it is not possible at this time to test this scenario against other possibilities.

Time-dependent horizontal and vertical motions after a strike slip event strongly depend on the viscosities under and near the fault zone. Although horizontal displacements are much larger than vertical displacement, in this study we found that the time dependent behavior of the vertical displacement is very sensitive to lateral heterogeneities of viscosity distribution. The bulge or subsidence formed after a great earthquake is of measureable magnitude. Thus levelling, in addition to horizontal geodetic measurements, after a great strike-slip earthquake may reveal the structure near the fault zone.

In all the models in this study, we have concentrated on the relaxation effects after a strike slip event. Some possible effects during an earthquake cycle are not explicitly modeled. The slow strain accumulation by tectonic stress and possible deep slip are not included in the finite element calculation. However, since linear material is assumed, the effects can be superimposed upon the relaxation process. If the recurrence time of the earthquake is on the order of hundred years and relaxation time of the asthenosphere is on the order of several years, then relaxation after the earthquake is a relatively fast process compared with

strain accumulation. If we take the state just before the earthquake as the reference state, the deformation and stress pattern should not be much influenced by the slow strain accumulation from the tectonic process.

Deep aseismic slip below the seismo-genic layer is suspected of playing an important role in earthquake mechanism (e.g. Thatcher, 1975a,b; Rundle and Jackson, 1977b; Savage and Prescott, 1978, Turcotte et al., 1979). Several studies have found that it is difficult to distinguish the effects of deep aseismic slip and viscoelastic relaxation from geodetic measurements alone (Barker, 1976; Rundle and Jackson, 1977a,b; Savage and Prescott, 1978). This argument was based on calculations using laterally homogeneous layered models and comparisons of the surface deformation caused by viscoelastic relaxation and a given dislocation at depth. As pointed out by Savage and Prescott (1978), there are inherent difficulties in using a simple layered model to compare these results, because in such cases a distribution of slip at depth can always duplicate the viscoelastic result. This inherent difficulty may not arise if the symmetry is broken by three dimensional inhomogeneity; in such cases the images dislocation may not lie on the fault surface. The relaxation is more intensive near a low viscosity zone, as we have shown in section III. Although present day available geodetic data are not constraining, geodetic measurements in the future could resolve this question.

In conclusion, we have implemented a versatile scheme to model the time dependent behavior after earthquakes. Non-uniform fault slip and three dimensional heterogeneities can be included in this scheme. The model results predict a stress diffusion phenomenon in front of fault tip after a strike slip event: if low viscosity extends to shallow depth near the fault zone, the shear stress in front of the fault tip will increase significantly with time. The time dependent deformation on free surface is more concentrated near the fault zone in that case than it is in the case of a laterally homogeneous layered structure. The time dependent behavior of vertical displacement near the fault may be completely altered by the presence of lateral inhomogeneities.

Figure Captions

Fig. 1. Fault for models G1, G2, and G3.

(a) Schematic diagrams of fault, double hatched area has maximum fault slip, single hatched area has tapered fault slip.

(b) Fault slip along strike direction (Y direction).

(c) Fault slip vs. depth (Z direction).

Fig. 2. Fault for models M1 and M2

(a) Schematic diagram of fault, double hatched area has maximum fault slip, single hatched area has tapered fault slip.

(b) Fault slip along strike direction (Y direction).

(c) Fault slip vs. depth (Z direction).

Fig. 3. Sectional views of viscosity distribution for models (a) G1, (b) G2, (c) G3. Numbers with exponent are viscosity in poise.

Fig. 4. Sectional view of viscosity distribution for model M1. Model M2 has the same structure except that the viscosity is 10^{20} poise in low viscosity zone.

Fig. 5. Top view of the finite element grid. The three dimensional model is made of seven identical plane grids.

Fig. 6. (a) Horizontal displacements on free surface due to strike slip event in model G1 at 0, 9.5, 25 and 49 years after the event. The location of the fault is indicated by a thick line segment and sense of motion is indicated by a pair of arrows.

Dots are the locations where displacements are calculated. Displacement is indicated by a line segment from the dot. A scale for the displacement (100 cm) and a scale for the map (400 km) are also shown in the figure.

(b) The same plot for model G2.

Fig. 7. (a) Horizontal displacement vs. time along the line perpendicular to the center of fault (x axis) on free surface for model G1. The distance from the center of the fault for points 1, 2, 3, 4, 5, 6 and 7 are 35, 70, 105, 140, 210 and 280 km. Schematic diagram of the locations are shown at the bottom of the graph.

(b) The same plot for model G2.

Fig. 8. (a) Contours of vertical displacement on free surface immediately after event for great earthquake models G1, G2, and G3. Broken lines (negative values) indicate subsidence; solid lines (positive values) indicate uplift. The location of fault is indicated by a thick line segment and a pair of arrows. The numbers near the contours are uplift or subsidence in mm. The tick marks on the frame are at half fault length interval (175 km). The elastic response is the same for model G1, G2, and G3.

(b) Contours of shear stress component σ_{xy} at 10 km depth immediately after the event for models G1, G2, and

G3. The numbers near the contours are stress in bars. Stress concentrations are placed near fault tips from interpolation, the actual grid resolution is 1/10 of the fault length.

Fig. 9. (a) The vertical displacement on free surface at 5 years after the event minus the elastic response for model G1. Numbers are amount of uplift or subsidence in mm. Ticks are at half fault length intervals.

(b) The same plot at 25 years after the event.

Fig. 10. (a) Vertical displacement on free surface at 5 years after the event minus the elastic response for model G2.

(b) The same plot at 25 years after the event.

Fig. 11. (a) Contours of shear stress component σ_{xy} at 10 km depth 25 years after the event for model G1.

(b) Same plot for model G2.

Fig. 12. (a) Shear stress component σ_{xy} vs. time at selected locations for model G1. The locations are at 10 km depth. A schematic diagram indicating the horizontal positions relative to the fault is given to the right of the figure. The distances from the fault center along the strike direction for points 1, 2, 3, 4, 5, 6, 7, 8, and 9 are 18, 53, 88, 123, 193, 228, 263, 307 and 385 km. The distance from the fault perpendicular to the strike direction is 35 km for point 9, 18 km for the rest of the points.

(b) Same plot for model G2.

Fig. 13. (a) Contour of vertical displacement on free surface at 25 years after the event minus the elastic response for model G2 (Identical to figure 10b, included for comparison).

(b) The same plot for model G3.

Fig. 14. (a) Shear stress component σ_{xy} vs. time at selected locations for model G2. The locations are at 10 km depth. A schematic diagram indicating the horizontal positions relative to the fault is given to the right of the graph (identical to figure 12b, included for comparison).

(b) The same plot for model G3.

Fig. 15. (a) Horizontal displacements on free surface due to strike slip event in model M1 at 0, 1, 3 and 9.5 years after the event.

(b) The same plot for model M2.

Fig. 16. Vertical deformation on free surface immediately after the event for models M1 and M2. Ticks are at half fault length interval (10 km). Numbers near the contours are uplift (positive values) or subsidence (negative values) in mm.

Fig. 17. (a) The vertical displacement on free surface at 9.5 years after the event minus the elastic response for model M1. Numbers are uplift or subsidence in mm. Ticks are at half fault length interval (10 km).

(b) The same plot for model M2.

Fig. 18. (a) Shear stress component σ_{xy} vs. time at selected locations for model M1. The locations are at 7.5 km depth. A schematic diagram indicating the horizontal positions relative to the fault is given to the right of the figure. The distance from the fault center along the strike direction for points 1, 2, 3, 4, 5, 6, 7, 8, 9 and 10 is 1.3, 3.8, 6.3, 11.3, 13.8, 16.3, 18.8, 21.9, 27.5 and 33.8 km. The distance from the fault perpendicular to the strike direction is 3.8 km for point 9 and 10, and 1.3 km for the rest of the points.

(b) The same plot for model M2.

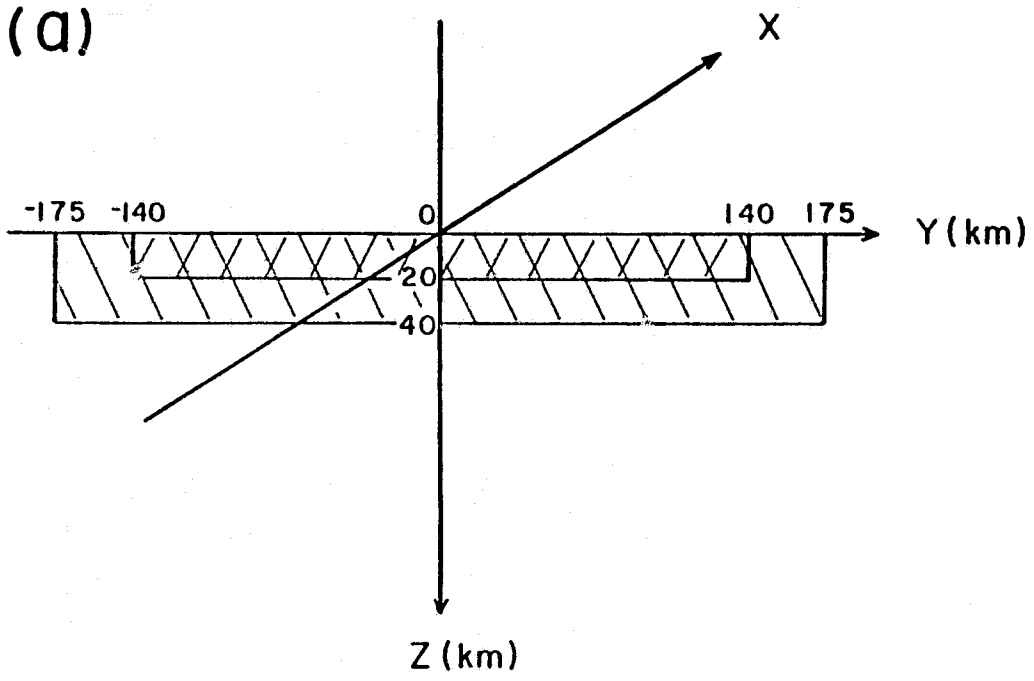
(a)
X
-175
-140
0
140
175
Y (km)
20
40
Z (km)

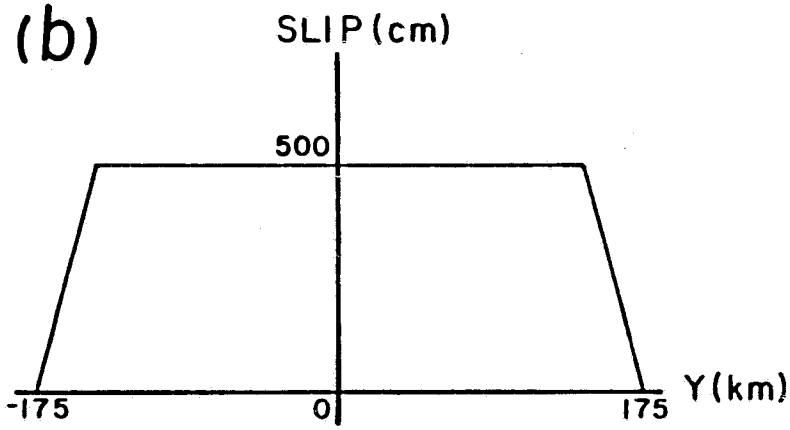
(b)
SLIP (cm)
500
-175
0
175
Y (km)

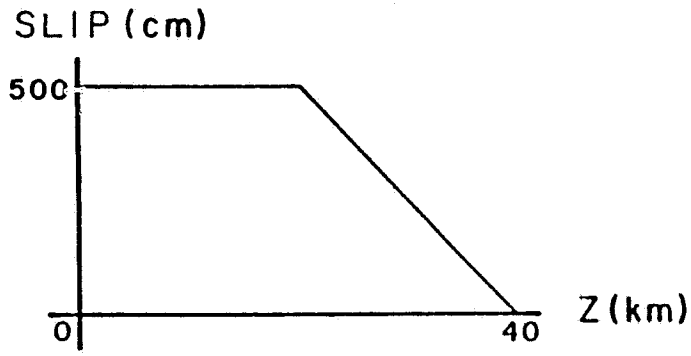
(C)
SLIP (cm)
500
0
40
Z (km)

Fig. 1

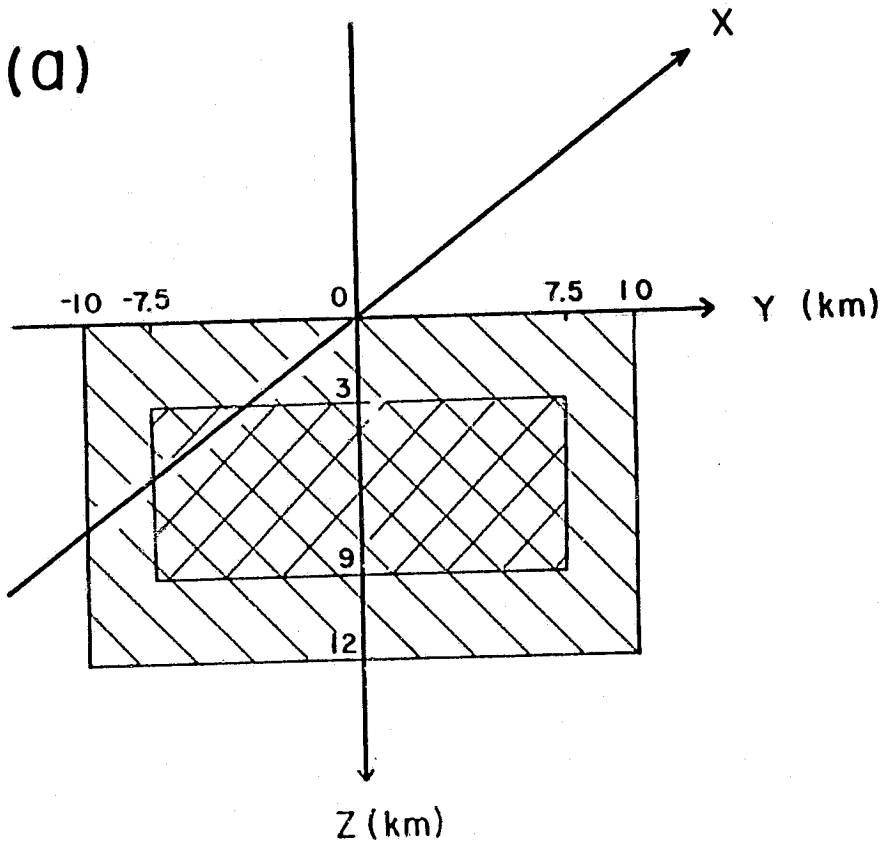
(a)
X
-10
-7.5
0
7.5
10
Y (km)
3
9
12
Z (km)

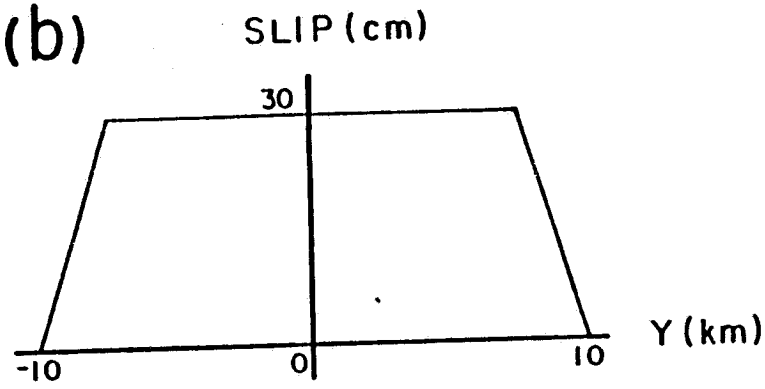
(b)
SLIP (cm)
30
-10
0
10
Y (km)

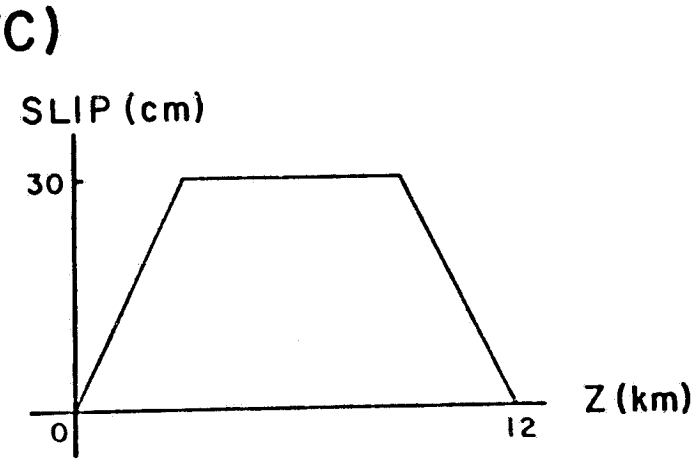
(c)
SLIP (cm)
30
0
12
Z (km)

Fig. 2

(a)

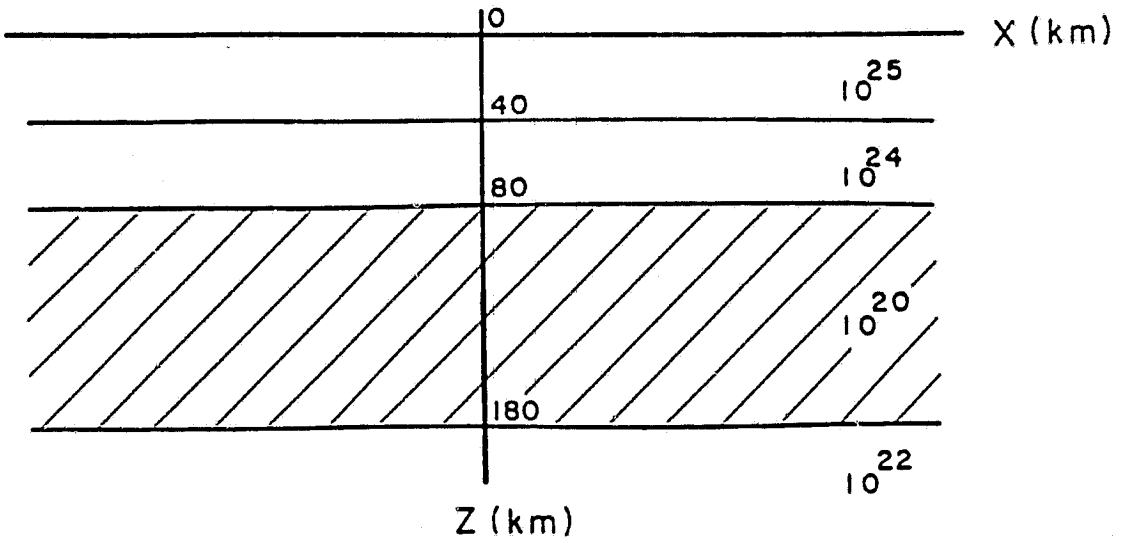
0
X (km)
40
10^{25}
80
10^{24}
10^{20}
180
10^{22}
Z (km)

(b)

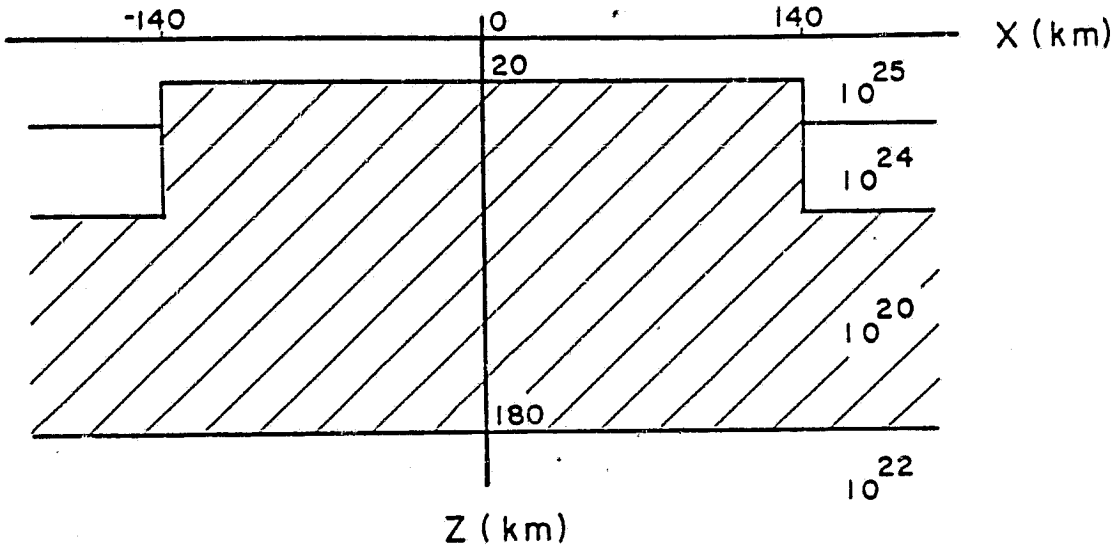
-140
0
140
X (km)
20
10^{25}
10^{24}
10^{20}
180
10^{22}
Z (km)

(c)

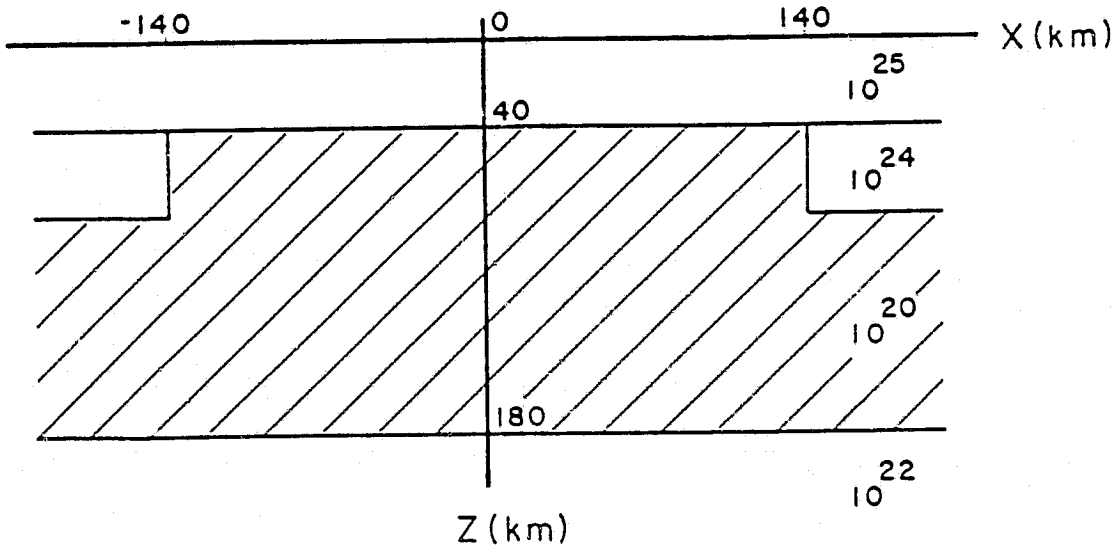
-140
0
140
X (km)
10^{25}
40
10^{24}
10^{20}
180
10^{22}
Z (km)

Fig. 3

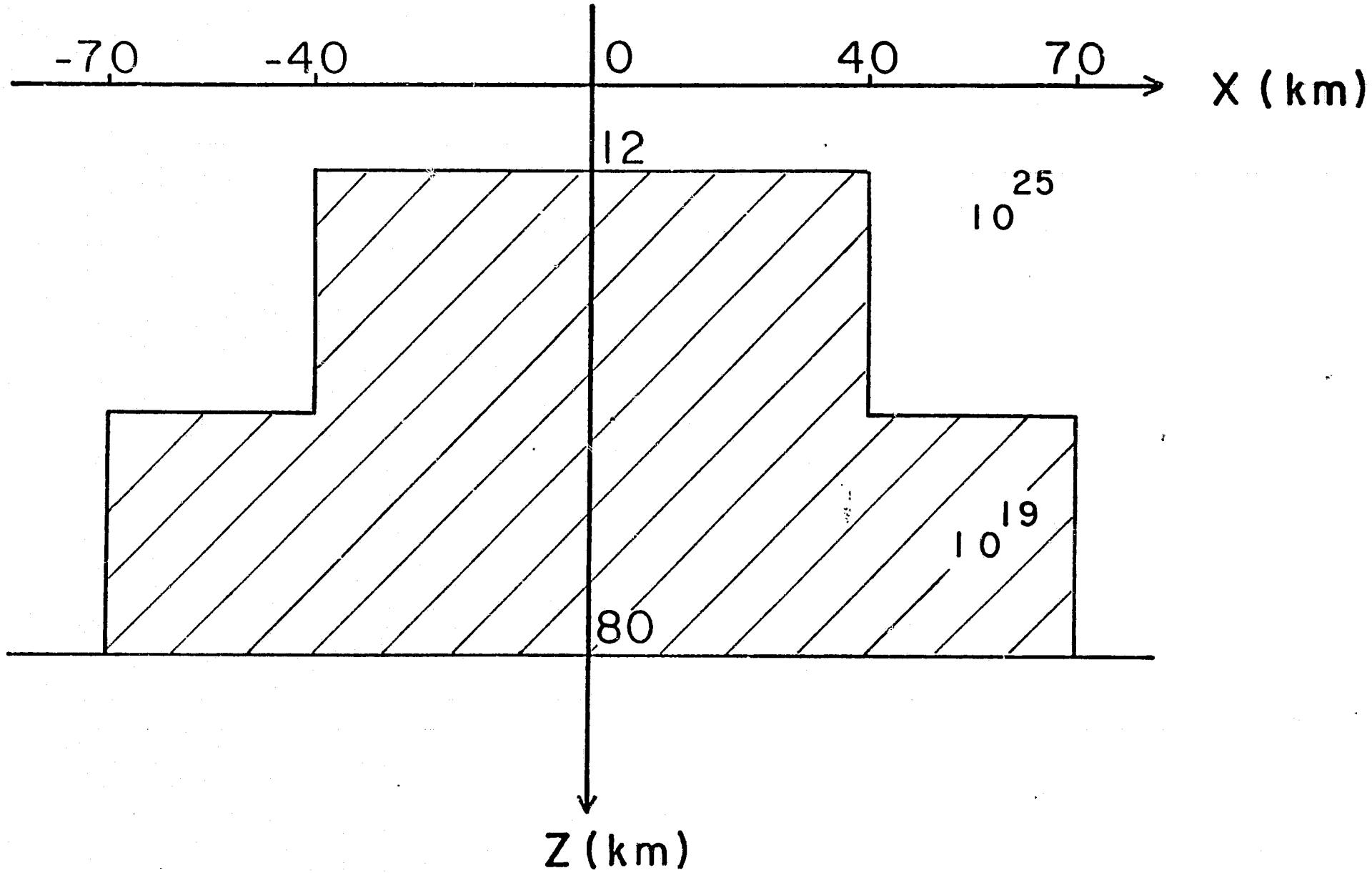

Fig. 4

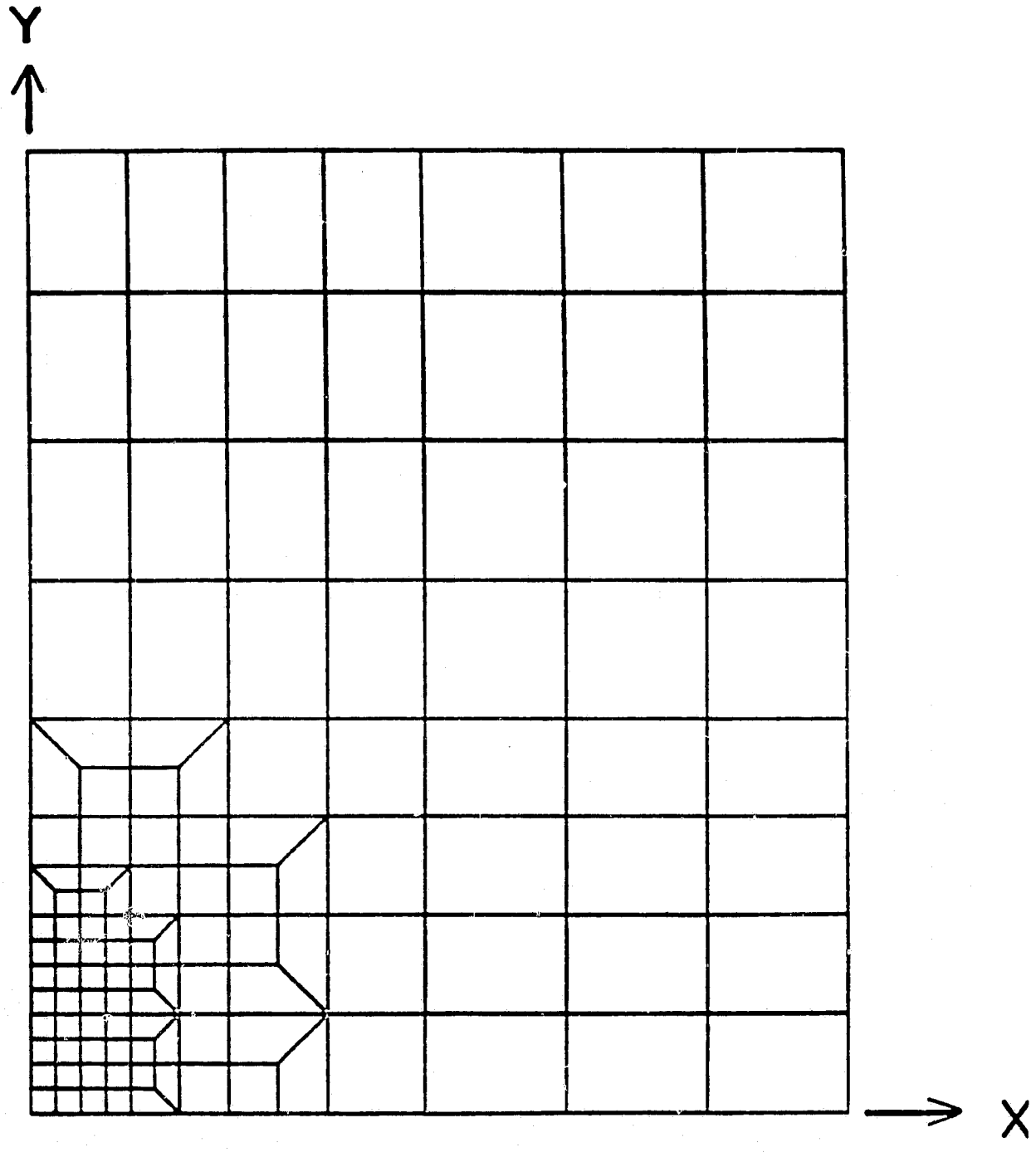

Fig. 5

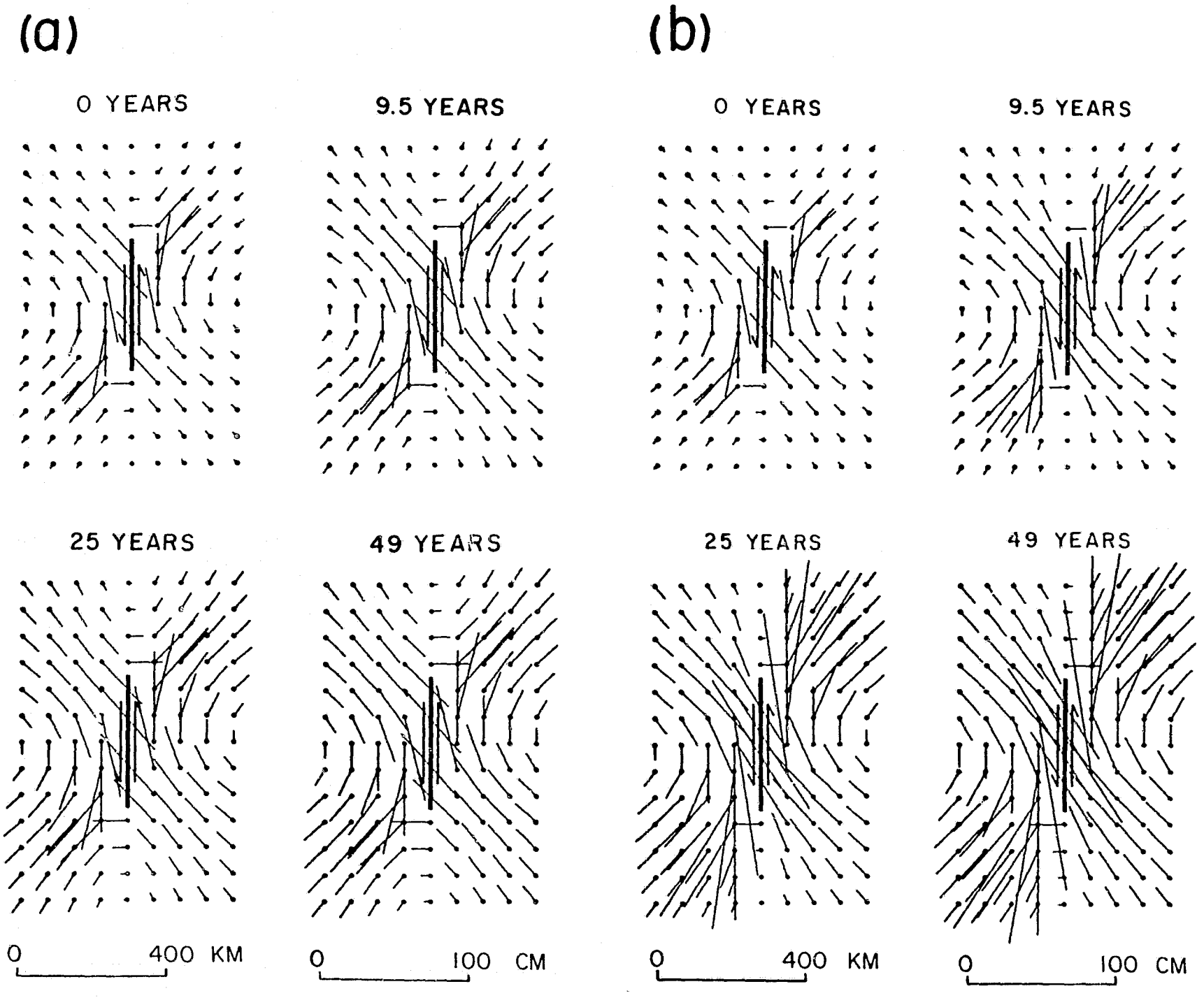
(a)
0 YEARS
9.5 YEARS
25 YEARS
49 YEARS
0
400 KM
0
100 CM
(b)
0 YEARS
9.5 YEARS
25 YEARS
49 YEARS
0
400 KM
0
100 CM

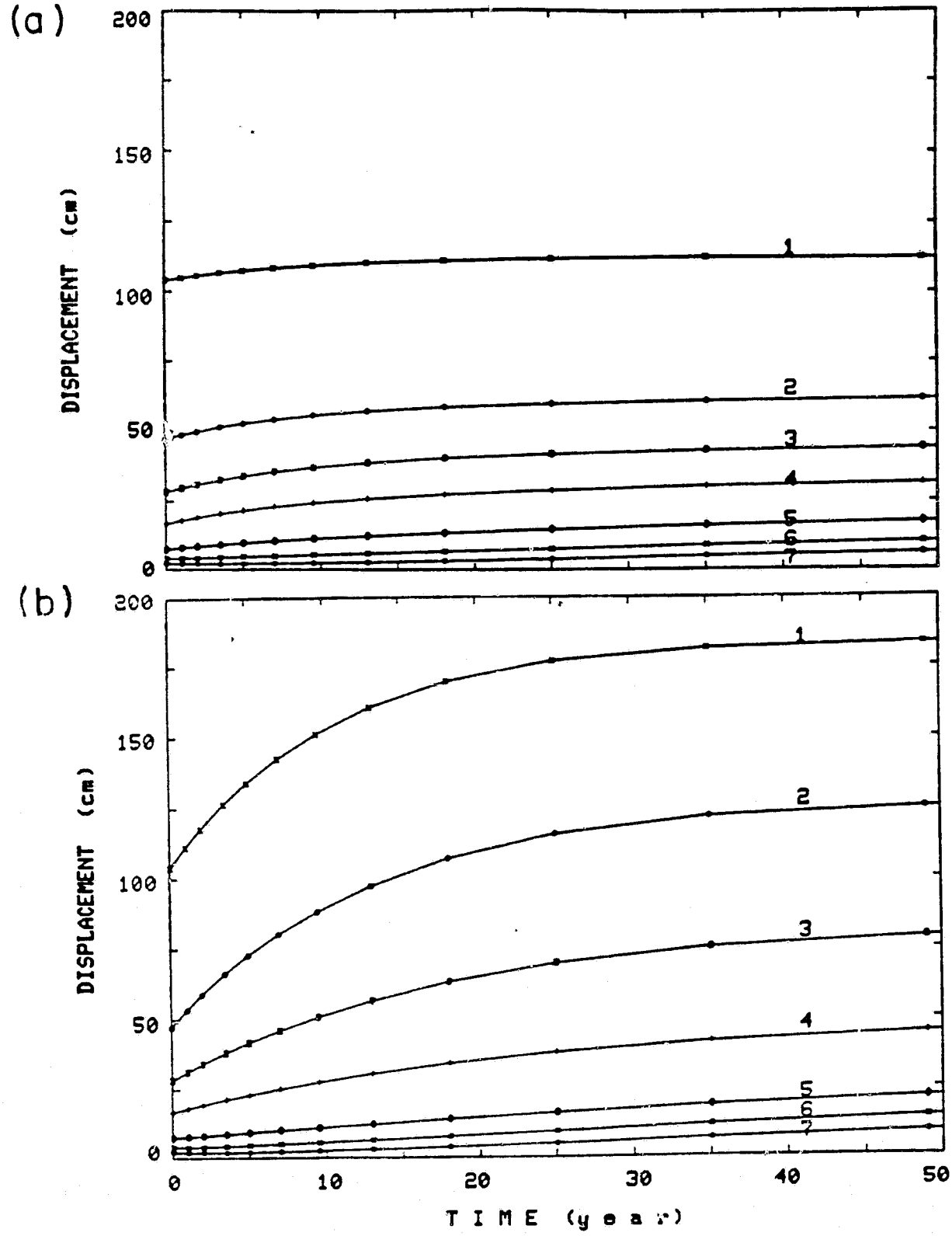
(a)
200
150
100
50
0
DISPLACEMENT (cm)
1
2
3
4
5
6
7
(b)
200
150
100
50
0
DISPLACEMENT (cm)
1
2
3
4
5
6
7
0
10
20
30
40
50
TIME (year)

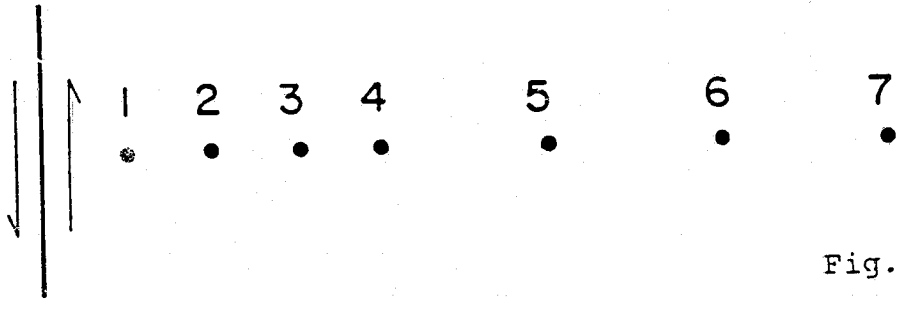
1
2
3
4
5
6
7

Fig. 7

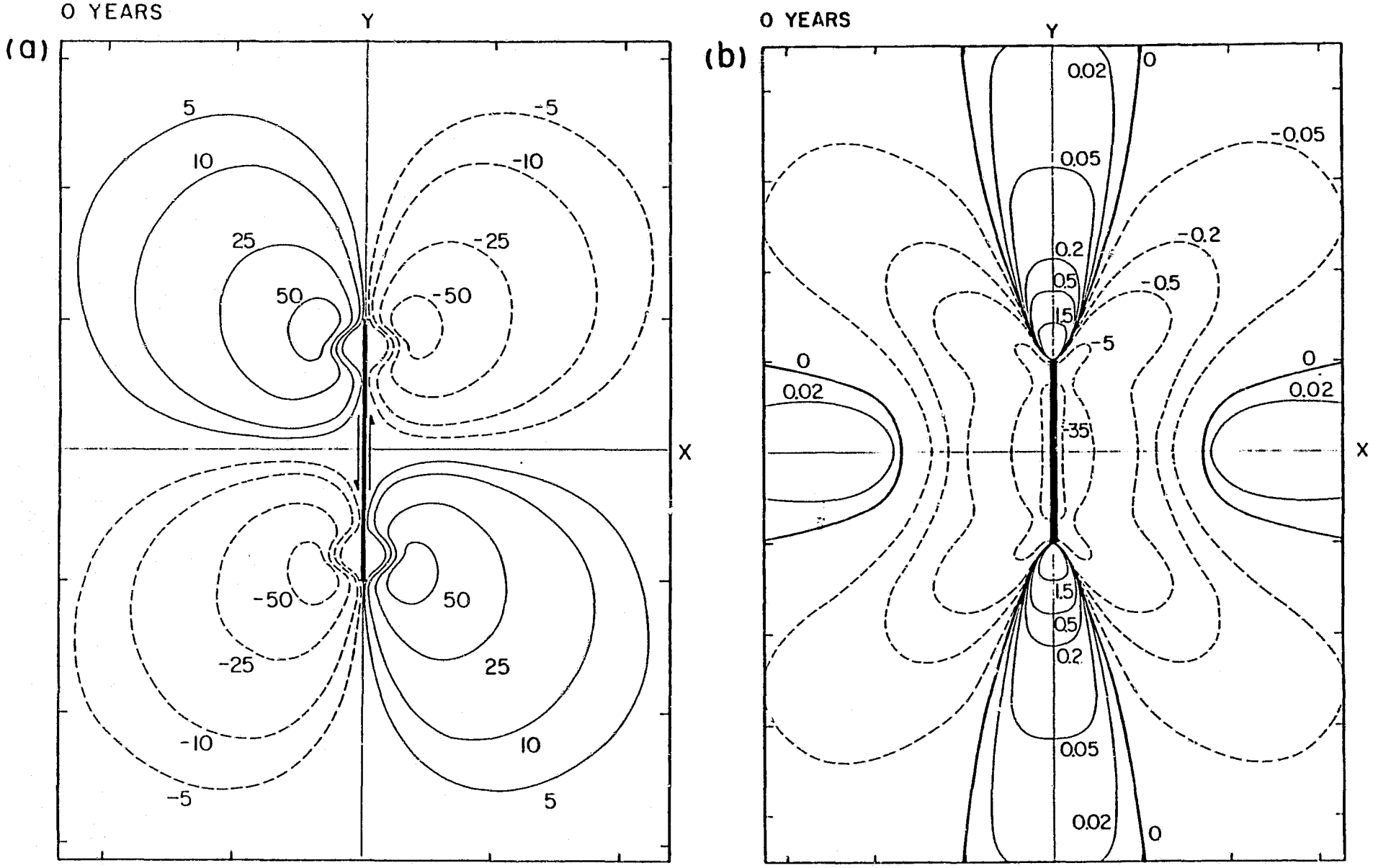
0 YEARS
(a)
Y
X
5
10
25
50
-5
-10
-25
-50
-50
-25
-10
-5
50
25
10
5
VERTICAL DISPLACEMENT
0 YEARS
(b)
Y
X
0.02
0
0.05
-0.05
0.2
-0.2
0.5
-0.5
1.5
-5
0
0.02
-35
0
0.02
1.5
0.5
0.2
0.05
0.02
0
SHEAR STRESS

Fig. 8

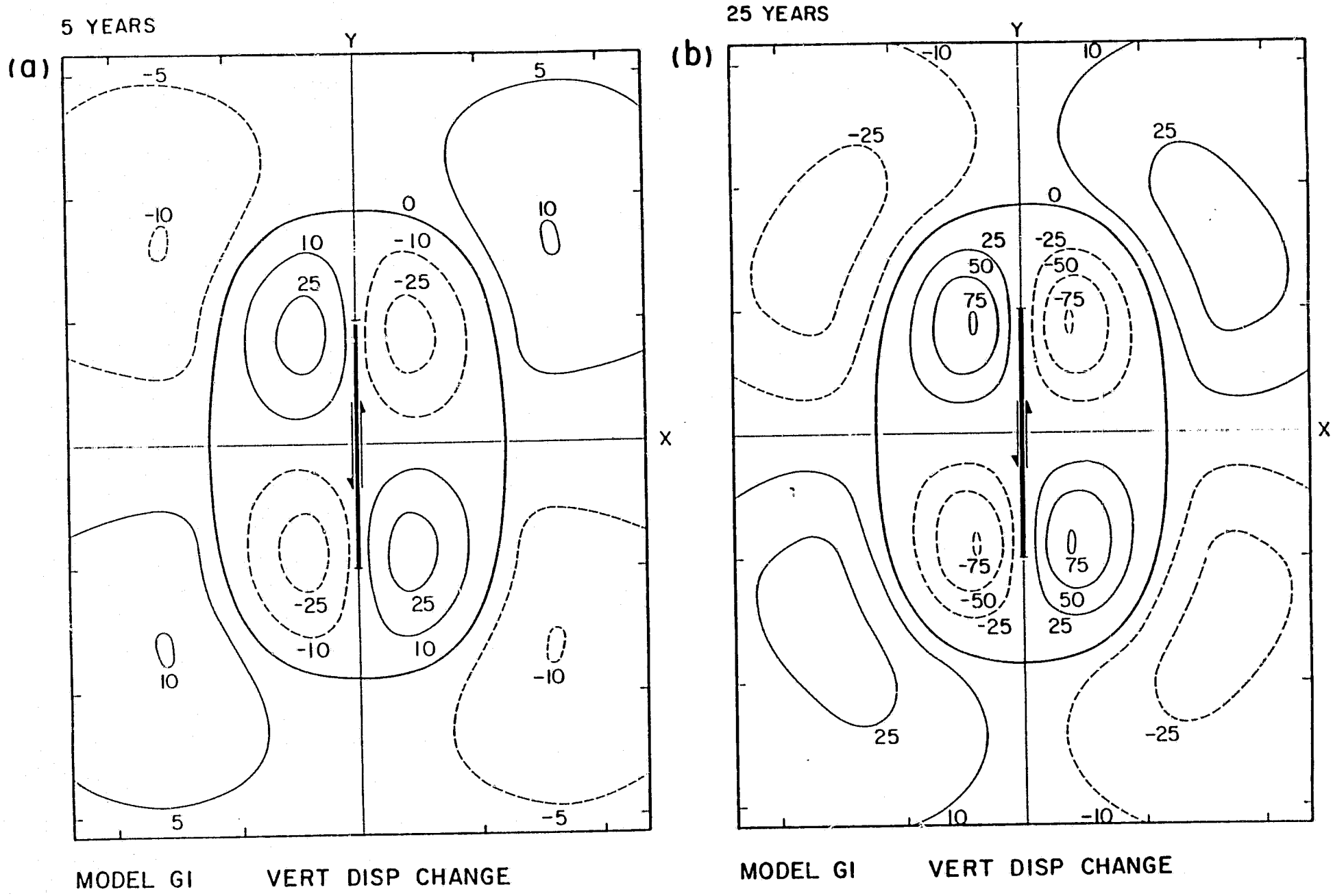
5 YEARS
(a)
Y
X
-5
5
-10
10
0
10
-10
25
-25
-25
25
10
-10
10
-10
5
-5
MODEL GI VERT DISP CHANGE
25 YEARS
(b)
Y
X
-10
10
-25
25
0
25
-25
50
-50
75
-75
0
0
-75
75
-50
50
-25
25
25
-25
10
-10
MODEL GI VERT DISP CHANGE

Fig. 9

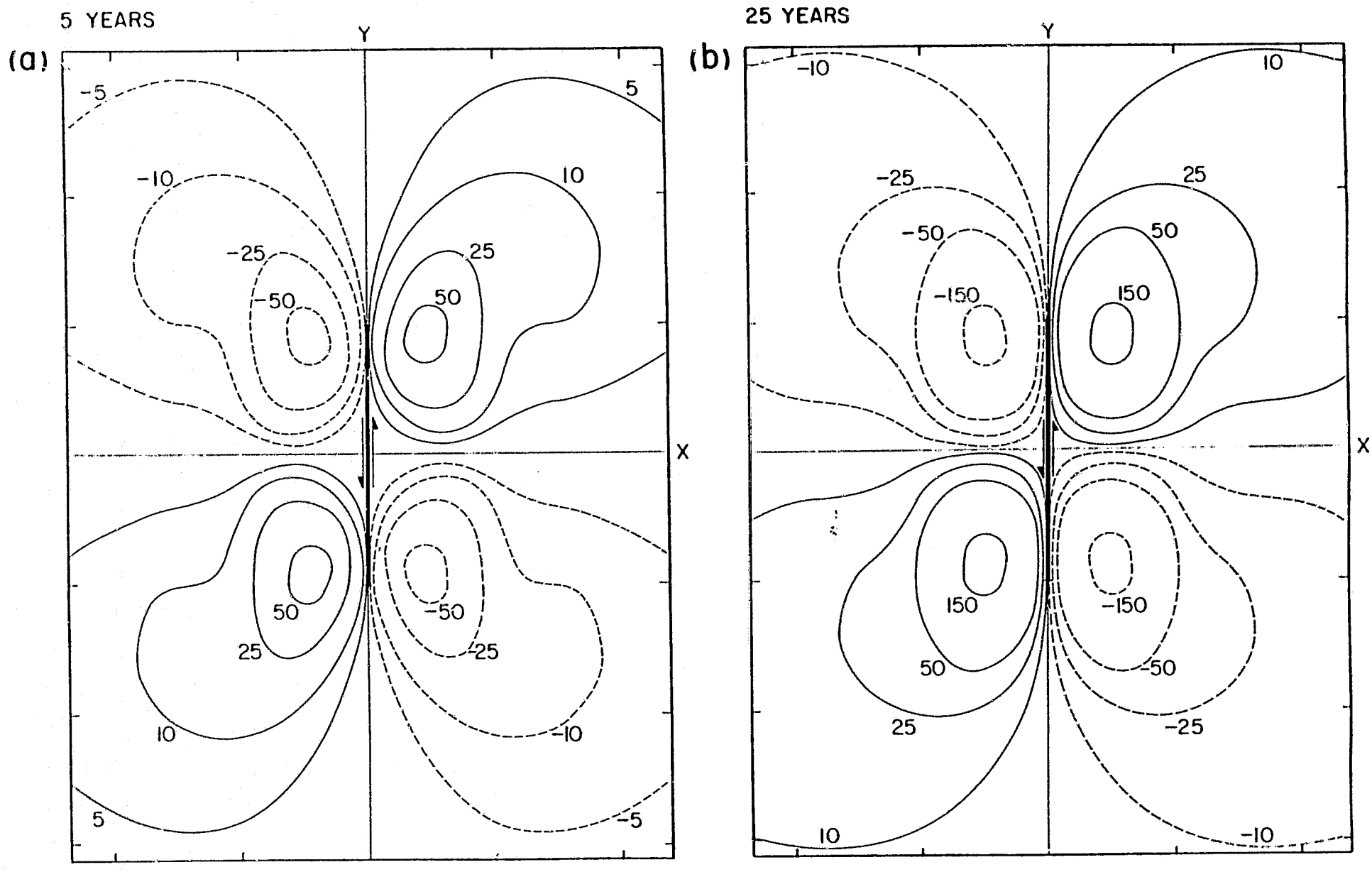
5 YEARS
(a)
Y
X
-5
5
-10
10
-25
25
-50
50
50
25
-50
-25
10
-10
5
-5
MODEL G2 VERT DISP CHANGE
25 YEARS
(b)
Y
X
-10
10
-25
25
-50
50
-150
150
150
50
-150
-50
25
-25
10
-10
MODEL G2 VERT DISP CHANGE

Fig. 10

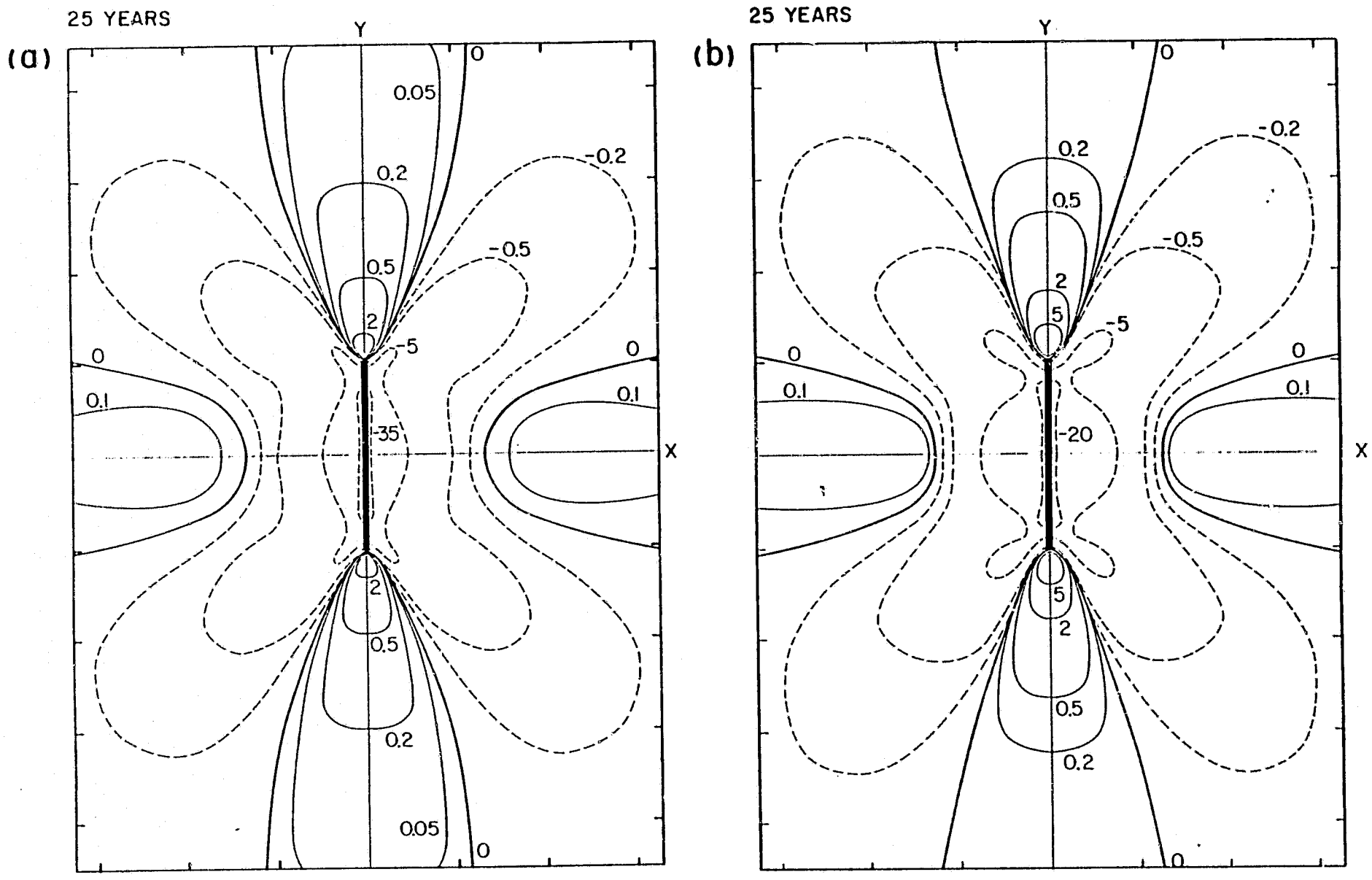

MODEL G1 SHEAR STRESS

MODEL G2 SHEAR STRESS

Fig. 11

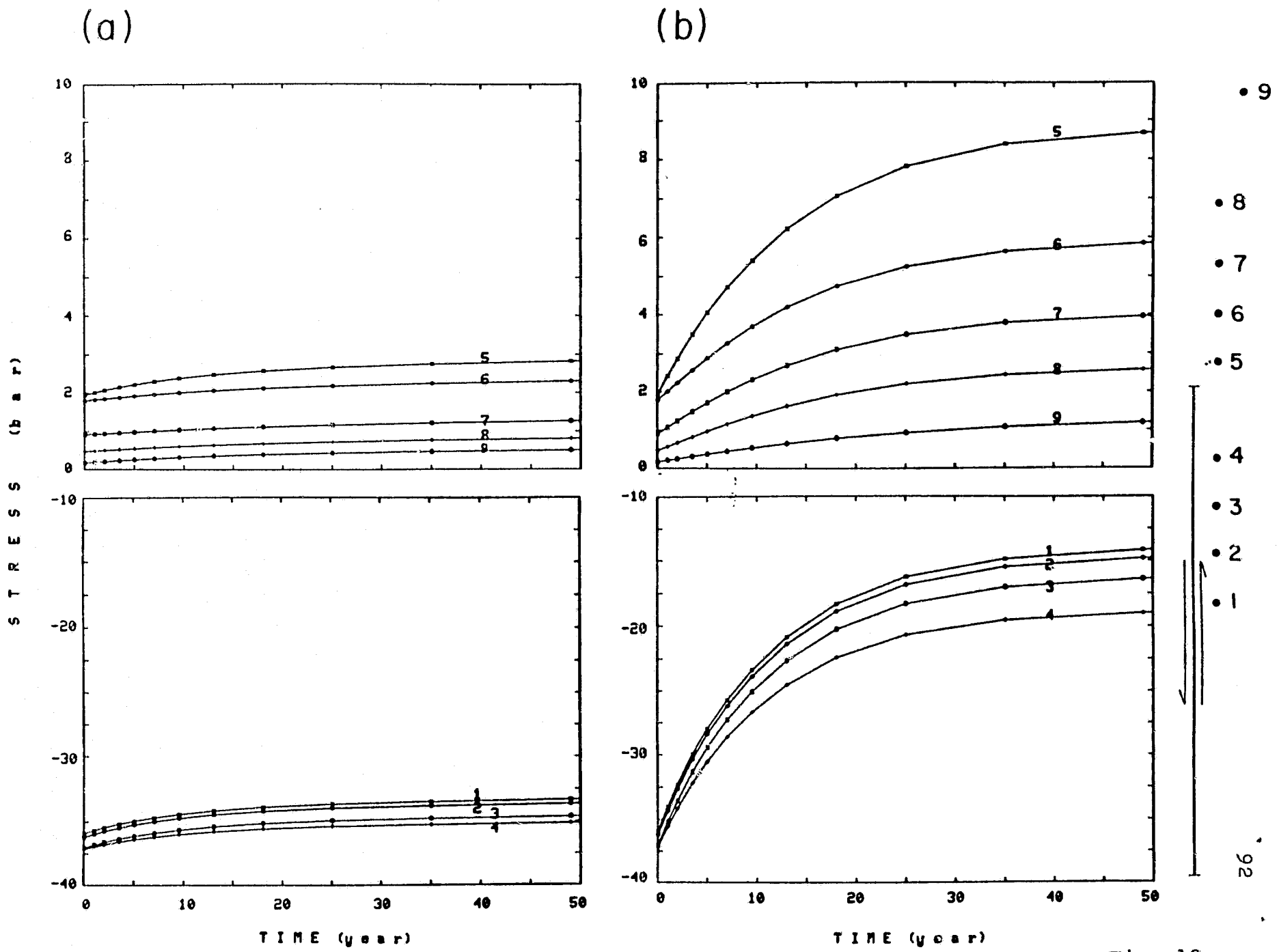
(a)
(b)
STRESS (bar)
TIME (year)
TIME (year)
10
8
6
4
2
0
-10
-20
-30
-40
0
10
20
30
40
50
1
2
3
4
5
6
7
8
9
• 9
• 8
• 7
• 6
• 5
• 4
• 3
• 2
• 1

Fig. 12

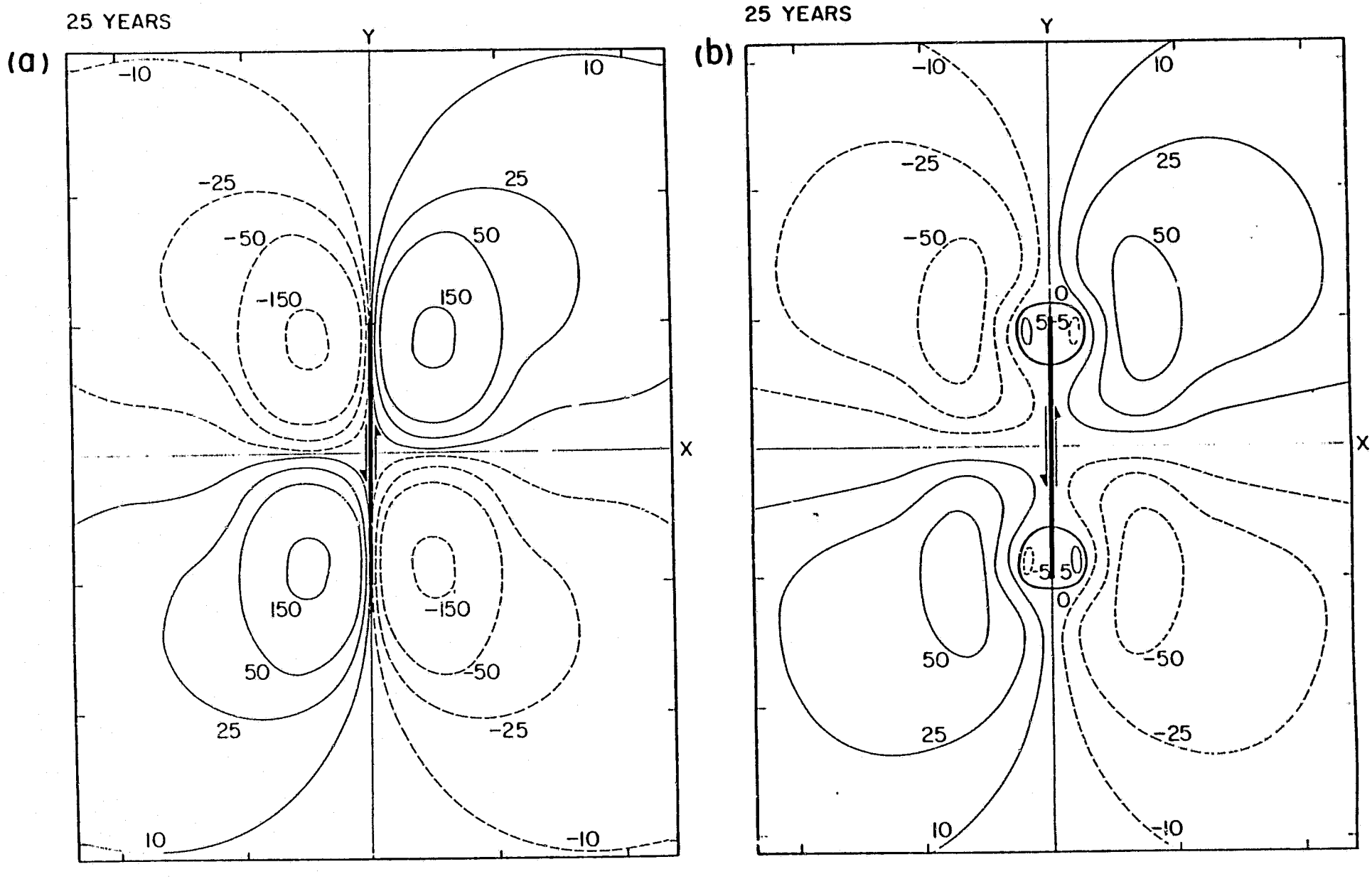

MODEL G2 VERT DISP CHANGE

MODEL G3 VERT DISP CHANGE

Fig. 13

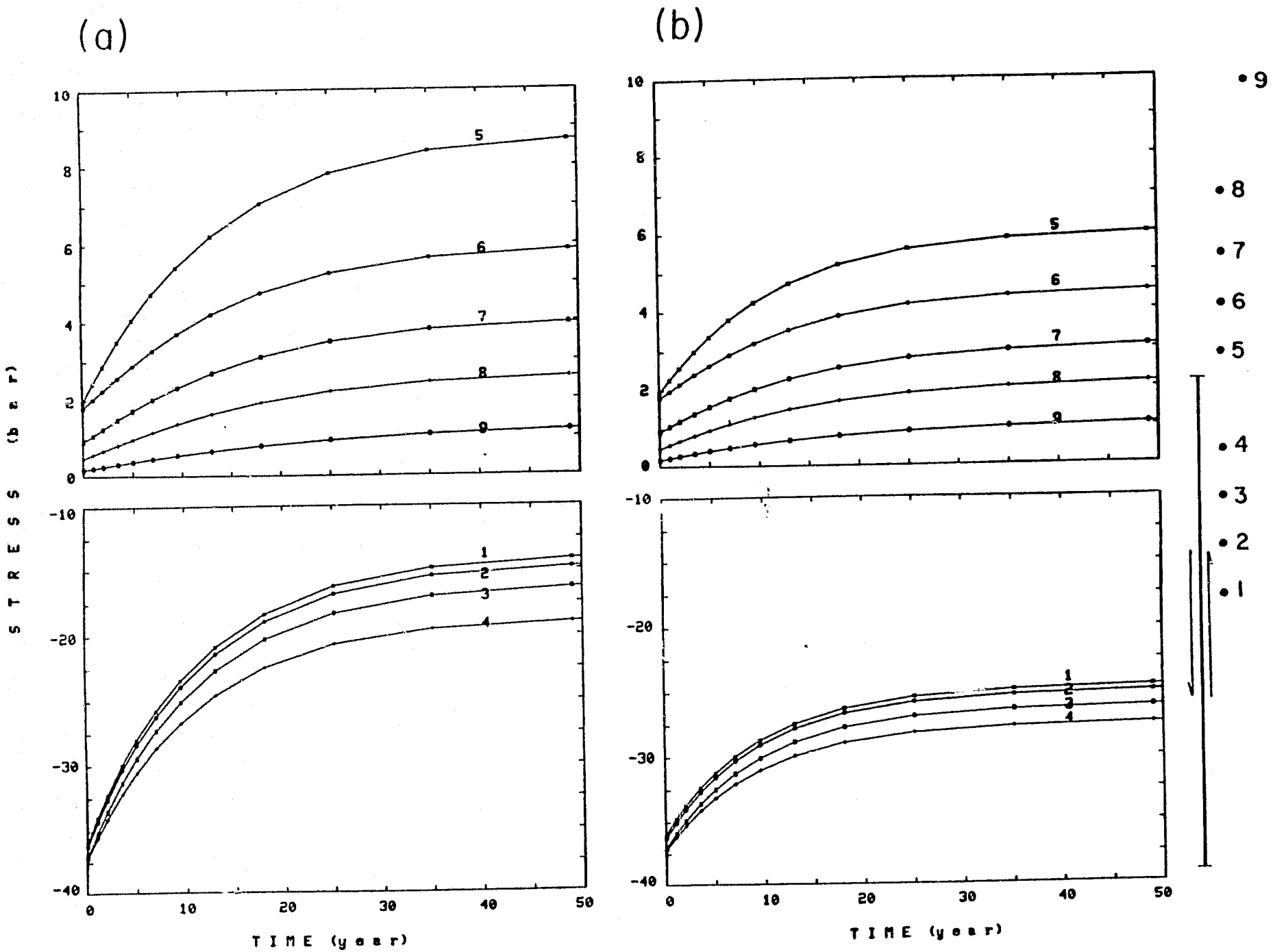

Fig. 14

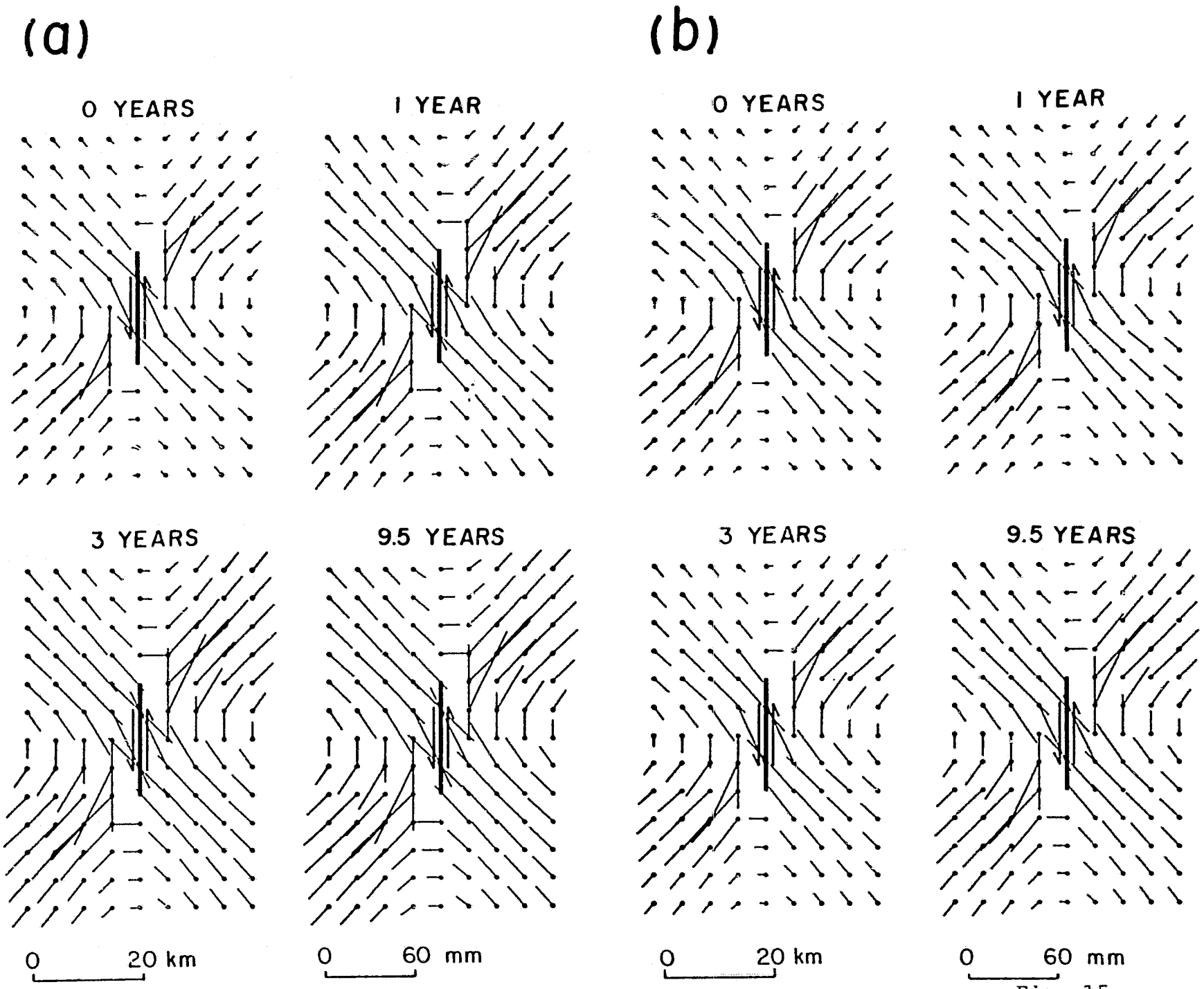
(a)
0 YEARS
1 YEAR
3 YEARS
9.5 YEARS
0 20 km
0 60 mm
(b)
0 YEARS
1 YEAR
3 YEARS
9.5 YEARS
0 20 km
0 60 mm

Fig. 15

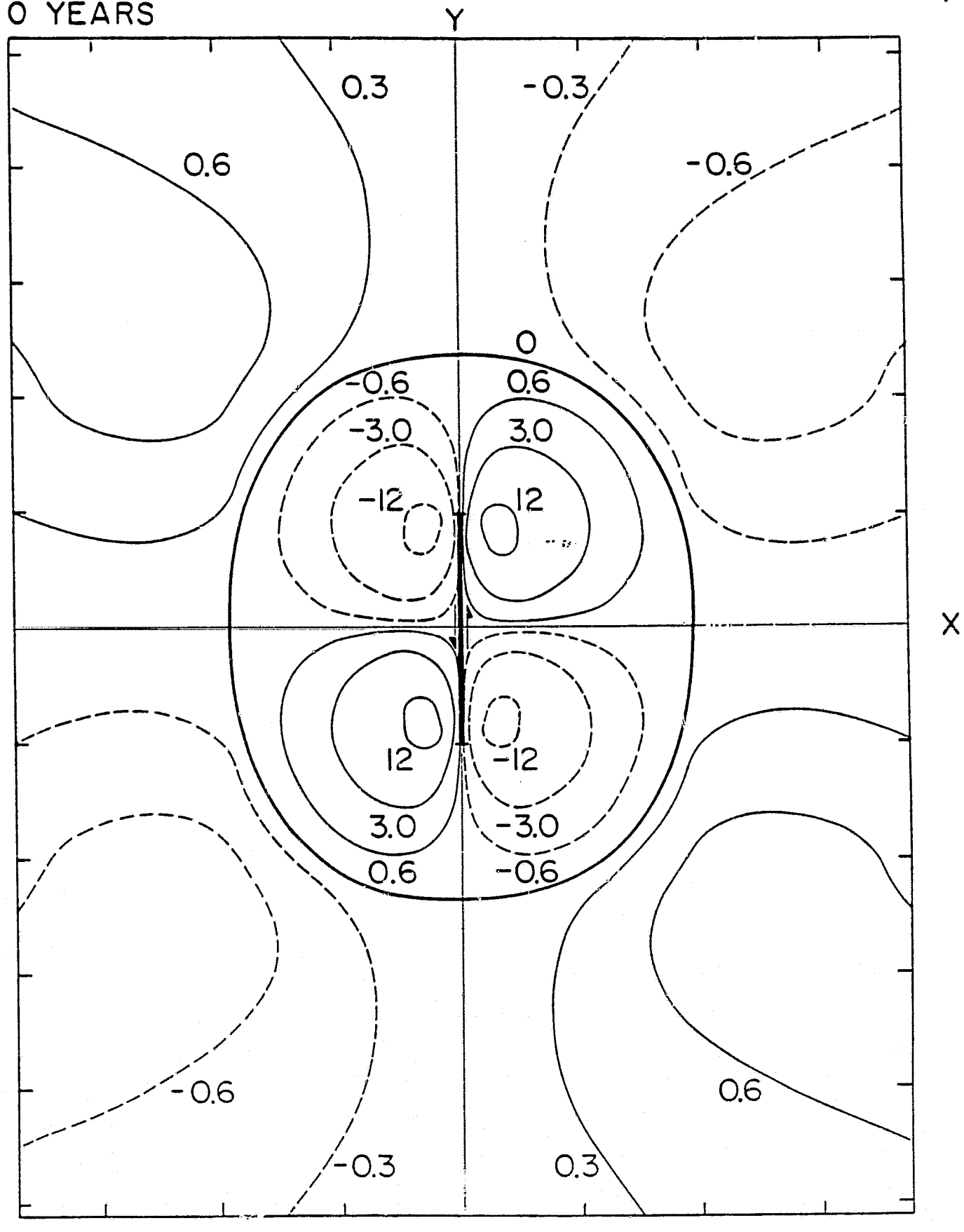

VERTICAL DISPLACEMENT

Fig. 16

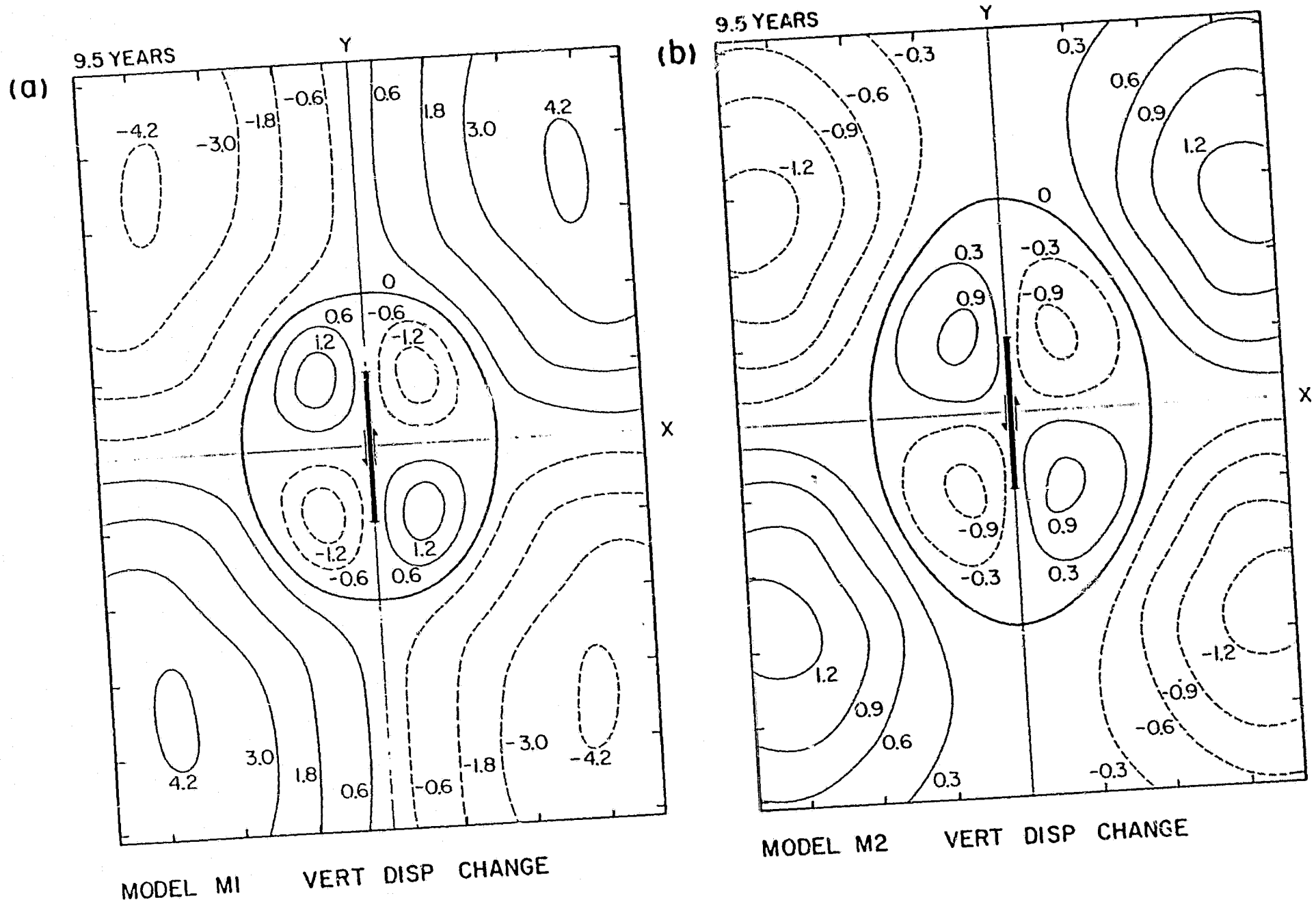
(a)
9.5 YEARS
Y
X
-4.2
-3.0
-1.8
-0.6
0.6
1.8
3.0
4.2
0
0.6
-0.6
1.2
-1.2
-1.2
1.2
-0.6
0.6
4.2
3.0
1.8
0.6
-0.6
-1.8
-3.0
-4.2
MODEL MI VERT DISP CHANGE
(b)
9.5 YEARS
Y
X
-0.3
0.3
-0.6
0.6
-0.9
0.9
-1.2
1.2
0
0.3
-0.3
0.9
-0.9
-0.9
0.9
-0.3
0.3
1.2
0.9
0.6
0.3
-0.3
-0.6
-0.9
-1.2
MODEL M2 VERT DISP CHANGE

Fig. 17

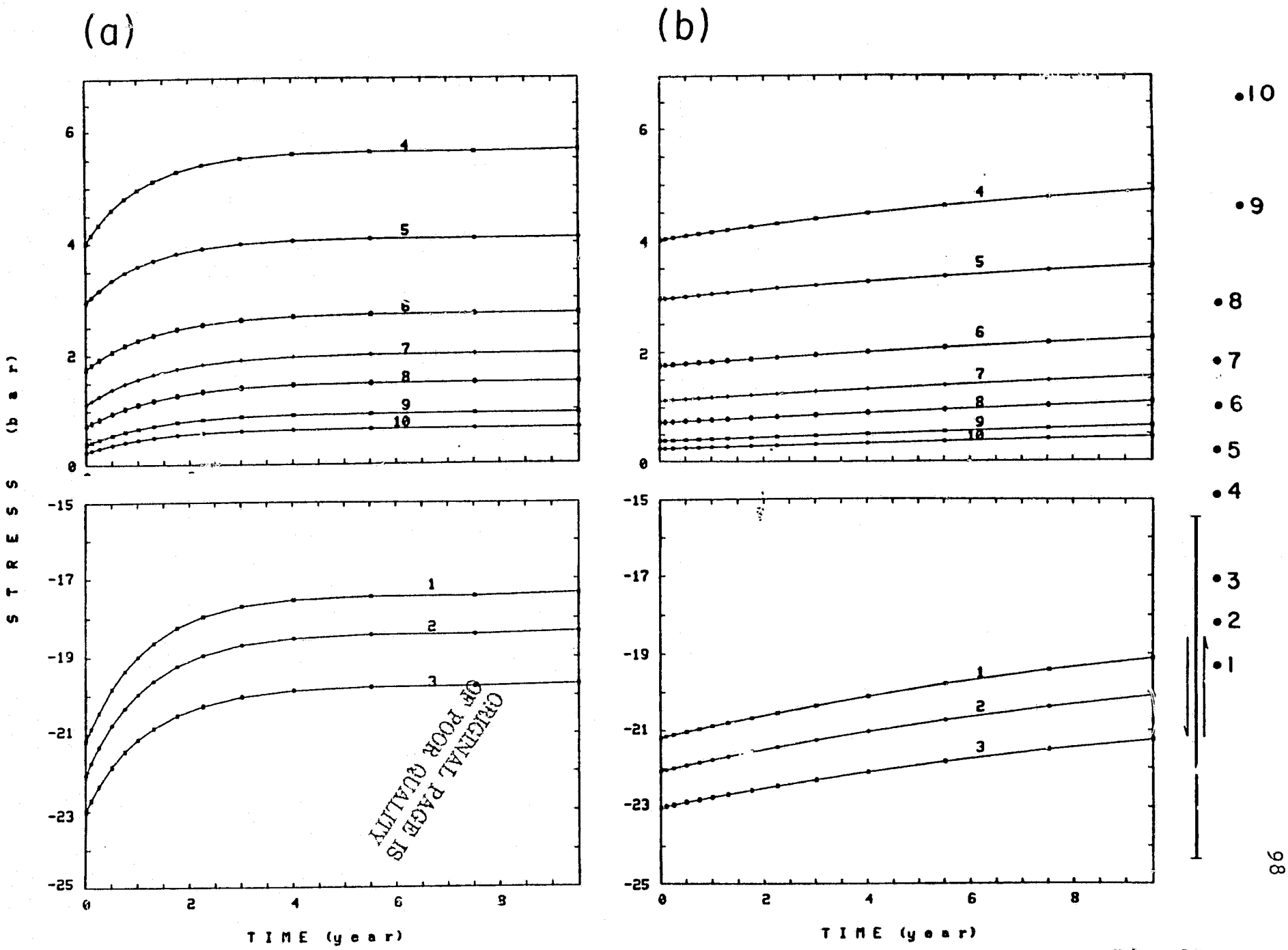
(a)
(b)
STRESS (bar)
TIME (year)
TIME (year)
1
2
3
4
5
6
7
8
9
10
ORIGINAL PAGE IS
OF POOR QUALITY

Fig. 18

Chapter 4

Two dimensional analysis of time dependent movements associated with dip slip earthquakes.

4.1 Introduction

In this chapter, we will study the time dependent deformations and stresses associated with dip slip earthquakes using two dimensional finite elements. Various fault zone structures and rheological properties are used in the calculations. Time dependent stresses and deformations for both abrupt and slow aseismic slips are modelled. An earthquake is modelled as a sudden slip (step function in time) on a dipping fault plane. An aseismic slip event is modelled as a prescribed time dependent slip. Viscoelastic relaxation is included in the calculation. The medium property is assumed to be elastic in bulk and viscoelastic in distortion. In this modelling, we are primarily interested in the large earthquakes in subduction regions. These earthquakes result from plate convergence; therefore they are very relevant to the dynamics of plate movements. Comparison of the model results of time dependent deformations and stresses with geophysical observations may help us understand the mechanisms of plate interactions in subduction regions.

A complete description of a region on earth should be three dimensional. However, three dimensional finite

element models are expensive to implement. The computing cost and human efforts in preparing three dimensional models can be an order of magnitude more than those of two dimensional models. In many cases, two dimensional models are adequate to describe the problem. In subduction regions, a great earthquake can have a fault length of about a thousand km. For example, the 1964 Alaskan earthquake had a fault length of about 600 to 800 km (press and Jackson 1965, Plafker 1969); the 1960 Chilean earthquake had a fault length of about 1000 km (Plafker 1972). The fault edges should have little effect on the surface deformations and stresses in the middle part of the fault, which can then be calculated using two dimensional models.

To study the phenomena associated with dip slip events, we'll use two dimensional and three dimensional models in a complementary way. In a subduction zone, where a two dimensional plane strain model is applicable, the stresses and deformations of a great dip slip earthquake are rapidly varying functions of the distance perpendicular to the trench; therefore a fine grid structure is needed to delineate these variations. We'll use two dimensional models with fine grids to study the phenomena near the fault zone. On the other hand, at a distance far away from the fault zone, two dimensional models cease to be valid. However, the stresses and deformations of an earthquake change slowly with space and time at far distances. Thus

coarse grid three dimensional models can be used. In chapter 5, we will use a three dimensional model with relatively large grid space to investigate the time dependent deformations and stress diffusion phenomena at far distances.

In section 2 of this chapter, we'll briefly review the relevant observations in subduction regions. In section 3 we will discuss some basic results of the relaxation of a dip slip earthquake in a viscoelastic medium. In section 4 we will discuss the interaction of deep aseismic slip and an earthquake along different segments of the fault. In section 5 we will apply relaxation models to the study of post-seismic uplift following the 1964 Alaska earthquake. In section 6 we will discuss and summarize the results of this chapter.

4.2 Brief review of deformation data in subduction regions

4.2.1 General structure of a subduction region

Subduction regions are among the most active and complex tectonic provinces on earth. They have been intensively studied by geophysicists, especially since the advent of plate tectonics theory. A comprehensive review is beyond the scope of this thesis. We will concentrate on the observations which are relevent to time dependent deformations. Topographically, a subduction region features a deep sea trench, an outer trench bulge, cordillera or island arc and sometimes a shallow marginal basin. There are volcanoes, heat flow and gravity anomalies. There is also intense seismic activity. 85% of the seismic energy released in the world is released in subduction regions. It is impressive that these complex phenomena are common to many subduction zones. This suggests that there are common physical processes operating in subduction regions. In plate tectonics theory, a subduction region is where a cold lithosphere descends into the mantle. All the features of subduction regions are probably related to the lithospheric subduction process.

The largest earthquakes in a subduction zone occur at shallow depth. To model a great shallow earthquake, attention must be given to the observed features there. An anomalously low attenuation and high seismic velocity body

in the mantle is identified to be the sinking lithosphere (Isacks et al 1968). The deep sea trench marks the place where subduction takes place. With few exceptions (Kanamori 1971a), great shallow earthquakes are of thrust type. These great shallow earthquakes occur along the zone of contact between the descending and overiding lithospheres. The descending lithosphere acts as a stress guide; intermediate and deep focus earthquakes occur inside it (Isacks and Molnar 1971, Smith and Toksoz 1972, Toksoz et al 1973). Volcanic activity is often present above the sinking lithosphere. High heat flow anomalies are often found in volcanic arcs and marginal basins while low heat flow anomalies are found near deep sea trenches (Uyeda and Vacquier 1968, Watanabe et al 1977). The high heat flow in volcanic arcs and marginal basins suggests that the temperature in the wedge area above a descending slab may be relatively high. This is also supported by the observations that the attenuations of seismic waves are often high in this wedge area (Oliver and Isacks 1967, Utsu 1971, Barazangi et al 1975), and that seismicity is absent beyond an aseismic front in the wedge (Yoshii 1979). The temperature distribution in subduction regions has been subjected to intensive investigations (e.g. McKenzie 1969, Turcotte and Oxburgh 1969, Minear and Toksoz 1970, Hasebe et al 1970, Griggs 1972, Toksoz et al 1973, Andrew and Sleep 1974, Schubert et al 1975, Toksoz and Bird 1977, Toksoz and

Hsui 1978, Hsui and Toksoz 1979, Sydora et al 1980). All the evidence indicates that large temperature variations exist in subduction regions. There is a cold descending lithosphere but a hot wedge area above the slab. It is not likely that a simple layered model can adequately describe these features in a subduction region.

The strain accumulation and relaxation of an earthquake are influenced by the viscosity distribution. From laboratory study of rock flow properties, the viscosity depends strongly on temperature and to a certain extent on pressure (Carter 1976, Goetze 1978, Ashby and Verall 1978). A complex thermal regime implies a complex viscosity structure. Since viscosity controls the time dependent behavior, we will include the viscosity variation of a subduction region in our model calculations of time dependent phenomena.

4.2.2. Crustal movements associated with earthquakes in subduction regions

Anomalous crustal deformations before and after an earthquake have often been reported (e.g. Imamura 1928ab, Tsuboi 1930, Okada and Nagata 1953, Tsubokawa et al 1964, Thatcher 1975ab, Fujii and Nakane 1979, Chang 1980). The deformations before an earthquake are indicators of strain accumulation, and they can serve as premonitary warnings for

a coming earthquake. The post-seismic deformations are related to the relaxation and redistribution of stresses near the fault zone. In this section, we will briefly review some observed time dependent crustal movements associated with earthquakes in subduction regions.

Although geodetic data associated with earthquakes have been reported for nearly a century, the information is still fragmentary, and the phenomena are diverse. Geodetic measurements are also prone to errors and at times are controversial (e.g. Savage 1975b, Jackson et al 1980). There is also the problem of uniqueness in the interpretation of geodetic data. At the present time, it is not likely that we can interprete the crustal movements in a region uniquely. Very often several mechanisms can produce the same observed phenomenon. However, geodetic measurements do put some constraints on possible models. In the future, with the frequent measurements covering broad areas using modern techniques like VLBI and laser ranging, it may be possible to gain a more thorough understanding of the dynamics of plate boundary movements through the modelling of geodetic measurements. At the present time, the best geodetic data associated with earthquakes in subduction zones are either from Japan or from the 1964 Alaskan earthquake. A review of the geodetic observations from these two regions are given in the following subsections.

a. Information from Japan

The largest body of geodetic mearsurements associated with dip slip earthquakes come from Japan. The Geographical Survey Institute of Japan and its predecessors carried out first order triangulations and levelings several times in the entire country since the last decade of last century (Harada 1976). The Geographical Survey Institute of Japan made a commendable effort to publish the survey data in Journals (Journal of Geodetic Society of Japan, Bulletin of Geographical Survey Institute of Japan). However, much of the data are still in notebooks and not easily accesible to outside users. This one hundred years covered several great earthquakes in Japan. As far as time dependent deformations are concerned, the most discussed event is probably the magnitude 8.2 Nankaido earthquake in 1946 (Nagata and Okada 1947, Okada 1950, Okada and Nagata 1953, Miyata 1955, Fitch and Scholz 1971, Kanamori 1972a,1973, Nur and Mavko 1974, Smith 1974, Bischke 1974, Ando 1975, Thatcher and Rundle 1979). This earthquake and the 1944 Tonankai earthquake (magnitude 8.0) broke much of the northern plate boundary between the Philippine plate and the Eurasian plate. The source mechanisms for both events were determined to be low angle thrust from geodetic and seismic studies (Fitch and Scholz 1971, Kanamori 1972a, Ando 1975). The combined fault area of these two events evaluated from seismological study was about 10,000 km^2 and the fault slip was about 3 meters (Kanamori 1972a), but the fault area

determined from geodetic data was about 25,000 km^2 and fault slip was from 3 to 18 m (Fitch and Scholz 1971). Kanamori(1973) interpreted the difference by long lasting aseismic and anelastic deformations. Precise levelings were carried out several times before and after the earthquake (Miyabe 1955). A typical set of geodetic data are shown in figures 4.2.1 and 4.2.2. Figure 4.2.1 shows a leveling route passing Muroto promontory on Shikoku Island, roughly perpendicular to the trench. Figure 4.2.2 shows the preseismic, coseismic and postseismic vertical deformations along the route (taken from Kanamori 1973). Before the earthquake, the trench side subsided with respect to the inland. The earthquake reversed the trend by uplifting Muroto promontory and subsiding the inland. After the event, the post-seismic deformation was uplift near the zero crossing line of the coseismic vertical deformation. Fitch and Scholz (1971) interpreted the preseismic subsidence near Muroto promontory as the overiding plate being dragged down by the descending oceanic plate. Thatcher and Rundle (1979) proposed that viscoelastic relaxation caused the subsidence. For the post seismic deformation, Nur and Mavko (1974) and Smith (1974) proposed that viscoelastic relaxation was the reason for the deformation. Thatcher and Rundle (1979) suggested that deep aseismic reverse slip caused the uplift. Fitch and Scholz (1971) proposed that the upper part of the fault was undergoing reverse slip while the lower part

slipped forward. This really demonstrates the nonunique nature of the probelm. At the present time, it is not possible to give a unique interpretation. Part of the difficulty is that the data were only available on land. All the models were forced to fit the data with the trailing part of the deformation on land while the largest deformation occurred in the sea. To understand the mechanism of trench earthquakes, we should seek more independent evidence.

Another often discussed example is the 1923 Kanto earthquake. This earthquake was located at the western end of Sagami Trough fault. Sagami Trough fault is a transform fault between the Asian plate and the Philippine sea plate. The levelings in Boso penisula, which started only 20 km away from Sagami trough, provided the deformations near the source. The fault determined from geodetic and seismic studies both indicated that the earthquake fault movement was an oblique slip on a dipping fault zone (Kanamori 1971b, Ando 1974). The earthquake fault parameters determined from geodetic measurements were 6 m of right lateral strike slip and 3 m of reverse dip slip. The dip angle of the fault plane is 45 degrees. Thus it is inappropriate to model this fault with a two dimensional dip slip model, especially near the end of the fault. The lack of symmetry of the fault makes such a three dimensional model expensive. In addition, the regional structures are complicated by

subsidiary faults and by blocks moving more or less independently from each other (Scholz and Kato 1978), making the modelling more complex. This can be seen from the data scattering around the theoretical values from simple models (Scholz and Kato 1978, Thatcher and Rundle 1979).

Two other often discussed earthquakes in Japan as far as geodetic measurements are concerned are the 1964 Niigata earthquake and the 1973 Nemuro-oki earthquake. There were premonitary crustal movements before the Niigata earthquake detected from geodetic measurements (Tsubokawa et al 1964). The fault parameters of the 1964 Niigata earthquake have been determined from seismic study by Aki (1966) and Abe(1975), and from geodetic study by Abe (1975). The fault parameters determined by Abe (1975) were a reverse fault dipping 56 degrees with 3.3 m average slip. The fault dimension was 80 km long and 30 km wide. Fujii (1978) examined the leveling data near Niigata since the turn of the century. He found that the precursory anomalous deformation near fault zone started about a decade before the event. The anomalous crustal movements started from the northern part and developed southwards. Near the middle section of the fault in the Nezugaseki region on the footwall side of the earthquake, the general trend of the vertical motion was continuous uplift since the turn of the century. The region started an accelerated uplift about one decade before the event, became subsidence a few years

before the earthquake. Fujii (1978) proposed a creep dislocation model to interpret this preseismic anomaly: due to tectonic stress, the deep part of the lithosphere (below about 50 km depth) started slipping aseismically about one decade before the event. This caused a broad uplift zone. As the dislocation extended near the free surface, part of the uplift zone located on the footwall side began to subside. The model in general seems to fit the preseismic observation. However, Niigata was a region under rapid subsidence because of heavy ground water pumping (Hayashi 1970), and some levelling results might not represent the tectonic movements. Even though the recent geodetic data can be explained, the significance of this earthquake in the context of long term tectonic movements is not certain. This earthquake was an intraplate event. It had a rather steep dipping fault as compared to the shallow dipping fault in Nankaido. Nezugaseki was an area of uplift since late Quaternary, as deduced from the heights of coastal terraces (Matsuda 1976). The earthquake caused Nezugaseki to subside; the subsequent motion of the tidal gage in Nezugaseki was continuous subsidence for several years after the event (Yohiko Crustal Movement Observatory 1973). Nakamura et al (1964) suggested that another earthquake would uplift the Nezugaseki region to match the coast terraces in the future. This earthquake has not happened yet.

The Nemuro-oki earthquake of 1973 was a predicted earthquake. Five great earthquakes ruptured much of the region from Kurile Islands to Hokkaido during the 17 years from 1952 to 1969; the only seismic gap in that region before 1973 was off the coast of Nemuro plane in eastern Hokkaido (Utsu 1972, 1974). The crustal deformations in eastern Hokkaido before 1973 were horizontal contractions in the direction perpendicular to the trench, and extensive subsidence with the subsidence rate increasing from the inland area toward the ocean. These were similar to the observations before the 1946 Nankaido earthquake, and it was consistent with the concept that the overiding plate was dragged down by the underthrusting plate (Shimazaki 1974a). From the levelling data collected since the turn of the century to 1973, the maximum subsidence rate was about 10 mm/year in Eastern Hokkaido (Tada 1974, Shimazaki 1974ab, Abe 1977a). However, from the fossil shell bed along the coast, the inferred subsidence is about 2 meters during the past five thousand years (Geological Survey of Japan 1974). Also from the height change of the marine terraces for the past half million years, the subsidence rate is only about 0.4mm/year (Shimazaki 1974a), an order of magnitude smaller than the subsidence rate in this century. If the sea level has remained more or less constant (Fairbridge 1961, Curray et al 1970), the rapid subsidence in Eastern Hokkaido for the past 70 years and the seismic gap strongly suggested a

coming earthquake (Utsu, 1972, Shimazaki 1974ab). The predicted earthquake occurred on June 17, 1973. The fault mechanism and location were exactly as predicted. The fault was determined to be a low angle thrust fault from both seismic and geodetic data (Shimazaki 1974b, Tada 1974). The aftershock zone almost exactly filled the gap left by the five previous great earthquakes (Shimazaki 1974b). But the magnitude of the earthquake (7.4) was smaller than expected. Based on the long term subsidence rate, the coast of eastern Hokkaido was expected to rebound upward following the earthquake (Kasahara 1975). However, the tidal stations at Hanasaki and Kushiro, which are located on the coast of eastern Hokkaido, did not rebound upward after the event (Abe 1977). Thus the significance of this earthquake is not certain yet.

The cases of Nemuro-oki and Niigata earthquake demonstrated some curious facts about the relationship between recent geodetic history and the long term behavior in Japan. In regions of recent subduction like southwestern Japan, where there are no deep earthquakes and no developed trenches, the seismic deformations conform to the Quaternary vertical deformation. Consistency of geological and geodetic deformations are also found in Kanto and Nobi basins, where rapid subsidence is happening (Matsuda 1976). On the other hand, in Northeastern Honshu and Hokkaido, where there are deep seismicity, developed trenches,

marginal basins and a long history of plate subduction, the recent geodetic deformation is not consistent with the Quaternary geological deformation. Kato (1979) compiled a map for the vertical deformation for the past seventy years in northern Honshu; in general there is a broad region of subsidence, and the subsidence is largest near the coast (about 30 cm in 75 years). However, northern Honshu was an uplift region during the Quaternary (Matsuda 1976). The area of subsidence is too extensive to be treated as a premonitary phenomenon for an earthquake in a specific region. The great Sanriku earthquake of 1933 happened off shore from this region, and it did not reverse the trend of the subsidence. Maybe in these regions, a great earthquake does not necessarily signal the beginning of a cycle of crustal movements. 70 years of geodetic measurements might not reveal all the phases of the crustal motion there. The genesis of the structures in these well developed trench-arc-back arc regions is not fully resolved yet (Uyeda 1977, Toksoz and Bird 1977, Hsui and Toksoz 1979, Toksoz and Hsui 1978). The forces acting in these regions may be complex, and this may well influence the geodetic observations.

To avoid the structural complexity and possible contaminations of geodetic data by artificial causes like industrial ground water pumping, we will not model the geodetic observations in Japan. Instead, we will look into the data from the great 1964 Alaskan earthquake, which is

reviewed next.

b. The 1964 Alaskan earthquake

Geodetic measurements in the subduction regions outside Japan usually do not have such a long history. However, two great subuction zone earthquakes which happened in the last two decades were outside Japan. They were the magnitude 8.5 Chilean earthquake of 1960, and the magnitude 8.2 Alaskan earthquake of 1964. Of these two events, there are more geodetic measurements associated with the 1964 Alaskan earthquake. Repeated surveys have been made since 1964 and may provide useful information (Brown et al 1977). Since this earthquake happened in the recent past, we will construct a model and calculate the time dependent deformation associated with it (section 4.5). It is hoped that future surveys will continue and new data can then be compared with the model results.

The 1964 Alaskan earthquake happened in the northeastern end of the Aleutian arc, where the arc gradually merges eastward into a zone of shallow seismicity and transform faulting (Plafker 1969). Surface deformation caused by this event has been reported by various investigators (Meade 1969, Parkin 1969, Plafker 1969, Small and Wharton 1969). The aftershock region in the continental shelf and the Gulf of Alaska has been surveyed by echo sounding (Huene et al 1967). The regional crustal movements

of the 1964 Alaskan earthquake are more extensive than any known historic seismic events. The significant tectonic deformations, involving uplift, subsidence and horizontal displacements, affected a minimum area of 200,000 km^2. The earthquake and its aftershocks were located between the trench and the volcanic arc in Alaska. All the larger aftershocks (magnitude >5.0) were shallower than 40 km (Algermissen 1965). Subsidiary faulting also occurred within the deformed region related to the Alaskan earthquake. The vertical deformation along a representative profile perpendicular to the strike of the trench is given in figure 4.2.3 (from Hastie and Savage 1970). There was a broad zone of hinterland subsidence, and the maximum subsidence was 2.3 meters. Very large uplift was found on Montague Island. The zones of uplift and subsidence were seperated by a line of zero land level change without abrupt offset (figure 4.2.3). The maximum uplift was 11.3 m on Montague Island. However, the uplift on Montague Island was probably associated with the Patton Bay fault, which is a subsidiary fault about 35 km long on land and extends to the Gulf of Alaska. Geological relations across the fault suggested that this fault was not a major tectonic boundary (Plafker 1969). The closest leveling data to the trench was on Middleton Island about 60 km off the trench; the vertical displacement there was about 4 m. The fault dip was determined to be 5 to 15 degrees from a body wave fault

plane solution (Stauder and Bollinger 1968), about 20 degrees from a surface wave nodal plane solution (Kanamori 1970), and only 3.7 degrees from geodetic data (Hastie and Savage 1970). Figure 4.2.3 also shows the theoretical surface deformation in the optimal dislocation model by Hastie and Savage (1970). The fault parameters given by Hastie and Savage had a reverse dip slip of 12.2 m, and a left lateral strike slip component of 9.7 m. The fault length was 600 km and width 204 km. The dip angle was 3.7 degrees and the depth of the top of the fault was 4.8 km. A secondary fault near Montague Island was included in the model to match the abrupt uplift on Montague Island. This secondary fault was 300 km long and the dip angle 37 degrees with a reverse slip component 17 m and left lateral strike slip 12 m. The secondary fault was considered to make an important contribution to the observed displacements only within 40 km of the fault trace (Hastie and Savage 1970). As can be seen from figure 4.2.3, the fit of observations with the dislocation model is not perfect. However, as pointed by Hastie and Savage (1970), a more complex model probably will add too much complexity without much physical significance. There are few data near the trench. It is not certain if the earthquake fault reached the surface there.

The coseismic deformation and geological record on the coast in Alaska in general were consistent with the concept of lithosphere subduction in plate tectonic theory. The Alaskan earthquake is the megathrust between the descending and overiding lithospheres. On Middleton Island, there were steplike flights of marine terraces. A 4 m terrace was identified as the marine surface uplifted during the 1964 earthquake (Plafker 1969). Radiocarbon dating for the older terraces suggests that the last previous uplift was about 1400 years ago, and the intervals for sudden uplifting was about 500 to 1400 years for the last several thousand years (Plafker 1969). The crustal movements along shorelines were generally consistent with the coseismic movement. Much of the zone which uplifted and part of the zone which subsided during the earthquake showed evidences of submergence for the past thousand years. This was interpreted as the subsidence caused by the dragging of the descending lithosphere before the earthquake (Plafker 1972), as in the case of the 1946 Nankaido earthquake.

The National Geodetic Survey performed first order leveling surveys from Whittier to Anchorage in 1964, 1965, 1968 and 1975. The results were given by Brown et al (1977). Figure 4.2.4 shows a simplified map of south central Alaska and the leveling route, and figure 4.2.5 shows the vertical deformation after the 1964 earthquake. The route from Whittier to Anchorage was approximately perpendicular to the trench strike. Figure 4.2.5 indicates

that a bulge was formed along the route. The leveling was tied to the tidal gage in Anchorage. The precision was believed to be better than 1.0 mm per km (Brown et al 1977). The uncertainty accumulates proportional to the square root of distance. The maximum uplift at the 1975 leveling occurred at bench mark D73, which is 40 km to Anchorage; the uplift was 54.8 cm there and the standard deviation was claimed to be less than 1 cm there. In the 1975 leveling, the route was extended from Anchorage to Palmer along a route roughly parallel to the trench (figure 4.2.4). There was no bulge along this route. This suggested the two dimensional nature of the deforamtion. From the studies in chapter 3 on the time dependent movements after the strike slip earthquakes, we know that the vertical deformation caused by strike slip motion is small near the middle part of the fault. We can thus use two dimensional plane strain models to study the time dependent uplift along this route. These data provided a rare set of precision leveling covering a long route. In the section 4.5, we will construct a model of the 1964 Alaskan earthquake and compare the model time dependent behavior with this data set.

Before we construct a model for the 1964 Alaskan earthquake in section 4.5, we'd like to look into some basic physical processes of the relaxation after an earthquake using simple models. This is given in section 4.3, where we discuss the effects of viscosity on the deformation pattern

after an earthquake.

4.3 Effects of layered structure on postseismic deformation

In this section we look into some basic features of the postseismic deformation of two dimensional dip slip earthquake models. Smith (1974) studied extensively the relaxation behaviors after thrust earthquakes. Our study in this section closely follows his approach. Time dependent deforamtions after two dimensional dip slip events have also been studied by Nur and Mavko (1974) and Thatcher and Rundle (1979) using layer over half space models. The purpose of this section is to demonstrate the effects of increasing viscoity with depth on relaxation, and to discuss the basic physical processes in viscoelastic interactions.

Smith (1974) found that vertical deformation following a dip slip earthquake is informative about the fault zone structure. He found that the ratio of fault depth to lithosphere thickness is an important controlling factor of the behavior of post seismic deformation. If the fault does not fracture the whole lithosphere, the area near the fault tip will subside after the earthquake. The results in this section are consistent with his findings. However, there are other parameters which will also affect the mode of relaxation. In order to understand the physical processes in relaxation, we use only simple models in this section. Throughout this chapter we will assume that the material is elastic in bulk and Maxwellian viscoelastic in distortion. We assume that the medium has a simple

instantaneous response of Poisson's ratio 0.25 and Young's modulus 2.0 x 10^{12} dyne/cm^2, the same values used in chapter 3. The first model (model 4A) has a buried shallow dipping fault. The schematic diagram of the fault and the finite element mesh used in this model is given in figure 4.3.1. In the coordinate system of the finite element grid, the fault is located between the horizontal coordinates -200 km and 0 km, and between 5 and 40 km in depth. The fault is a thrust fault dipping 10 degrees. The maximum fault slip is assumed to be 12 m, and it tapers off to zero along the broken line near the ends in figure 4.3.1. The viscosity structure of model 4A simulates a flat elastic lithosphere overlying a viscoelastic half space. The lithosphere is 80 km thick and has viscosity 10^{25} poise. For transient phenomenon lasting for decades the response of this high viscosity material is practically elastic. The viscoeleastic half space has a viscosity 10^{20} poise. We calculate the displacement vectors at selected locations at time = 0.0, 1.1, 3.6 and 11 years after the earthquake. The snapshots of the deformation are given in figures 4.3.2a to 4.3.2d. In these figures, the small circles indicate the locations where the calculations are made. The line segment stemming from a circle indicates the displacement vector at that location. The scale for the displacement is given in the lower left corner while the scale for the map is given in the lower right corner. The thick line indicates the

location of the fault. Figure 4.3.2a is the elastic deformation associated with the earthquake. Due to the presence of the free surface, the deformation pattern differs from the symmetric pattern of a dislocation in full space; however, the basic deformation pattern still retains the features of a double couple source. The displacements above the fault zone in general are larger than those below the fault. On the free surface, there is a broad zone of subsidence near the lower part of the fault. The subsidence changes continuously to uplift toward the upper part of the fault. The maximum uplift occurs near the upper tip of the fault. Beyond the upper tip of the fault, the vertical surface deformation suddenly drops to near zero. This feature is well known for shallow dipping thrust faults (Mansinha and Smylie 1971).

Although the largest coseismic deformation and stresses are located near the fault, the most important cause of postseismic deformations lies in the low viscosity region below the lithosphere. The elastic lithosphere cannot have time dependent deformation by itself. When the low viscosity region starts to flow in response to stresses, the elastic lithosphere will deform to maintain continuity and equilibrium. The region below the lower tip of the fault is under compression after the earthquake, as can be seen easily from the deformation pattern. Thus material tends to move away from that region. In the regions on

either side of the fault, the material at far distances is drawn towards the fault zone because of the tension created by the earthquake. Thus the basic time dependent pattern of material movement is that material moves away from the compressed region below the fault, and moves towards the fault zone from the two sides. This phenomenon can be seen more clearly from the snapshots of the postseismic displacement changes (total displacement minus coseismic displacement) in figures 4.3.3a to 4.3.3c, which show the postseismic displacement changes at 1.1, 3.6 and 11 years at the selected locations. Two circuits of material movements are formed after the earthquake. The resulting vertical deformation changes on the free surface are shown in figure 4.3.4. There is a subsidence region near the lower fault tip and two uplift regions on the two sides of the subsidence region.

The postseismic deformations are very much affected by the viscosity structure in the mantle. If a low viscosity channel exists below the lithosphere but below this low viscosity channel the viscosity starts to increase, then the resulting time dependent deformation will be different from that of the low viscosity half space. In the low viscosity half space case, it is relatively easy for the material to move downwards; but if the viscosity increases with depth, it will then be easier for the material to move sideways in the low viscosity channel. Model 4B

demonstrates such an effect. The model has the same lithosphere and fault as in model 4A, but it has a low viscosity channel from 80 to 160 km with viscosity 10^{20} poise; below this depth the viscosity is assumed to be 10^{22} poise. The deformation at 0.0, 1.1, 3.6, and 11 years at the same selected locations are given in figure 4.3.5a to 4.3.5d. The post-seismic deformation changes at 1.1, 3.6 and 11 years at the same locations are given in figure 4.3.6a to 4.3.6c. As expected, the material in the compressed region tends to move sideways in the low viscosity channel. On the free surface, the vertical deformation will be a smaller subsidence near the lower fault tip, because it is more difficult for the material to move downward; and there are two larger uplift regions adjacent to the subsidence region, because the material also flows sideways from the compressed region and material piles up on both sides. This phenomenon can be seen in figure 4.3.7, where the vertical displacement change on the free surface are given.

To test if the same phenomenon exists for steeply dipping fault, we construct two additional models. Model 4C and model 4D have the same fault model and lithosphere structure. The fault is a reverse fault dipping 60 degrees, the fault offset is 10 m from surface to 40 km deep and tapers off to zero at 45 km deep. Model 4C simulates an elastic lithosphere over a viscoelastic half space. The

elastic lithosphere is 80 km thick and has viscosity 10^{25} poise. Below 80 km the viscosity is 10^{20} poise. Model 4D has a low viscosity channel from 80 to 180 km deep, with viscosity 10^{20} poise. Below 180 km deep the viscosity is assumed to be 10^{22} poise. The schematic diagram of the fault and the viscosity model are given in figure 4.3.8. The finite element grid used in these calculation are given in figure 4.3.9. 1050 degrees of freedom and 496 elements are used in these models. The displacement patterns for model 4C at time = 0.0, 5.2, and 25.7 years after the event are given in figures 4.3.10a to 4.3.10c, and the displacement changes at time = 5.2 and 25.7 years are given in figure 4.3.11a and 4.3.11b. The basic pattern of the postseismic deformation (figure 4.3.11) is similar to that of the shallow dipping model 4A (figures 4.3.3a to 4.3.3c). Two circuits of movement are formed on the two sides of of the fault. This similarity indicates that the same mechanism is operating in both cases, namely, the material moves away from the compressed region below the fault and moves toward the fault zone from the two sides. The resulting vertical deformation changes for model 4C on the free surface are given in figure 4.3.12. As expected, there is subsidence near the fault and uplifts on both sides of the subsidence region.

The displacement patterns for model 4D at time = 0.0, 5.2, and 25.7 years after the event are given in figure

4.3.13a to 4.3.13c, and the displacement change patterns at time = 5.2 and 25.7 years are given in figures 4.3.14a and 4.3.14b. Here the basic mechanism for the postseismic movement is similar to that of model 4B. The material below the fault tends to flow sideways because the viscosity increases with depth. The vertical displacement changes at 5.2 and 25.7 years after the event are given in figure 4.3.15. Compared with the half space mode 4C, the subsidence is smaller while the uplifts are larger. Increasing viscosity with depth thus has evident effects on the deformation patterns for both shallow and steep dipping events.

Thatcher and Rundle (1979) calculated the deformation following a thrust event in a viscoelastic medium. Their model used an elastic layer over a viscoelastic half space. They found that for events that partially fracture the lithosphere, there is large subsidence near the fault zone due to viscoelastic relaxation after an dip slip earthquake. They also pointed out that the region below the fault zone is under compression and the material there tends to flow away, which will cause subsidence. They also found that buried reverse slip causes uplift. They proposed a model for the earthquake cycle in a subduction zone: The uplift after great thrust events is mainly due to deep aseismic slip while viscoelastic relaxation causes the interseismic

subsidence. From the examples in this section, we see that the large extent of subsidence caused by relaxation partially depends on the model. It must be relatively easy for the material to flow downwards to cause a large extent of subsidence. The deformation patterns after an earthquake are rather sensitive to viscosity structure. The main cause of post-seismic deformation lies in the low viscosity zone: when the material in the low viscosity zone moves in response to the stress state there, the high viscosity regions deform accordingly in order to maintain continuity and equilibrium. In a subduction zone, the viscosity structure is much more complex than a layer over a half space. The complexity in viscosity structure may produce different postseismic deformation patterns. With realistic conditions for a subduction region, post-seismic uplift in a fault zone may be explained by viscoelastic relaxation. We will discuss this further in section 4.5 when we construct models of the 1964 Alaskan earthquake.

4.4 Interaction of deep aseismic slip and a shallow earthquake

In this section, we study the interaction of deep aseismic slip and shallow earthquake along the same fault in a subduction region. Premonitory slow slips were observed before abrupt slips in rock mechanics experiments (Byerlee 1967, Scholz et al 1972, Byerlee and Summers 1975, Dietereich 1978, 1979ab). Aseismic slip on surface has been observed along the San Andreas fault zone (Nason 1973, King et al 1973, Nason and Weertman 1973). Many investigators believe that deep aseismic slip relieves the stress below the stick slip layer in San Andreas fault zone (Brace and Byerlee 1970, Thatcher 1975ab, Rundle and Jackson 1977, Turcotte et al 1979). In a subduction region, aseismic slip may also play a role both before and after the earthquake (Fitch and Scholz 1971, Scholz 1972, Kanamori 1973, Kasahara 1975, Brown et al 1977, Fujii 1978, Fujii and Nakane 1979, Thatcher and Rundle 1979). It is conceivable that aseismic slip happens in the lower portion of the fault zone before an earthquake, especially if there are forces acting on the fault zone from the deeper part of the earth either by gravitational sinking or convection (Isacks and Molnar 1971, Toksoz et al 1973, Forsyth and Uyeda 1975, Solomon et al 1975, Richardson 1978a). The aseismic slip loads the upper stick slip region, which then ruptures during an earthquake. Deep aseismic slip has also been used to explain the crustal movements after the earthquake. The possible reason for

postseismic slip is that an earthquake loads the deeper portion of the fault, and the subsequent aseismic slips relieve the stress loaded by the earthquake.

Figure 4.4.1 and 4.4.2 give two examples of the theoretical vertical deformation on the free surface due to buried slips. Model 4E has a fault dipping 21.8 degrees. The slipping fault surface is located between the depths 40 km and 80 km. The maximum fault slip is 1 m and the slip tapers off near the fault ends, as shown in figure 4.4.1. Model 4F has a fault dipping 45 degrees and is located between the depths of 40 km and 80 km, also with a maximum fault slip of 1 m (figure 4.4.2). The surface deformations in both models are mainly uplift. In the case of a normal fault, the vertical deformation will be mainly subsidence (except for the special case of vertically dipping faults). Thus a buried slip can be conveniently used to explain either uplift or subsidence. Since a buried slip cannot be observed directly, we have the freedom to choose its size, location, slip sense, and dip angle. Aseismic slip with properly chosen parameters can thus explain many observations. Discreet judgements must be used so that these interpretations make physical sense.

In the following, we construct two kinematic models for the interaction of deep aseismic slip with an earthquake along the same fault. We are interested in modelling the

way the aseismic slip loads the stick slip region before the earthquake, and the way the earthquake loads the aseismic slip region after the event. The finite element grid used in this study is given in figure 4.4.3. For the purpose of comparison, first let's examine the behavior of a fault in an elastic medium. Model 4G has elastic constants of Young's modulus 2.0×10^{12} dyne/cm^2 and Poisson's ratio 0.25 as in other models in this chapter. The fault extends from surface to 80 km depth dipping 45 degrees. The lower 40 km is assumed to undergo slow aseismic slip while the upper 40 km will rupture abruptly. The time dependence of the slip is given in figure 4.4.4. We assume that at the time zero the stress in the fault zone reaches a critical level and the lower portion of the fault starts aseismic slip. The slip is assumed to be a reverse slip along the 45 degree fault dip. In a numerical scheme, we have to discretize the continuous aseismic slip, we assume the slip between the depths 45 km and 75 km increases from 0 to 5 m in 40 steps during the first 20 years. The fault slip tapers off between 40 and 45 km deep and between 75 and 80 km deep. At 20 years the upper section ruptures abruptly with 5 m reverse slip, thus bringing equal slip displacement from the surface to 75 km deep, and tapers off from 75 to 80 km deep. The shear stress parallel to the dip direction at 6 locations along the fault zone are given in figure 4.4.5 and 4.4.6. Positive shear stress tends to produce reverse slip

on fault while negative shear stress tends to relieve the prestress for a thrust fault. Figure 4.4.5 shows the shear stress at three locations along the stick slip region. The aseismic slip continuously loads the stick slip region for 20 years until the earthquake happens and the stress is relieved (becomes negative). Since there is no relaxation, the stress stays the same after 20 years. In figure 4.4.6, the shear stress along the aseismic slip region is given. The aseismic slip continuously relieves the stress in that region until at 20 years the earthquake happens and reloads the aseismic region. For this elastic medium, the load from the earthquake is not sufficient to bring the aseismic region back to zero stress (i.e. the reference stress level which caused the aseismic slip to happen). Actually the stress state after the earthquake is simply that of a uniform slip from 0 to 75 km deep and tapers off from 75 to 80 km deep, because there is no relaxation in the model. Thus everywhere along the fault zone the stress is relieved.

In model 4H we introduce viscoelastic relaxation. The rheological structure is given in figure 4.4.7. The lithosphere is assumed to be 80 km thick and has a viscosity of 10^{25} poise. There is a descending slab, also with the viscosity 10^{25} poise. Outside the descending slab, the viscosity is 10^{20} poise from 80 to 160 km depth, and below 160 km the viscosity is assumed to be 10^{22} poise. We also assume there is a low viscosity wedge above the shear zone

between the descending and overiding lithospheres, and the viscosity is assumed to be 10^{20} poise there. The resulting shear stress parallel to the dip direction at the same locations are given in figure 4.4.8 and 4.4.9. In the stick slip region, the results are similar to those of the elastic model (figure 4.4.8), except that the magnitude of loading from the aseismic slip is slightly reduced, and after the earthquake the stress slowly recovers towards zero. In the aseismic slip zone, where we assumed low viscosity, the shear stress is quite different from the elastic case. In the first 20 years, the effect of viscoelastic interaction is to recover the prestress. The end result is that the stress relief at 20 years is considerably less than that of the elastic case. The earthquake can then load the upper part of the aseismic slip zone back to positive stress (i.e. stress larger than the reference stress which started the aseismic slip). The behavior after the earthquake is that shear stress relaxes towards zero.

Admittedly this simple model is far from perfect. For example, it is probably not reasonable to assume that the aseismic slip starts simultaneously along the whole aseismic region. Maybe it should start from one end and propagate to the other end. We will not attempt to model this mode (and infinitely many other modes) of slips in this thesis. However, this simple numerical experiment does tell us something about the interaction between the earthquake

and the aseismic slip: the aseismic slip stresses the stick slip zone before the earthquake, the earthquake in turn loads the aseismic slip zone. The stress caused by the earthquake on the aseismic zone usually decreases with distance from the source. Viscoelastic interaction with the aseismic slip has a stress recovery effect in the aseismic slip zone. Combination of the loads from the earthquake and the stress recovery due to viscoelastic relaxation can sometimes bring the region near the earthquake fault tip to the stress level which started the aseismic slip.

4.5 Modelling of the 1964 Alaskan earthquake

4.5.1 General descritptions

The coseismic deformations of the 1964 Alaska earthquake are very complex. Many subsidiary faults were activated during the earthquake and contributed locally to the deformations (Plafker 1969). On the other hand, repeated leveling data showed a rather smooth profile over a long levelling route (figure 4.2.5); this suggested the nonlocal nature of the time dependent deformation. This deformation was probably associated with the main fault rather than the subsidiary local effects. We set up a model to calculate the relaxation associated with the main fault of the 1964 earthquake. The observed data indicated that the variation of uplift in the direction perpendicular to the leveling route was small (figure 4.2.5). Thus we can use two dimensional plane strain models. All the models in this section have the same finite element grid, fault parameters, and instataneous response. The finite element grid has 1412 degrees of freedom and 651 elements (see figure 4.5.1). The model region is 2200 km long and 1000 km deep. As usual we assume that the material in the models is elastic in bulk and Maxwellian viscoelastic in distortion. The elastic parameters are assumed to be Young's modulus 2.0 x 10^{12} dyne/cm^2 and Poisson's ratio 0.25. The differences between the models will be due to different viscosities.

The purpose of this study is not to fit the geodetic data in detail with a complicated model. We are interested in using the features in the data to bring out the physical processes occurring after the earthquake. The models are constructed according to our knowledge of subduction regions. Starting with a simple layered model, one by one we add the features observed in a subduction region to the simple model. We then compare the model results with the uplift data. Hopefully with this process we can gain some insights into the physics of the time dependent movements in a subduction region.

4.5.2 Fault model

The schematic model of the fault is shown in figure 4.5.1. The values for the maximum fault slip (12 m) and the fault width (203 km) are similar to those of the optimal model of Hastie and Savage (1970). However, the dip angle of the fault plane in Hastie and Savage's model is only 3.7 degrees, while we used a dip angle of 10 degrees. Our value is closer to the values determined by seismic studies (20 degrees from surface wave analysis by Kanamori, 5 to 15 degrees from body wave analysis by Stauder and Bollinger). We also assume that the fault slip tapers off linearly to zero near where the fault ends instead of ending abruptly with a uniform slip. As in the optimal model by Hastie and Savage, we assume that there is no surface rupture. The

topmost point of the fault is 5 km deep. There are few data near the trench, and it is not certain if the main fault reached the surface. However, the detailed configuration of the fault near the upper fault tip should have little effect on the deformation from Whittier to Anchorage, which are located near the lower tip of the fault some 200 km away. We chose a buried fault partly for computational economy. In order to maintain the proper aspect ratio of the elements in the wedge area above a shallow dipping fault, many elements are needed near the intersection of the fault and the free surface if we use quadrilateral elements. The grid structure is simpler for a buried fault. In the coordinate system of the finite element grid, the fault is located between the horizontal coordinates -200 km and 0 km, and between 5 and 40 km of depth.

4.5.3 Coseismic response

All the models have the same elastic parameters, thus they have the same coseismic responses. Figure 4.5.2 shows the coseismic vertical deformation on the free surface from the model calculation. The general behavior is subsidence in the inland side and uplift toward the trench on the overiding lithosphere, and little deformation on the footwall side. This is expected for a shallow dipping dislocation (Plafker 1972, Mansinha and Smylie 1971). The vertical deformation does not have the spectacular uplift

associated with steep dipping subsidiary faults as in the Hastie and Savage model, but the general features are similar. The maximum uplift is located about 30 km from the fault tip. The rather rapid increase of uplift there is due to the material pile up near the buried fault tip. The same fault model has also been used in section 4.3 to study the deformation patterns of the shallow dipping event. The displacement vectors at selected nodes were given in figure 4.3.2a of section 4.3.

The town of Whittier is located near the maximum coseismic subsidence along the leveling. In the model result, this point is near the horizontal coordinate -180 km. We will use the segment from -280 km to -180 km as the leveling route when comparing the model results with the uplift data.

4.5.4 The layered models

For comparison purposes, we calculated the time dependent response of two simple layered models. Model 4I is identical to model 4B in section 4.3. We assumed that the lithosphere is 80 km thick and has a viscosity of 10^{25} poise. Below the lithosphere is a layer of low viscosity 10^{20} extending from 80 to 160 km deep. Below 160 km the viscosity is 10^{22} poise. The vertical displacement changes at 1.1, 3.6 and 11 years after the event are given in

figure 4.5.3. Superimposed on this figure is the uplift data of surveys in 1965, 1968 and 1975. Theoretical results are subsidence near the lower tip of the fault and uplift on both sides of the subsidence area. It is interesting that the uplift on the inland side has a magnitude of about 60 cm in 11 years, comparable to the observed uplift data. On the whole though, the match between the model result and the observation is not satisfactory. The position of the inland uplift in the model is located more to the inland side. Nevertheless, this simple model illustrates an important point: for reasonable values of viscosity, great earthquakes like the 1964 Alaska earthquake can produce measurable deformation years after the event. In the case of the Alaska earthquake, the amount of uplift in the model is comparable to the leveling result. This suggests that it is important to include the effects of viscoelastic relaxation in the analysis of time dependent geodetic measurements.

Model 4J is identical to model 4A in section 4.3, it simulates an elastic lithosphere over a viscoelastic half space. This model differs from model 4I only in that the viscosity below 160 km is assumed to be 10^{20} poise instead of 10^{22} poise. As discussed in section 4.3, this would cause a larger subsidence zone because it is easier for the material to move downwards. The result of the vertical displacement change is given in figure 4.5.4. The amplitude and the extent of the subsidence are larger than those in

the layered case model 4I; and the uplift in the inland side is reduced (notice the scale change in the figure). The results of this model are still not compatible with the observations, however, the uplifts are still of measurable magnitude.

4.5.5 Model with descending lithosphere

In model 4K, we introduce a short descending lithosphere (see figure 4.5.5). Alaska is a part of the circum-Pacific seismic belt. Seismicity studies indicated that intermediate earthquakes exist in this region (Gutenberg and Richter 1954, Isacks and Barazangi 1977, Van Wormer et al 1974); therefore the existence of a descending slab is expected from plate tectonics theory. We assumed that a short descending slab exists in model 4K. The descending lithosphere is assumed to be 80 km thick, and the maximum depth of the descending slab is 160 km. We assume that the viscosity within the descending slab is the same as the lithosphere above 80 km. The viscosity in the other area is the same as in the layered model (model 4I). The result for vertical deformation is given in figure 4.5.6. Compared with the result of model 4I (figure 4.5.3), both the uplifts in the inland and the subsidence are reduced. The physical reason for this difference can be explained in the following way: Since the descending lithosphere blocks the low viscosity channel, it is more difficult for the

material under the fault zone to move to the inland side. Thus the uplift in the inland side is reduced. The subsidence near the fault is also reduced, because less time dependent movement can be induced due to the high viscosity descending lithosphere. As seen in figure 4.5.6. This model result also does not explain the uplift data.

4.5.6 Model with descending slab and low viscosity wedge

The wedge areas above the descending slabs often are regions of high heat flow (Watanabe et al 1977) and high seismic wave attenuation (Oliver and Isacks 1967, Molnar and Oliver 1971, Utsu 1971, Barazangi et al 1975). Shear heating between the descending and overiding lithospheres may have raised the temperature in this region (Toksoz et al 1973, Hsui and Toksoz 1979). Since viscosity depends strongly on temperature, it is conceivable that the region above the shear zone can have a rather low viscosity. In addition, if strain rate depends on higher power of stress, the effective viscosity near the fault zone will be lower because the stress is higher there. In model 4L we assume that the low viscosity extends to a thin layer above the boundary between the descending and overiding lithospheric plates, as shown in figure 4.5.7. We assumed that the viscosity in this low viscosity zone is 2.0×10^{19} poise. Other aspects of this model are the same as those for model 4K.

The deformation changes on the free surface at 1.1, 3.6 and 11 years after the event are given in figure 4.5.8. Superimposed on this figure are the leveling data from 1965, 1968 and 1975 surveys. The features of the model results and the observations match very well. The basic features of the theoretical displacement profile are still two uplift areas separated by a subsidence region near the fault tip, as in the case of layered model 4I (cf. figure 4.5.3). But the uplift region on the inland side is narrower than that in the layered model. The position of the uplift has also shifted towards the trench side. The points of maximum uplift migrate towards the trench with time. This feature also exists in the uplift data, as pointed out by Brown et al (1977). Figure 4.5.9 shows the enlarged figure of the model results superimposed on the observed uplift data . The match at 11 years after the event is excellent. Such a good match is rare in the modelling of geodetic data, and probably is fortuitous, because the true structure of the earth is certainly more complex than the simple model. Nevertheless, it is gratifying to find that a model constructed from our knowledge about the subduction region can produce the features in the data, and gives better fit than other less realistic models. The model uplift at 1.1 and 3.6 years after the event is smaller than the 1965 and 1968 survey data. This is not surprising though: We have assumed that the earthquake happens instataneously. For the first

several years, the crustal movements associated with the aftershocks and deep slips probably contributed to the observed deformation. The relaxation effect became dominant only after the phase of rapid adjustments like aftershocks had decayed. Notice that the discrepancies between data and theoretical results is larger near the fault end (which is located at -200 km in the horizontal coordinate) than near the inland side for the early years. Some extension of the earthquake fault may have occurred through aseismic slip. The buried aseismic slip in general will cause uplift above it, as we have seen in section 4.4. It is also reasonable that the aseismic slip is larger near the fault end, where the stress caused by the earthquake is largest.

The displacement vectors at selected locations at time = 0.0, 1.1, 3.6, and 11 years after the event are given in figure 4.5.10a to 4.5.10d. The general pattern is still that of a double couple source. However, the downward displacements under the lower fault tip in general decrease rather than increase with time, indicating that the material there moves upwards rather than downwards after the event. The direction of the material movements in the compressed region is thus opposite to those in the cases of the half space and the layered model (model 4A and 4B in section 4.3). This behavior is more clearly seen in figure 4.5.11a to 4.5.11c, where the displacement changes at 1.1, 3.6, and 11 years are given. This deformation pattern is probably

due to the interaction of the low viscosity zone and the high viscosity descending slab. Because the high viscosity descending lithosphere underneath the low viscosity region serves as a guide for the material movements, the material in the low viscosity zone above the descending slab cannot move downwards into the descending slab; it will move either downdip or updip. To maintain continuity and equilibrium the materials above and below this low viscosity region will move towards it. This created the complex deformation pattern in figure 4.5.11. To show the displacement change pattern more clearly, we reduced the scale of displacement and replotted figure 4.5.11c in figure 4.5.11d. Notice that in the downdip extension region of the fault, the deformation pattern is very similar to that of a reverse fault along the segment indicated by the dashed line. This is hardly surprising, as this configuration tends to relieve the earthquake load in that region.

4.5.6 The effects of slab geometry

In model 4K and 4L, we have kept the shape of the descending slabs simple. The real situation may be more complicated. Seismicity profiles in this region are rather diffused (Van Wormer et al 1974). Van Wormer et al (1974) suggested that there are two blocks in South central Alaska. The boundary between the two blocks extends from the Yetna River through Prince William Sound, perhaps as far as the

continental shelf break near Yakutat Bay. The leveling route discussed in this section and the epicenter of the 1964 Alaskan earthquake are located near this boundary. The subduction direction north of this block boundary is about N40W, while to the south of the boundary it is about N77W. We cannot take this complexity into account in our two dimensional models. However, this difference was inferred from the seismicity in the intermediate depth. If any split of the descending slab does exist, it should exist only in the deeper part of the slab. In the shallow part of the descending slab it should be continuous. In model 4M we investigate the effects of the deep structure of the descending slab on the relaxation. The model is given in figure 4.5.12. Model 4M is the same as model 4L except for the addition of a deeper descending slab. The result of the surface deformation is given in figure 4.5.13. The uplift data are also shown on the figure. The effect of the deeper part of the descending lithosphere on the surface deformation is very small. On the other hand, this also means that it is not very useful to use surface deformation to probe the deep structure of a descending lithosphere.

4.5.7 The effect of viscosity

The viscosity in the earth is still a controversial issue. Since viscosity depends strongly on temperature and temperature anomalies exist in subduction regions, the

viscosity in a subduction region may be quite different from that in other areas. The value of viscosity in a subduction region is largely speculative. Several investigators have pointed out that great thrust earthquakes in a subduction zone may provide an opportunity to investigate the viscosity there (Nur and Mavko 1974, Smith 1974, Kasahara 1975, Thatcher and Rundle 1979). We have found for the case of the Alaskan earthquake, the leveling data put some constraint on the possible models. The models with a descending slab and low viscosity wedge above the descending slab can reproduce the features in the data, while the simple layer models and the model without a low viscosity wedge produced less satifactory results. To see the sensitivity of surface deformation on the viscosity, we constructed one additional model with different viscosity in the low viscosity channel. Model 4N is similar to model 4L, except the low viscosity below 80 km deep is 5×10^{19} poise instead of 10^{20} poise. The result of the vertical displacement changes are given in figure 4.5.14, and the uplift data are superimposed on the model result. This model gives a less satisfactory fit to the uplift data than model 4L. The result has a broader extent of uplift compared with the data, and the uplift amplitude in the model is larger. This illustrates that the surface deformation is sensitive to the viscosity structure, and geodetic measurements can be used to constrain the possible

viscosity models.

4.6 Discussion

In this chapter, we will look at the data and models of the time dependent deformations in subduction zones. In general, a region with a long subduction history like Hokkaido and North Honshu has a rather complex structure. The origin of the tectonic features are not fully understood at the present time. The geodetic data also cannot be easily explained by a simple underthrust and rebound cycle. On the other hand, in Southwest Japan and Alaska, geodetic data seem to suggest a simple picture of an earthquake cycle: The coastal region is dragged down by the descending lithosphere before the great shallow earthquake, and it rebounds upward following the earthquake. We looked into some basic physical processes in this cycle. In section 4.3, we noticed that the time dependent deformations are very sensitive to the viscosity distribution. The movements induced by the earthquake originate primarily in the low viscosity zone. The high viscosity regions deform in response to the movements in the low viscosity region to maintain continuity and equilibrium. This sensitivity of deformation to viscosity makes geodetic data a valuable tool for probing the viscosity structure of a fault zone. In section 4.4, we looked into the interaction of preseismic slow slip and the earthquake. We found that deep preseismic slip stresses the earthquake fault zone and the earthquake in turn will load the deep aseismic slip zone. Viscoelastic interaction with the aseismic slip causes a stress recovery

effect in the aseismic slip region. Due to the load of the earthquake and the stress recovery effect, it is possible that afterslip occurs near the earthquake fault tip. In section 4.5, we constructed a series of models for the 1964 Alaskan earthquake and compared the model results with the time dependent geodetic data. The most important finding in this modelling is that with a realistic viscosity structure of a subduction zone, viscoelastic relaxation can explain the uplift data. In the modelling of a subduction zone, it is essential to include a high viscosity descending slab and a low viscosity region above the shear zone between the descending slab and the overiding lithosphere. Simpler model results can not fit the uplift data. Since surface deformations are sensitive to the viscosity in the fault zone, geodetic data can put stringent constraints on the possible viscosity models. As the viscosity is vitally relevent to stress accumulation and earthquake occurrence, the modelling should be used with the high quality data from space techniques to investigate earth structure.

As we have mentioned, the purpose of this study is not to fit the Alaskan data in detail with some complicated model. Rather, we are interested in bringing out the important physical processes for an observed time dependent phenomenon, and investigating the approach we can follow in the future when more data become available. In the process of finding earth structure from observed geodetic data,

there is the problem of uniqueness of the solution. With only one set of leveling data, there are other possible explanations. Brown el al (1977) examined the possible processes that could explain the uplift following the 1964 Alaskan earthquake. The possible processes were (1) creep on a buried fault, (2) viscoelastic rebound, (3) strain accumulation due to lithosphere loading, (4) magma intrusion, and (5) dilatancy effects. Brown et al (1977) concluded that magma intrusion and dilatancy effects were not the probable explanations for the observed phenomenon: there was no indication of magma activities in the region; and dilatancy predicts subsidence rather than uplift, contrary to what was observed. They thought that strain accumulation due to lithospheric loading and viscoelastic rebound might play a part in the uplifting process, but they did not think these two processes were important. Strain accumulation is too slow a process to cause such a rapid uplift. On the viscoelastic rebound, they quoted the results of Nur and Mavko (1974) to estimate the effects of viscoelastic relaxation. The magnitude of theoretical uplift was found different from the observed data. This is not surprising since a layered model does not reflect the structural features of a subduction zone. In addition, the solution of Nur and Mavko is a doubtful one; it has been criticized by Smith (1974) and Thatcher and Rundle (1979). Brown et al (1977) also doubted if the viscosity in the

fault zone could be as low as 5 x 10^{19} poise, as implied in the calculations by Nur and Mavko. There is no definite evidence to argue against or for this viscosity value in a fault zone. We are not aware of any heat flow measurements near the leveling route. There are volcanos about 100 km away from Anchorage. On the other hand, Barazangi et al (1975) studied the body wave attenuation in the Aleutian arc about 1000 km away from this region and found no evidence of a high attenuation zone there. We think the problem of the viscosity value in a fault zone is still open. However, when modelling a subduction zone, we should not be bound to use the viscosity value derived from the post glacial rebound data in continental areas. The shear heating may reduce the viscosity near the fault zone. In addition, the exact form of a constitutive relation between stress and strain is not known. If strain rate is proportional to a certain power of stress, the effective viscosity in a fault zone will be lowered due to the high stress there.

The favored explanation of the uplift data by Brown et al (1977) is the deep aseismic slip on an extension of the fault plane which ruptured during the 1964 earthquake. A 2.3 m slip dipping 25 degrees on a buried fault segment about 50 km wide near Anchorage gives a satisfactory fit to the uplift at 1975 (Brown et al 1977). In order to expalin the migration of maximum uplifts from the inland toward the trench, Brown et al suggested the following process: In

south central Alaska, the megathrust zone between the North American plate and the underthrusting Pacific plate can be divided into two major segments. The 1964 Alaskan earthquake ruptured the upper section of the lithosphere where the material is brittle. The lower segment of lithosphere is dominated by viscous creep. The segment of the fault which is inferred to be responsible for the postseismic movement is in a transition zone between the pure stick slip and the pure creep behavior. The rupture of the brittle upper segment loads the transition zone, which then proceeds to fail via viscous creep. If the time constant of the creep mechanism decreases with depth along the fault, the effects of the slip on the lower portions will be felt first and peak out before those of the upper portions. Smaller time constants imply smaller effective viscosities, which may be associated with the geothermal gradient in the area. The lower portions, being hotter, should have smaller time constant of creep.

In the process proposed by Brown et al, it is assumed that a zone of low viscosity exists in the downdip extension region of the earthquake fault. The relaxation time of the region should be less than ten years so that the effects of migration of maximum uplifts can be seen within one decade after the event. The existence of such a low viscosity region is essential in the interpretations by Brown et al: If such a low viscosity zone does not exist,

the aseismic slip should occur near the earthquake fault tip rather than further downdip, since the load caused by the earthquake decreases rapidly with distance and the frictional strength of the fault increases with depth. It would then be difficult to explain the gap between the aseismic slip zone and the earthquake fault; it would also be difficult to explain why the slip went updip. If such a low viscosity zone exists, the viscoelastic relaxation effect after the earthquake should be evaluated. In section 4.5 we see that the deformation pattern due to relaxation in the downdip extension region of the fault is that of a reversed slip (cf. figure 4.5.11d). In a sense, the relaxation has produced some kind of aseismic slip, except that the slip does not occur discontinuously across a surface, and the deformation pattern changes continuously but rapidly in a zone. However, in the relaxation model, the trenchward migration of maximum uplift comes about as a natural result of the structure of the subduction zone. Brown et al assumed the existence of a low viscosity zone but did not calculate the effect of the viscoelastic relaxation, instead they imposed aseismic slips to fit the data. In a sense, the relaxation models give a more complete description of the physical process. We don't have to imposed the aseismic slip in an ad hoc fashion, and the viscosity model used in the calculation is a realistic model of the subduction zone. The roles of a descending slab and

a low viscosity zone above the descending slab are essential in the relaxation model: The descending slab guides the flow direction in the low viscosity zone. Had there been no desending slab, the vertical deformation on the surface would be dominated by subsidence near the lower fault tip, because the material movement will be mainly downwards there, as in the layered models in section 4.5

Thus in some sense the relaxation model contains the aseismic slip model. However, the relaxation model is constructed with our knowledge of the subduction zone; the comparison of geodetic data and models thus provides us with the information on the viscosity structure in a subduction zone. If our interpretation is correct, the vertical deformation from Whittier to Anchorage should still be uplift in the next decade but with decreased uplift rate. Figure 4.6.1 gives the prediction by using the results of model 4L. The theoretical uplifts at 1.1, 3.6, 11, 13.2, 19.1 and 27.5 years after the event are shown in figure 4.6.1. It must be clarified that even if this prediction comes true, by using only one leveling route, it is not possible to acertain the viscosity structure of Alaska. We have few constraints on the trench side. However, the general features of the uplift data can be explained by viscoelastic relaxation in a fault zone with a descending slab, a low viscosity layer below the lithosphere, and a low viscosity zone above the shear zone. These are probably the

basic elements of a subduction zone structure. For more detailed structures of subduction regions, more geodetic measurements are needed.

Addendum:

A paper (Wahr and Wyss 1980) appeared after this thesis had been drafted. Wahr and Wyss (1980) modelled the post-seismic uplift of the 1964 Alaskan earthquake with a two dimensional finite element model. Their model consists of an elastic half space and a viscoelastic inclusion. The viscoelastic inclusion models the low viscosity wedge above the shear zone. They found that the uplift from Whittier to Anchorage at 1975 can be fit by a model having an inclusion viscosity 1.2×10^{19} to 2.2×10^{19} poise. This viscosity value is similar to our results in this chapter. However, the maxima of uplift migrate away from the trench in their model, in the opposite direction as the data indicated. Models 4L and 4M in this chapter included more features of the subduction region and the migration direction of maximum uplift conformed to what was observed.

Figure Captions - Chapter 4

Figure 4.2.1. Tonankai and Nankaido earthquakes. The aftershock area 1 day after the main shock is shown by solid curves and that after one month by dashed curves. The solid polygon shows the projection of the theoretical fault plane from Fitch and Scholz (1971). The leveling result from points a to b is given in figure 4.2.2. Point b is Muroto Promontory, which is the closest point to the trench along the leveling route. (Reproduced from Kanamori 1973).

Figure 4.2.2 Pre-, co- and post-seismic vertical deformation along the route from a to b in figure 4.2.1. (Reproduced from Kanamori 1973).

Figure 4.2.3 Observed and calculated vertical displacements for the 1964 Alaska earthquake along a cross section through Montague and Middleton Islands. (Reproduced from Hastie and Savage 1970).

Figure 4.2.4 Simplified tectonic map of South Central Alaska. The epicenter of the 1964 Alaska earthquake is denoted by a circled star. The route of the leveling profile is shown as a light dashed line. (Reproduce from Brown et al 1971).

Figure 4.2.5 Profile of the elevation change along the leveling line shown in figure 4.2.4. (Reproduced from Brown et al 1977).

Figure 4.3.1 (a) The finite element grid used for model 4A and 4B. The grid region is 2,200 km long and 1,000 km deep. It has 1412 degrees of freedom and 651 elements. (b) The fault model used for model 4A and 4B. The fault is located between -200 km and 0 km in the horizontal coordinate and between 5 and 40 km in depth in the finite element grid coordinate system. The fault has 12 m reverse slip along the solid line segment and the slip tapers off near the ends along the segments of dashed lines.

Figure 4.3.2 (a) The displacement vectors at selected locations immediately after the event for model 4A. The small circles indicate the locations where the calculations are made. The small line segments stemming from the circles indicate the displacements at the locations. A scale of the displacement is given in the lower left corner and a scale of the map is given in the lower right corner. The thick line indicates the location of the earthquake fault. (b) The same plot at 1.1 years after the event. (c) The same plot at 3.6 years after the event. (d) The same plot at 11.0 years after the event.

Figure 4.3.3 (a) The changes of displacement vectors at selected locations at 1.1 years after the event for model 4A. The small circles indicate the locations

where the calculations are made. The small line segments stemming from the circles indicate the changes of displacements at the locations. A scale of the displacement is given in the lower left corner and a scale of the map is given in the lower right corner. The thick line indicates the location of the earthquake fault. (b) The same plot at 3.6 years after the event. (c) The same plot at 11.0 years after the event.

Figure 4.3.4 The vertical displacement changes on the free surface at 1.1, 3.6 and 11.0 years after the event for model 4A

Figure 4.3.5 (a) The displacement vectors at selected locations immediately after the event for model 4B. The small circles indicate the locations where the calculations are made. The small line segments stemming from the circles indicate the displacements at the locations. A scale of the displacement is given in the lower left corner and a scale of the map is given in the lower right corner. The thick line indicates the location of the earthquake fault. (b) The same plot at 1.1 years after the event. (c) The same plot at 3.6 years after the event. (d) The same plot at 11.0 years after the event.

Figure 4.3.6 (a) The changes of displacement vectors at

selected locations at 1.1 years after the event for model 4B. The small circles indicate the locations where the calculations are made. The small line segments stemming from the circles indicate the changes of displacement at the locations. A scale of the displacement is given in the lower left corner and a scale of the map is given in the lower right corner. The thick line indicates the location of the earthquake fault. (b) The same plot at 3.6 years after the event. (c) The same plot at 11.0 years after the event.

Figure 4.3.7 The vertical displacement changes on free surface at 1.1, 3.6 and 11.0 years after the event for model 4B Figure

Figure 4.3.8 The schematic diagram of the fault and the viscosity structure for model 4C. The fault has uniform slip of 10 m from 0 to 40 km deep and tapers off to zero at 45 km deep. The numbers with exponents are viscosity values in poise.

Figure 4.3.9 Finite element grid for models 4C and 4D.

Figure 4.3.10 (a) The displacement vectors at selected locations immediately after the event for model 4C. The small circles indicate the locations where the calculations are made. The small line segments stemming from the circles indicate the displacements at

the locations. A scale of the displacement is given in the lower left corner and a scale of the map is given in the lower right corner. The thick line indicates the location of the earthquake fault. (b) The same plot at 5.2 years after the event. (c) The same plot at 25.7 years after the event.

Figure 4.3.11 (a) The changes of displacement vectors at selected locations at 5.2 years after the event for model 4C. The small circles indicate the locations where the calculations are made. The small line segments stemming from the circles indicate the changes of displacements at the locations. A scale of the displacement is given in the lower left corner and a scale of the map is given in the lower right corner. The thick line indicates the location of the earthquake fault. (b) The same plot at 25.7 years after the event.

Figure 4.3.12 Vertical displacement change on the free surface at 0.0, 5.2 and 25.7 years after the event for model 4C.

Figure 4.3.13 (a) The displacement vectors at selected locations immediately after the event for model 4D. The small circles indicate the locations where the calculations are made. The small line segments stemming from the circles indicate the displacements at

the locations. A scale of the displacement is given in the lower left corner and a scale of the map is given in the lower right corner. The thick line indicates the location of the earthquake fault. (b) The same plot at 5.2 years after the event. (c) The same plot at 25.7 years after the event.

Figure 4.3.14 (a) The changes of displacement vectors at selected locations at 5.2 years after the event for model 4D. The small circles indicate the locations where the calculations are made. The small line segments stemming from the circles indicate the changes of displacements at the locations. A scale of the displacement is given in the lower left corner and a scale of the map is given in the lower right corner. The thick line indicates the location of the earthquake fault. (b) The same plot at 25.7 years after the event.

Figure 4.3.15 Vertical displacement change on the free surface at 0.0, 5.2 and 25.7 years after the event for model 4D.

Figure 4.4.1 The vertical displacement on the free surface for a buried fault model (model 4E). The fault model is given in the lower figure. The fault is located between 40 and 80 km deep. The dip angle is 21.8 degrees. The maximum slip is 1 m and the fault slip

tapers off along the dotted line near the ends of the fault.

Figure 4.4.2 The vertical displacement on the free surface for a buried fault model (model 4F). The fault model is given in the lower figure. The fault is located between 40 and 80 km deep. The dip angle is 45 degrees. The maximum slip is 1 m and the fault slip tapers off along the dotted section near the ends of the fault.

Figure 4.4.3 The finite element grid for model 4G and 4H.

Figure 4.4.4 (a) The time dependence of the slip between 45 and 75 km deep of the fault in model 4G and 4H. The slip tapers off to zero between 45 and 40 km deep and between 75 and 80 km deep. (b) The time dependence of slip along the upper 40 km of the fault in model 4G and 4H.

Figure 4.4.5 The shear stress parallel to 45 degree dip at three locations in the stick slip region for model 4G. The locations are indicated in the inset. Positive stress implies that stress is accumulating and negative stress implies that stress is relieved from the reference stress state.

Figure 4.4.6 The shear stress parallel to 45 degree dip at

three locations in the aseismic slip region for model 4G. The locations are indicated in the inset.

Figure 4.4.7 Schematic diagram for model 4H. The hatched area has a low viscosity 10^{20} poise. The lithosphere and the descending slab has a viscosity of 10^{25} poise. The fault dip is 45 degrees and extends from 0 to 80 km. The lower 40 km slips aseismically; the upper 40 km ruptures abruptly during the earthquake.

Figure 4.4.8 The shear stress parallel to 45 degree dip at three locations in the stick slip region for model 4H. The locations are indicated in the inset.

Figure 4.4.9 The shear stress parallel to 45 degree dip at three locations in the aseismic slip region for model 4H. The locations are indicated in the inset.

Figure 4.5.1 (a) The finite element grid used for studying the 1964 Alaska earthquake. The grid region is 2,200 km long and 1,000 km deep. It has 1412 degrees of freedom and 651 elements. (b) The fault model used for studying the 1964 Alaska earthquake. The fault is located between -200 km and 0 km in horizontal coordinate and between 5 and 40 km in depth in the finite element grid coordinate system. The fault has 12 m reverse slip along the solid line segment and the slip tapers off near the ends along the segments of the dashed lines.

Figure 4.5.2 The coseismic vertical displacement on the free surface for the fault model in figure 4.5.1

Figure 4.5.3 The vertical displacement change on the free surface for model 4I. The observed uplift data from Brown et al are also superimposed on the figure. The model results are at 1.1, 3.6 and 11 years after the event for curves 1, 2 and 3. The observed uplifts at 1965, 1968 and 1975 are denoted by crosses, circles and stars.

Figure 4.5.4 The vertical displacement change on the free surface for layered model 4J. The observed uplift data from Brown et al are also superimposed on the figure. The model results are at 1.1, 3.6 and 11 years after the event. The observed uplifts are from 1965, 1968 and 1975. Notice the vertical scale change from figure 4.5.3.

Figure 4.5.5 The viscosity distribution for model 4K. There is a short descending lithosphere to 160 km deep. The descending lithosphere has a viscosity 10^{25} poise. Other parameters are the same as model 4I.

Figure 4.5.6 The vertical displacement change on the free surface for model 4K. The observed uplift data from Brown et al are also superimposed on the figure. The model results are at 1.1, 3.6 and 11 years after the

event. The observed uplifts are at 1965, 1968 and 1975.

Figure 4.5.7 The viscosity distribution for model 4L. The descending slab is the same as in model 4K, but there is a low viscosity zone above the shear zone between the descending and overiding lithospheres. The viscosity is assumed to be $2.\times 10^{19}$ poise there.

Figure 4.5.8 The vertical displacement change on free surface for model 4L. The observed uplift data from Brown et al are also superimposed on the figure. The model results are at 1.1, 3.6 and 11 years after the event. The observed uplifts are at 1965, 1968 and 1975.

Figure 4.5.9 The vertical displacement change from -280 km to -180 km for model 4L. Results are enlarged from figure 4.5.8. The uplift from Whittier to Anchorage is superimposed on the figure.

Figure 4.5.10 (a) The displacement vectors at selected locations immediately after the event for model 4L. The small circles indicate the locations where the calculations are made. The small line segments stemming from the circles indicate the displacements at the locations. A scale of the displacement is given in the lower left corner and a scale of the map is given

in the lower right corner. The thick line indicates the location of the earthquake fault. The boundaries of low viscosity zones and the descending slab are also indicated on the plot. (b) The same plot at 1.1 years after the event. (c) The same plot at 3.6 years after the event. (d) The same plot at 11.0 years after the event.

Figure 4.5.11 (a) The changes of displacement vectors at selected locations at 1.1 years after the event for model 4L. The small circles indicate the locations where the calculations are made. The small line segments stemming from the circles indicate the changes of displacements at the locations. A scale of the displacement is given in the lower left corner and a scale of the map is given in the lower right corner. The thick line indicates the location of the earthquake fault. The boundaries of the descending slab and the low viscosity zone are also indicated on the plot. (b) The same plot at 3.6 years after the event. (c) The same plot at 11.0 years after the event. (d) The same plot as figure (c) with a reduced displacement scale. The boundaries of descending slab and low viscosity zones are also indicated in the figure. Notice that along the two sides of the dashed line, the displacements have opposite directions as if there were a dislocation there.

Figure 4.5.12 The viscosity ditribution for model 4M. The only difference from model 4L is that there is a longer descending slab. The zigzag contour of the descending slab is due to the finite element discretization, but it has little effects on the vertical displacement on free surface.

Figure 4.5.13 The vertical displacement change on free surface for 4M. The observed uplift data from Brown et al are also superimposed on the figure. The model results are at 1.1, 3.6 and 11 years after the event. The observed uplifts are from 1965, 1968 and 1975.

Figure 4.5.14 The vertical displacement change on free surface for layered model 4N. The observed uplift data from Brown et al are also superimposed on the figure. The model results are at 1.1, 3.6 and 11 years after the event. The observed uplifts are form 1965, 1968 and 1975.

Figure 4.6.1 The predicted vertical displacement change from Whittier to Anchorage from model 4L. The curves indicated by 1, 2, 3, 4, 5 and 6 are at 1.1, 3.6, 11, 13.2, 19.1 and 27.5 years after the event

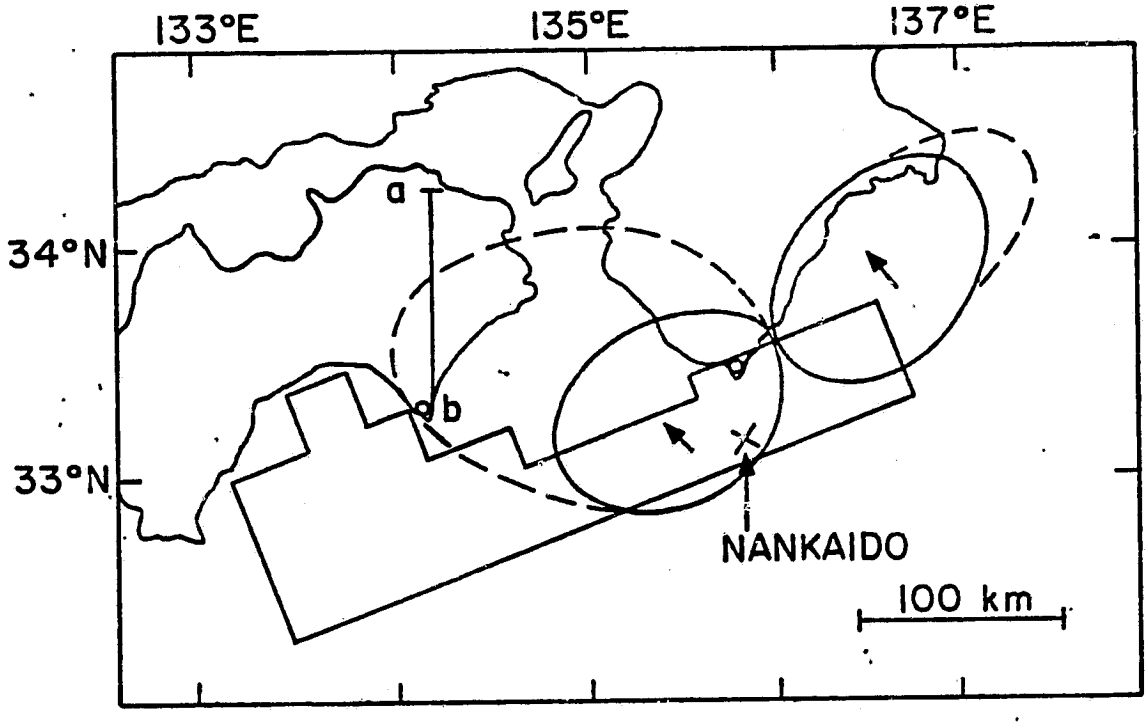

Fig. 4.2.1

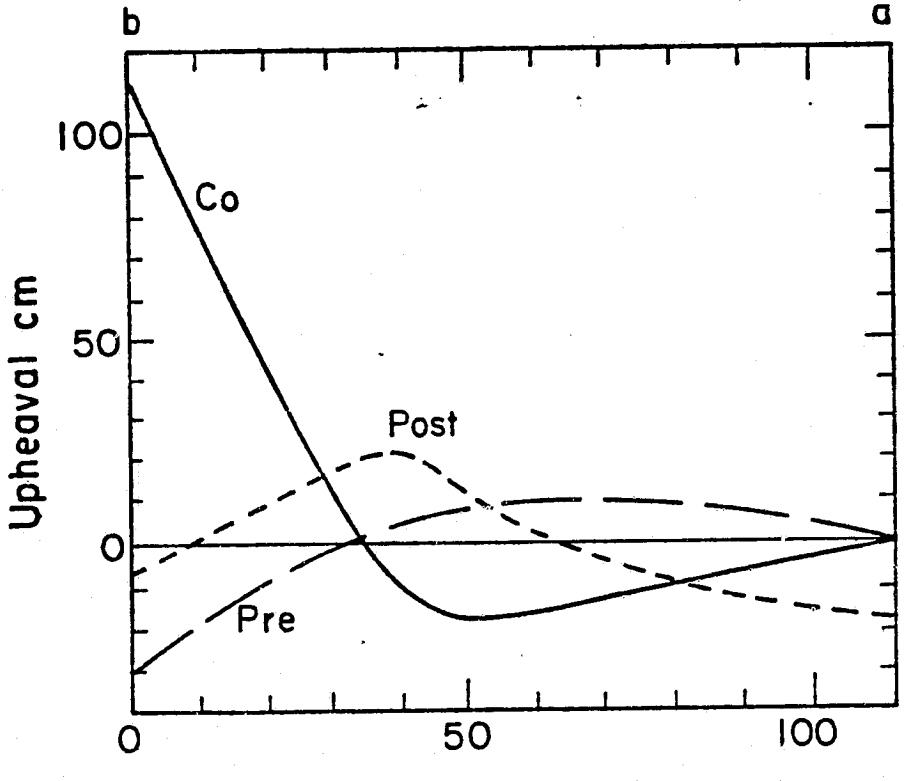

Fig. 4.2.2

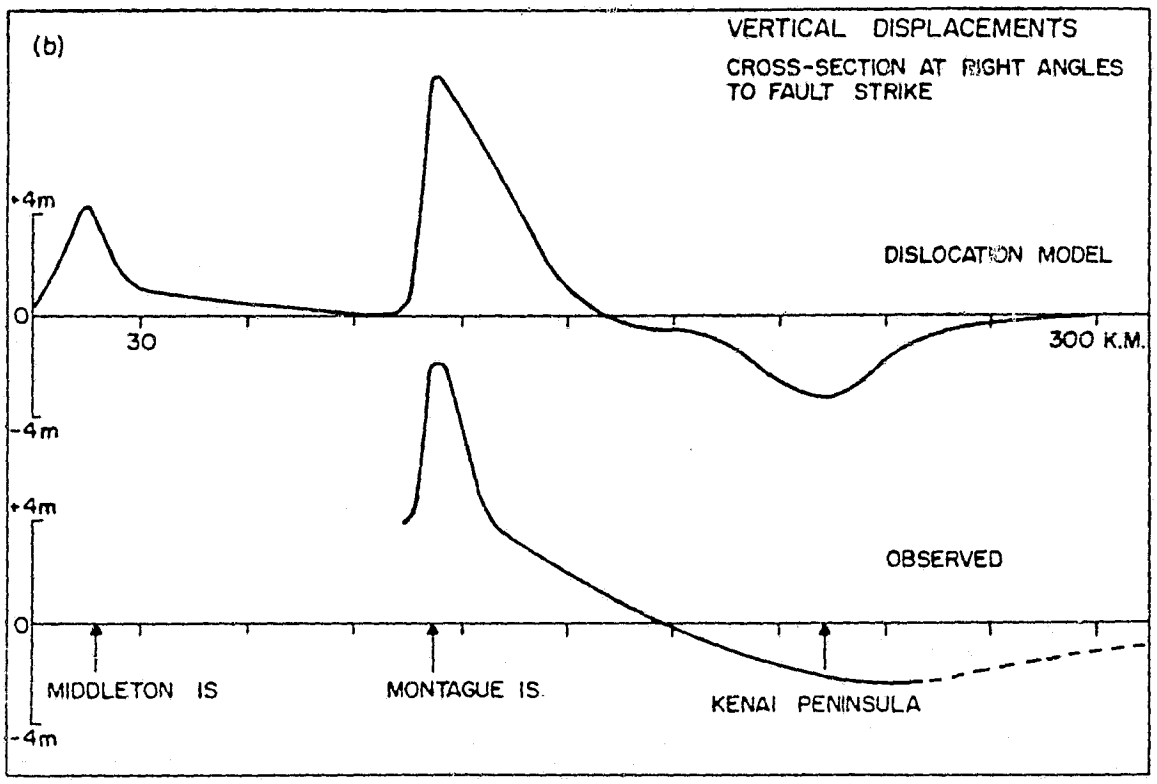
(b)
VERTICAL DISPLACEMENTS
CROSS-SECTION AT RIGHT ANGLES TO FAULT STRIKE
+4m
0
-4m
DISLOCATION MODEL
30
300 K.M.
+4m
0
-4m
OBSERVED
MIDDLETON IS
MONTAGUE IS.
KENAI PENINSULA

Fig. 4.2.3

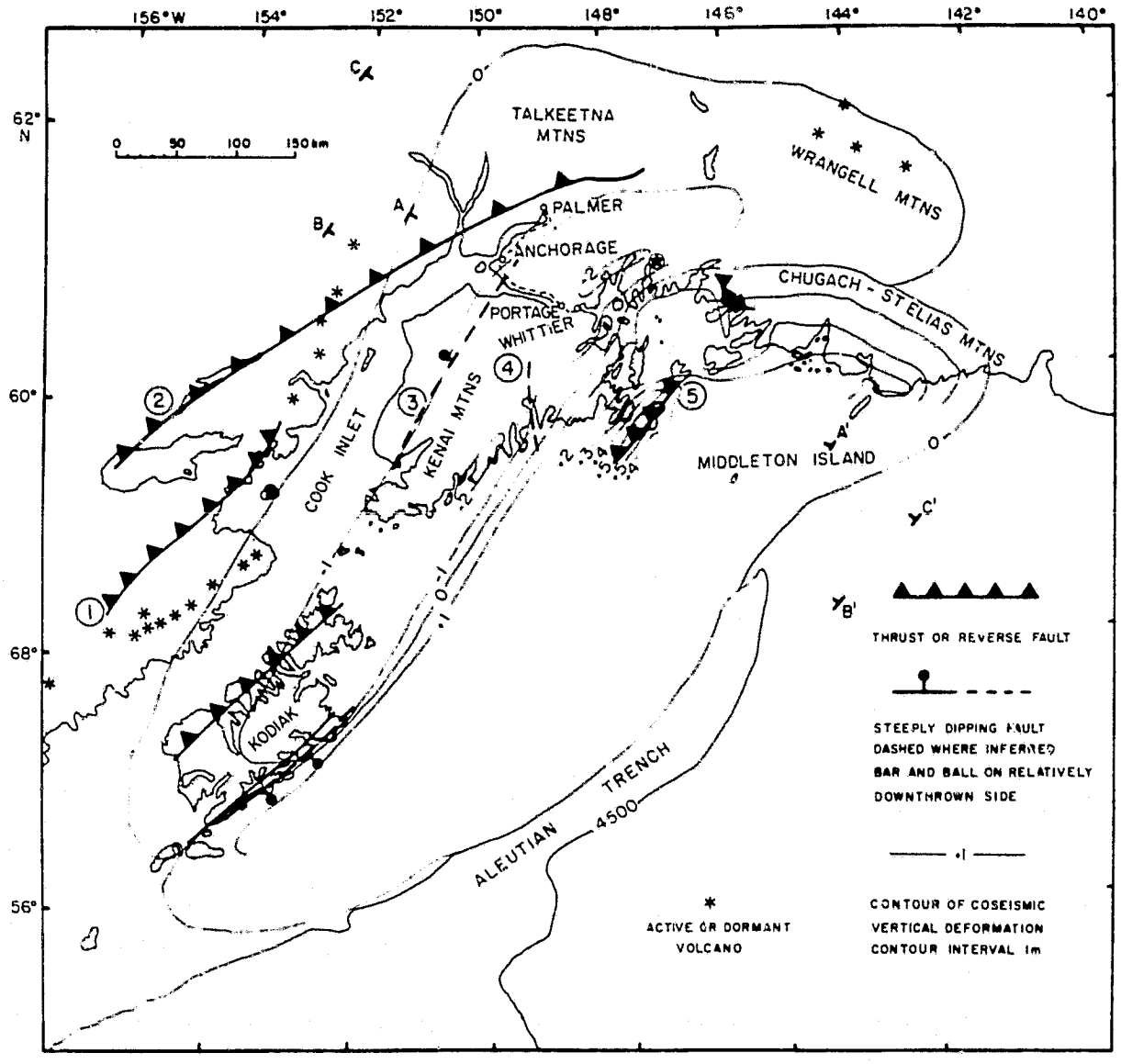
156°W
154°
152°
150°
148°
146°
144°
142°
140°
62° N
60°
68°
56°
0 50 100 150 km
TALKEETNA MTNS
WRANGELL MTNS
PALMER
ANCHORAGE
PORTAGE
WHITTIER
CHUGACH - ST ELIAS MTNS
COOK INLET
KENAI MTNS
MIDDLETON ISLAND
KODIAK
ALEUTIAN TRENCH
4500
A
A'
B
B'
C
C'
THRUST OR REVERSE FAULT
STEEPLY DIPPING FAULT
DASHED WHERE INFERRED
BAR AND BALL ON RELATIVELY
DOWNTHROWN SIDE
CONTOUR OF COSEISMIC
VERTICAL DEFORMATION
CONTOUR INTERVAL 1m
ACTIVE OR DORMANT
VOLCANO

Fig. 4.2.4

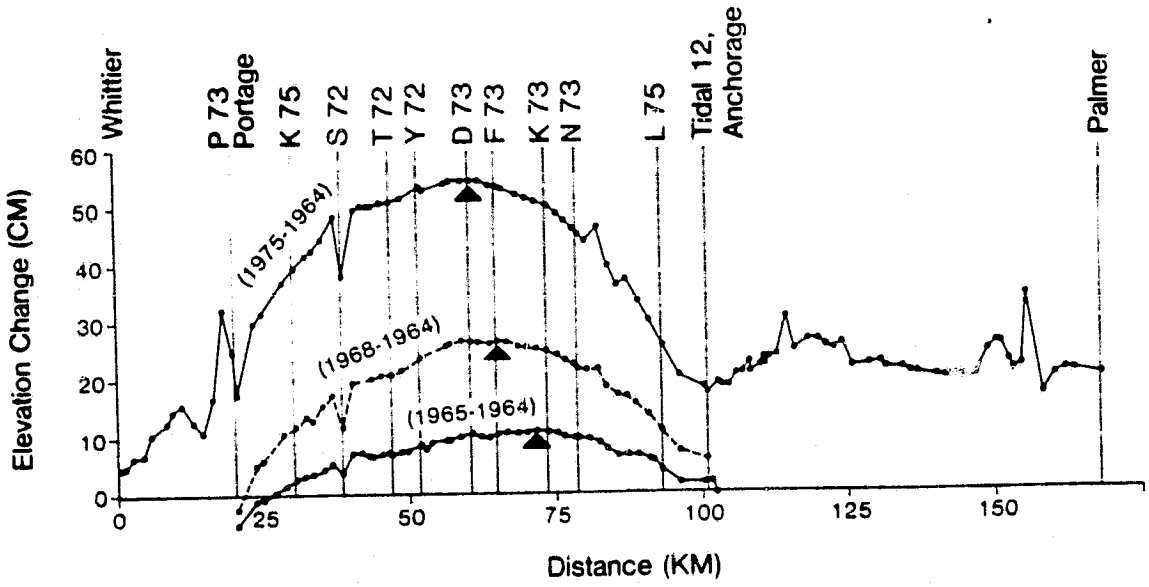
Whittier
P 73
Portage
K 75
S 72
T 72
Y 72
D 73
F 73
K 73
N 73
L 75
Tidal 12,
Anchorage
Palmer
(1975-1964)
(1968-1964)
(1965-1964)
Elevation Change (CM)
60
50
40
30
20
10
0
0
25
50
75
100
125
150
Distance (KM)

Fig. 4.2.5

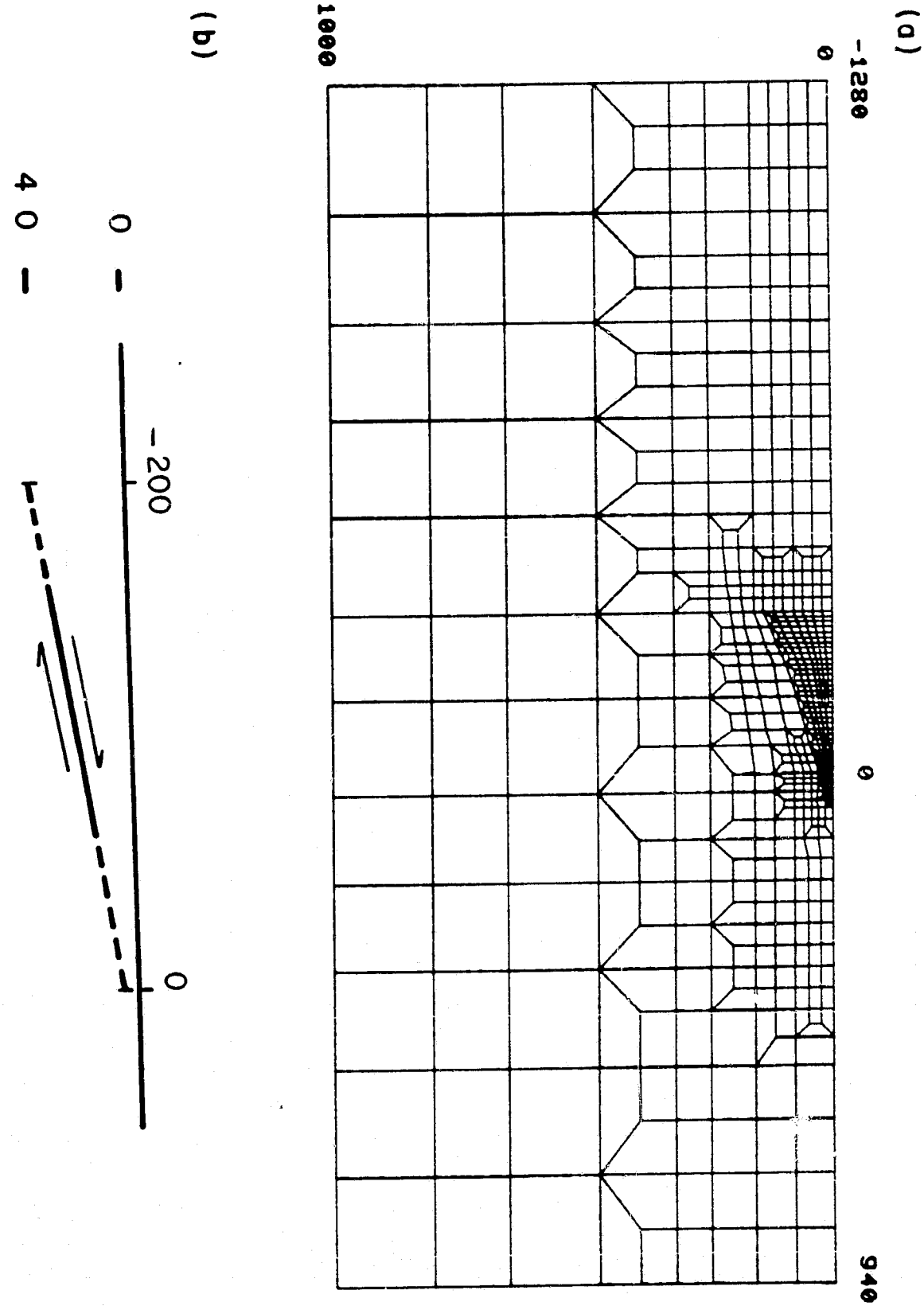

Fig. 4.3.1

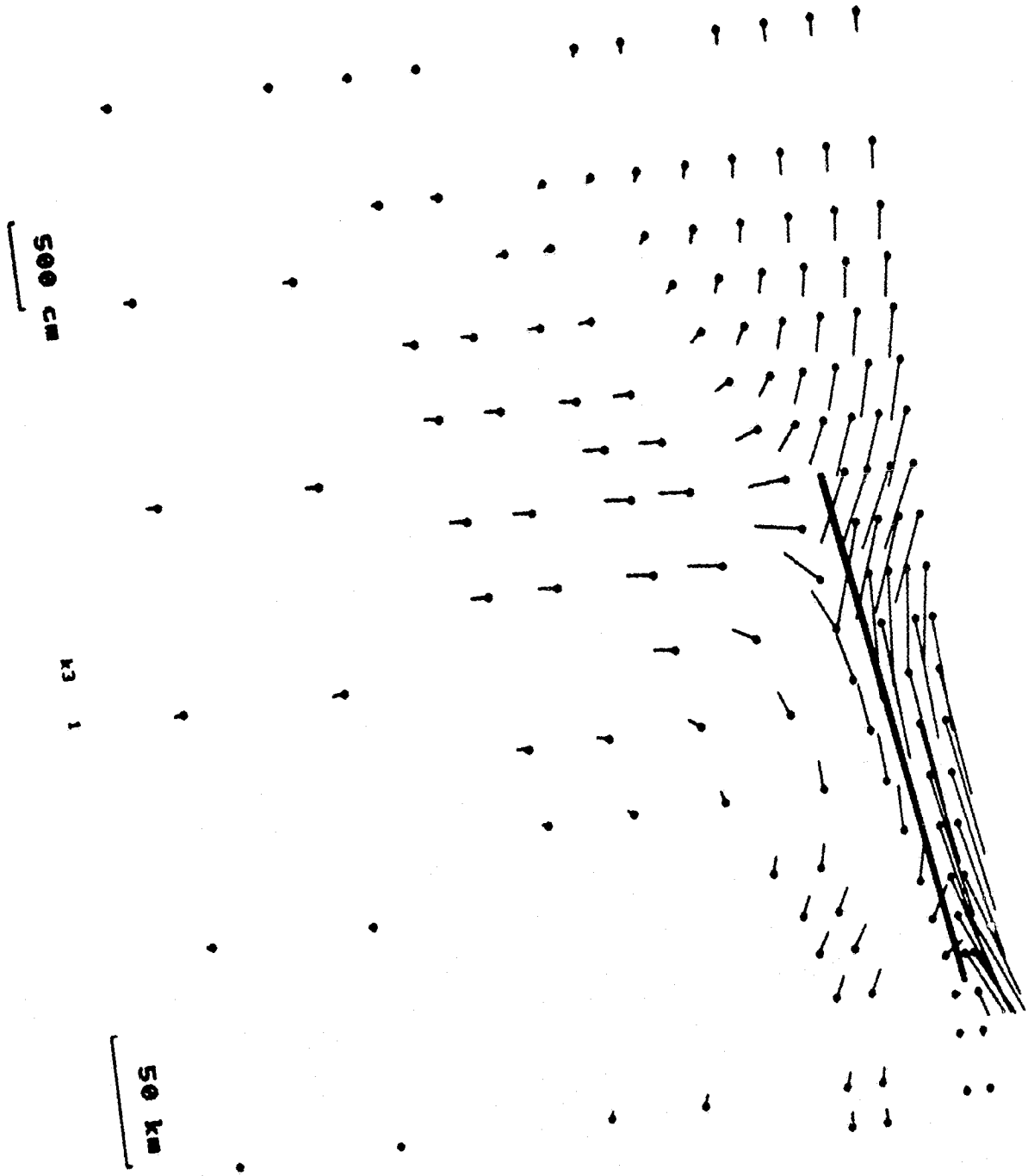

Fig.4.3.2 a

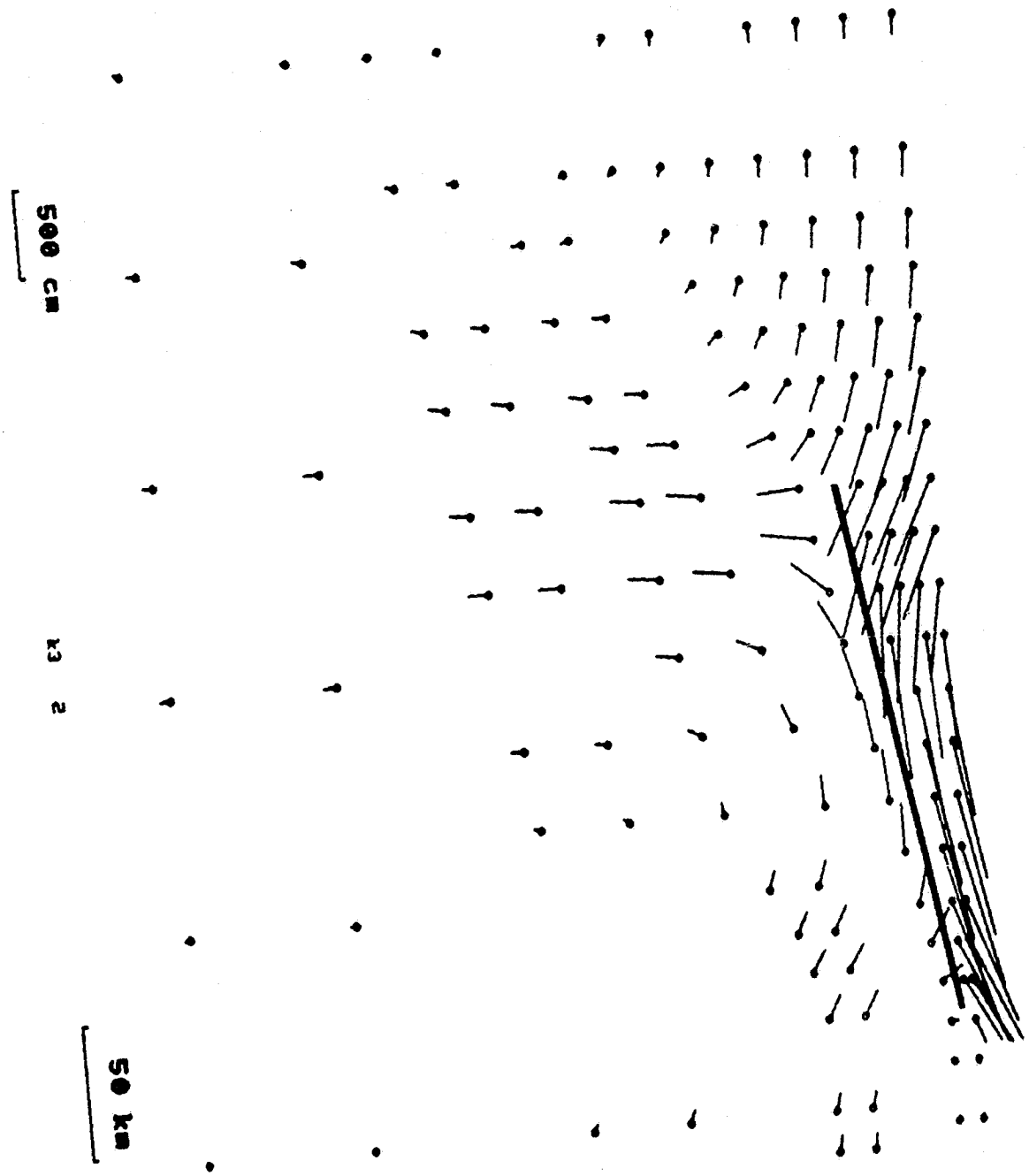

Fig. 4.3.2 b

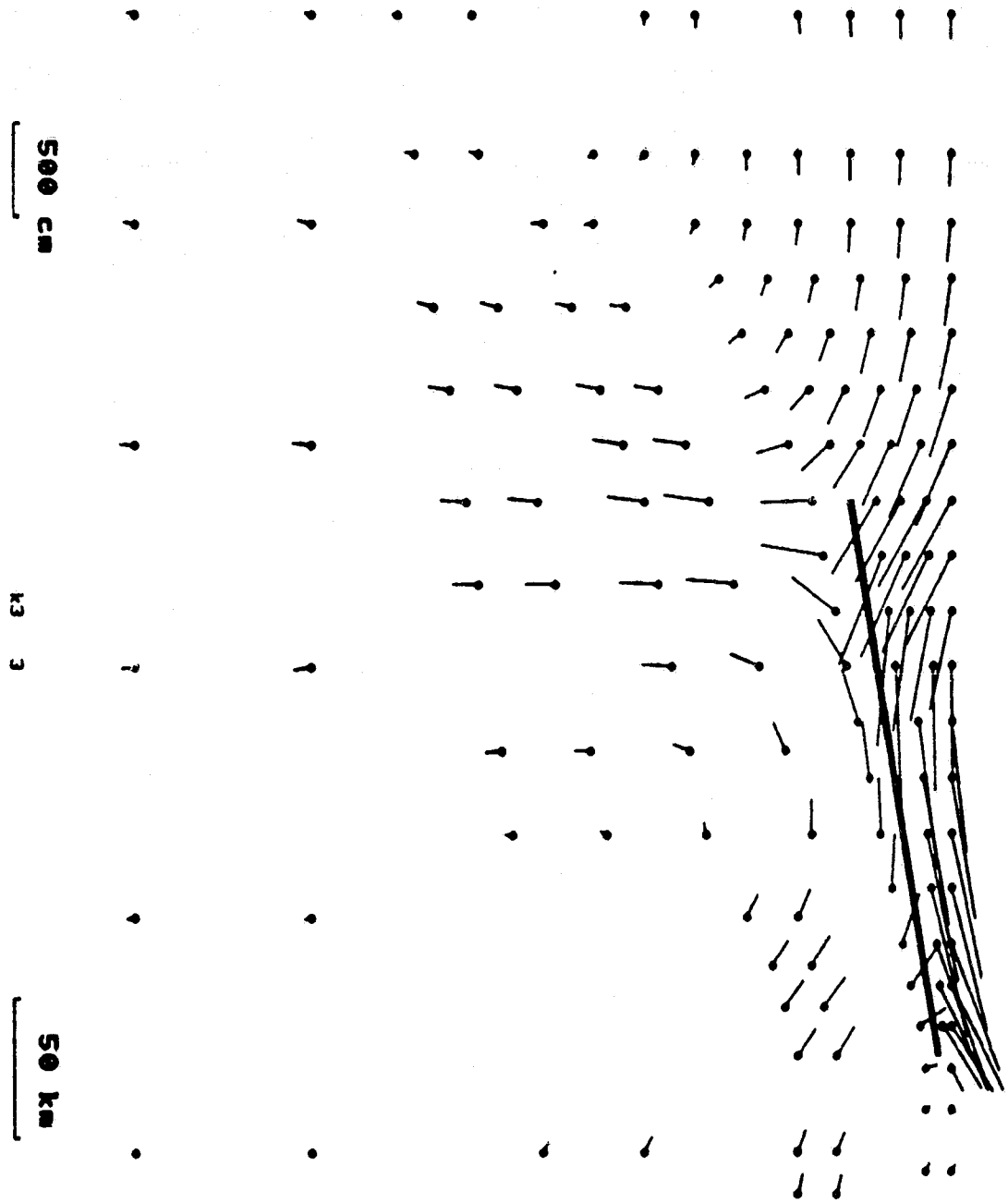

Fig. 4.3.2 c

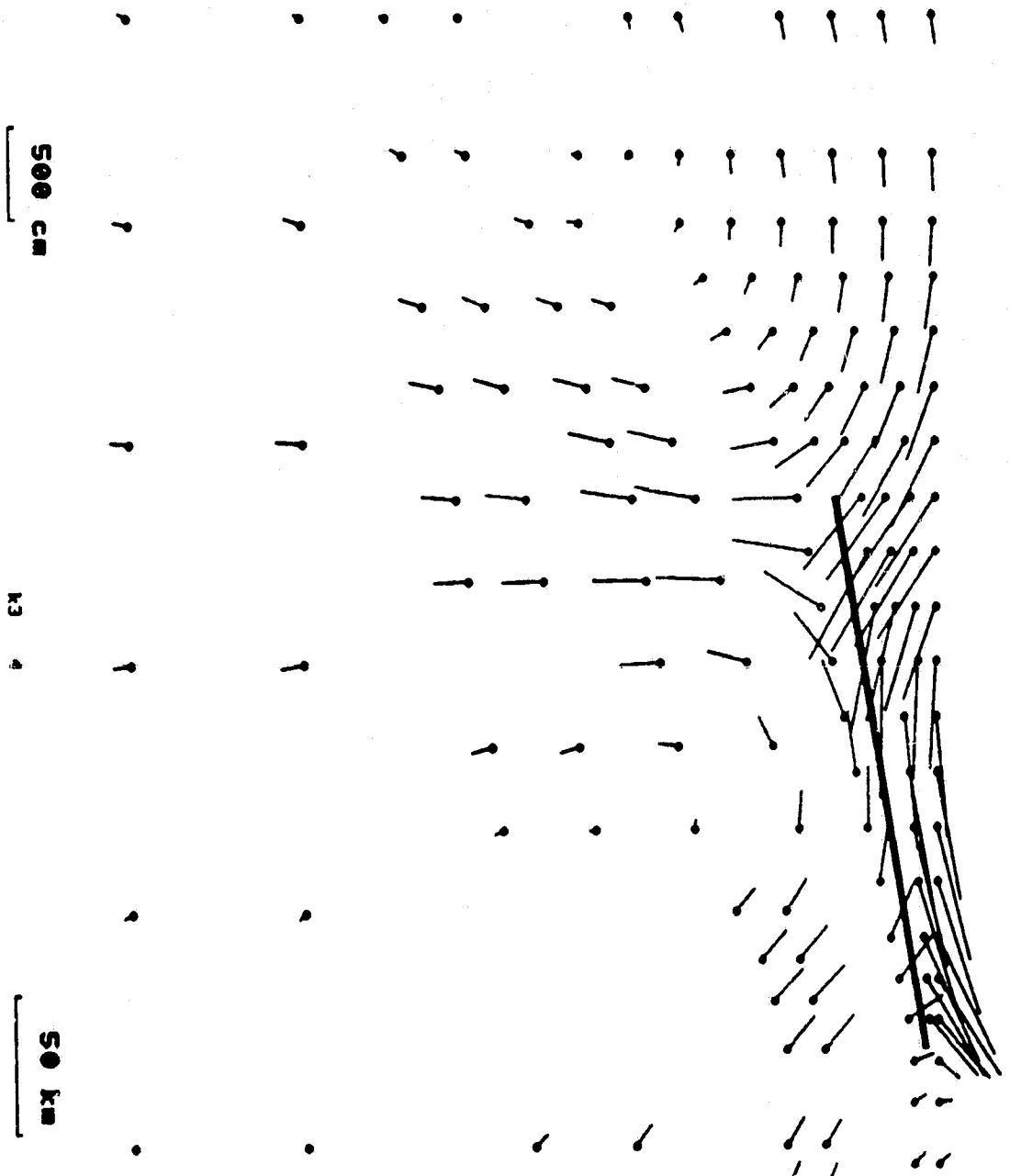

Fig. 4.3.2. d

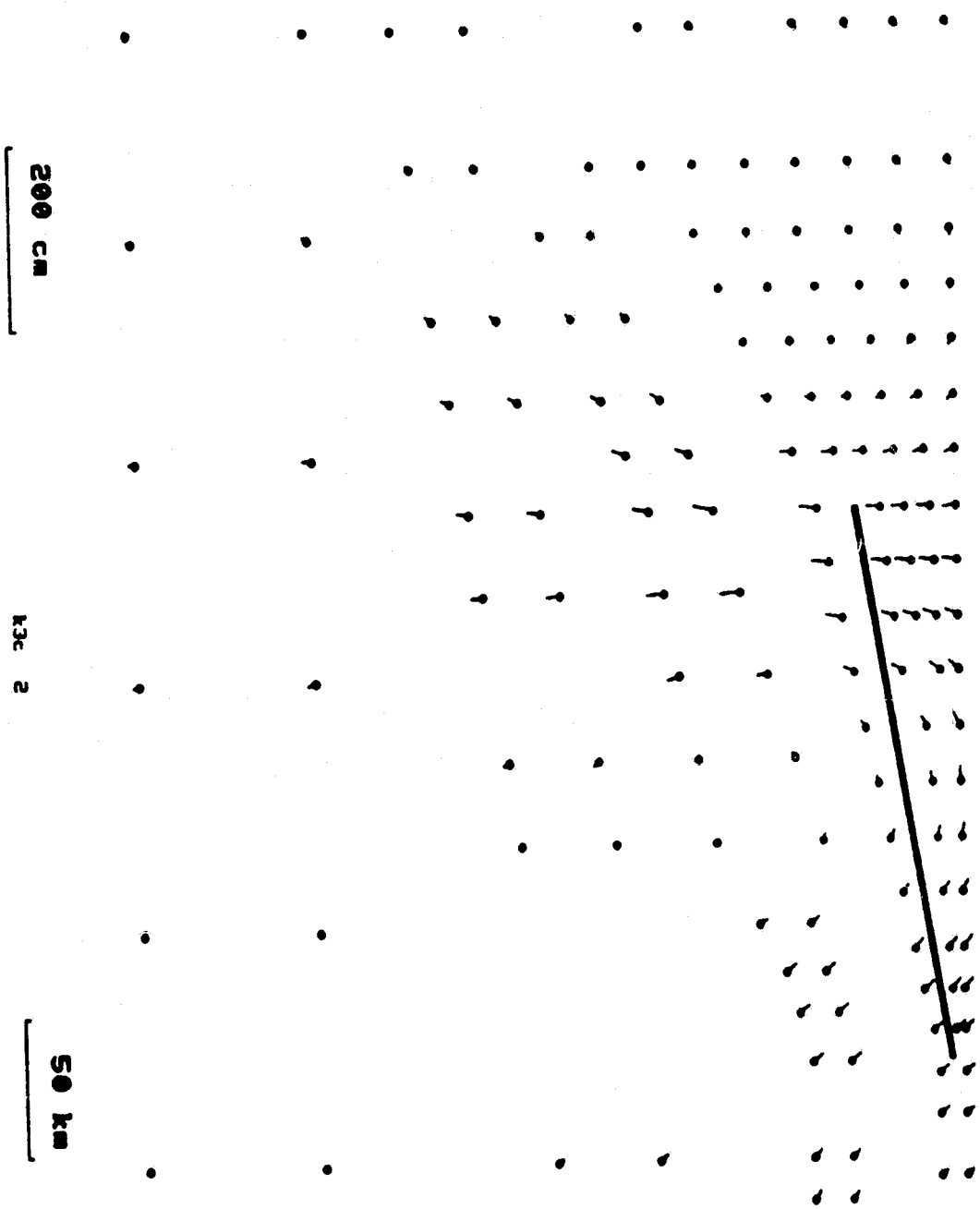

Fig. 4.3.3 a

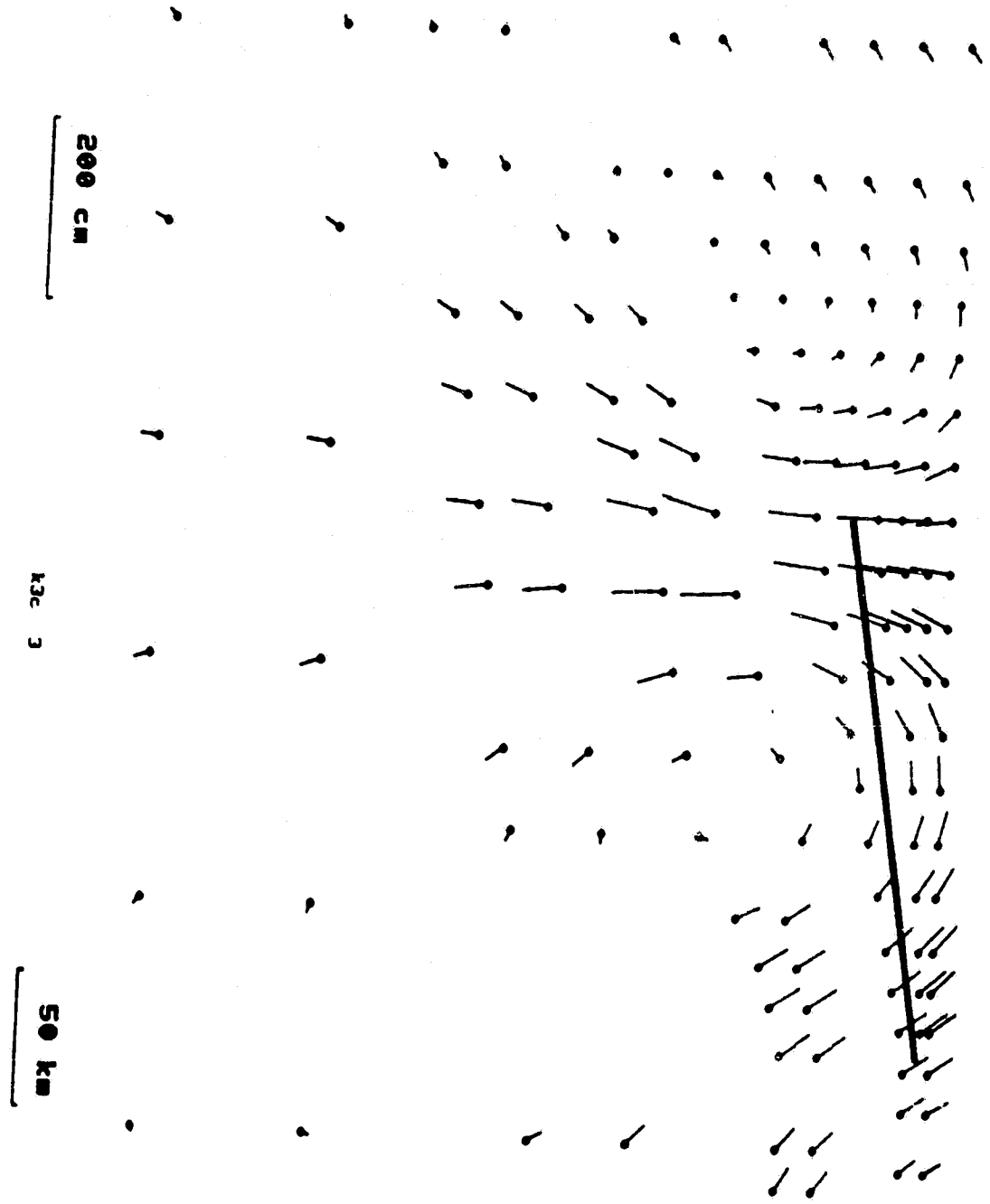

Fig. 4.3.3 b

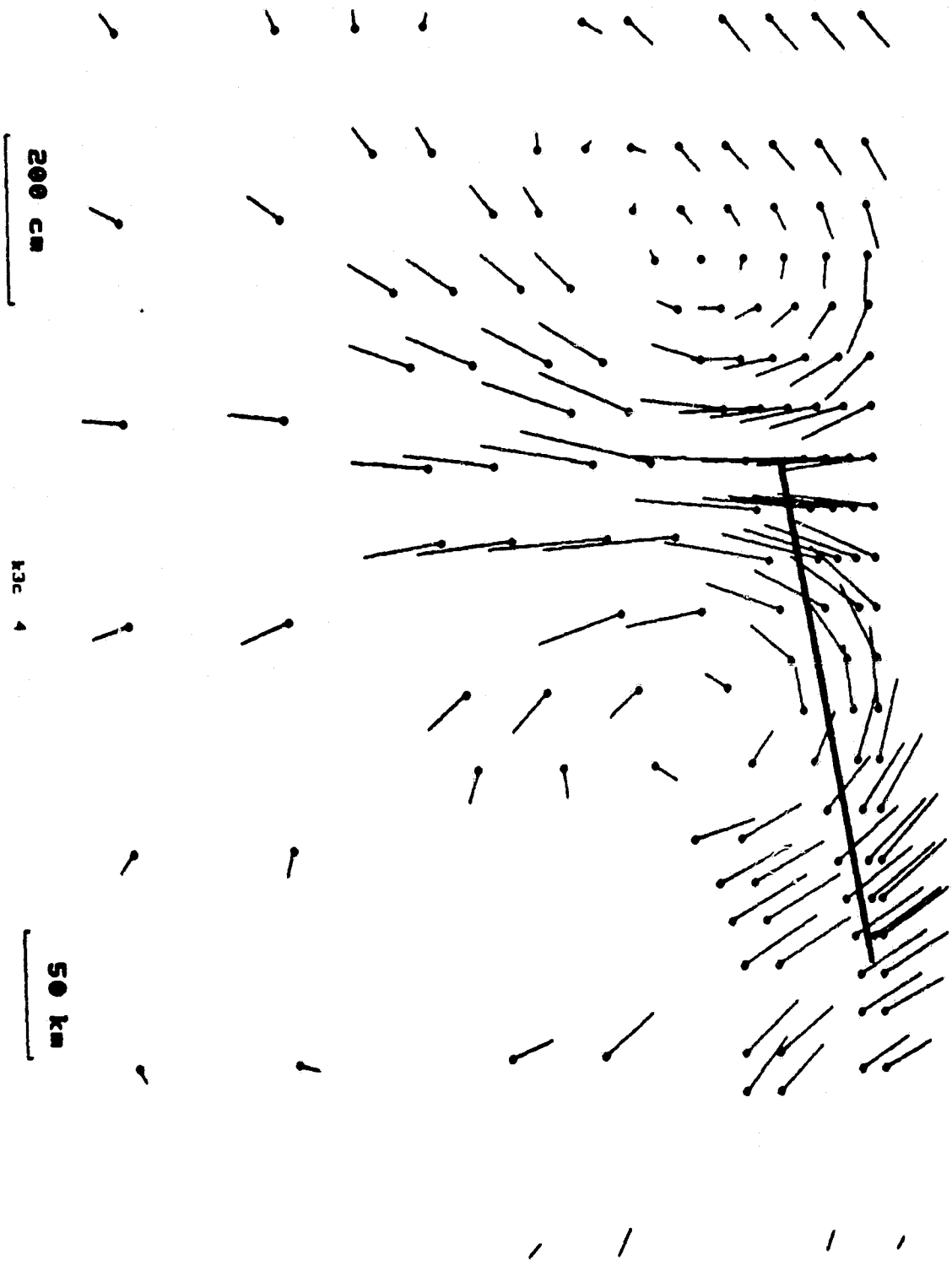

Fig. 4.3.3 c

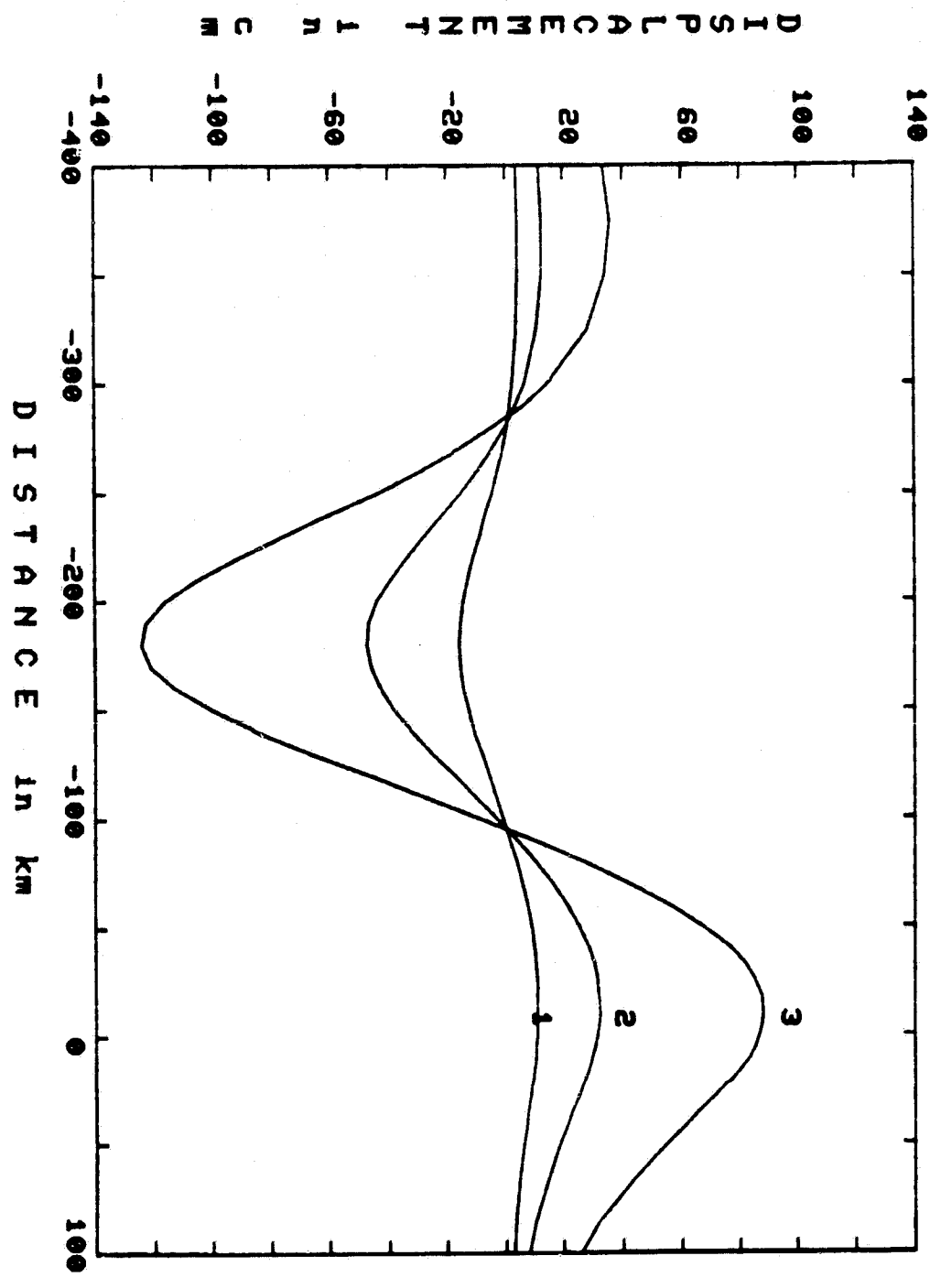
DISPLACEMENT in cm
-140
-100
-60
-20
20
60
100
140
-400
-300
-200
-100
0
100
DISTANCE in km
1
2
3

Fig. 4.3.4

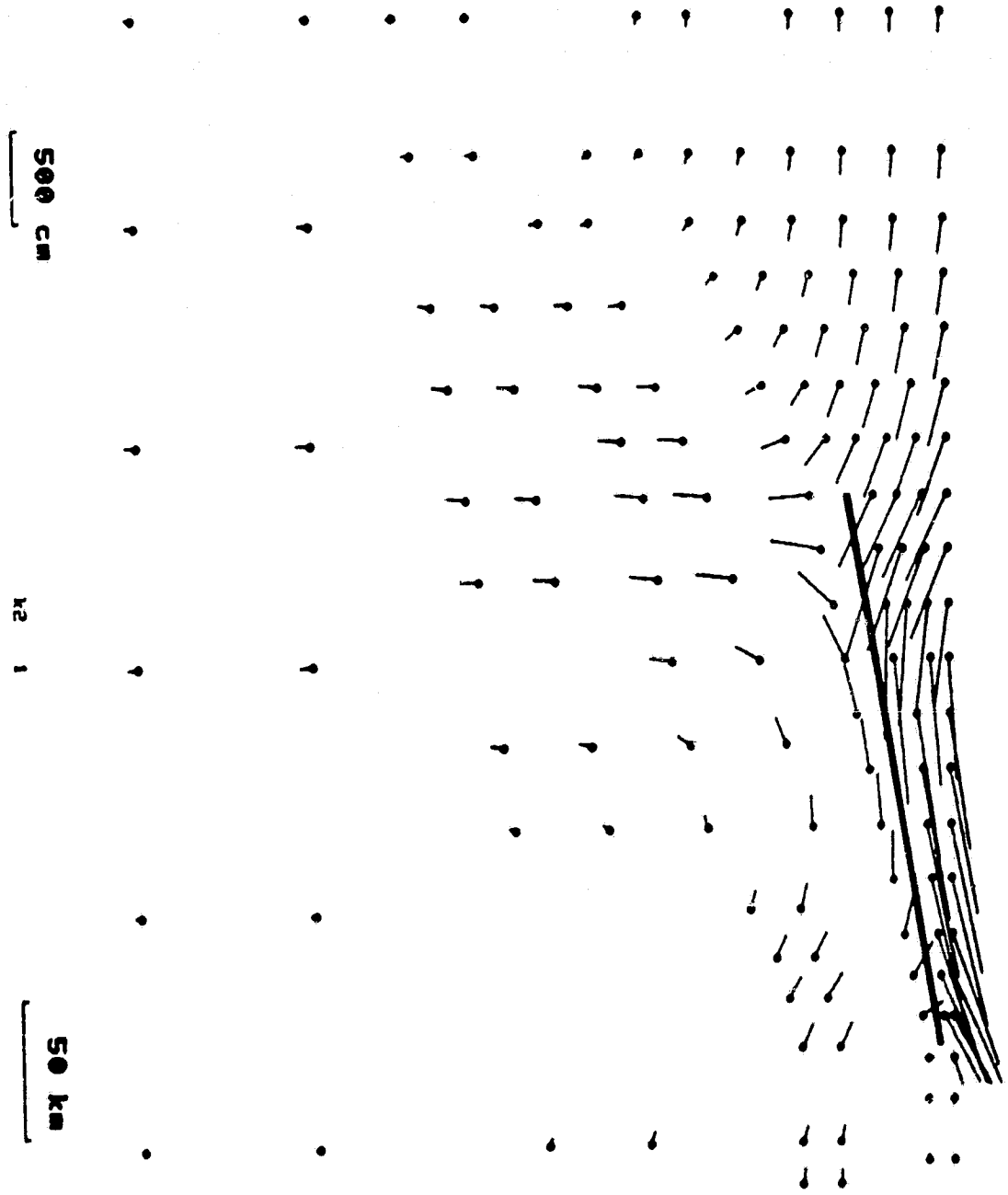

Fig. 4.3.5 a

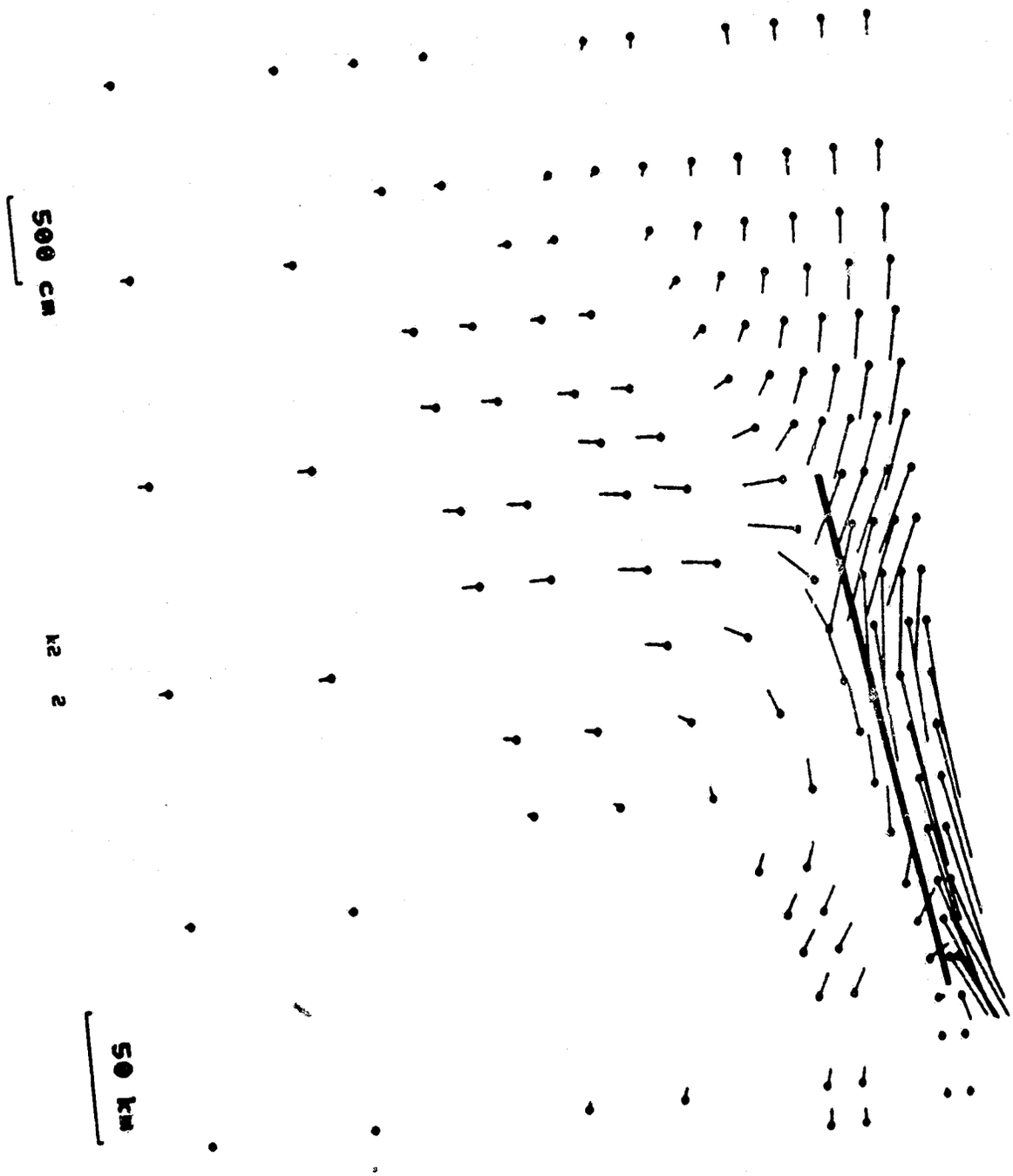

Fig 4.3.5 b

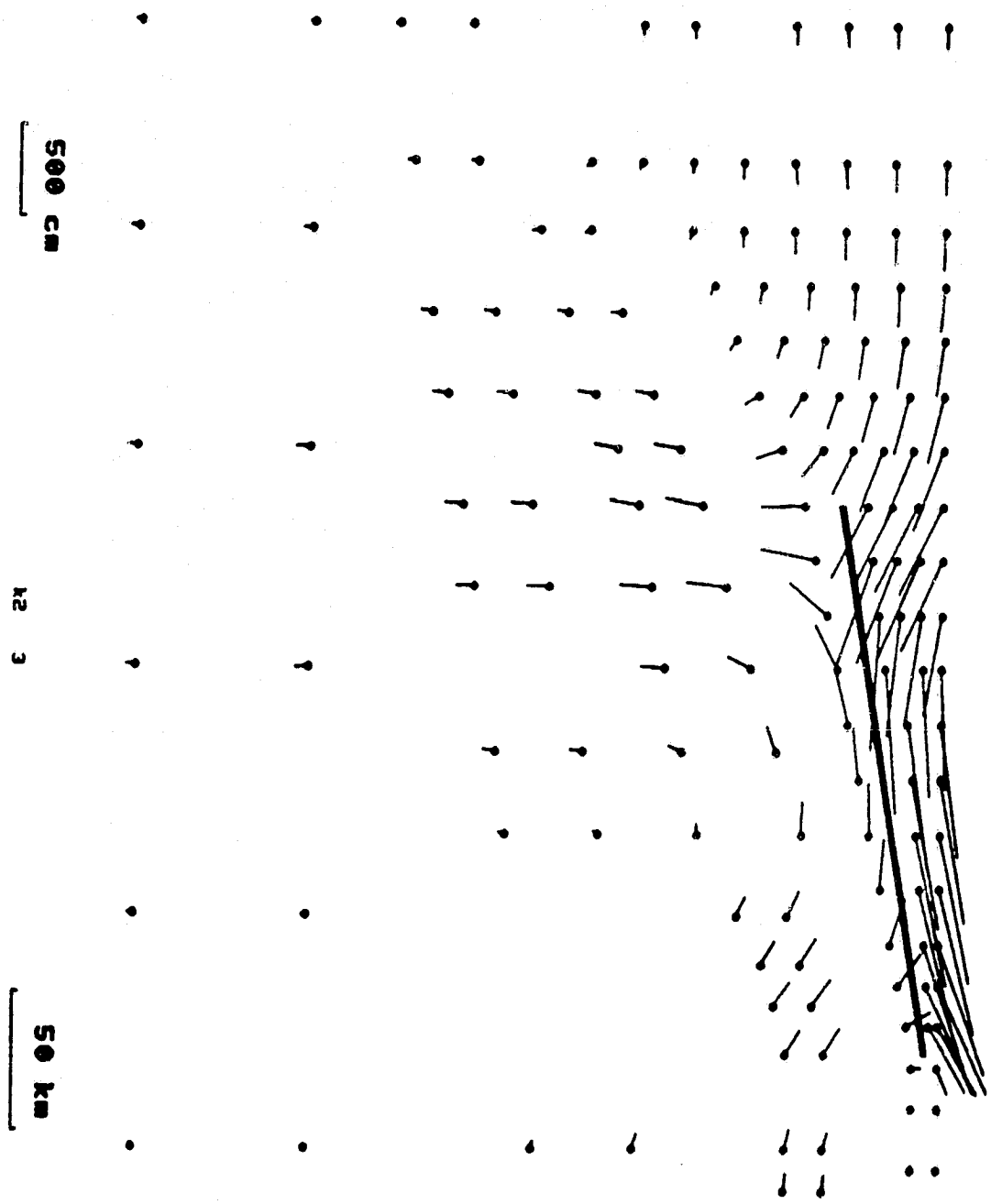

Fig 4.3.5 c

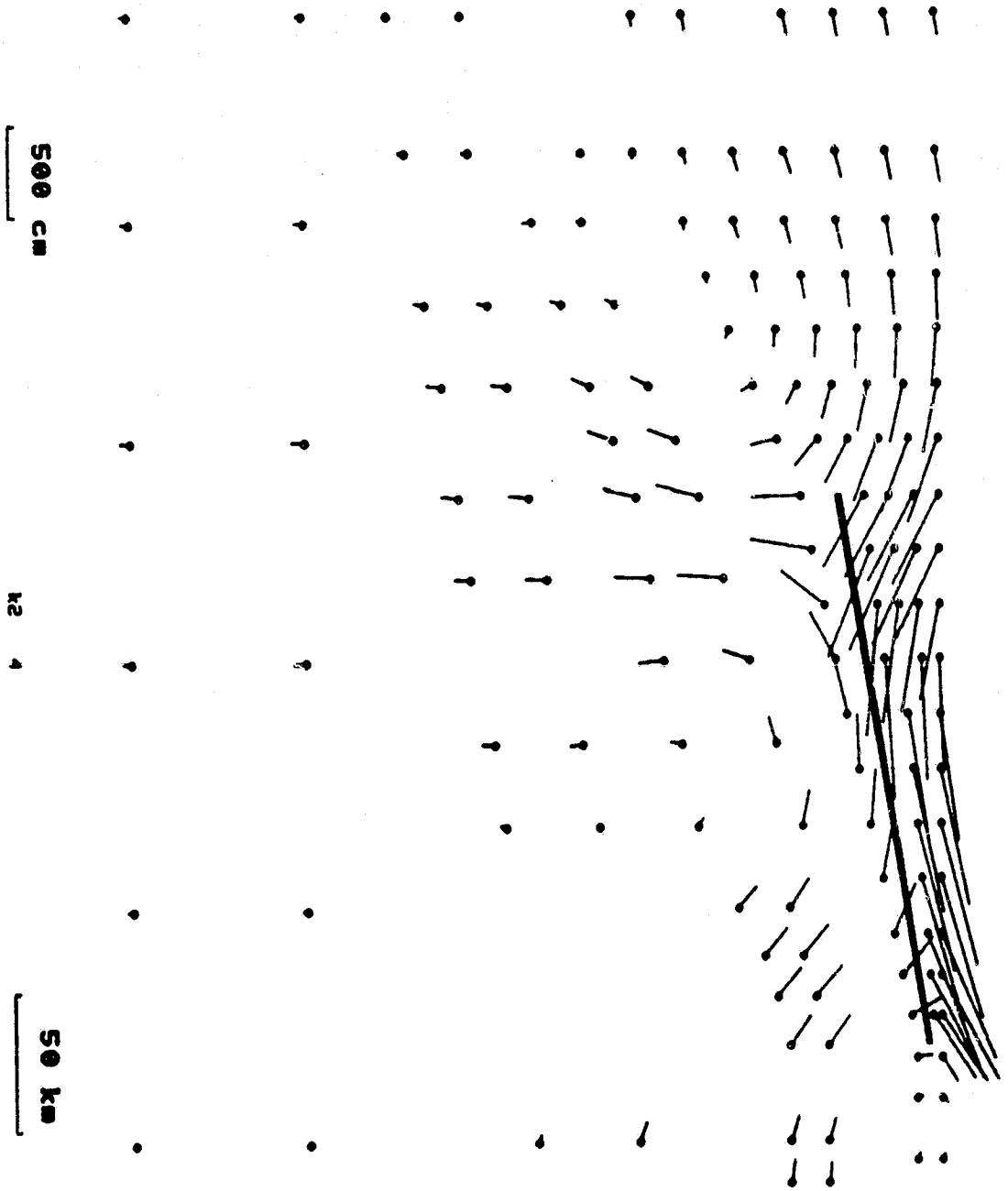

Fig 4.3.5 d

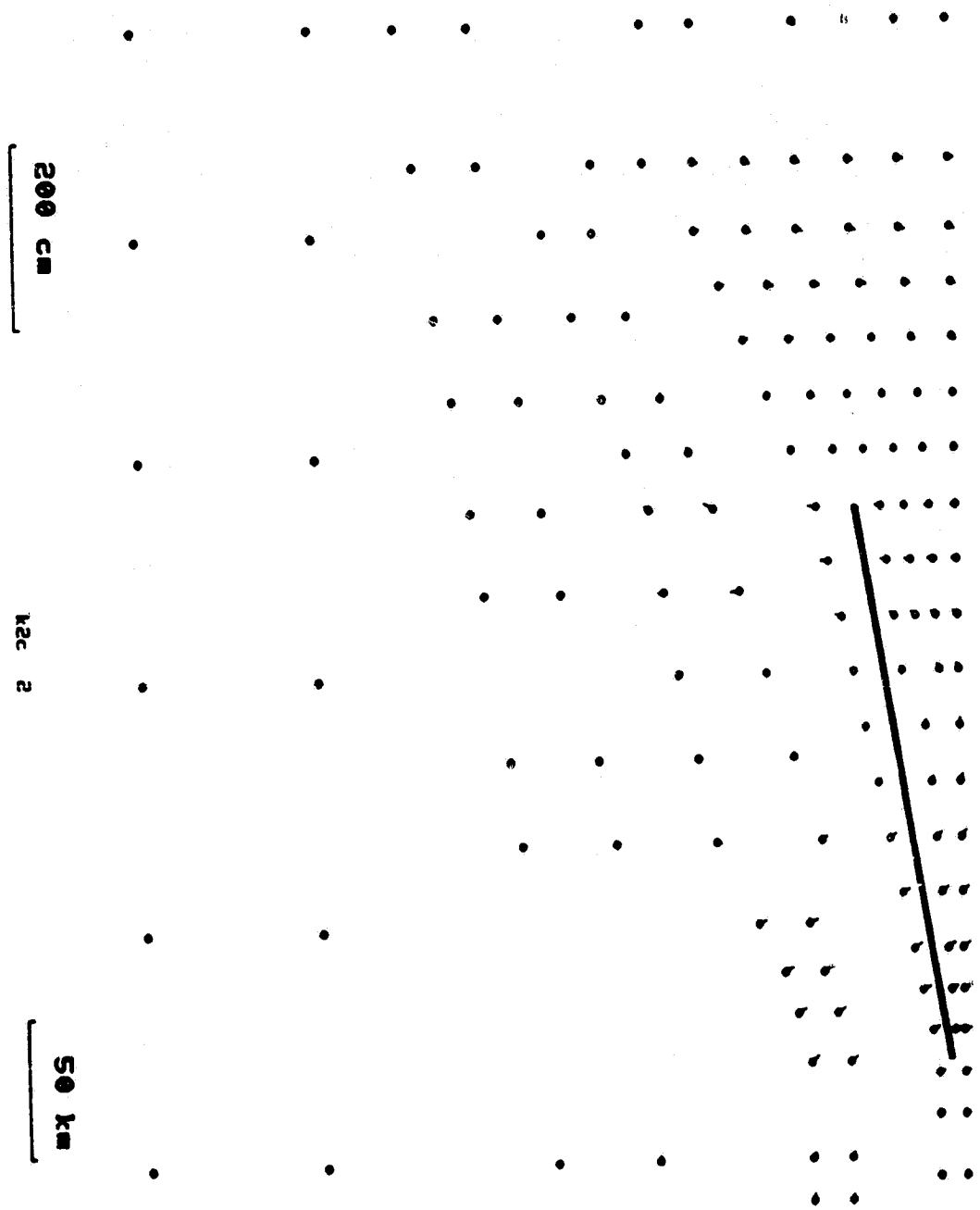

Fig 4.3.6 a

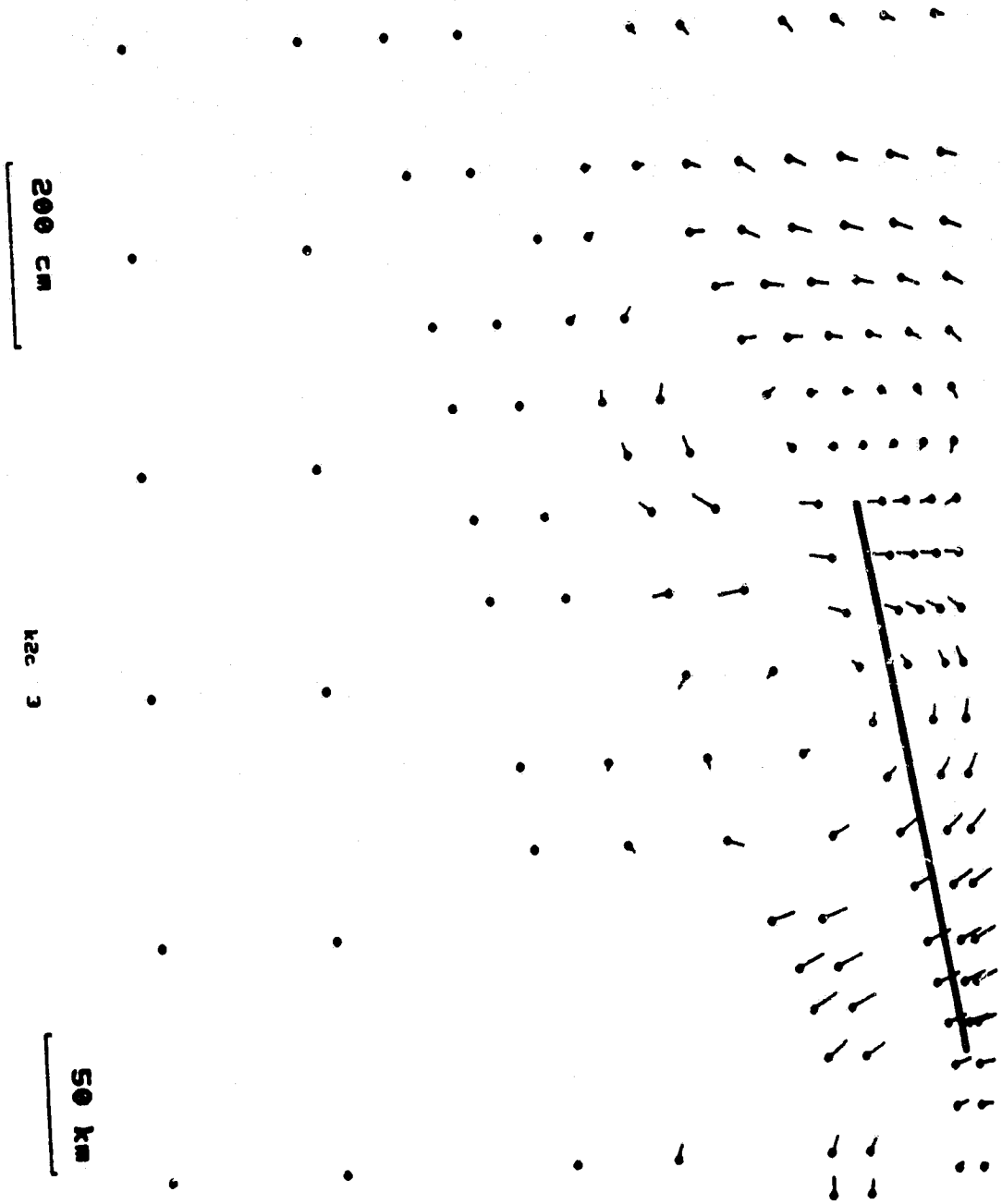

Fig 4.3.6 b

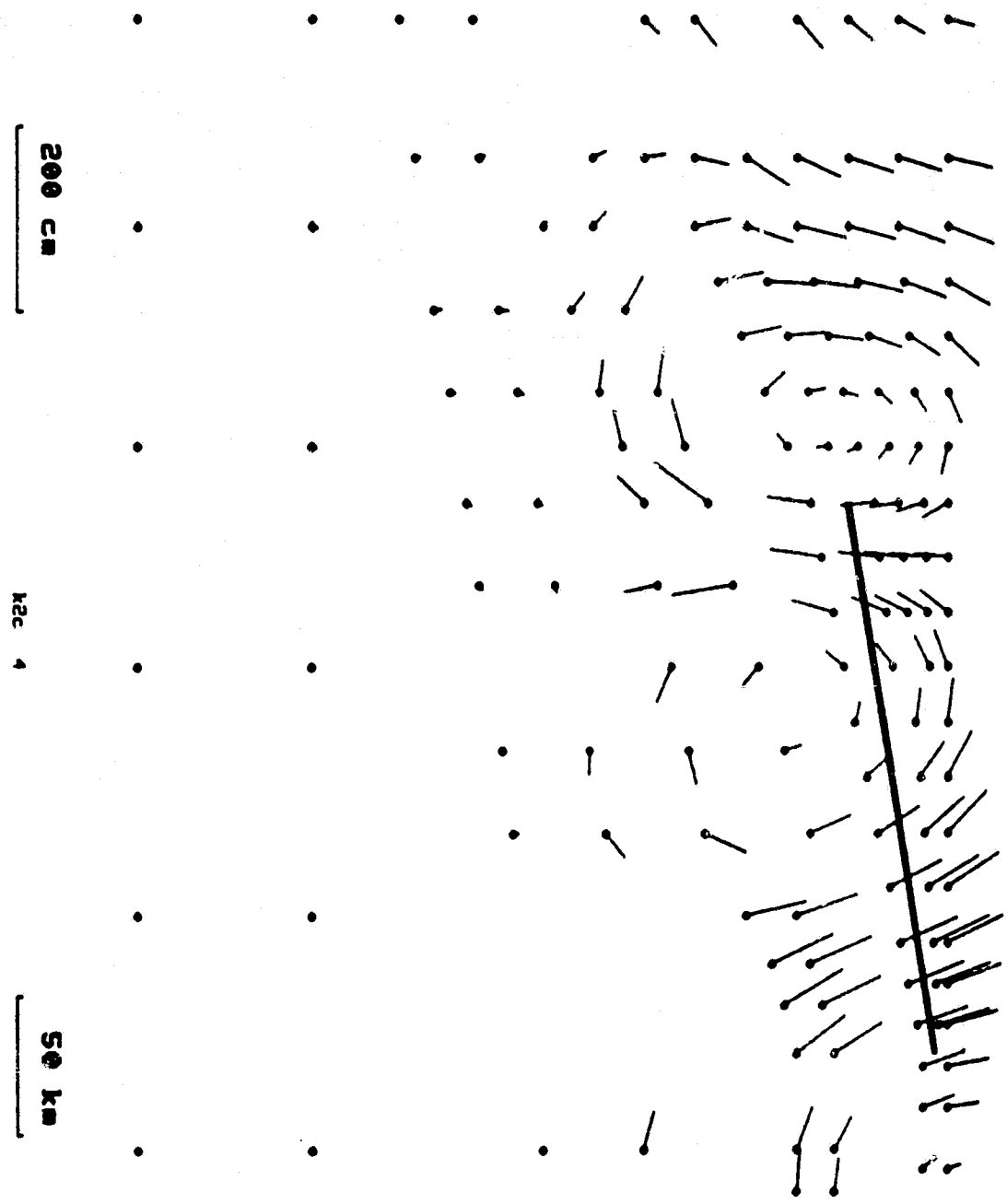

Fig 4.3.6 c

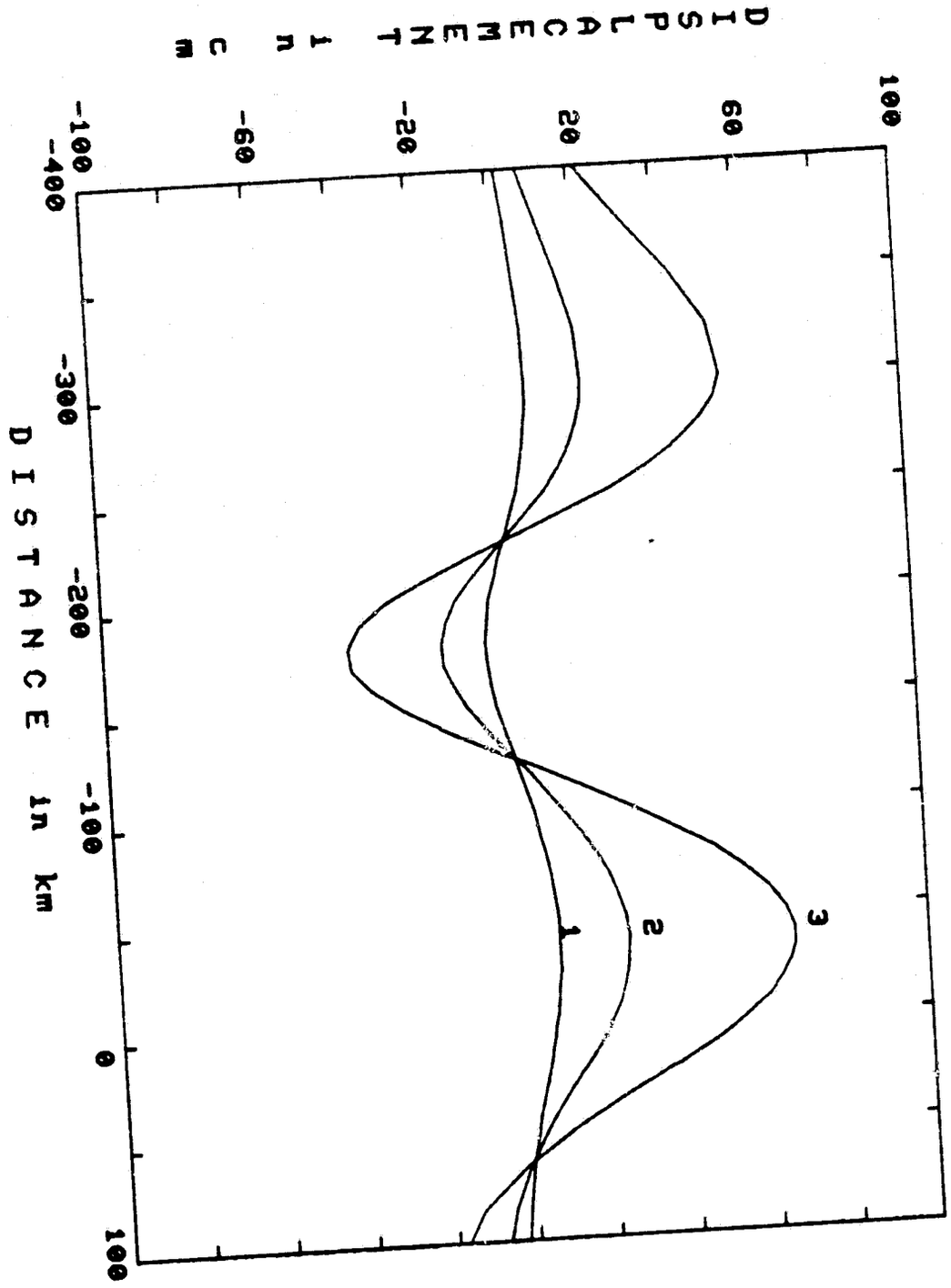
DISPLACEMENT in cm
100
60
20
-20
-60
-100
-400
-300
-200
-100
0
100
DISTANCE in km
1
2
3

Fig 4.3.7

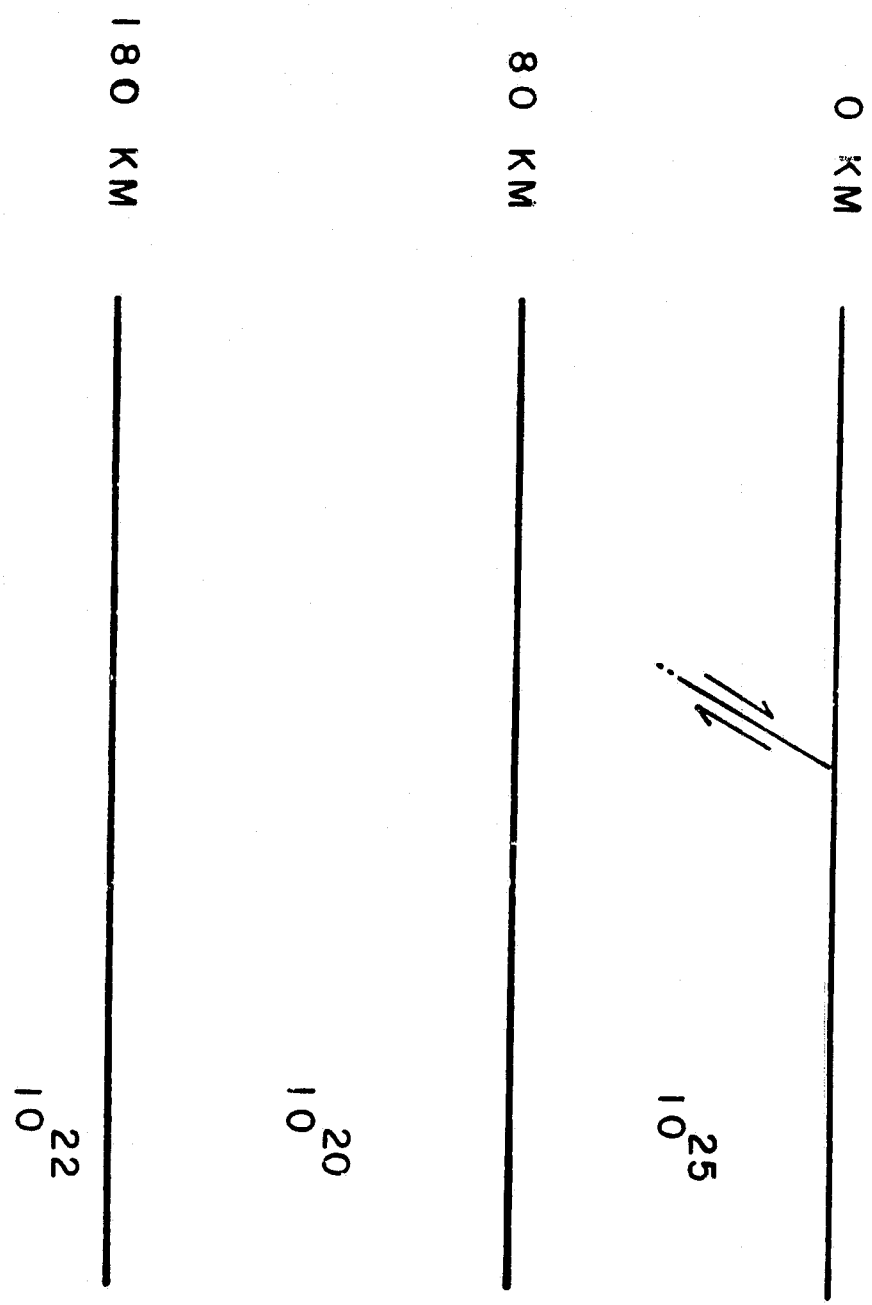

Fig 4.3.8

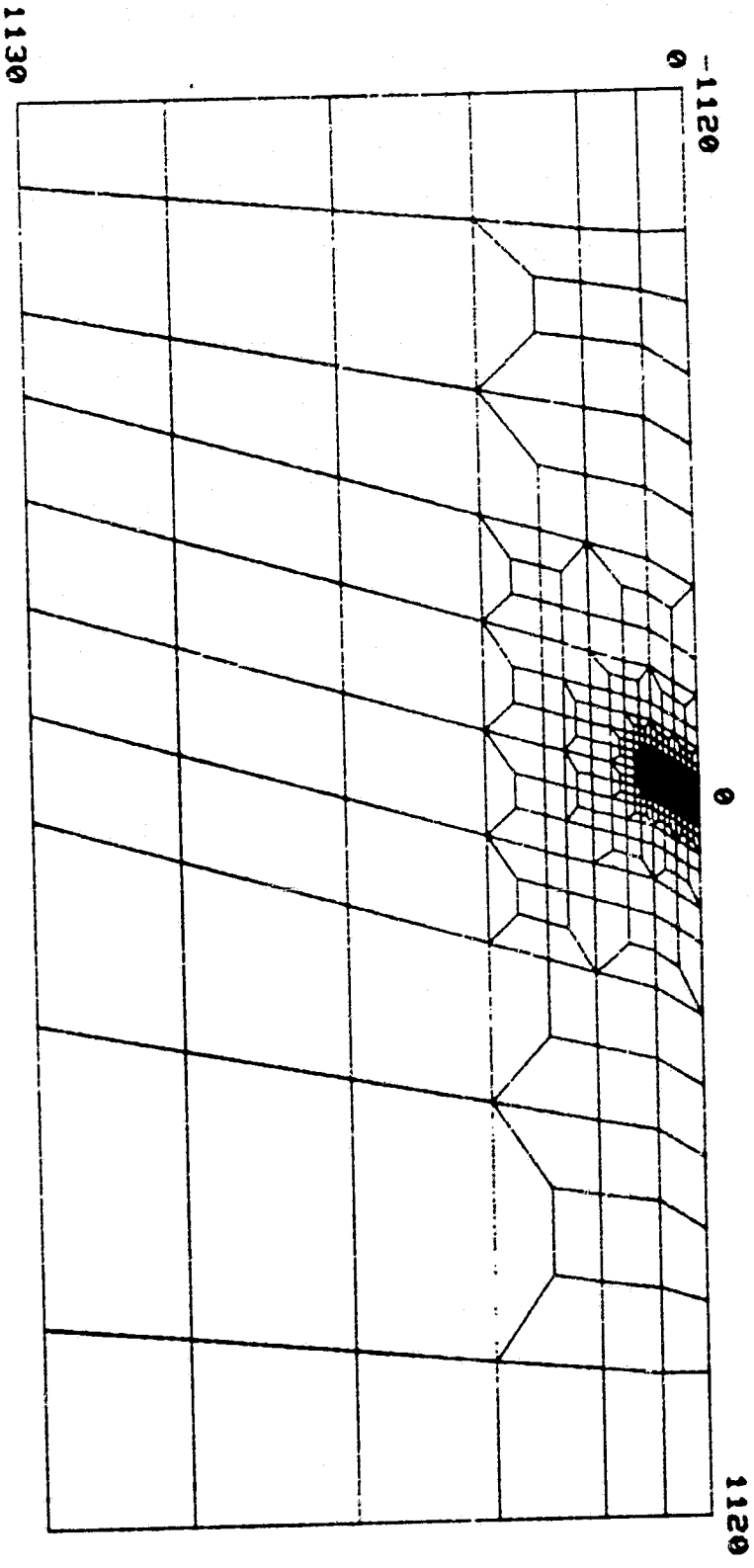

Fig. 4.3.9

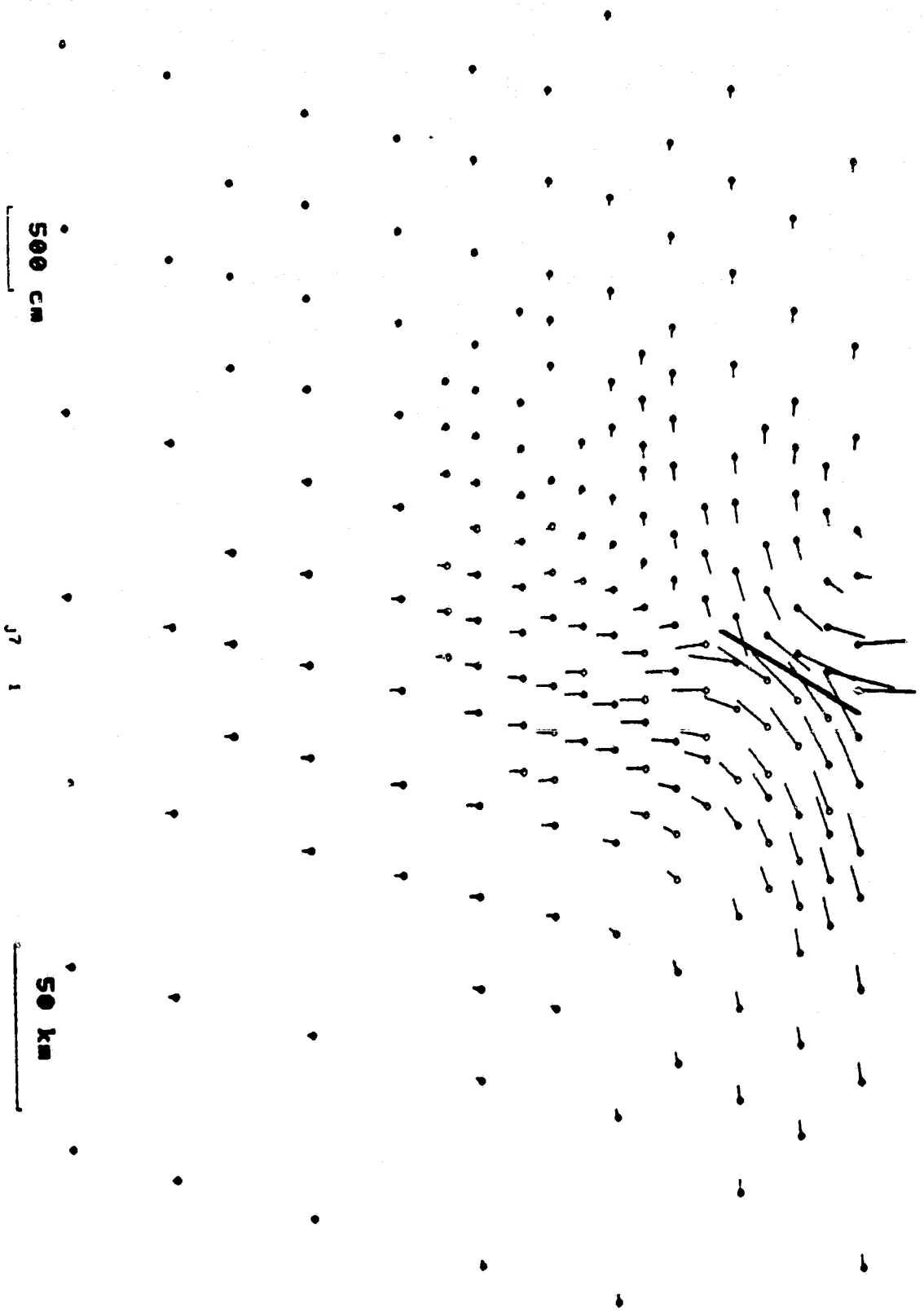

Fig 4.3.10 a

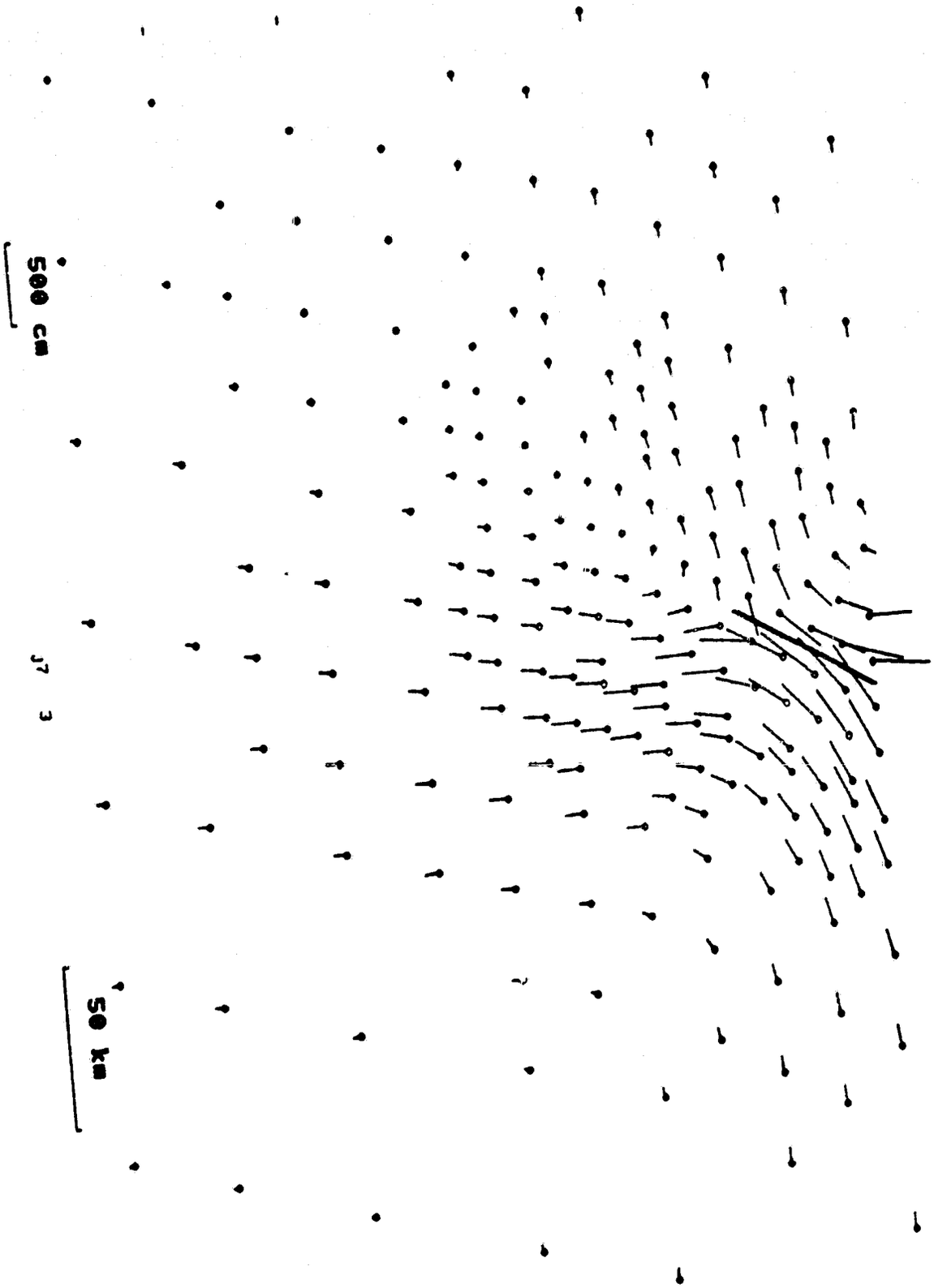

Fig 4.3.10 b

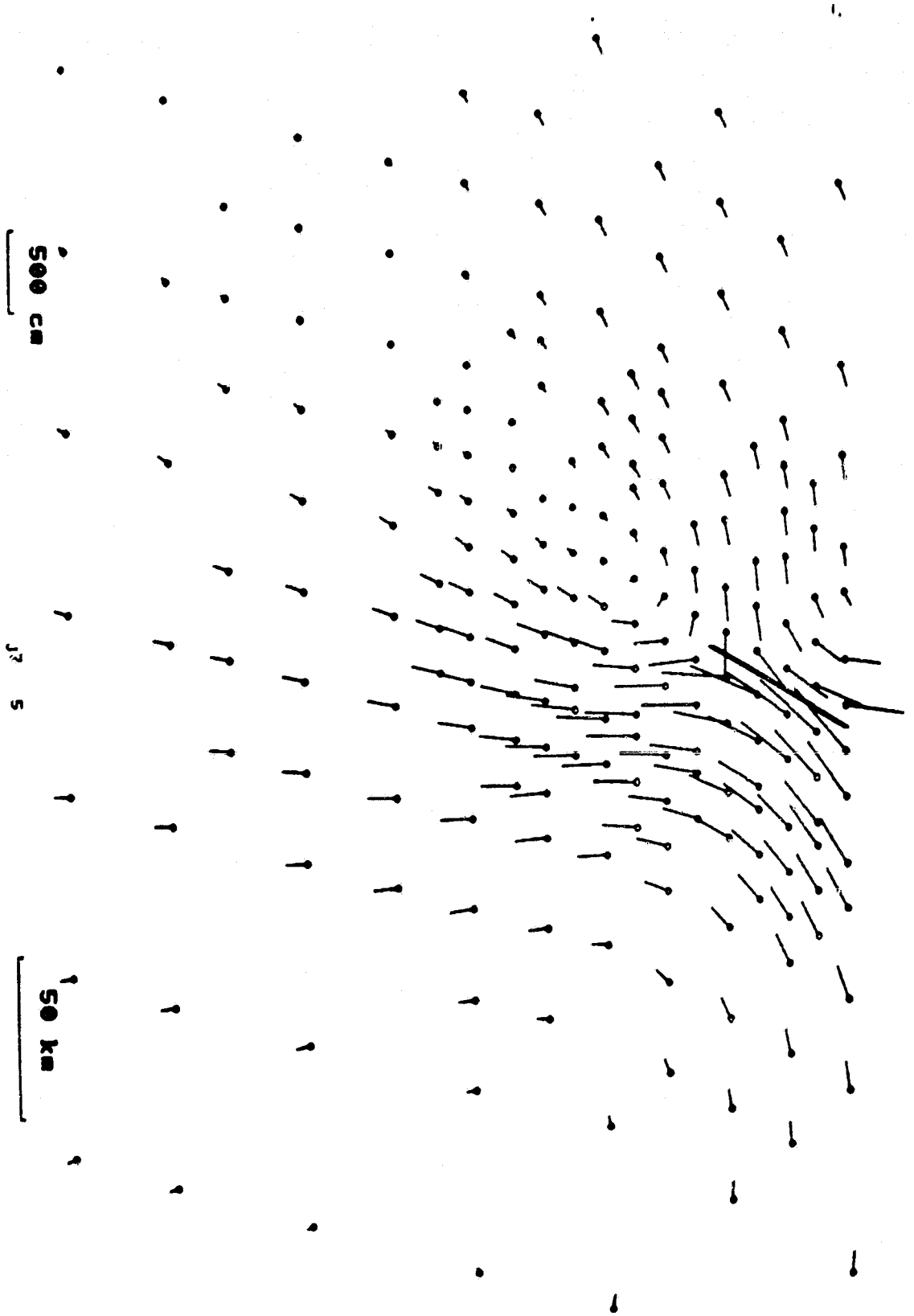

Fig 4.3.10 c

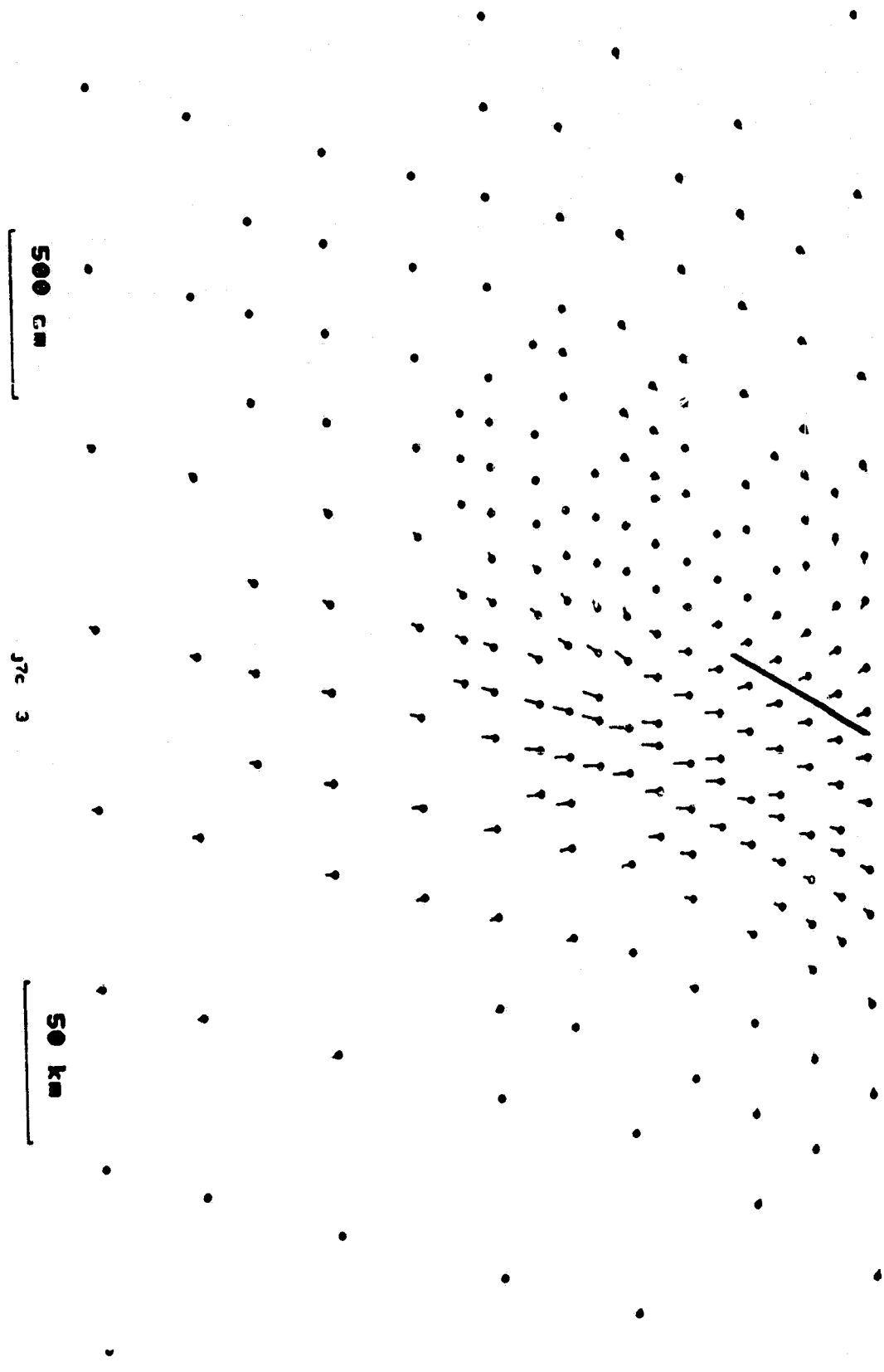

Fig 4.3.11 a

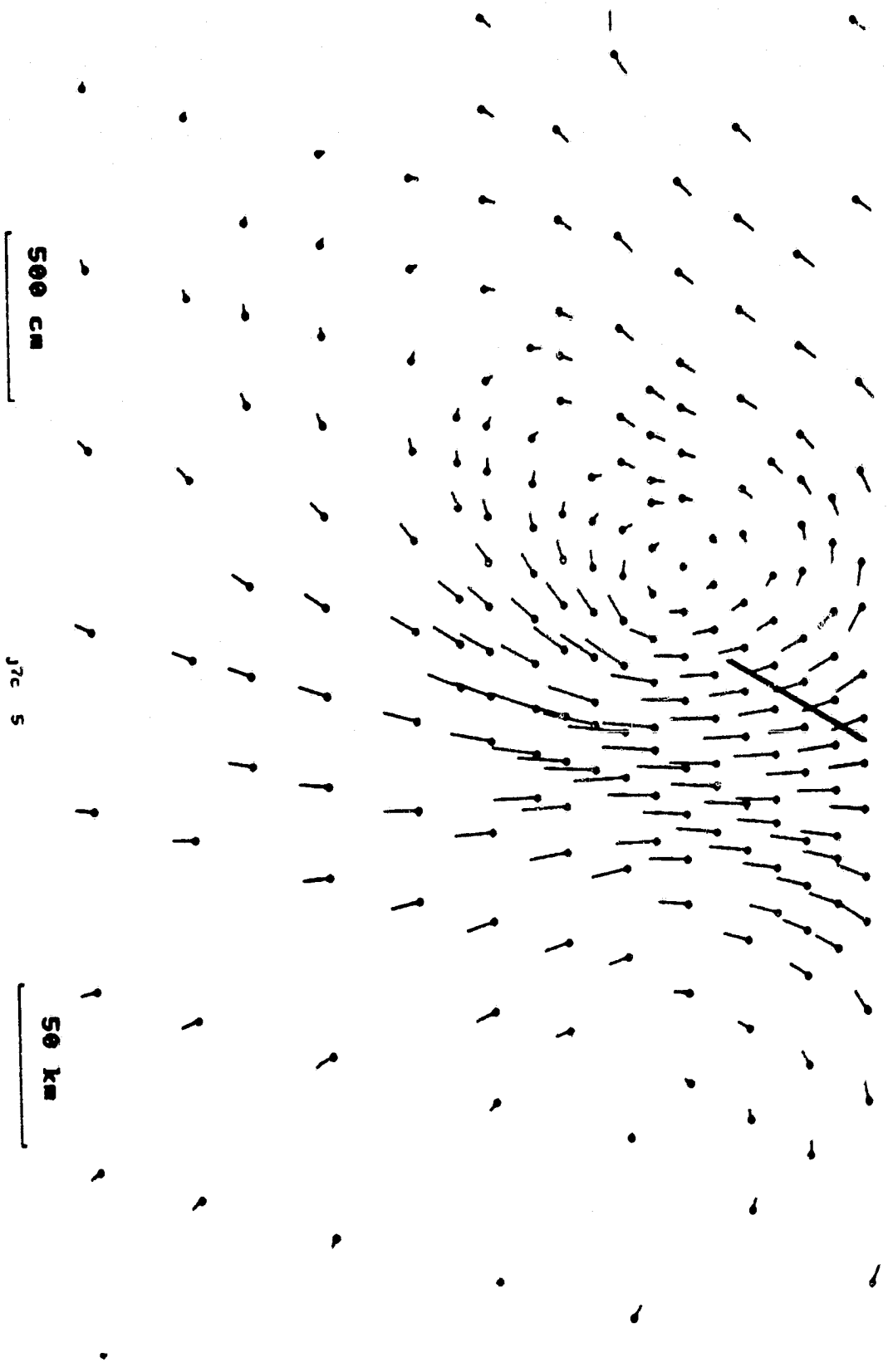

Fig 4.3.11 b

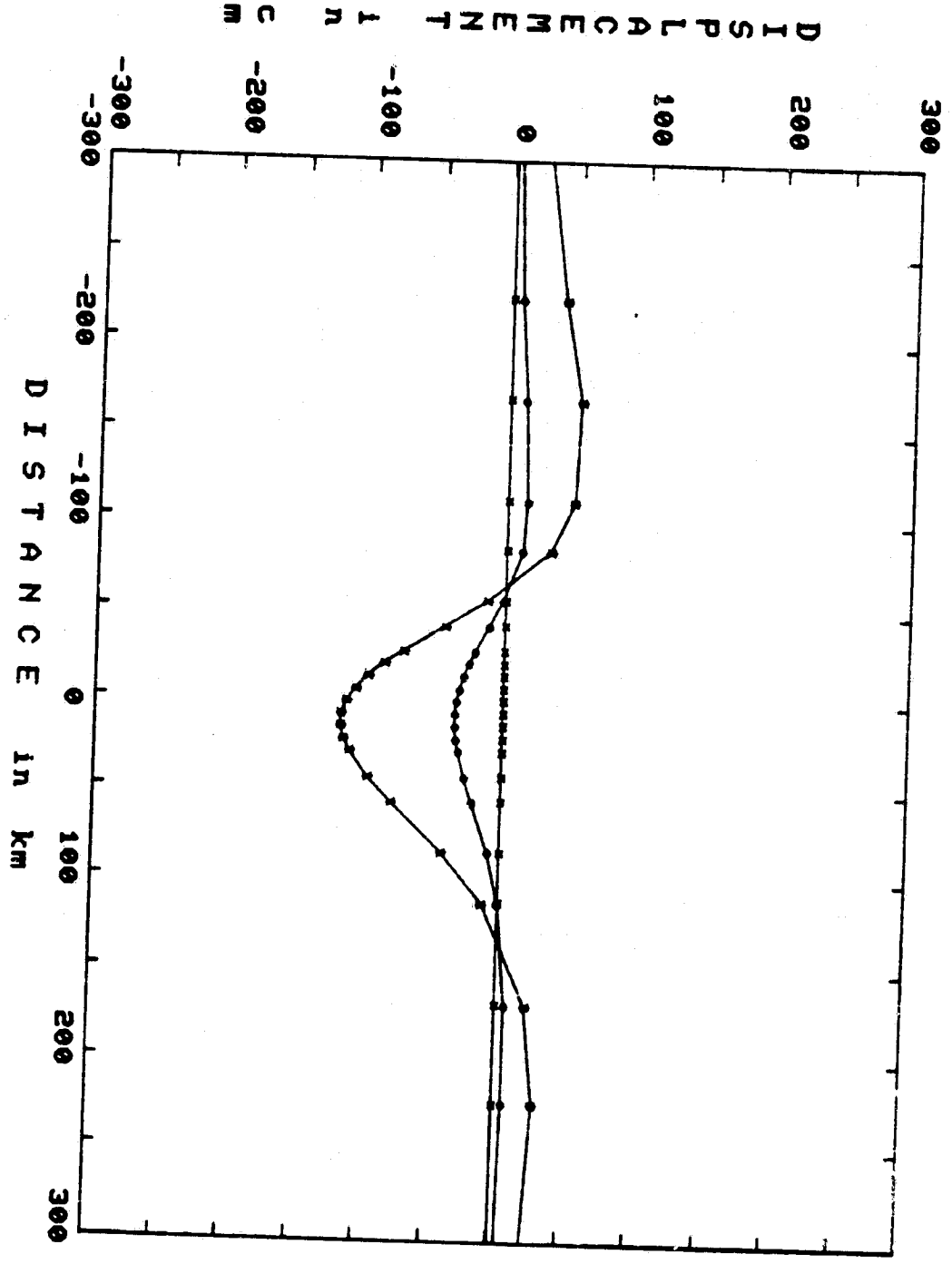
DISPLACEMENT in cm
-300
-200
-100
0
100
200
300
DISTANCE in km
-300
-200
-100
0
100
200
300

Fig 4.3.12

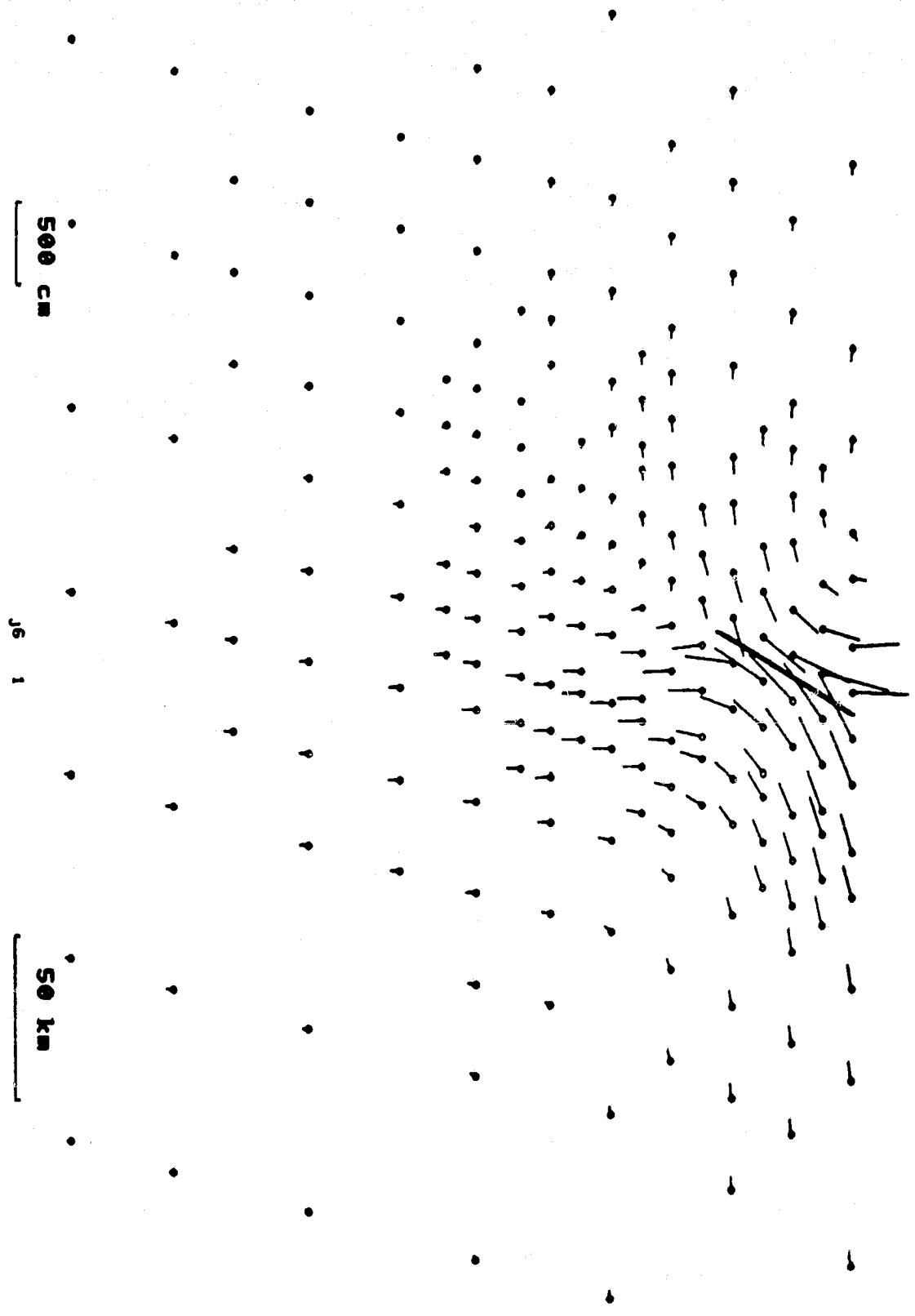

Fig 4.3.13 a

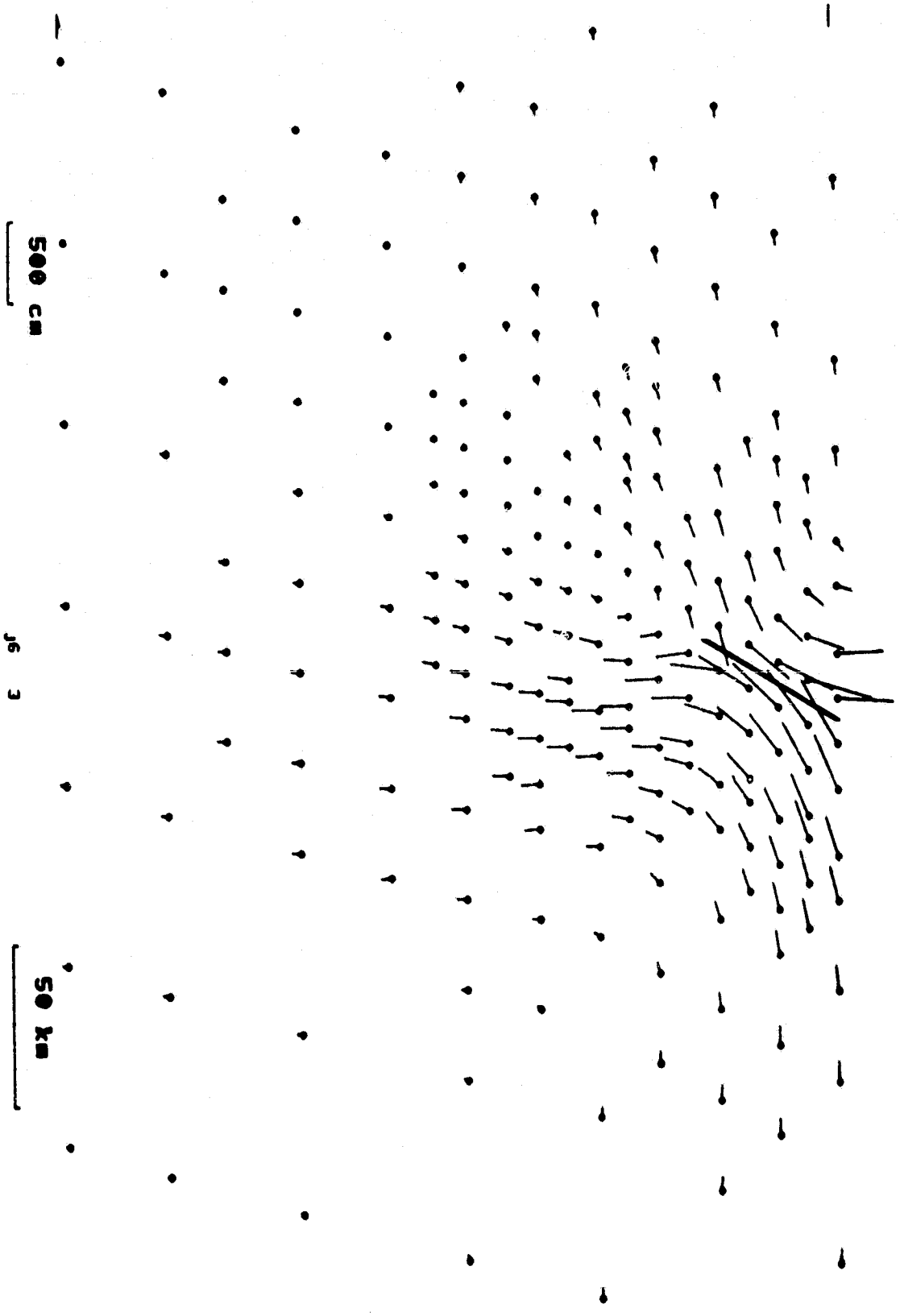

Fig 4.3.13 b

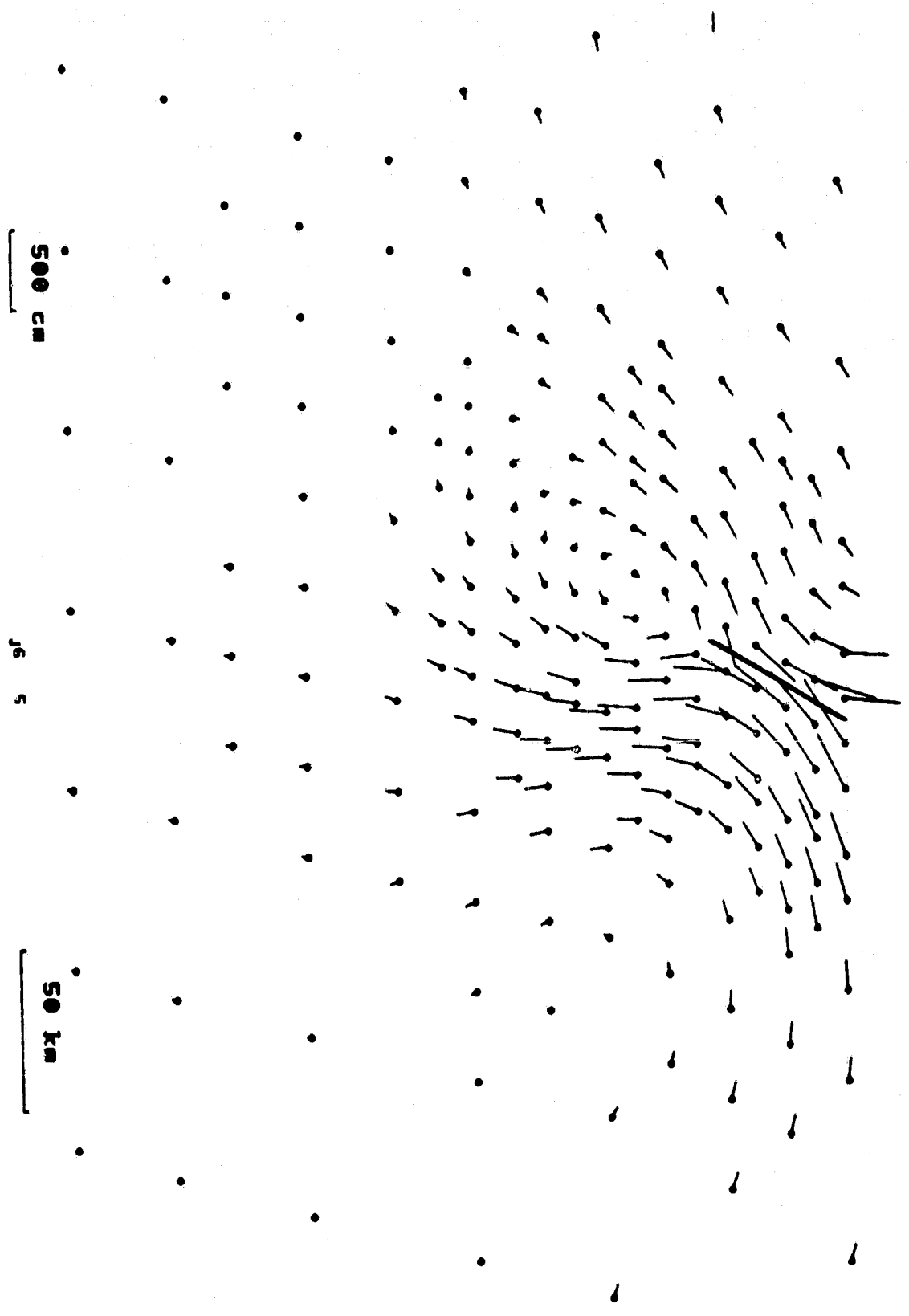

Fig 4.3.13 c

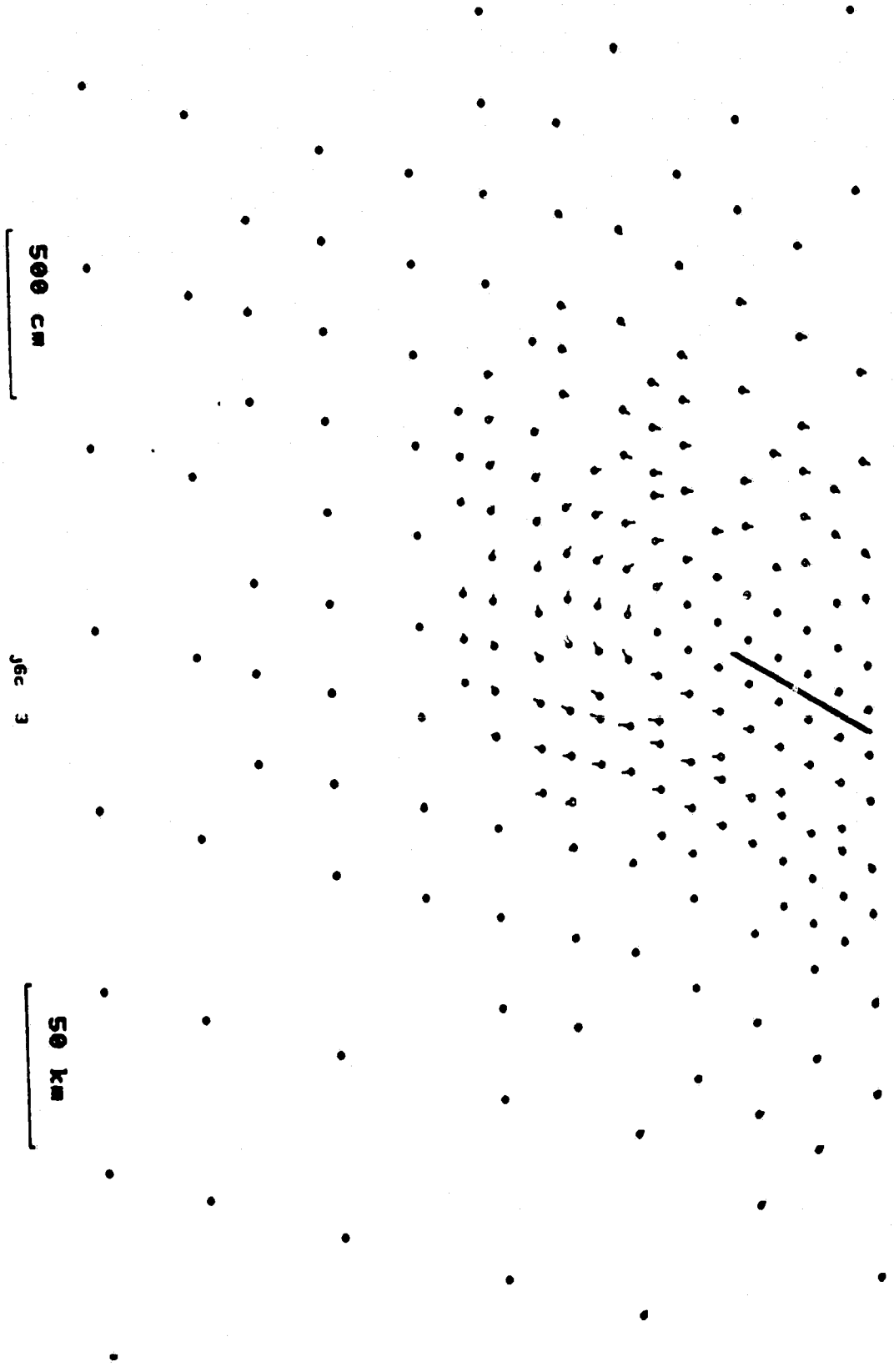

Fig 4.3.14 a

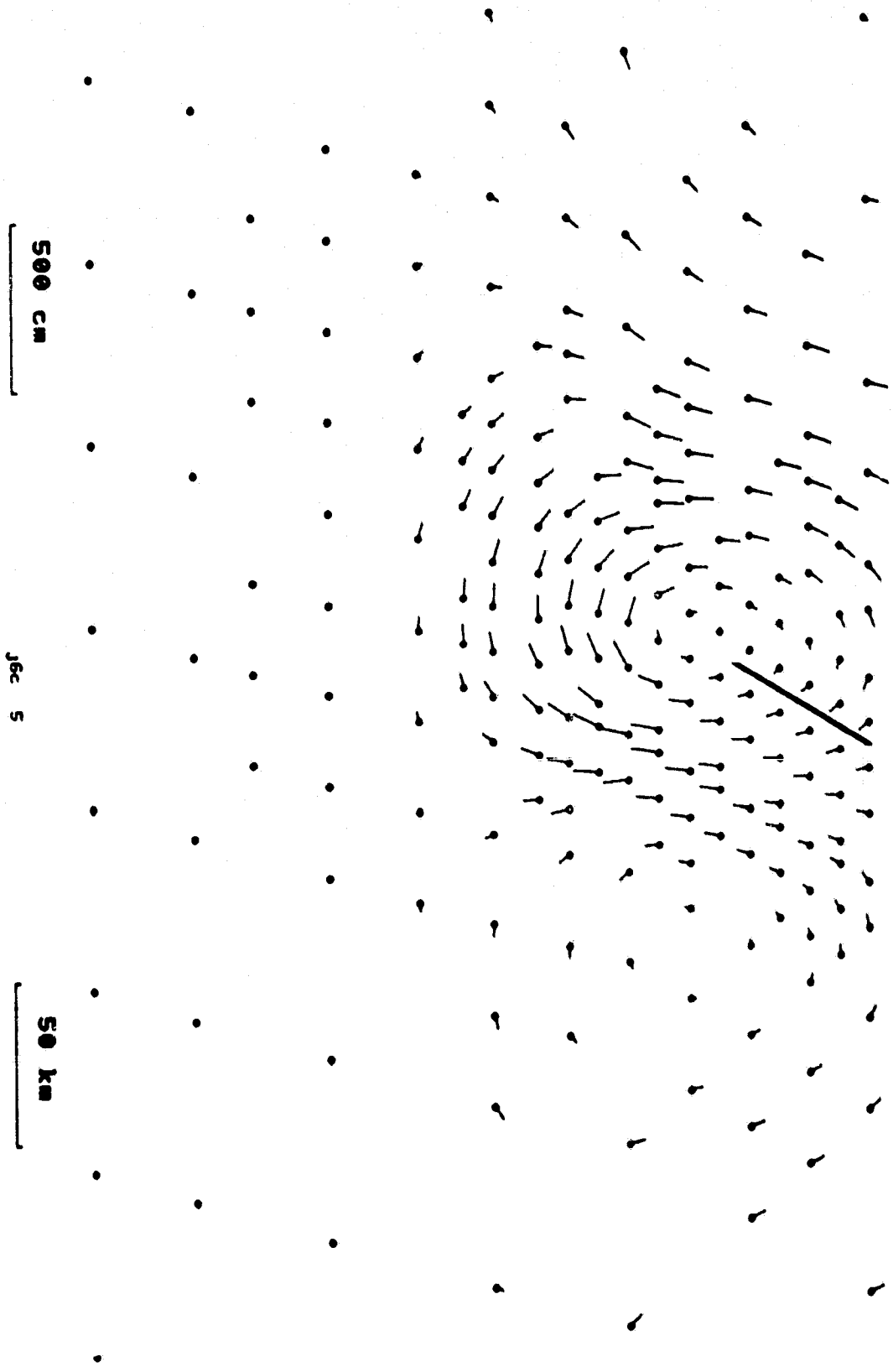

Fig 4.3.14 b

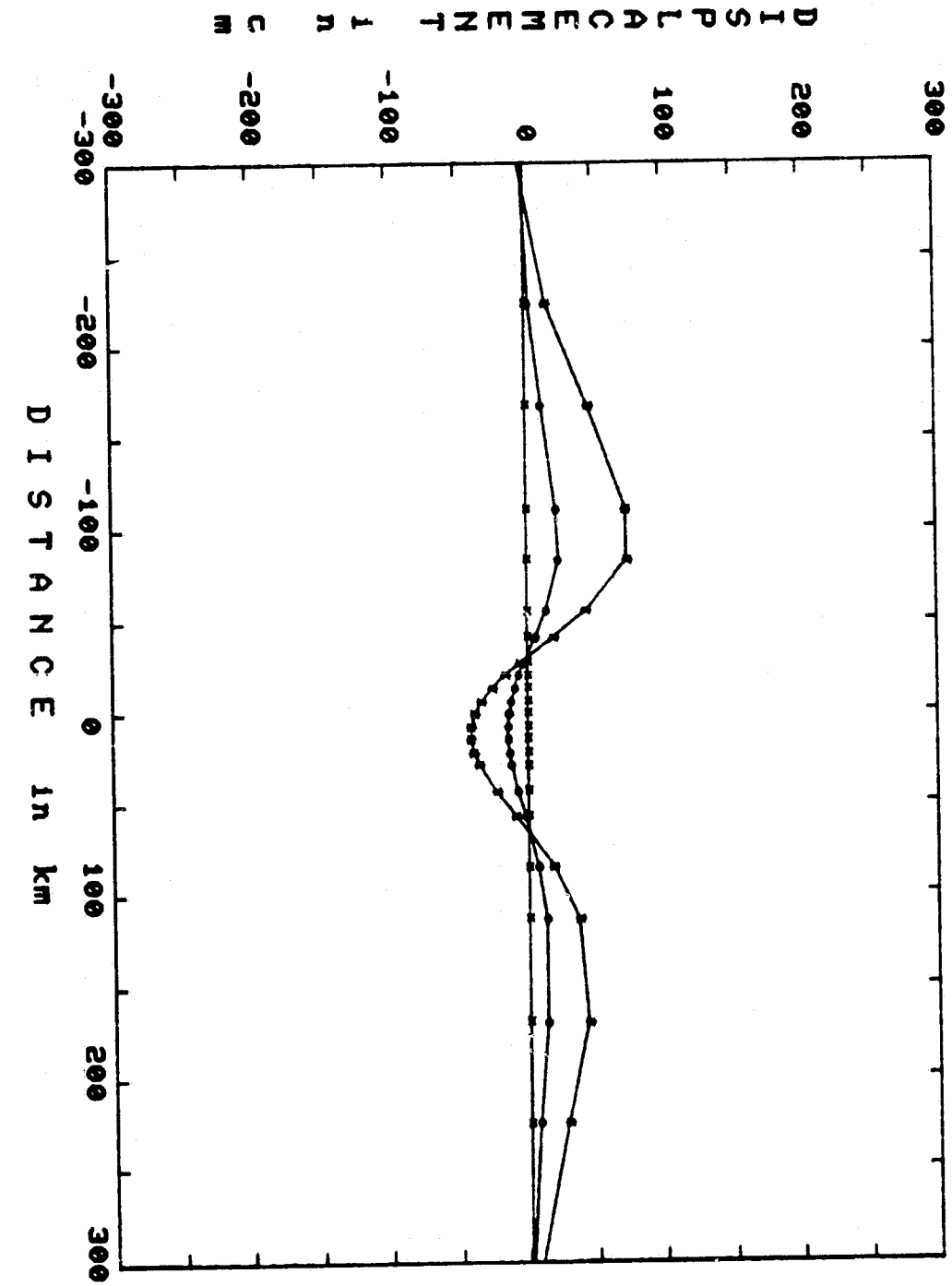
DISPLACEMENT in cm
-300
-200
-100
0
100
200
300
DISTANCE in km
-300
-200
-100
0
100
200
300

Fig 4.3.15

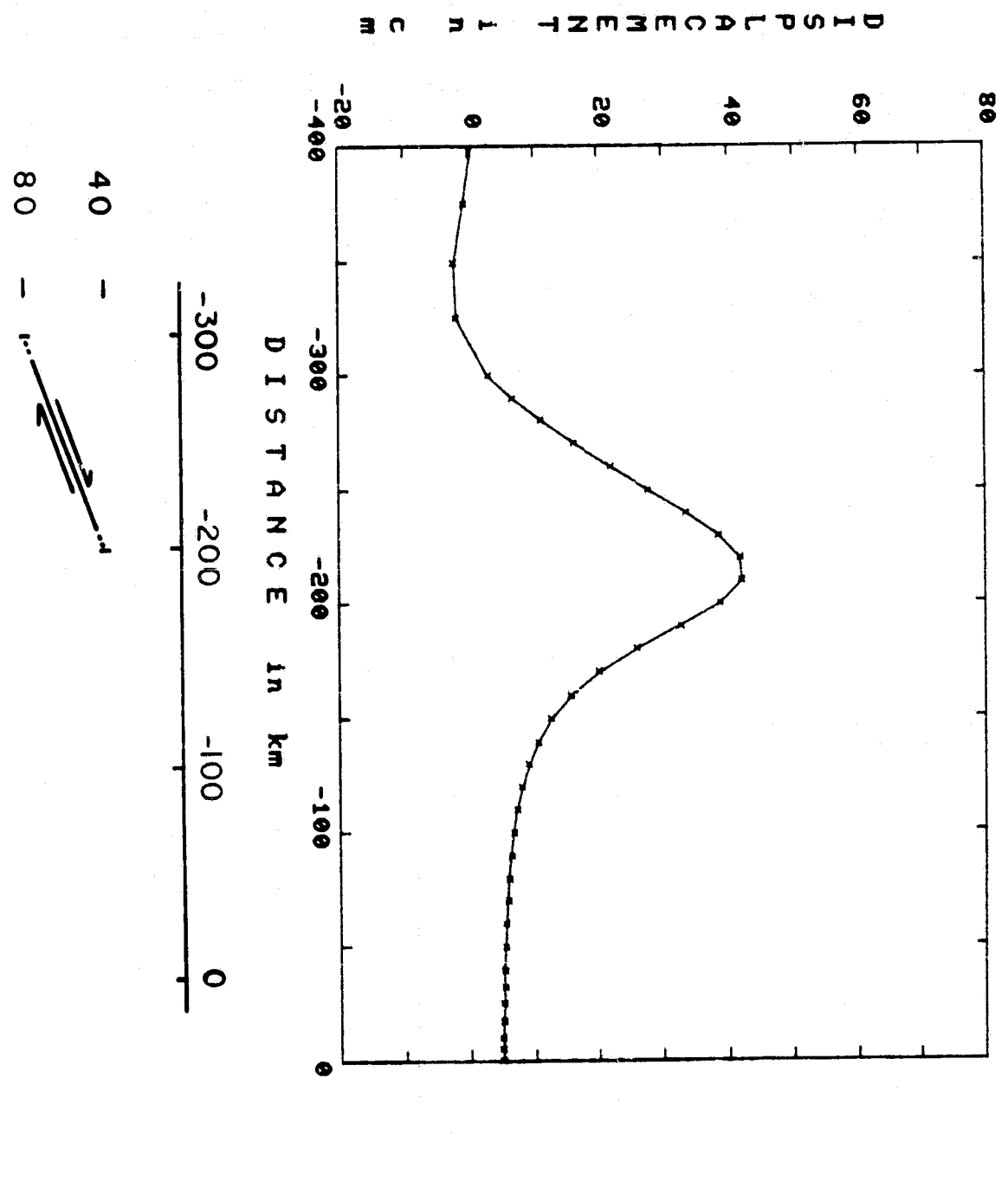
DISPLACEMENT in cm
-20
0
20
40
60
80
-400
-300
-200
-100
0
DISTANCE in km
-300
-200
-100
0
40
80

Fig 4.4.1

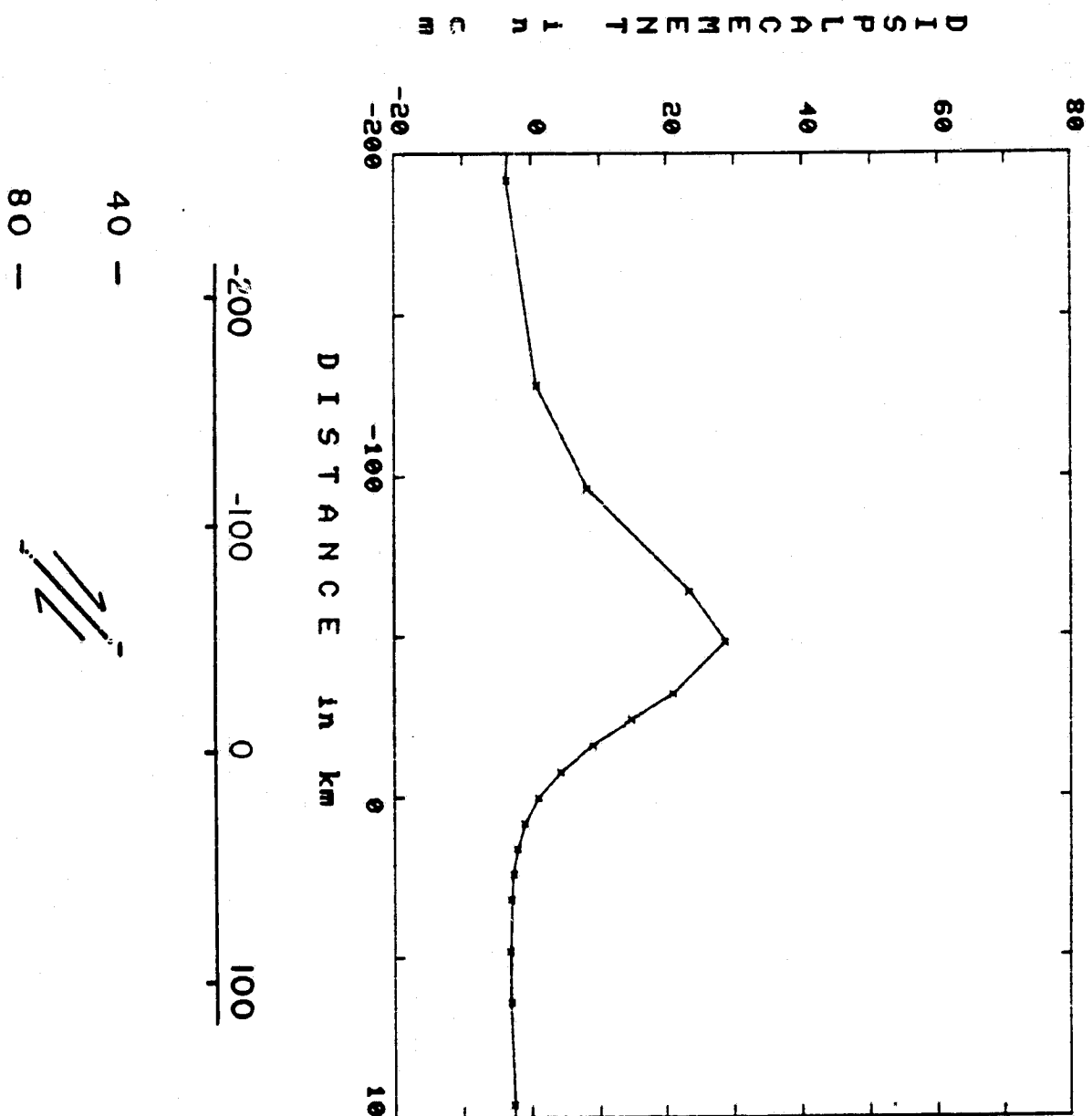
DISPLACEMENT in cm
-20
0
20
40
60
80
-200
-100
0
100
DISTANCE in km
-200
-100
0
100
40 —
80 —

Fig 4.4.2

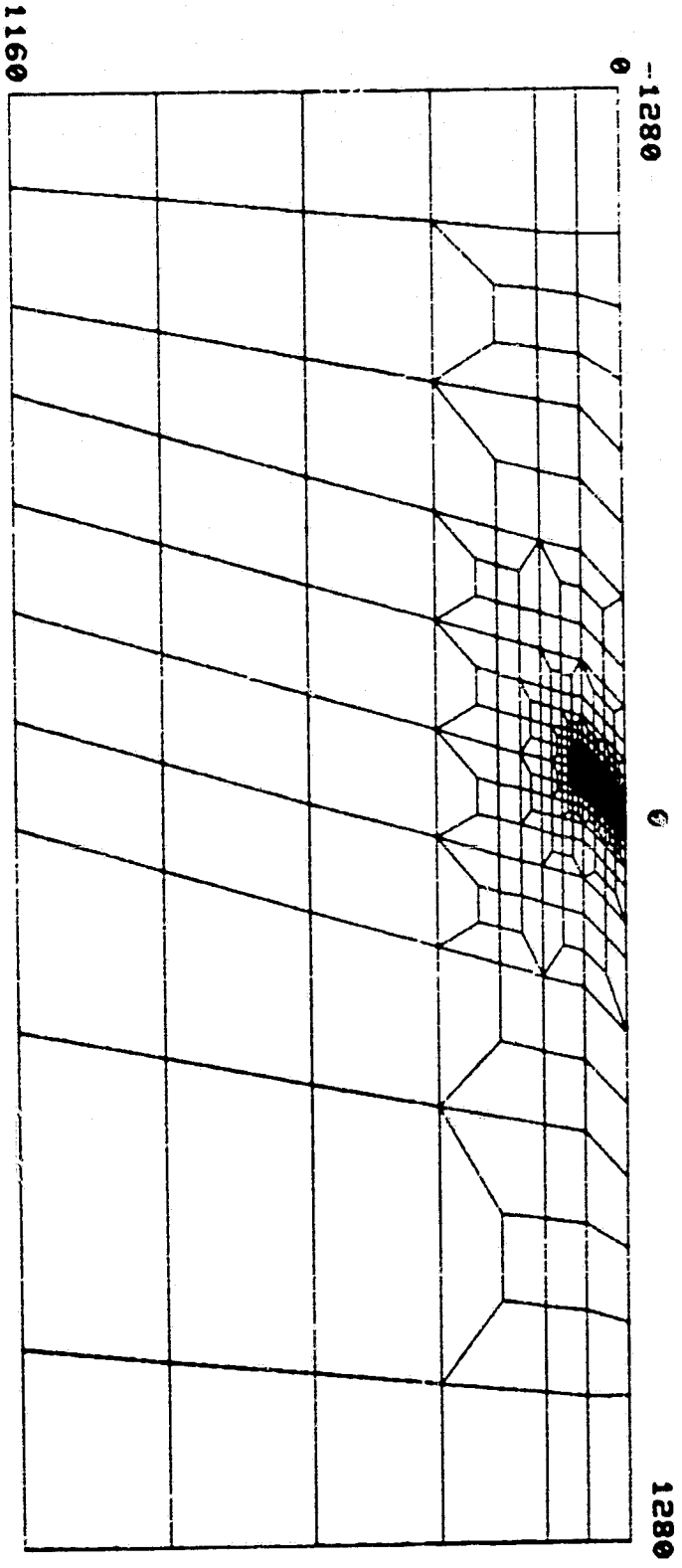

Fig 4.4.3

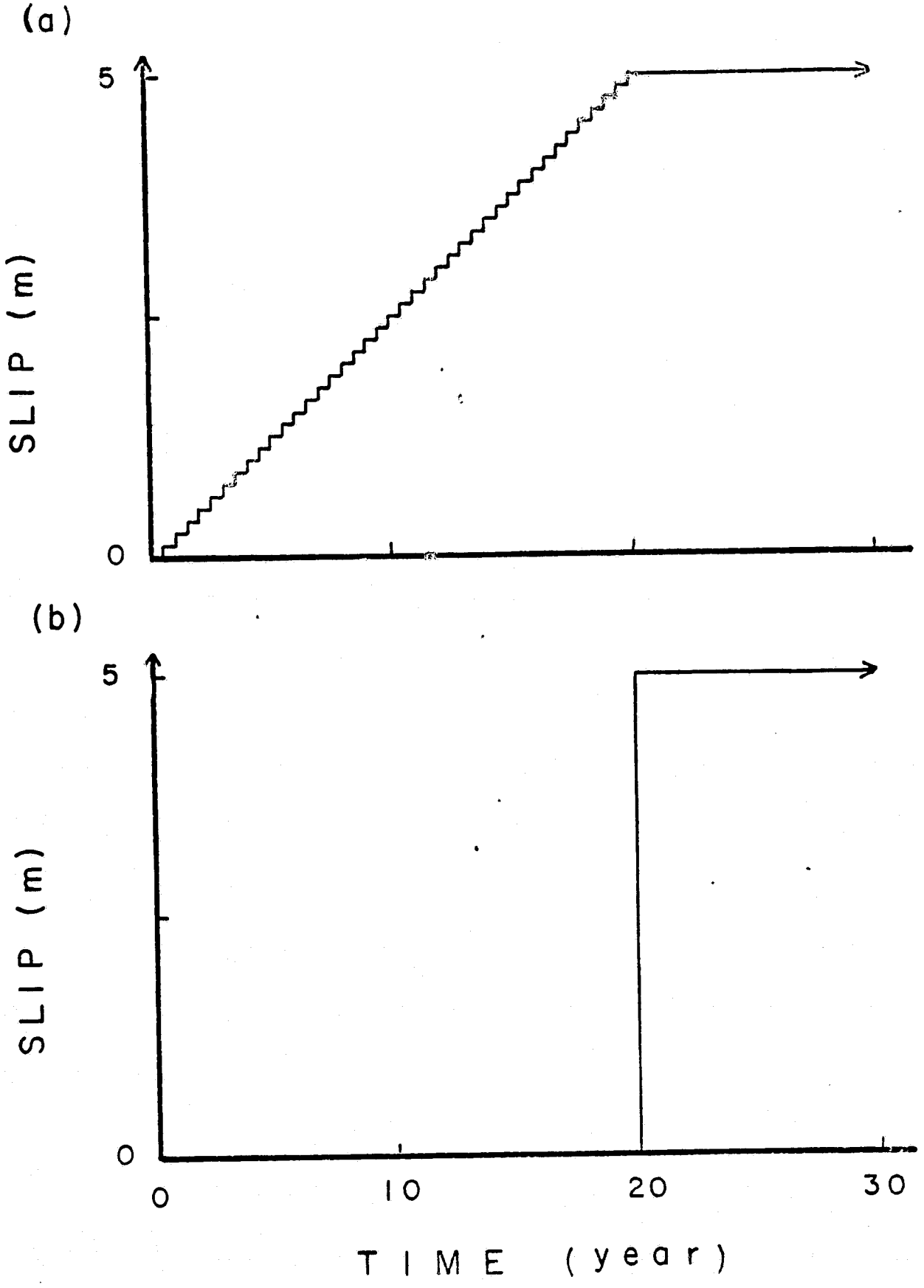

Fig 4.4.4

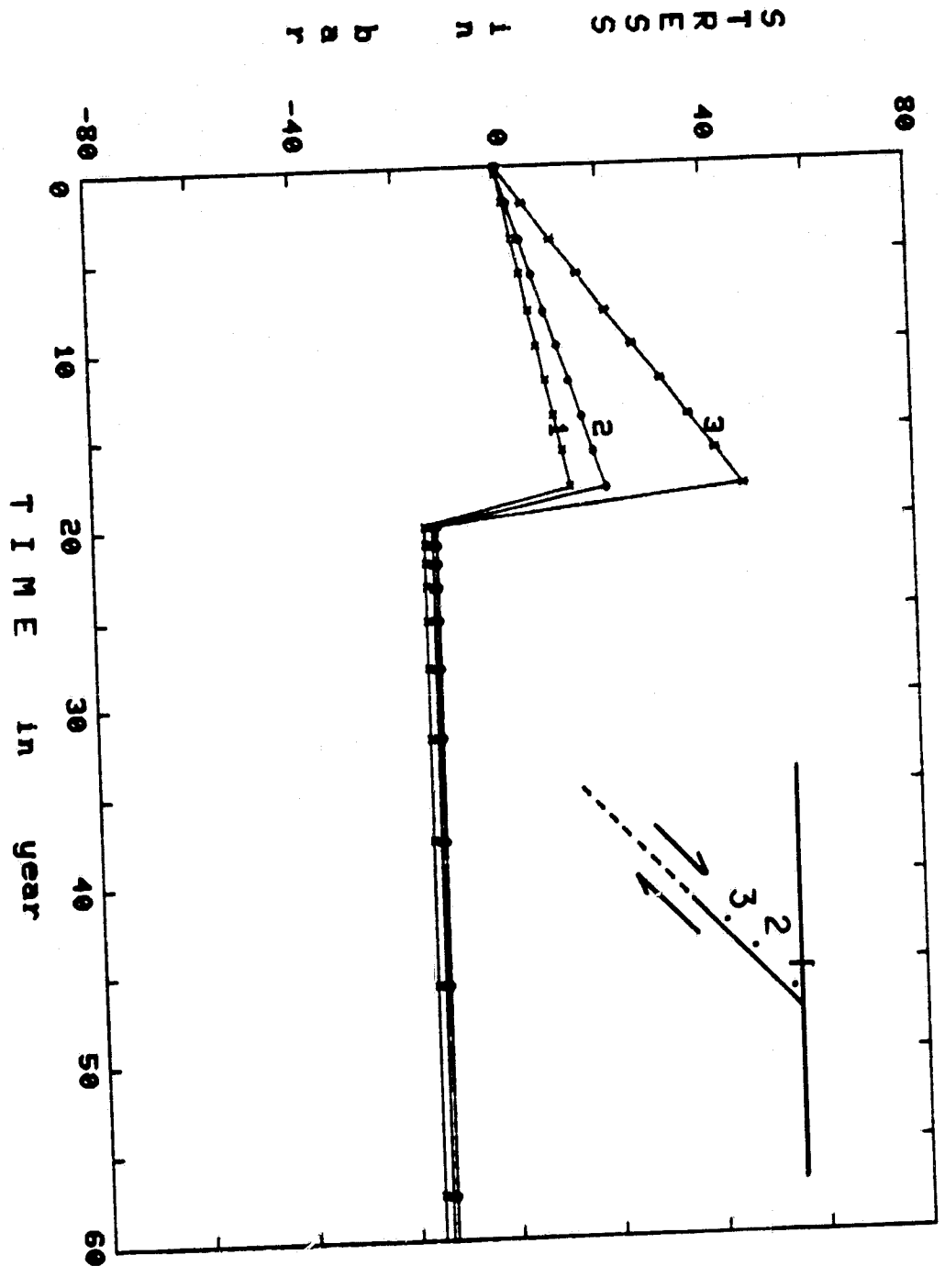

Fig 4.4.5

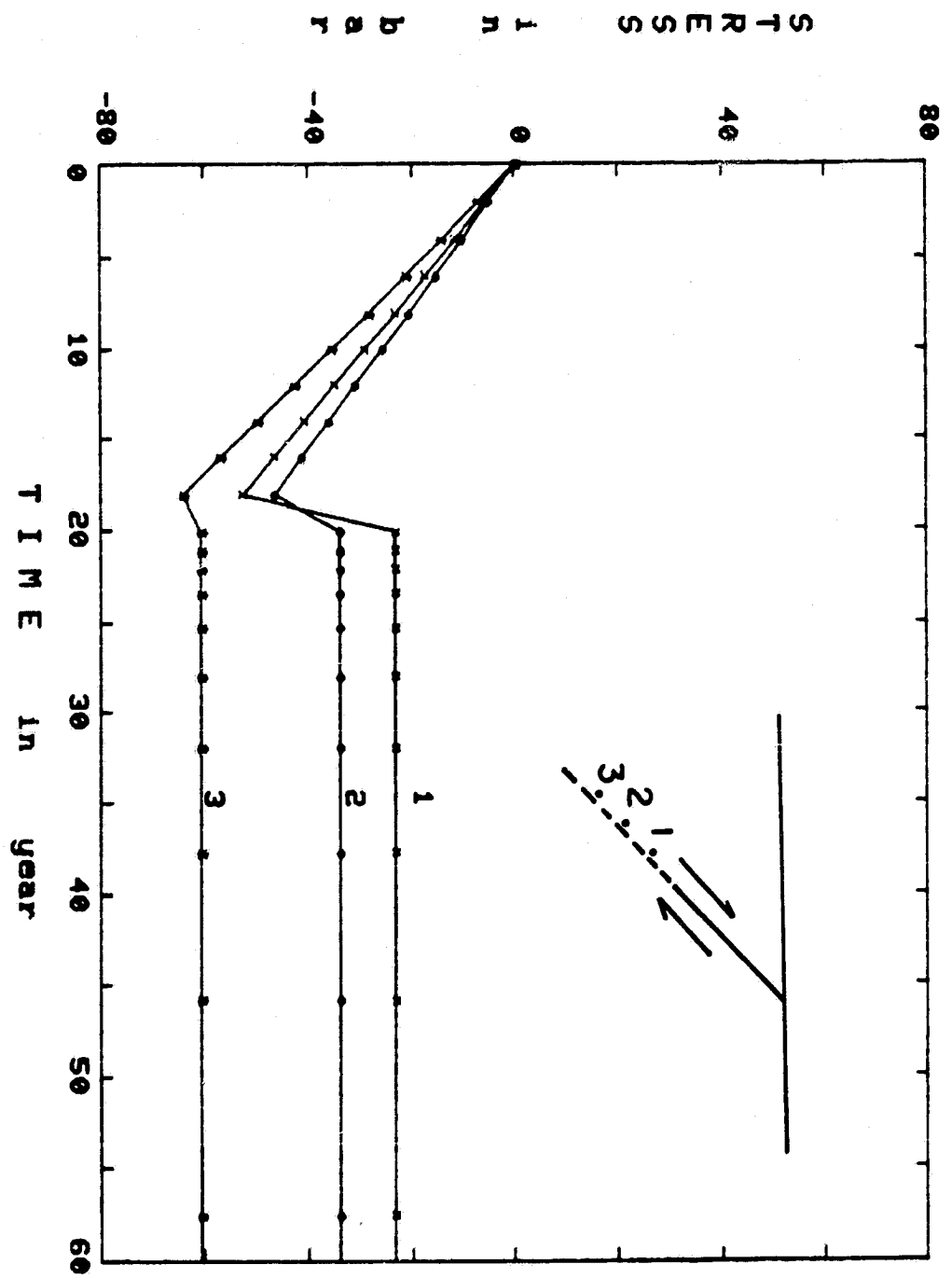

Fig 4.4.6

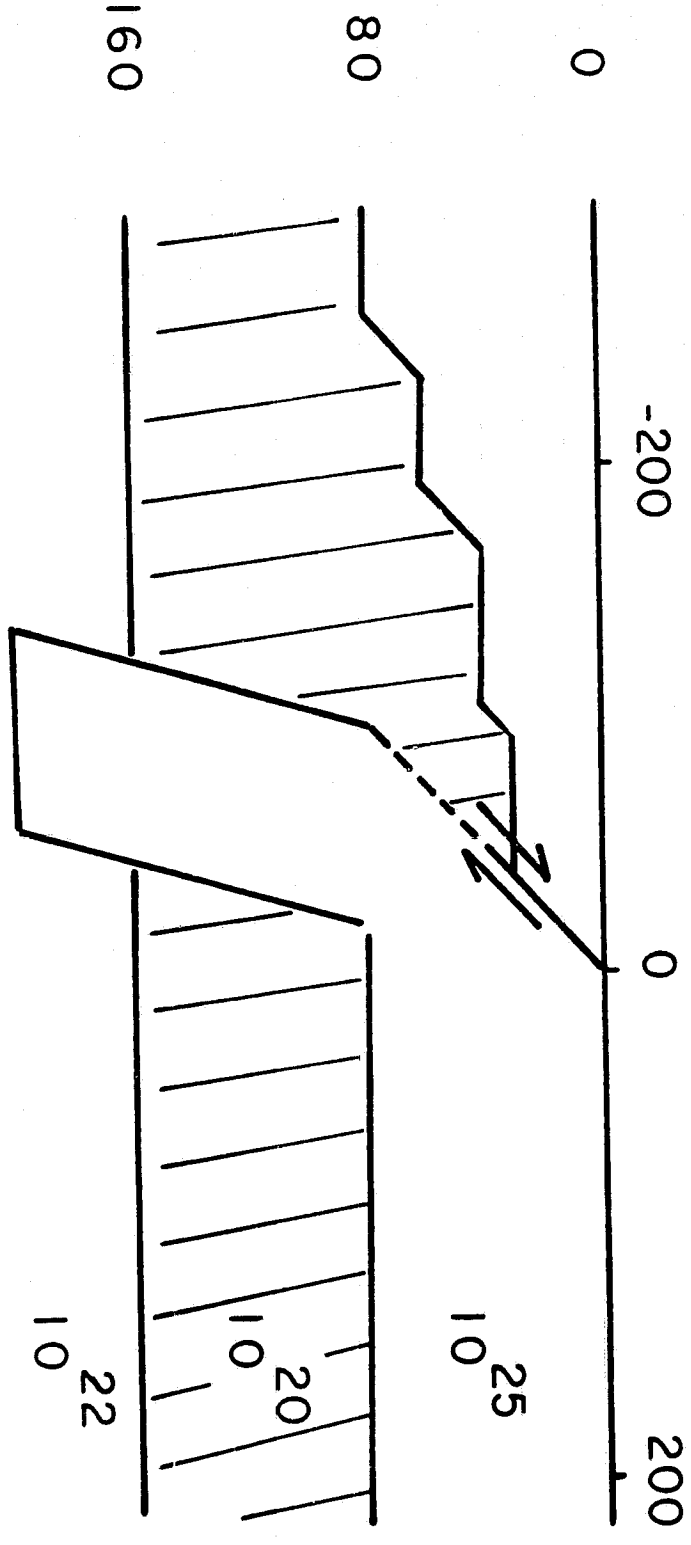

Fig 4.4.7

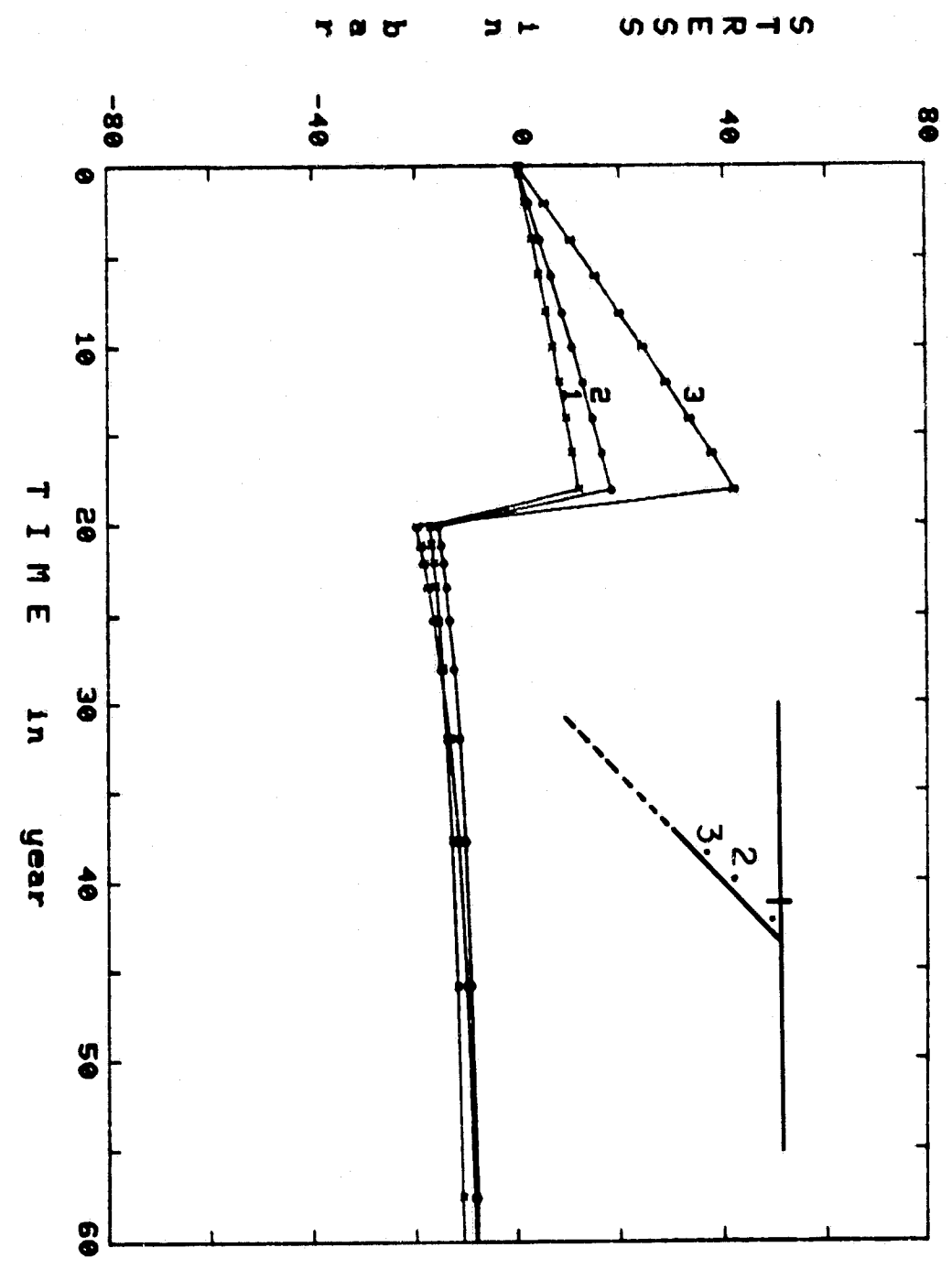

Fig 4.4.8

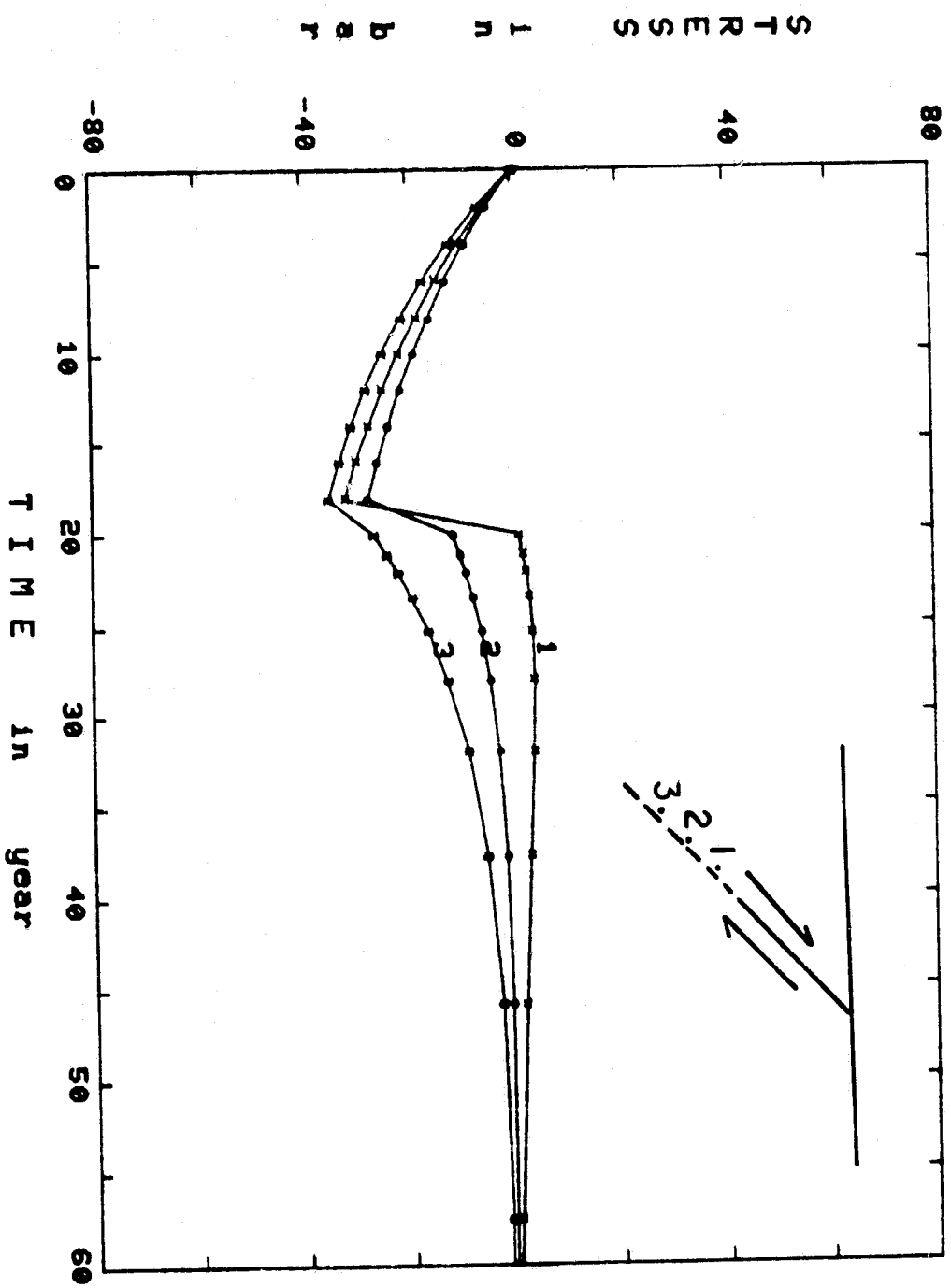

Fig 4.4.9

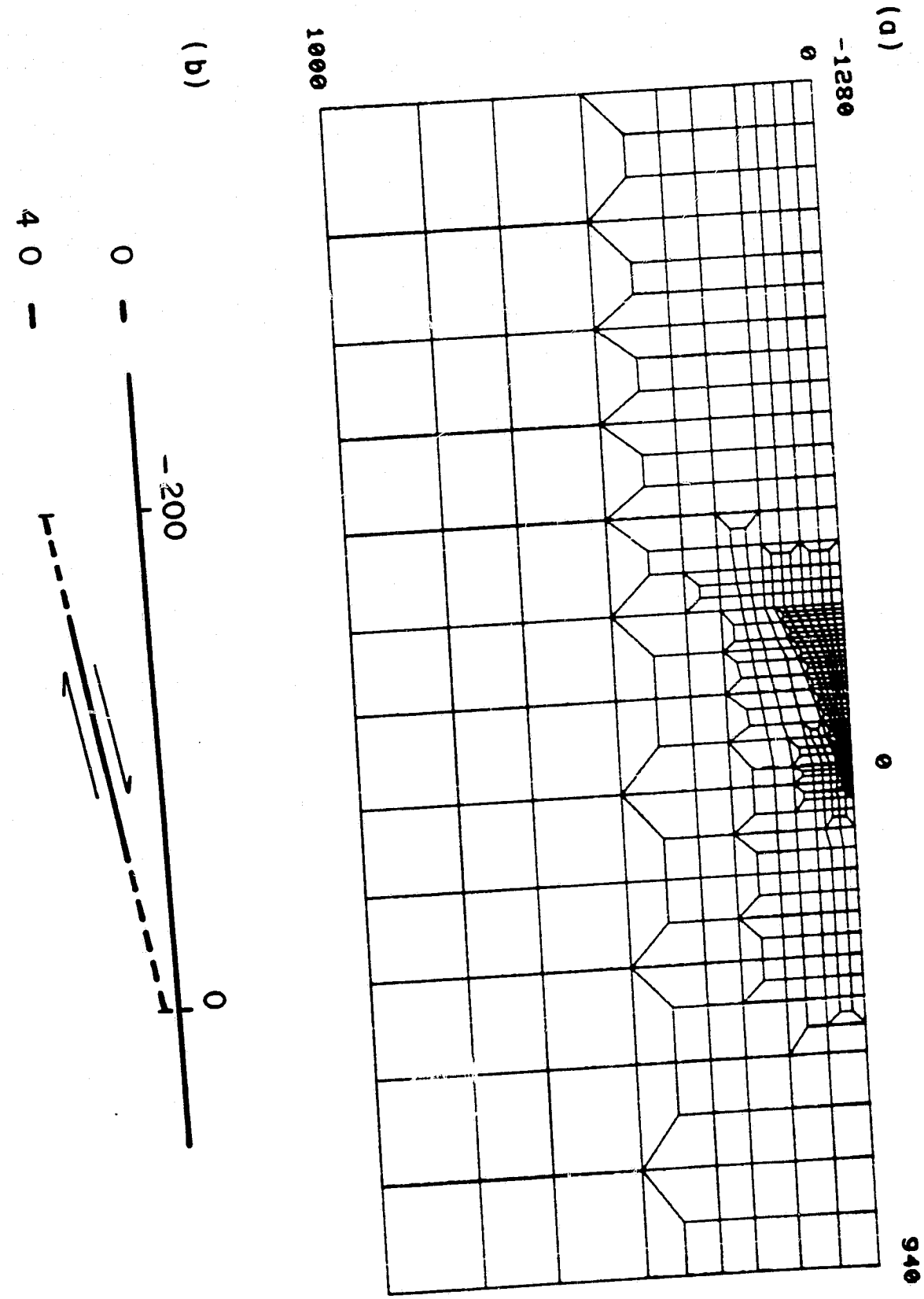

Fig 4.5.1

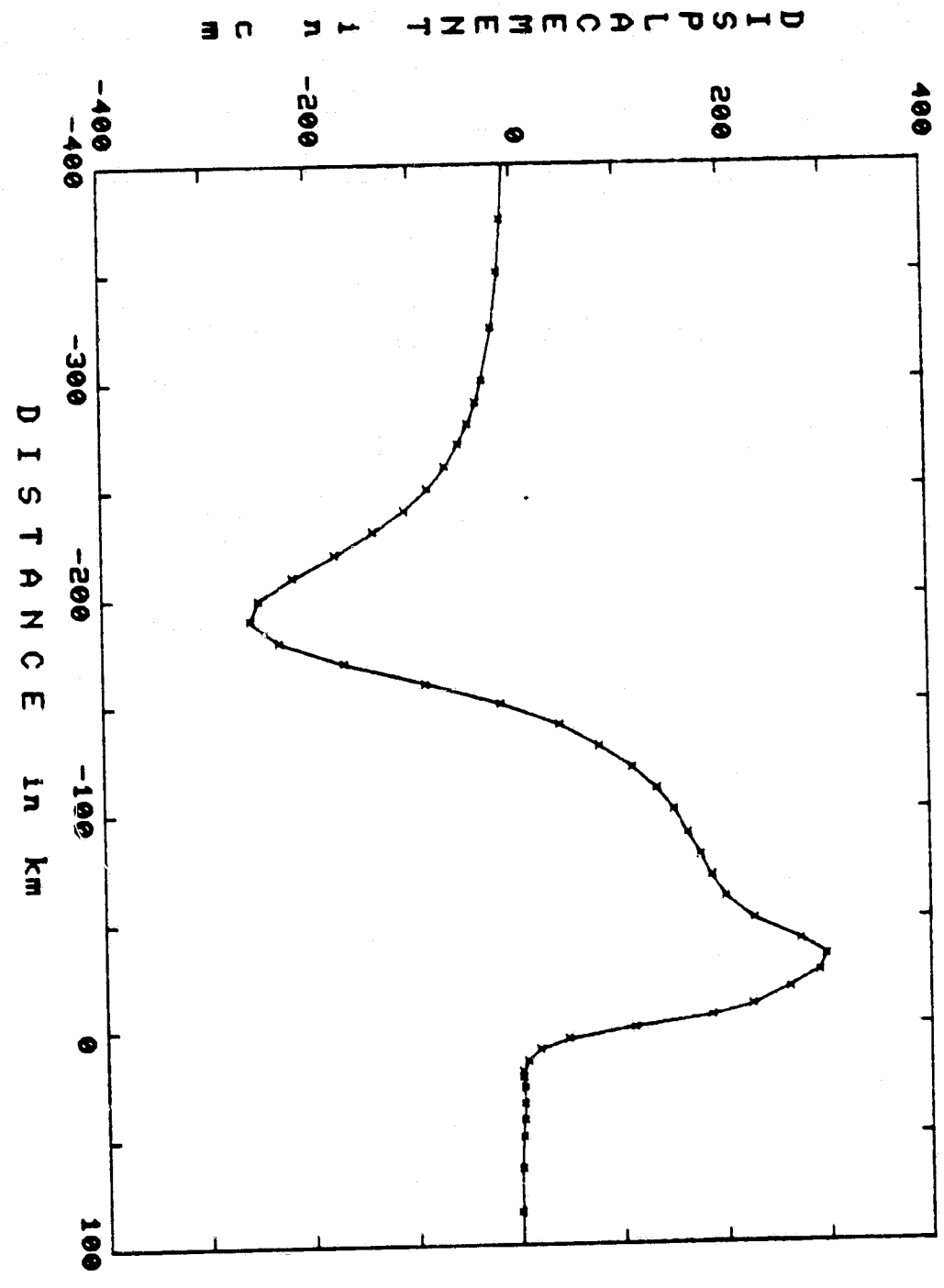
DISPLACEMENT in cm
-400
-200
0
200
400
DISTANCE in km
-400
-300
-200
-100
0
100

Fig 4.5.2

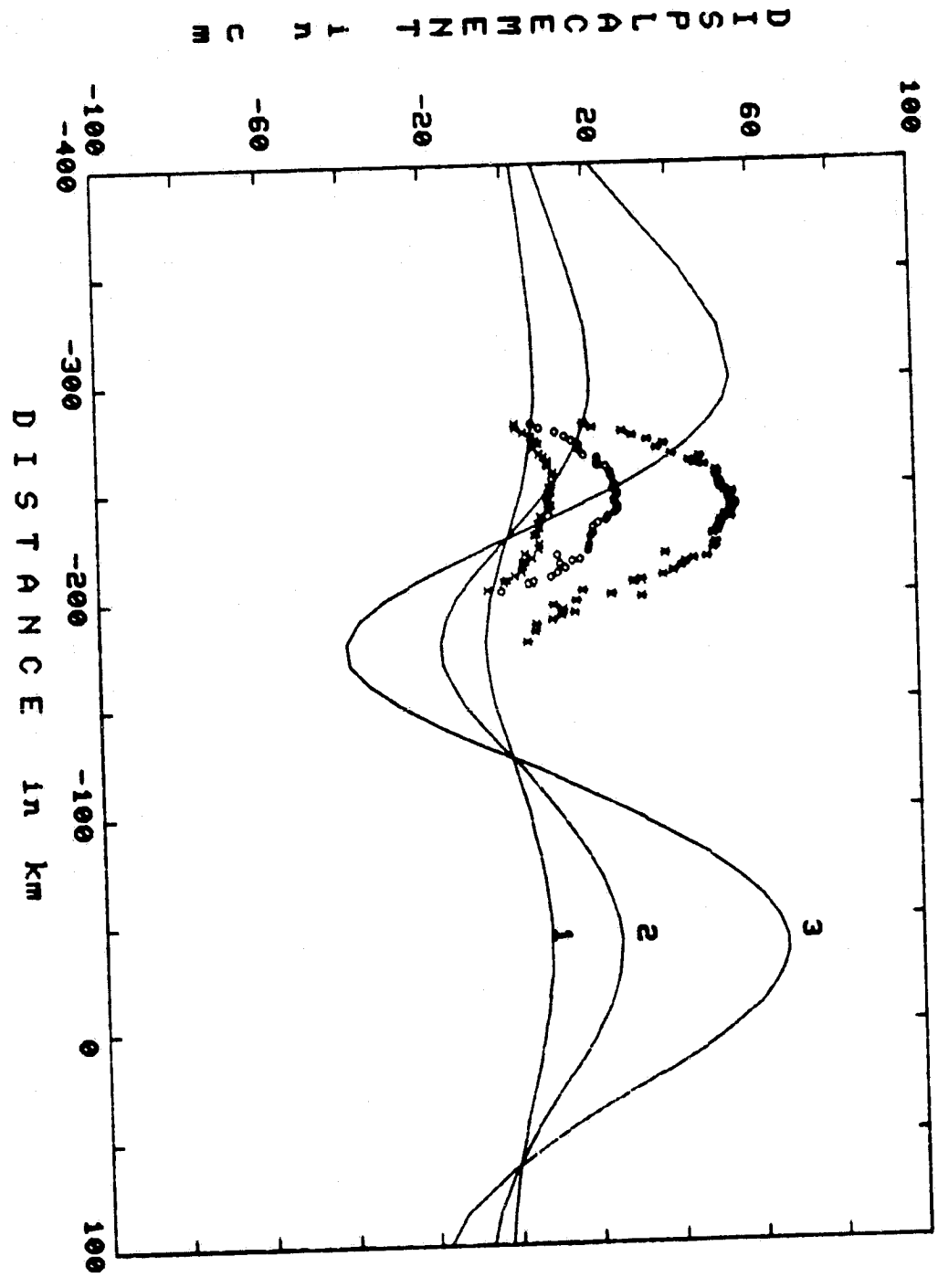
DISSAPLACEMENT in cm
-100
-60
-20
20
60
100
-400
-300
-200
-100
0
100
DISTANCE in km
1
2
3

Fig 4.5.3

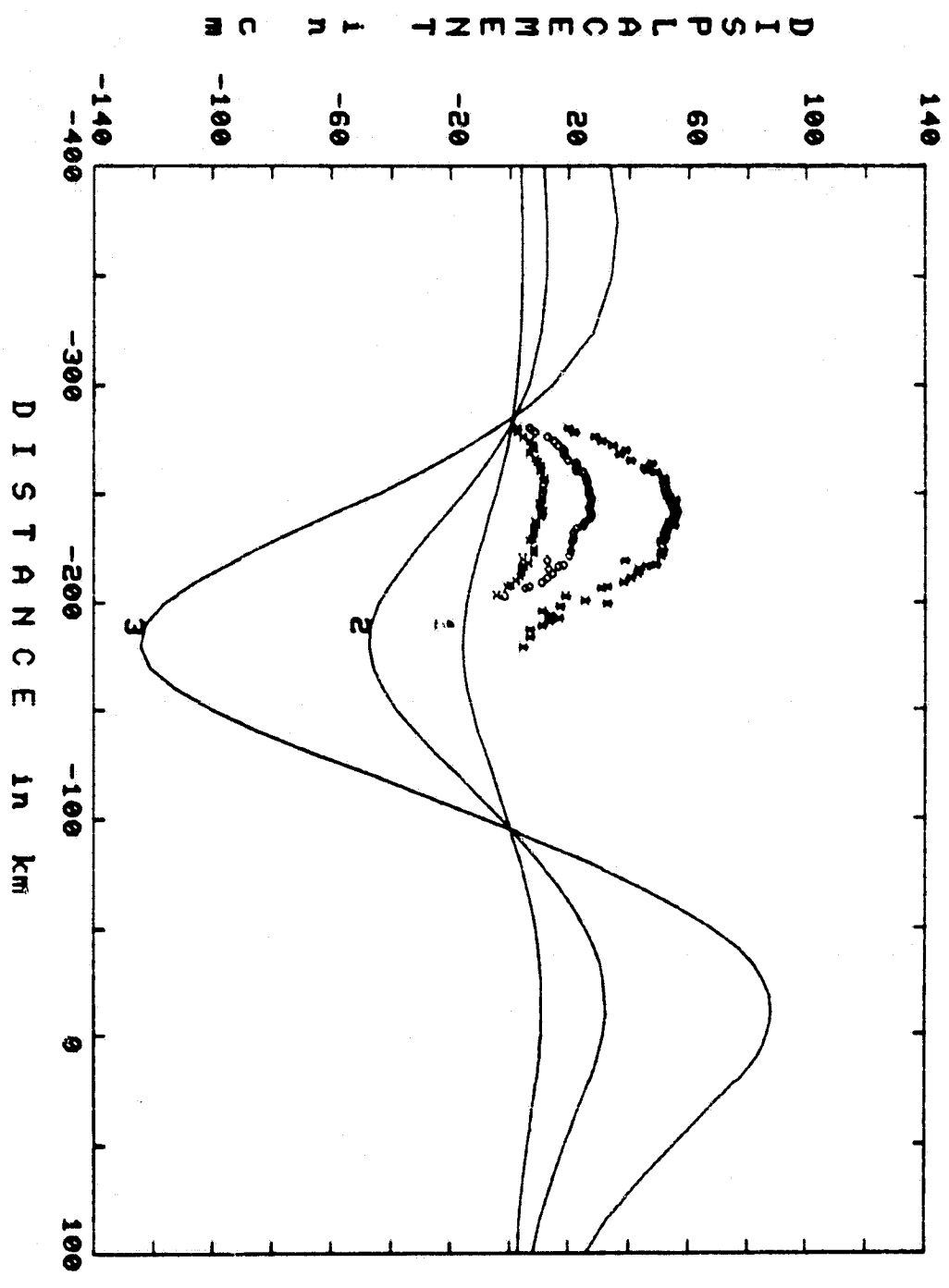
DISPLACEMENT in cm
-140
-100
-60
-20
20
60
100
140
DISTANCE in km
-400
-300
-200
-100
0
100
1
2
3

Fig 4.5.4

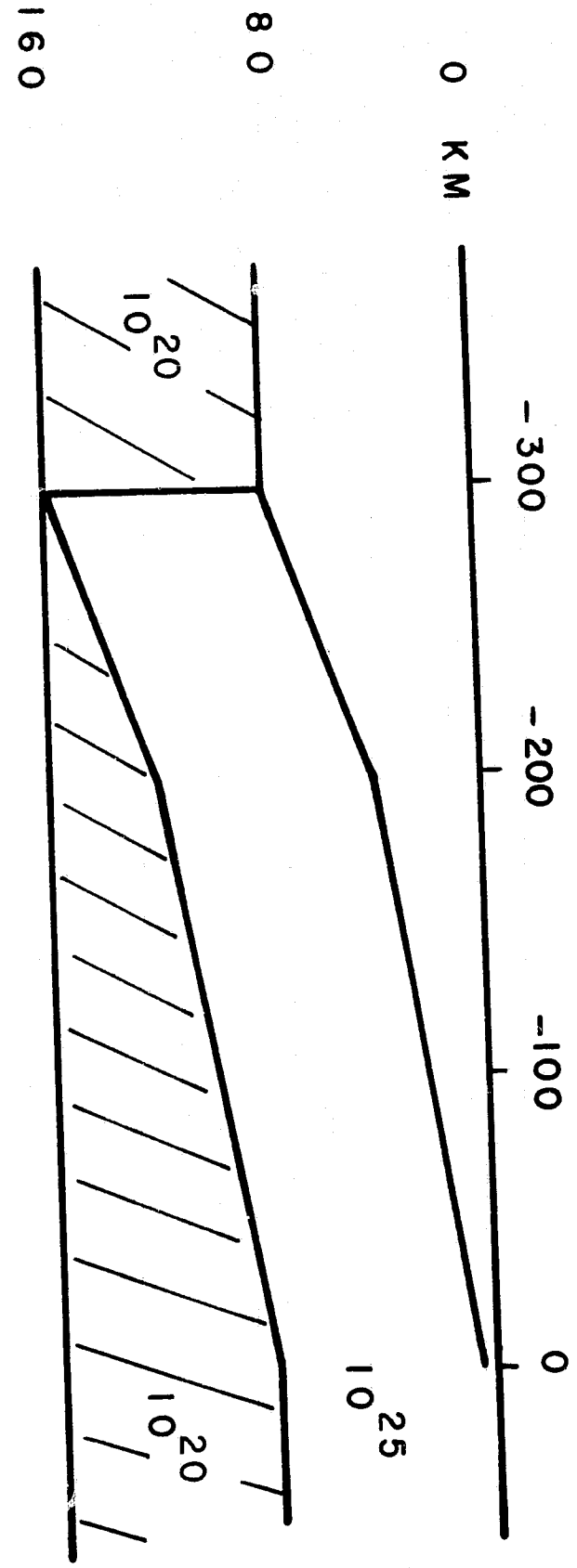

Fig 4.5.5

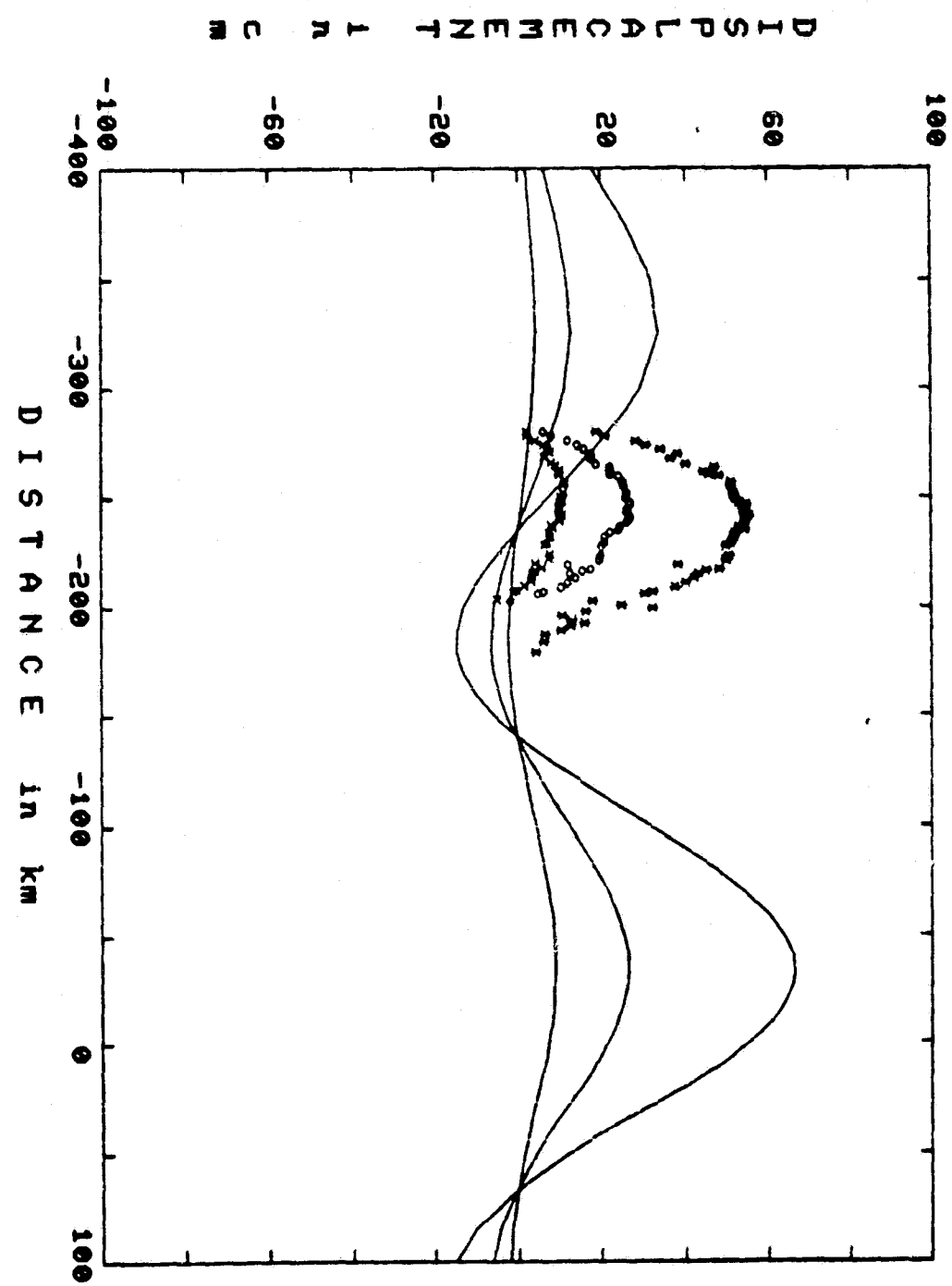
DISPLACEMENT in cm
-100
-60
-20
20
60
100
-400
-300
-200
-100
0
100
DISTANCE in km

Fig. 4.5.6

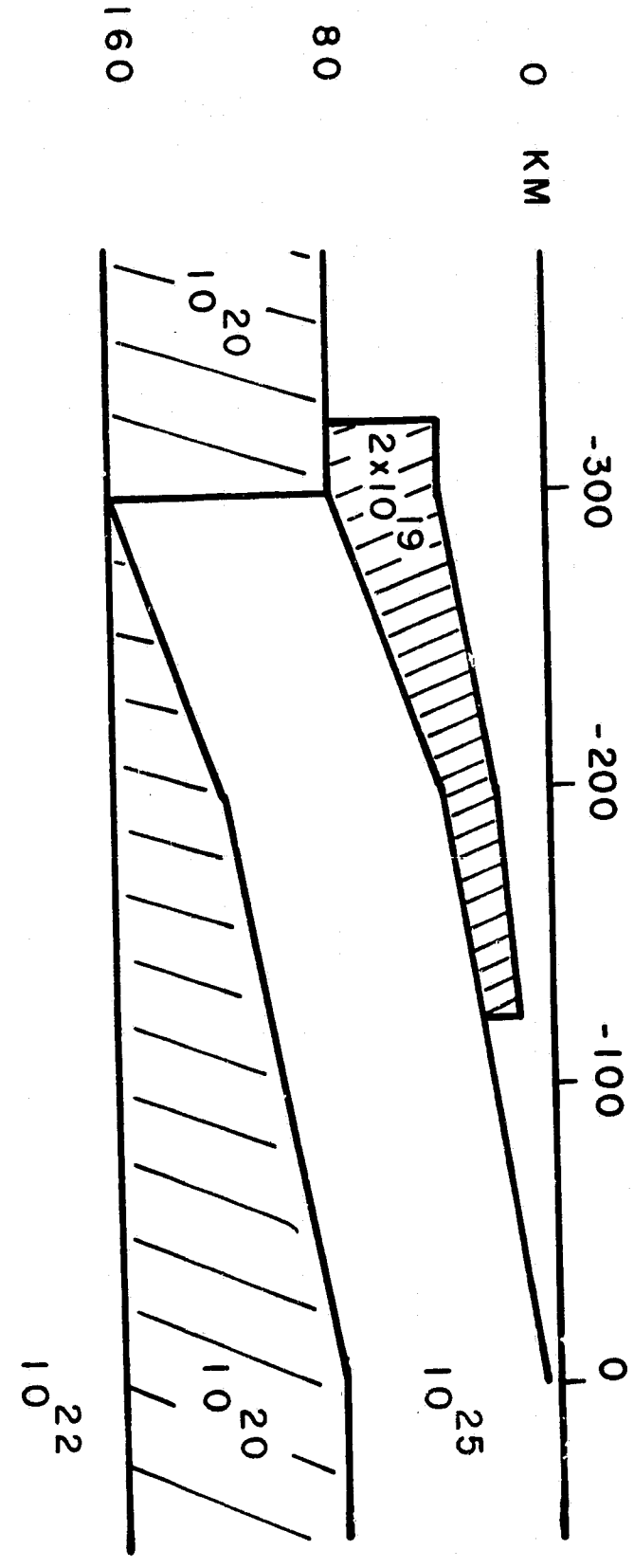

Fig 4.5.7

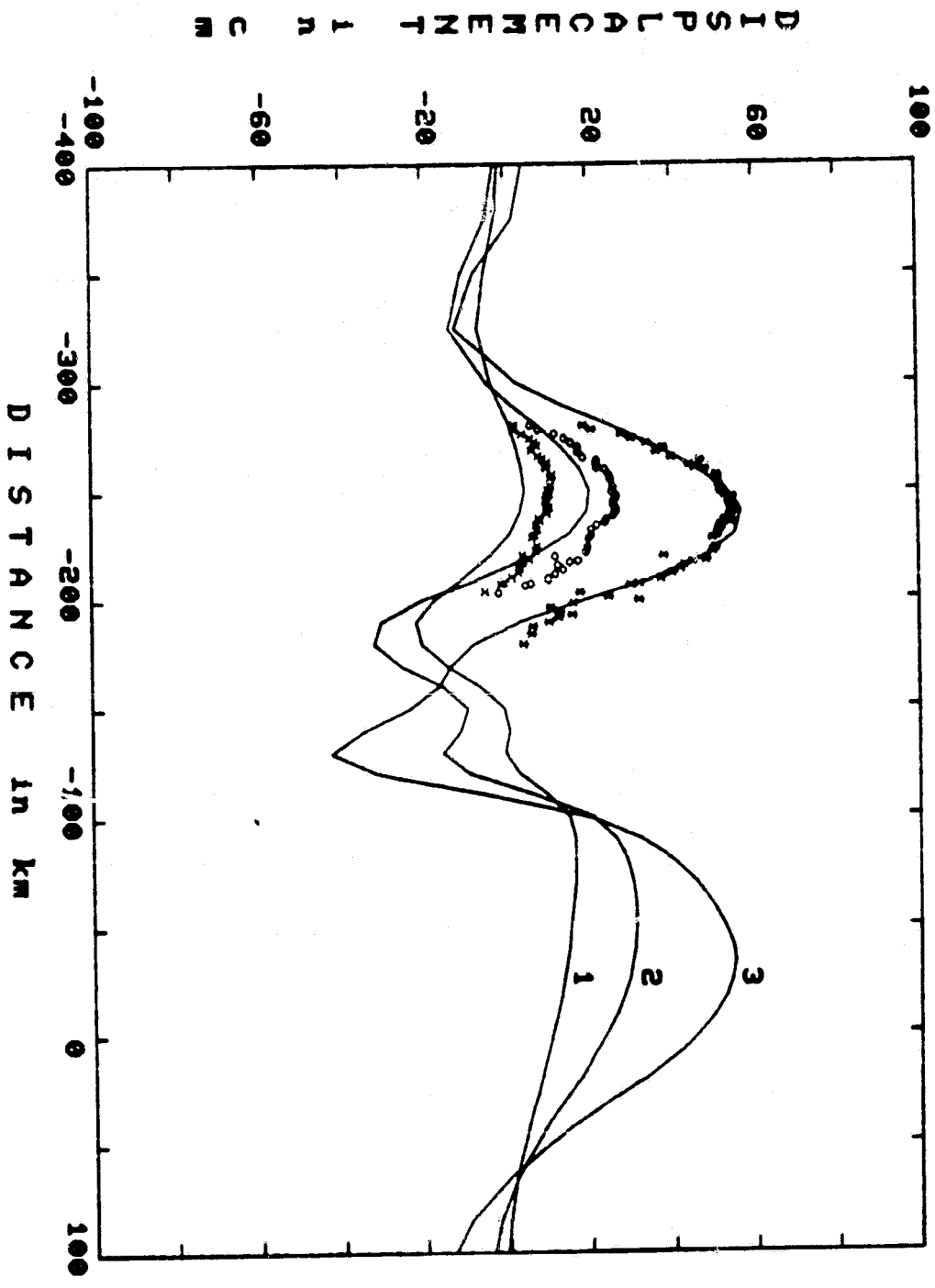
DISPLACEMENT in cm
-100
-60
-20
20
60
100
-400
-300
-200
-100
0
100
DISTANCE in km
1
2
3

Fig 4.5.8

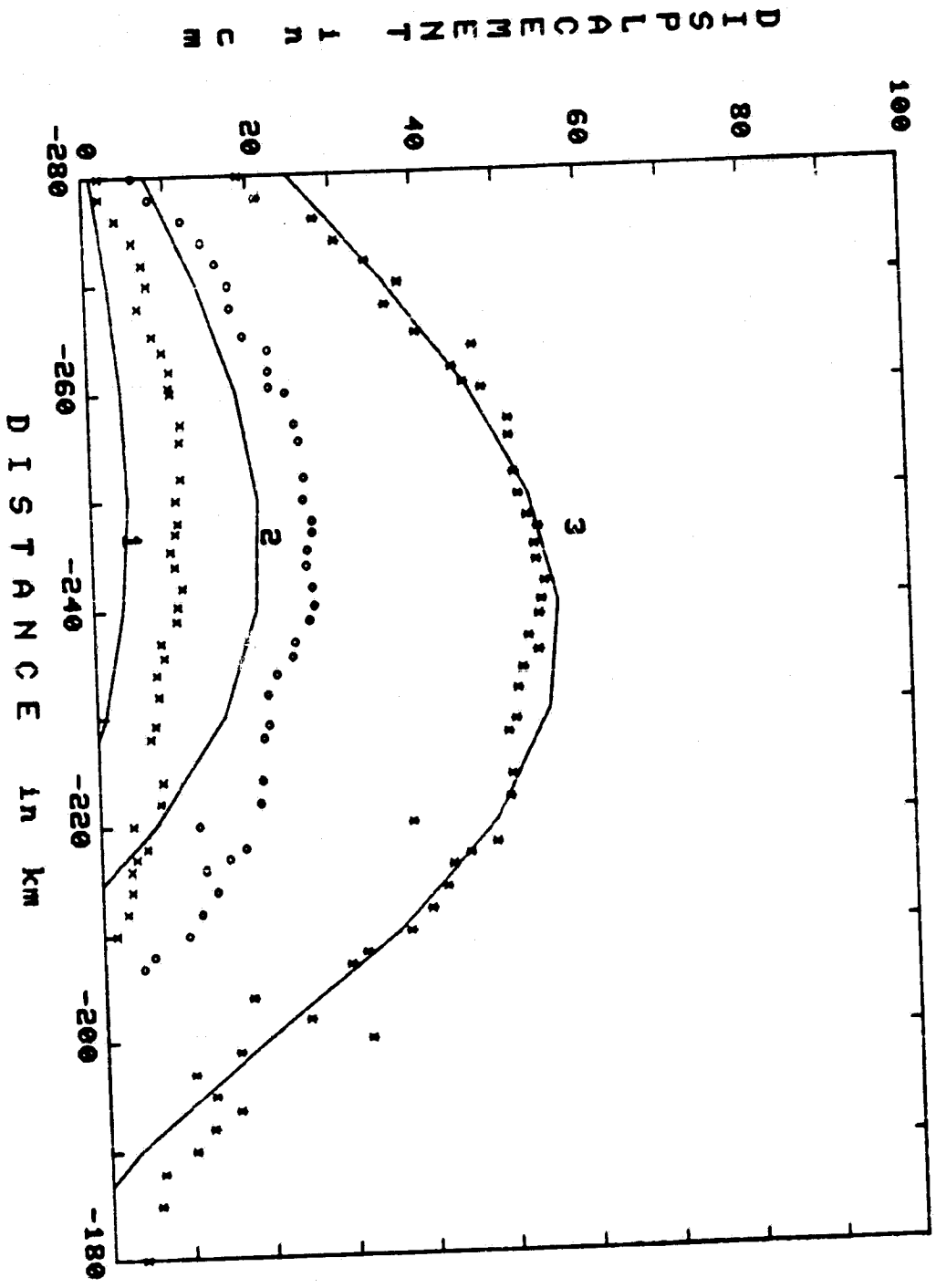
DISPLACEMENT in cm
0
20
40
60
80
100
-280
-260
-240
-220
-200
-180
DISTANCE in km
1
2
3

Fig 4.5.9

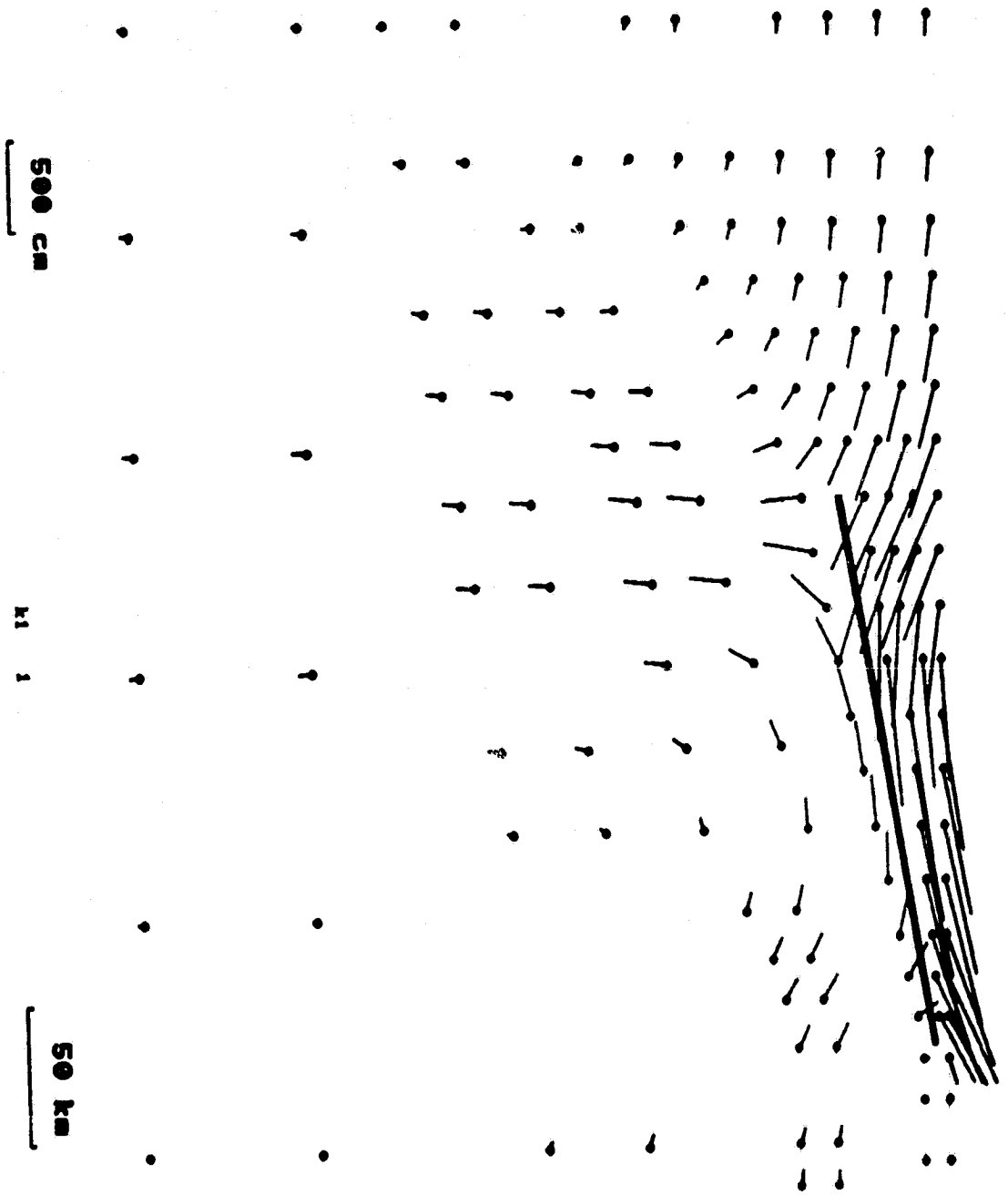

Fig 4.5.10 a

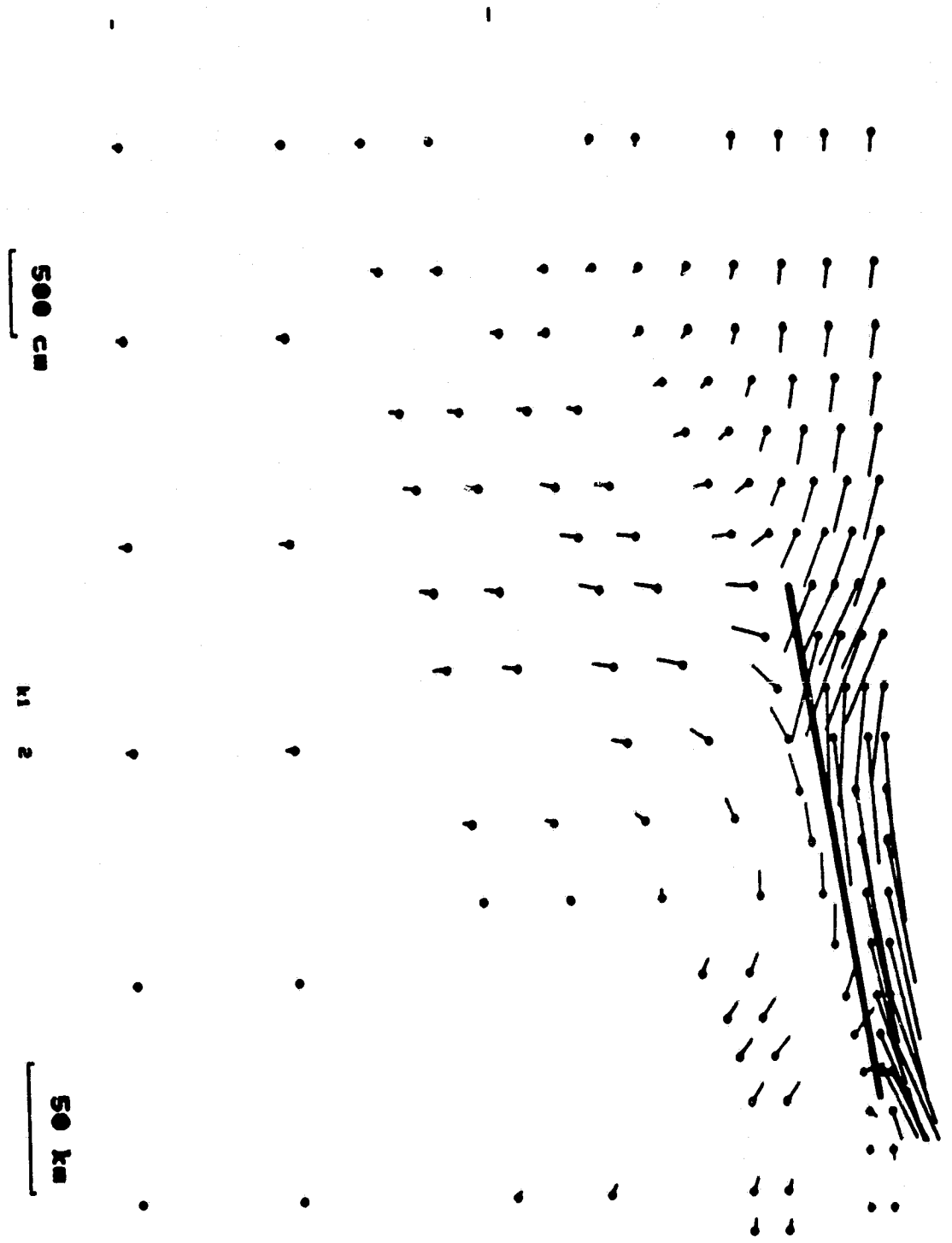

Fig 4.5.10 b

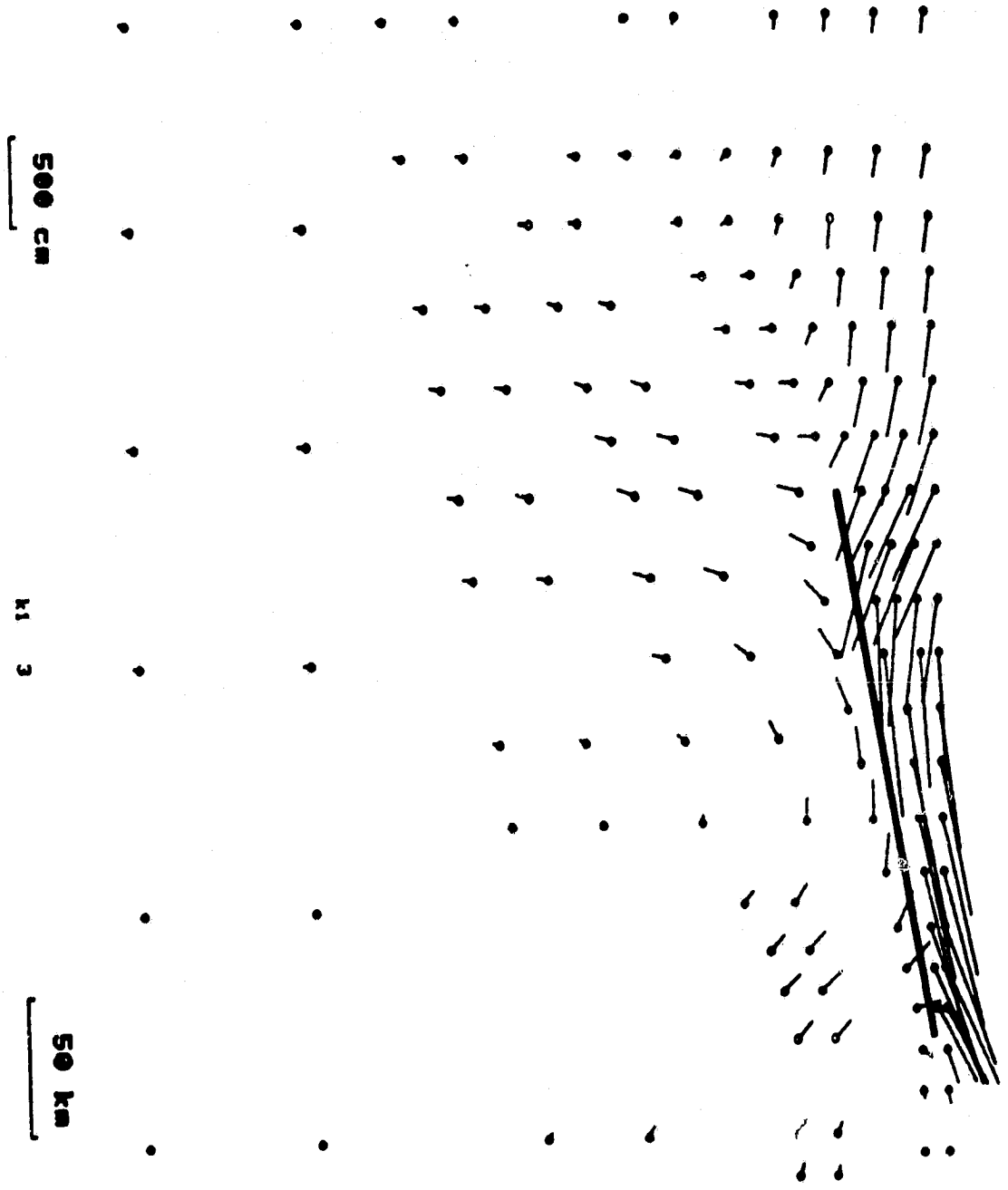

Fig 4.5.10 c

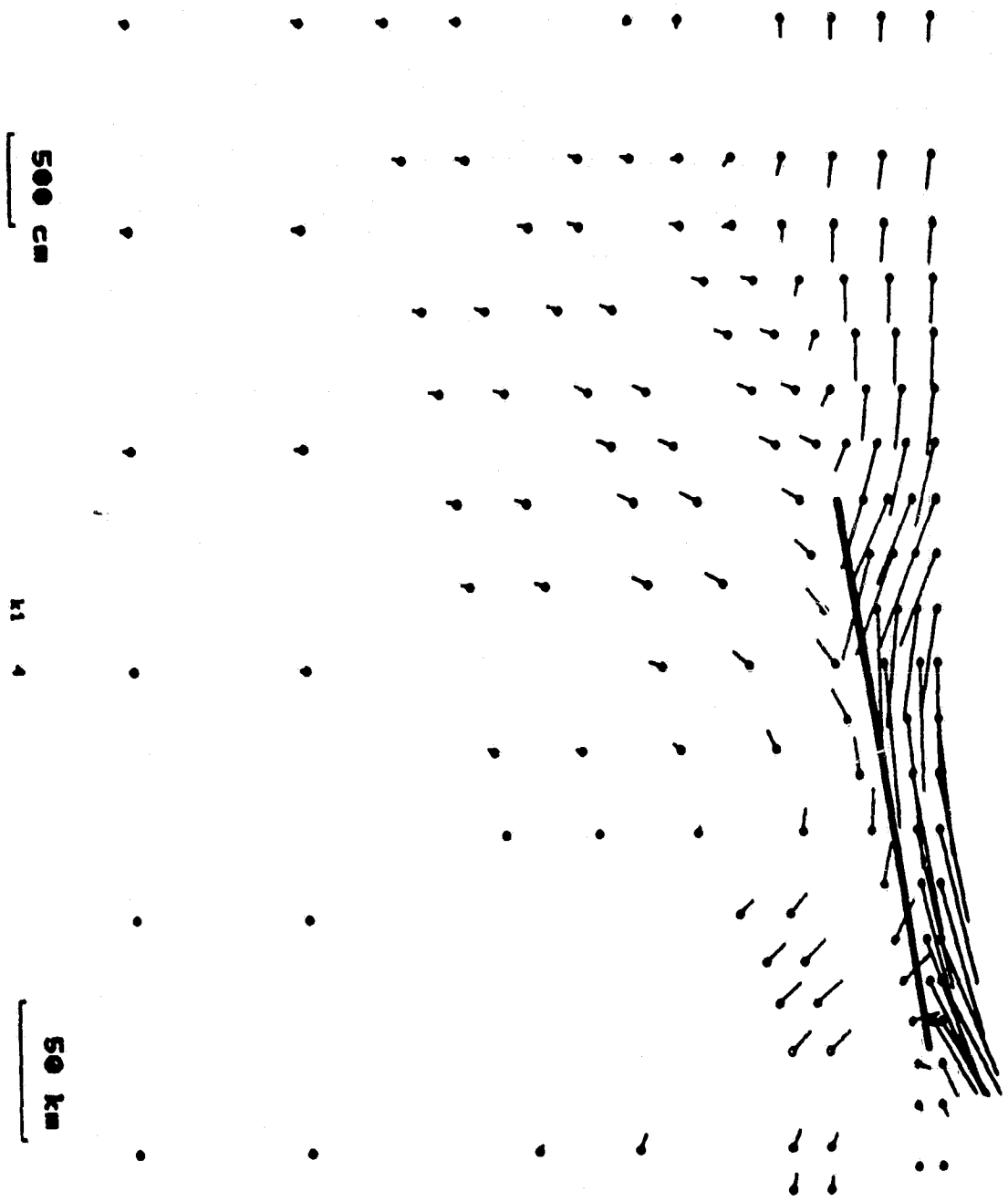

Fig 4.5.10 d

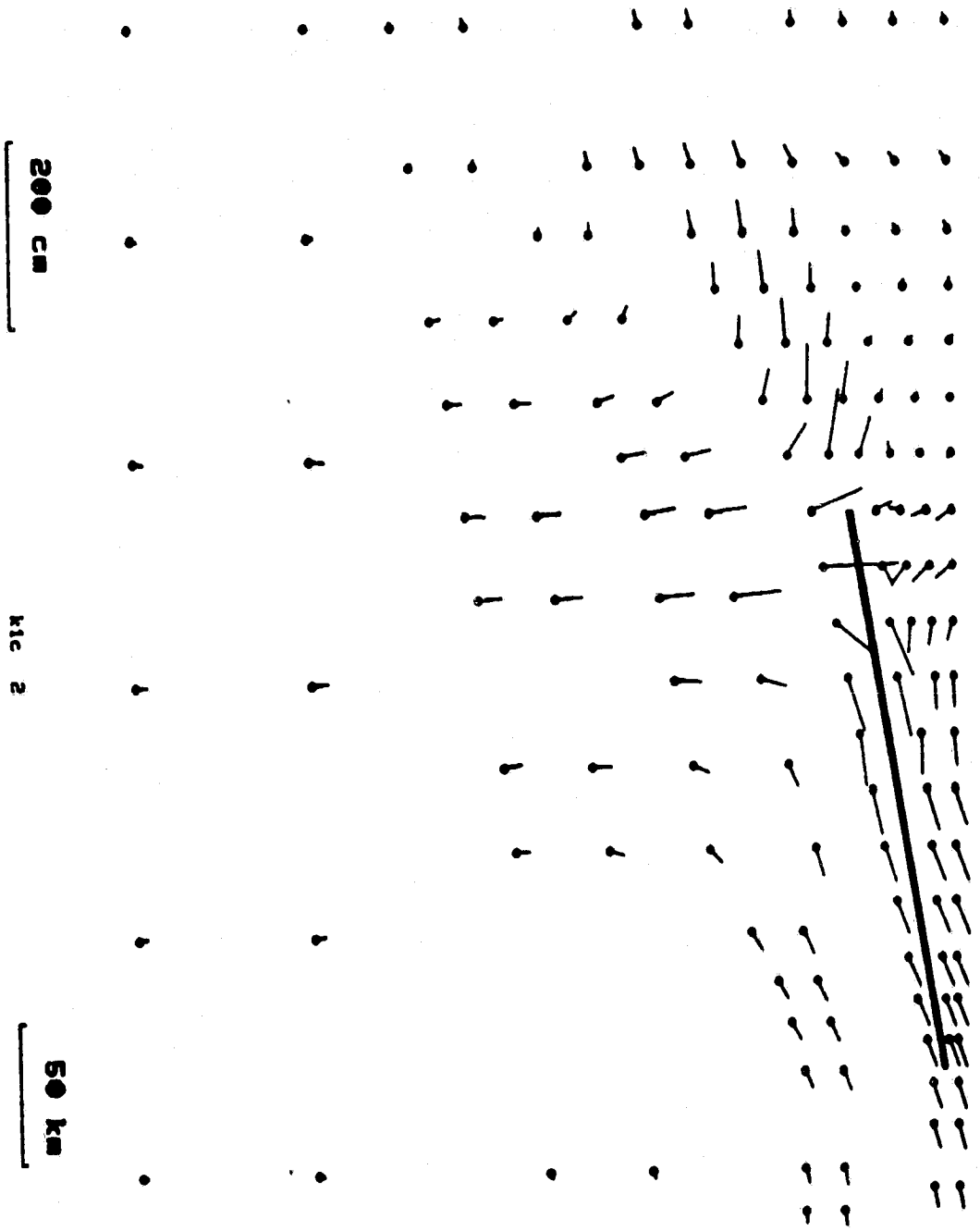

Fig 4.5.11 a

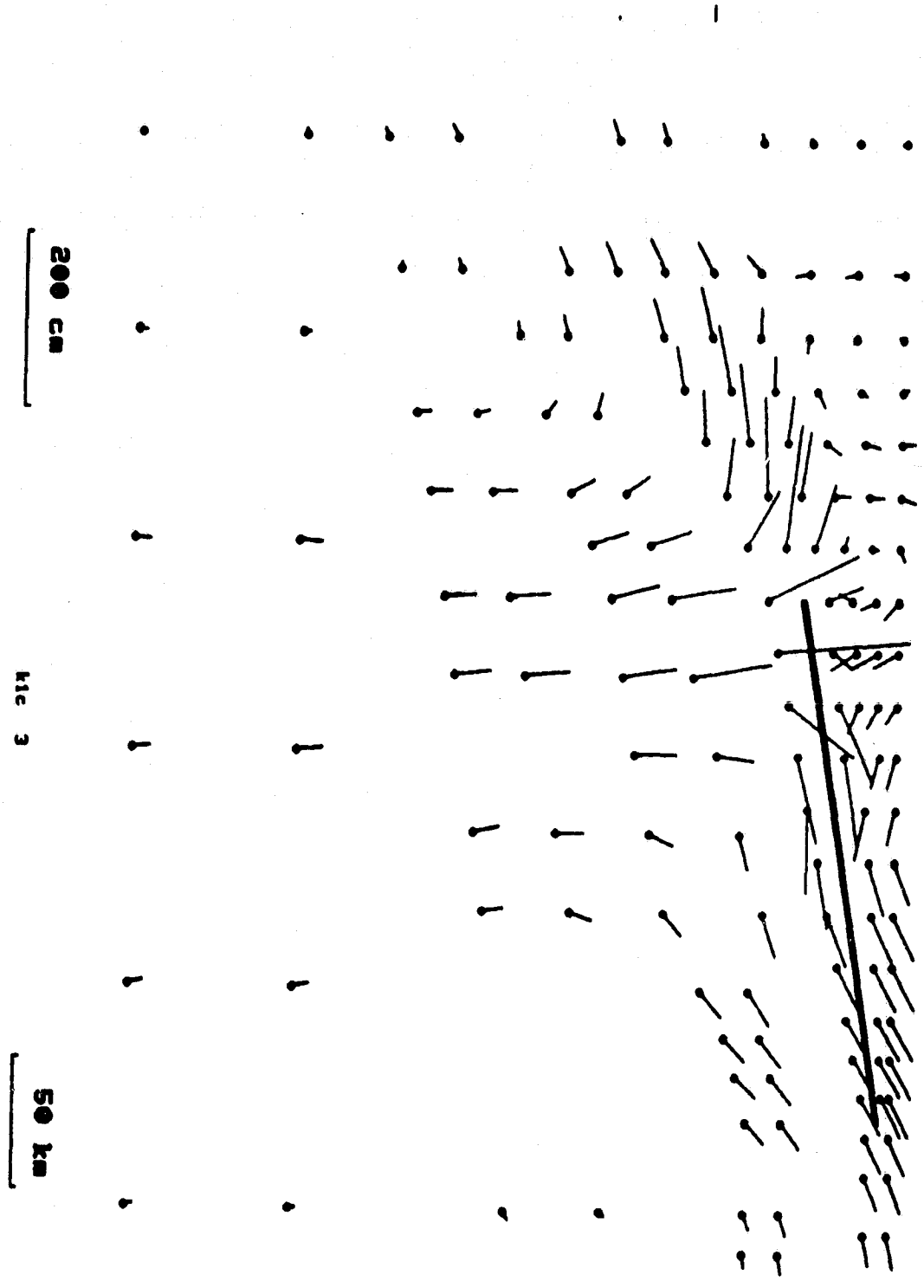

Fig 4.5.11 b

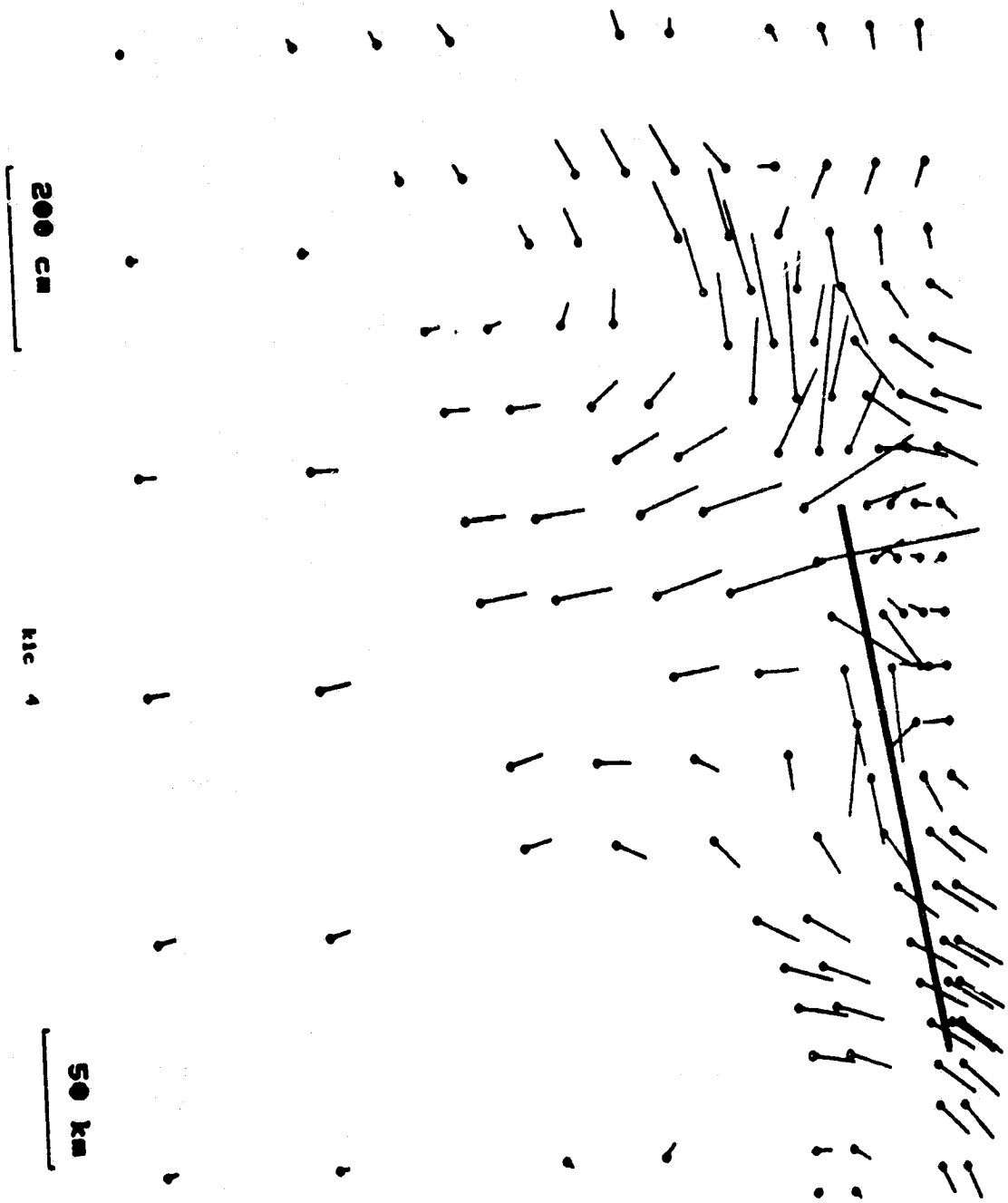

Fig 4.5.11 c

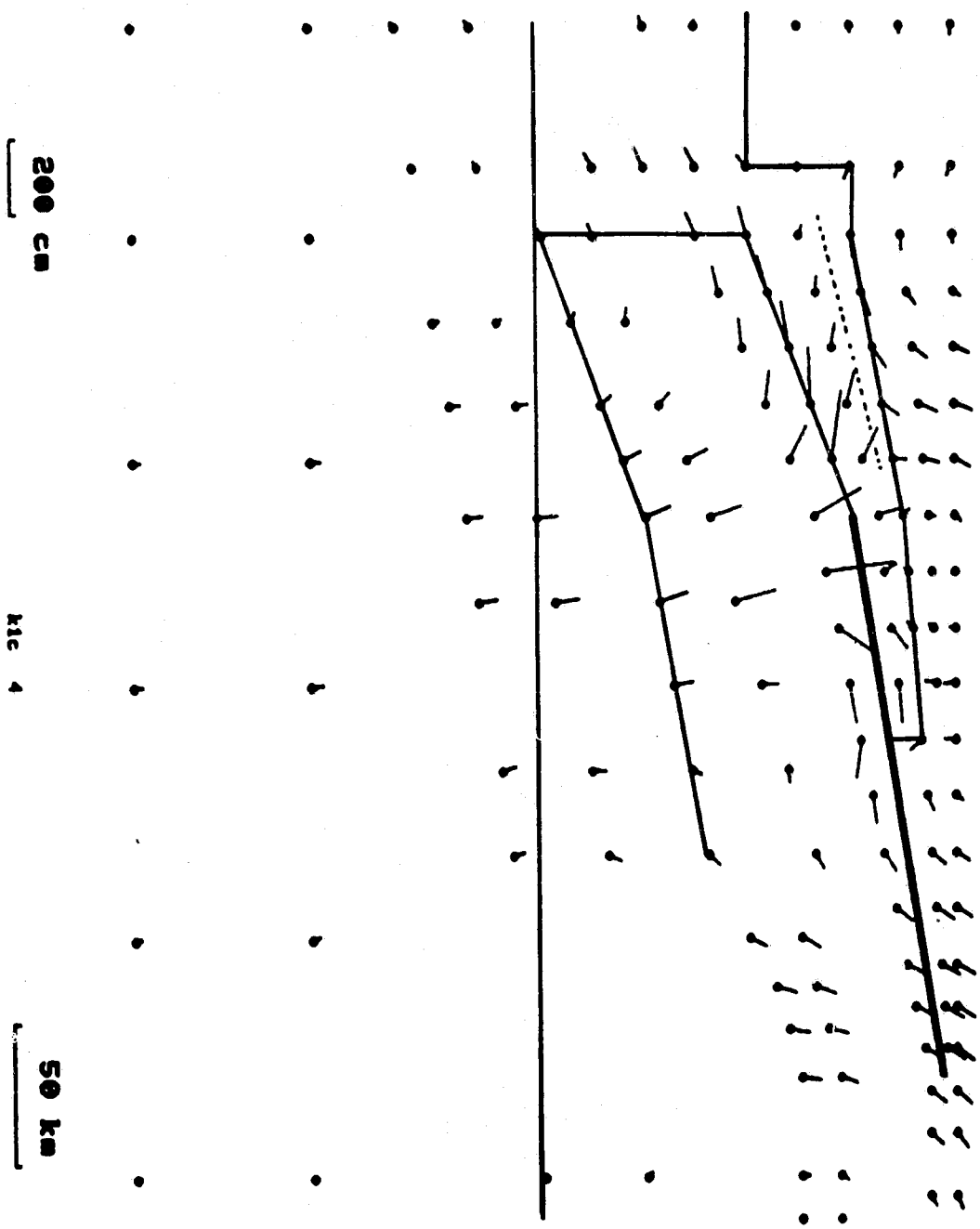

Fig 4.5.11 d

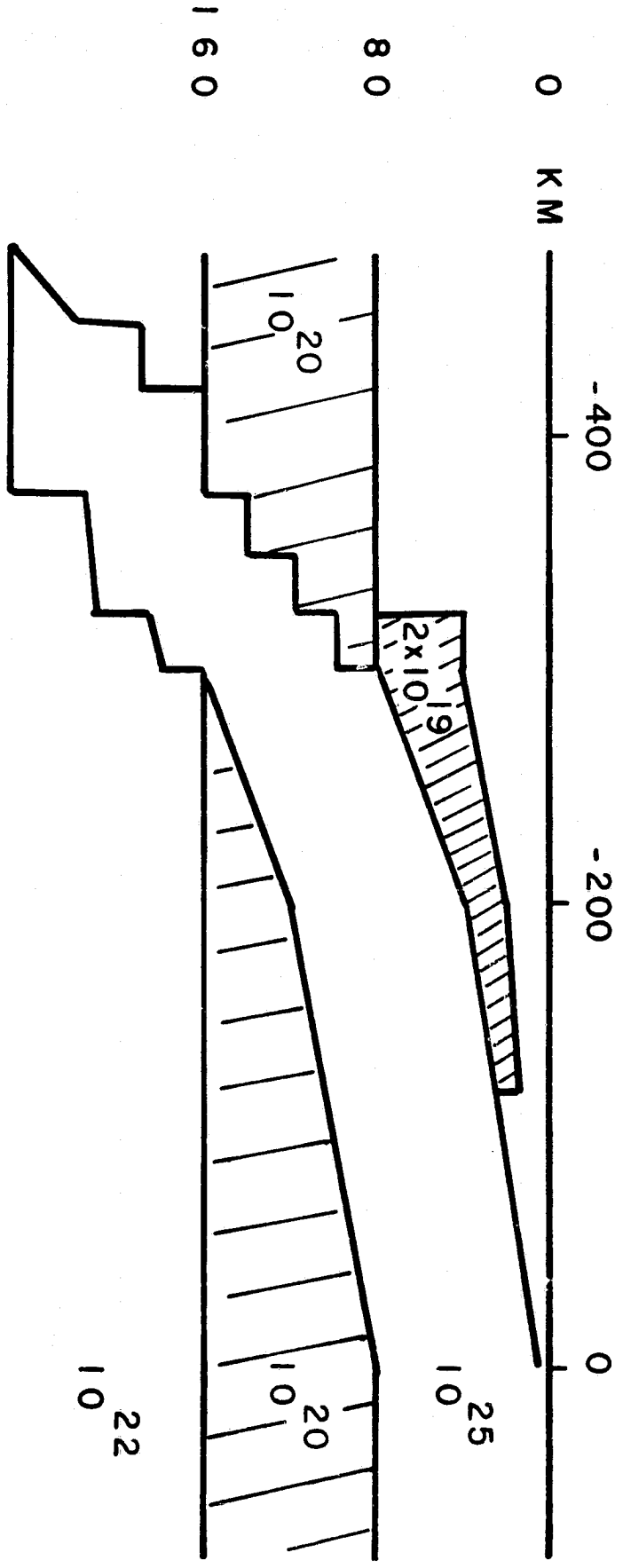

Fig 4.5.12

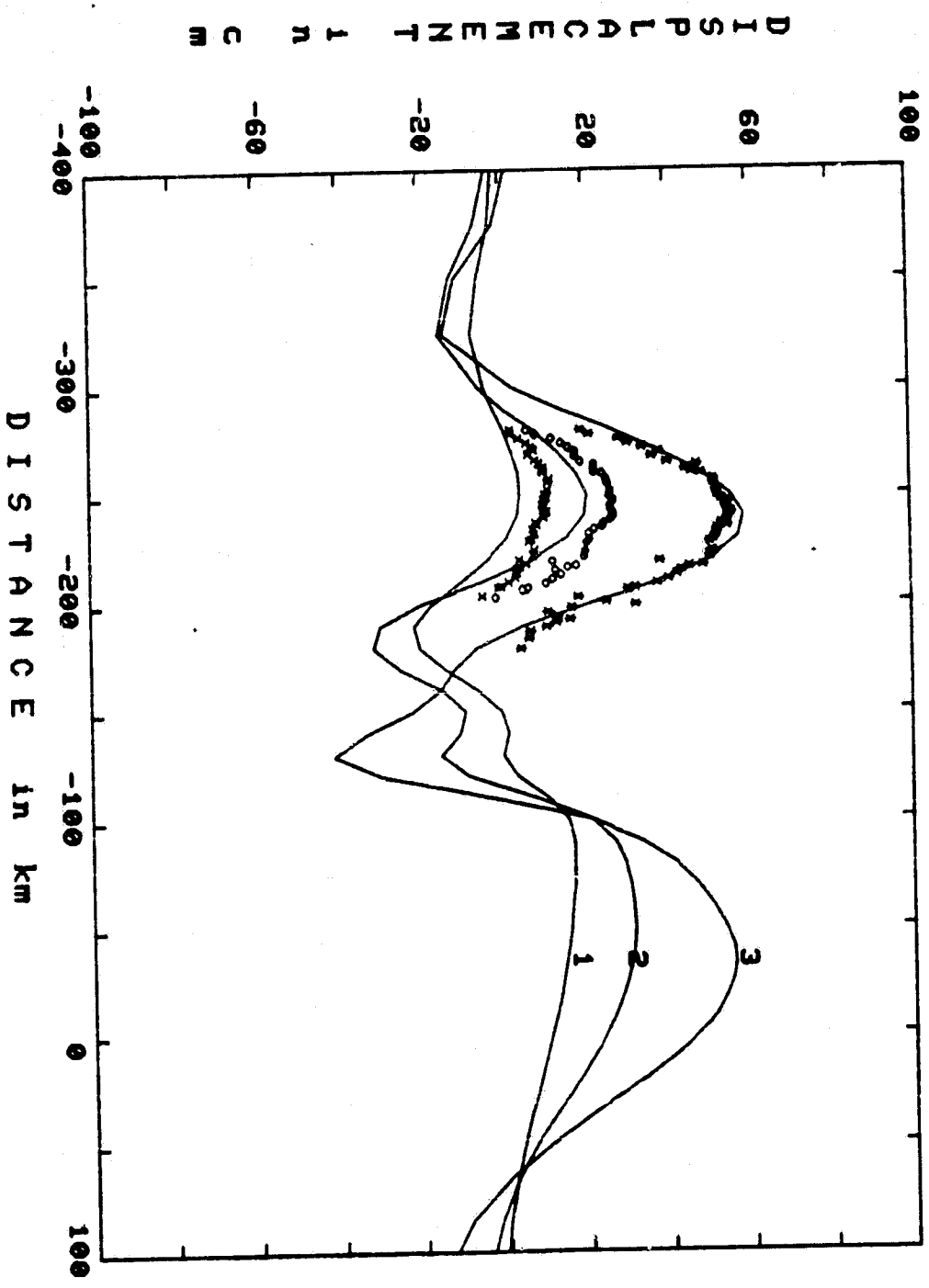
DISPLACEMENT in cm
-100
-60
-20
20
60
100
-400
-300
-200
-100
0
100
DISTANCE in km
1
2
3

Fig 4.5.13

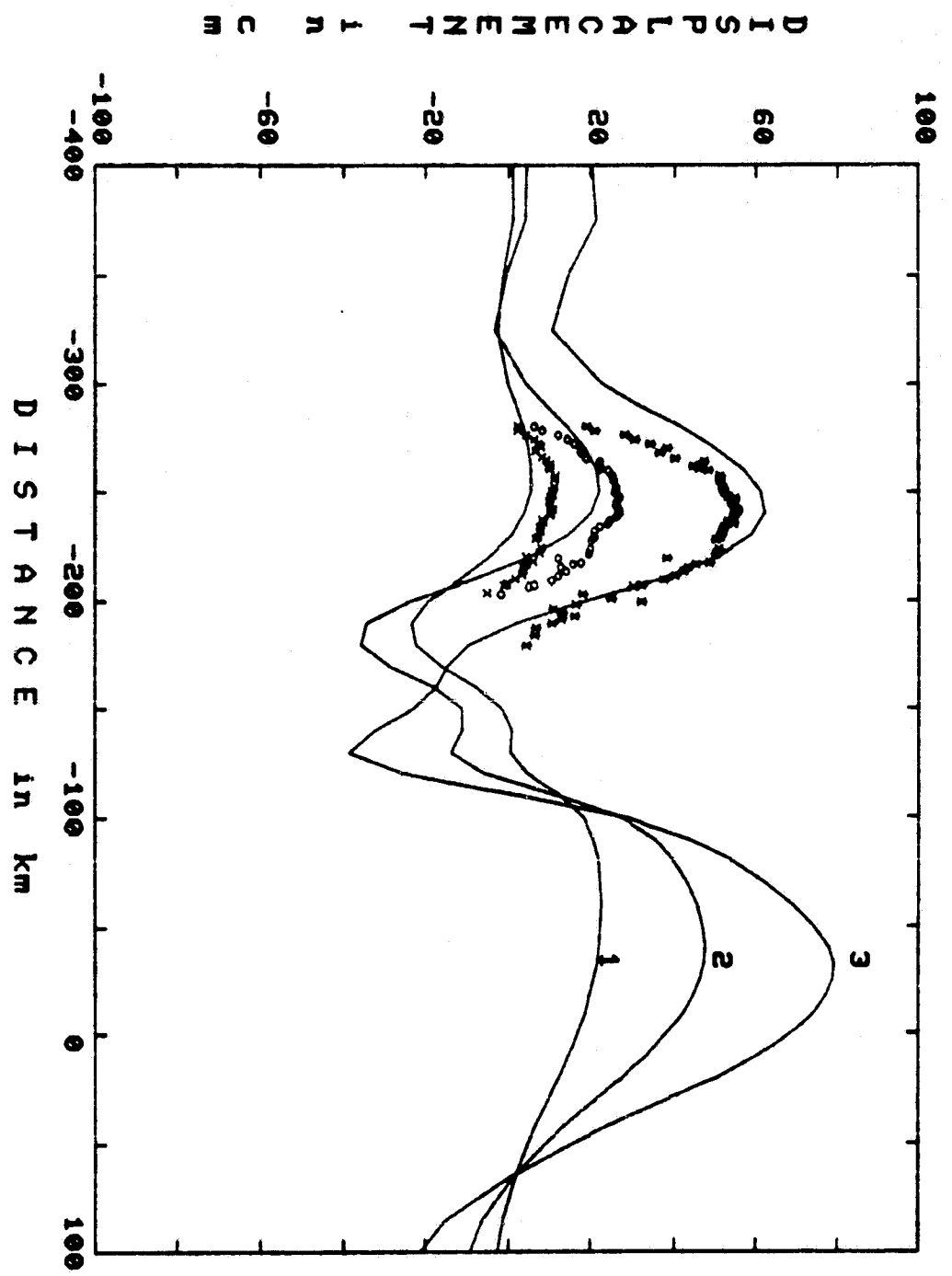
DISPLACEMENT in cm
-100
-60
-20
20
60
100
-400
-300
-200
-100
0
100
DISTANCE in km
1
2
3

Fig 4.5.14

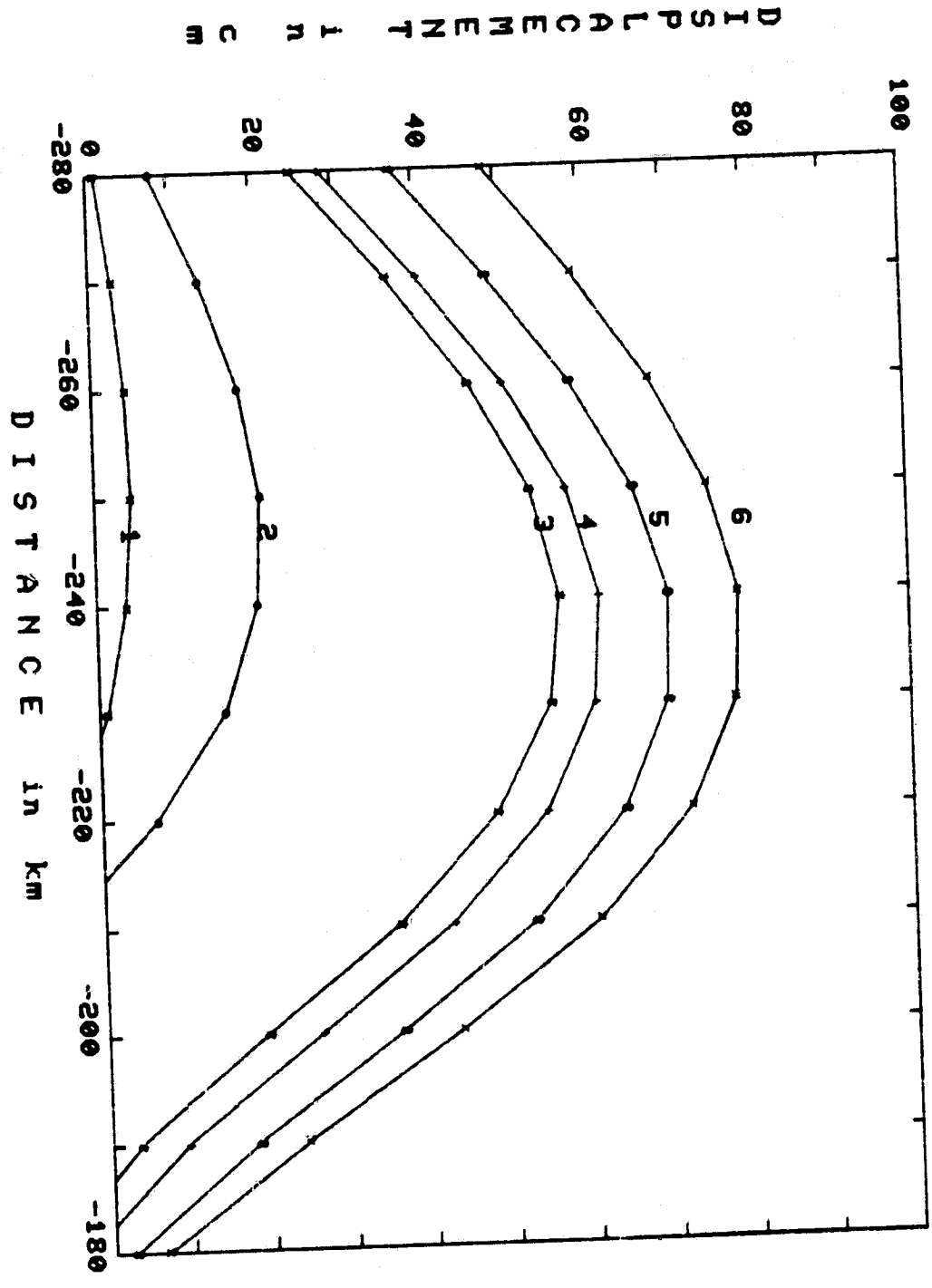
DISPLACEMENT in cm
0
20
40
60
80
100
-280
-260
-240
-220
-200
-180
DISTANCE in km
1
2
3
4
5
6

Fig 4.6.1

Chapter 5

Three dimensional analysis of dip slip earthquakes

5.1 Introduction

Great earthquakes may cause static crustal deformations detectable by modern instruments at teleseismic distances (Press 1965). This offers the possibility of studying earthquake mechanisms with teleseismic residual displacements, strains, and tilts. Great advances have been seen in new techniques of geodetic measurements in the last decade. In particular, lunar laser ranging (Bender and Silverberg 1975), satellite ranging (Agreen and Smith 1974, Smith et al 1979) and very long baseline interferometry (Counselman 1973, Coates et al 1975, Niell et al 1979) all promise to provide distance measurements with the precision of a few cm per thousand km. A network of stations for zero frequency seismology will be feasible in the near future. Geodetic measurements can be used not only to study earthquake mechanisms but also to measure plate velocities in plate tectonics. The contributions to the fundamental understanding of geo-dynamics from such measurements will be tremendous. On the other hand, the modelling and interpretation of these data covering a great scope of space and time will certainly be a challenge for theoreticians.

In anticipation of the coming data, in this chapter we will make the first step in the modelling of the large

scale time dependent problem with our finite element scheme. We will look into the problems of time dependent crustal movements at far away distances from the source and the stress diffusion due to a great dip slip event.

The static displacements due to the 1964 Alaska earthquake were detected in Hawaii (Press 1965). The model of the 1960 Chilean earthquake also indicated that the static effects caused by the earthquake were measurable in the plate interior (Richardson 1978b). However, the time dependent displacements due to great earthquakes at teleseismic distances have not been adequately studied. This information is essential in the deduction of plate velocities from geodetic data, since great plate boundary earthquakes may produce significant effects at the stations of geodetic measurement. On the other hand, seismic activities in different regions are often correlated. Migration of earthquakes along the transform faults have been reported, as discussed in chapter 3. Migration and correlation of earthquakes in subduction zones have also been found (Fedotov 1965, Mogi 1968, 1969ab, Kelleher 1970, Sykes 1971, Kanamori 1972, Kelleher 1972, Mogi 1973, Utsu 1974,1975, Shimazaki 1976,1978, Yamashina 1979). Correlation of global seismicity has been discovered using time series analysis (Chinnery and Landers 1975). Discussion of the migration of seismicity along subduction zones needs a three dimensional model, because a two

dimensional plane strain model assumes that the fault length is infinite. In this chapter, we will investigate the possible triggering effects of a dip slip event.

The modelling of large scale three dimensional problems is often hampered by the cost of computation. The number of operations in solving a system of linear equations in finite element analysis is proportional to NB^2, where N is the degree of freedom and B is the bandwidth of the stiffness matrix, which also often correlates with the size of the problem. When we discussed vertical strike slip earthquakes in chapter 3, the symmetry properties of the vertical strike slip fault were fully exploited. Only a quarter of the physical region was used in the computation. This constituted a great savings in computation cost. A dip slip event, except for the special case of a vertically dipping fault, can at best have a mirror symmetry. At least half of the physical region must be used in the computation. At the present time, there are no suitable geodetic data for comparison with the model results; we will use a coarse grid model to look at the general features of relaxation. However, the same scheme can be used with a finer grid model when data become available.

5.2 Model description

We model the earthquake as a sudden slip (step function in time) on a fault surface. The medium is assumed to be elastic in bulk and viscoelastic in distortion. The elastic properties are Young's modulus 2×10^{12} dyne/cm^2 and Poisson's ratio 0.25. For the disturbances caused by the earthquake at far distances, the detailed structure in the source region is not important, and a layered model should be adequate. The model lithosphere has a thickness of 80 km and a viscosity of 10^{25} poise. From 80 km to 180 km the viscosity is 10^{20} poise, and below 180 km the viscosity is 10^{22} poise. The schematic diagram of the fault and the viscosity model is given in figure 5.2.1. The fault is 500 km long and 80 km deep, with dip angle 30 degrees. The fault slip is 10 m from 0 to 40 km deep, and it tapers off linearly from 10 m at 40 km deep to zero at 80 km deep; the fault slip also tapers off linearly to zero along the 50 km segments near the two fault edges along the strike direction. The finite element model uses half of the physical region. The top view of the finite element grid is given in figure 5.2.2. The plane y = 0 is the symmetry plane bisecting the fault. The fault intersects the free surface at coordinates x = 0 km and y = 0 to 250 km in the finite element model, as indicated by the dark line in the figure. The y displacement on the symmetry plane (y=0) is set to zero because of the symmetry. The lower boundary is assumed to be rigid while the side boundaries are assumed to

have spring boundary condition. The region is large enough that the external boundaries far away from the source have insignificant effects on the results. The physical model region is 3200 km long, 2200 km wide, and 700 km deep. Six grid surfaces and five layers of solid elements are used. The elements are eight node isoparametric hexahedrons with eight integration stations. There are 850 elements and 3456 degrees of freedom in the model. Admittedly this grid is too coarse to delineate the rapid variations near the source, however, it should be adequate to assess the general behavior away from the fault.

5.3 Model results

We will only present the model results relevent to plate motion and stress diffusion. Figure 5.3.1 shows the surface horizontal displacement along the x axis (on the symmetry plane) at time = 0 and at 25 years after the event. More detailed time dependence can be seen from the plots of horizontal displacements vs. time at selected nodes. Figure 5.3.2 shows the surface horizontal displacements on the symmetry plane (y=0) at x = 0, -100, -400, -760, and -1000 km on the overiding plate side, and figure 5.3.3 shows the same quantities at x= 0, 100, 400, 760, and 1000 km on the underthrusting plate side. The magnitude of the displacements gradually increase with time except near the source. The increase is about 70 cm in four decades at 400 km away from the source, and it is less than 20 cm at 1000 km away. The horizontal plate velocity due to the event averaged over four decades is less than 2 cm/year everywhere. However, the plate motion is nonuniform. Most of the time dependent adjustments take place within the first decade after the event. This can be seen more clearly in the plot of horizontal plate velocity in the x direction (V_x) vs. time. Figure 5.3.4 gives V_x vs. time at the selected locations on the overiding plate side and figure 5.3.5 gives V_x on the underthrusting plate side. The magnitude of V_x decreases monotonically with time. At intermediate distance (x=400 km), V_x is about 4 cm/year for the first several years after the event. This velocity is

comparable to the long term plate velocities in plate tectonic theory, and certainly is a measurable quantity in high precision geodetic measurements. On the other hand, V_x is always less than 1 cm/year at 1000 km away from the source; this perturbation will be barely detectable with present day capabilities.

Since the fault length is finite, the plate velocity caused by the earthquake varies with distance along the direction perpendicular to the symmetry plane. Figure 5.3.6 shows V_x along the line x = -400 km at y = 0, 120, and 250 km, and figure 5.3.7 shows V_x along the line x=-1000 km at y = 0, 210, and 540 km. V_x in general decreases away from the symmetry plane (y=0). The edge effect of the source is significant at intermediate distance; along the line x = -400 km, the maximum V_x decreases by 45% at half fault length (250 km) away from the symmetry plane. This effect should be measurable but can not be described in two dimensional models. Along the line x = -1000 km, V_x is again always less than 1 cm/year.

Next we examine the stress diffusion caused by the earthquake. The largest stress component near the x axis is the horizontal normal stress along the x direction (S_{xx}). Figure 5.3.8 shows the stress component S_{xx} at 20 km depth near the x axis at time = 0 and 25 years after the event. Positive S_{xx} indicates horizontal tension and negative S_{xx}

indicates horizontal compression. The magnitude of S_{xx} decreases with time near the source but increases with time at far distances, indicating a stress diffusion effect. The stress diffusion can be seen more clearly in the plot of stress vs. time. Figure 5.3.9 gives the stress component S_{xx} at x = -60, -165, -385, -695, and -1175 km on the overiding plate side, and figure 5.3.10 gives S_{xx} at x = 10, 95, 225, 445, and 845 km on the underthrusting plate side. Near the source, the maxima of S_{xx} occur at time = 0. At far away distances, the peaks of the stress arrive later, as if the stress is diffused away from the source region. If the source region is under horizontal compression before the earthquake, as expected for a thrust event, the thrust earthquake relieves the prestress near the source along the x axis. At some distance away from the source, the prestress state may be different from that of the source region. For example, the bending of the oceanic plate may produce tensile stress seawards of the thrust fault zone. A thrust fault event may reenforce the prestress there and trigger a normal fault event.

The magnitude of the stress decreases rapidly with distance. At x= 1000 km, the magnitude of the stress is less than 2 bars. This stress probably can not produce significant physical effects by itself. However, the stress is long lasting and the cummulative effects due to many events may be significant.

Earthquake migration along subduction zones has been reported (Mogi 1968, Kelleher 1970,1972). This may be related to the time dependent stress along the strike direction of a thrust earthquake. Figures 5.3.11 shows S_{xx} vs. time at selected locations along the fault near the y axis. Figure 5.3.12 shows S_{xx} at locations beyond the fault edge near the y axis. S_{xx} changes sign near the fault edge along the strike direction. Along the fault zone S_{xx} is positive (tension) while beyond the fault edge S_{xx} is negative (compression). If the prestress near the source is horizontal compression, the thrust event relieves the prestress along the fault zone but reenforces the prestress in the zone beyond the fault edges along the strike direction. This is very similar to the stress diffusion associated with strike slip faults (chapter 3). Physically, this is not difficult to understand: if we consider the overiding plate to be stationary, the event tends to pull the underthrusting plate with it; this causes the compression in the adjacent regions. A great thrust earthquake thus increases the possibility of thrust earthquake occurrence in the zone adjacent to the source region along its strike direction. Notice that the magnitude of the compressional stress due to the event increases with time; thus it is possible that the triggered event happens years after the triggering event. This is consistent with the earthquake migration phenomenon.

We would like to remind the reader that this model is a layered model. The effects due to the lateral viscosity variation in a subduction zone have not been included in the model. Those effects need to be calculated if detailed near source phenomena are discussed.

5.4 Discussion

In this chapter, we made the first attempt to model the time dependent displacements and stress changes following a three dimensional dip slip earthquake. The main purpose of this study is to assess the time dependent effects of the earthquake on plate motion and stress diffusion. We used a simplified viscosity model and a coarse finite element grid. The effort needed in preparing a realistic three dimensional time dependent model of a subduction zone, including irregularly shaped descending slab and low viscosity zone, is huge; it should be reserved to the time when data warrant more detailed studies. However, the same computational scheme and programs can be used with little modification.

The results in this chapter indicate that the perturbation on the plate motion by a great thrust event is highly non-uniform in both space and time. For an earthquake with 10 m maximum slip, 500 km fault length, and 30 degrees dip, on the symmetry plane the maximum horizontal surface velocity is about 4 cm/year at intermediate distance (about 400 km) from the source. This is comparable to long term average plate velocity. The maximum perturbation of plate velocity decreases to less than 1 cm/year at 1000 km away from the source. The results on the symmetry plane are similar to those of a two dimensional model. Figure 5.4.1 gives the plate velocity at 380 and 900 km away from the

source for a two dimensional model. The model uses the finite element grid of figure 4.4.3 in chapter 4. The fault dip is 45 degrees and the slip is 10 m from surface to 40 km and tapers to zero at 80 km depth. The viscosity model is similar to that in this chapter. The maximum plate velocity is about 4 cm/year at 380 km and 1 cm/year at 900 km. The maximum adjustments occur immediately after the event. These are similar to the three dimensional model. However, the decay of velocity with time is slower in the two dimensional model. Two dimensional model also cannot describe the effects off the symmetry plane. As we see in figure 5.3.6 and 5.3.7, the horizontal plate velocity varies considerably along the strike direction.

The transient results in this chapter do not agree with the analyses using an elastic plate overlying a purely viscous fluid model (Elsasser 1967, Bott and Dean 1973, Anderson 1975, Melosh 1976). The difference is demonstrated in the following example. Figure 5.4.2 shows the schematic diagram for such a model: An elastic plate of thickness h_1 simulates the lithosphere while a layer of viscous fluid of thickness h_2 simulates the asthenosphere. A step function displacement on the edge of the elastic plate simulates a plate boundary earthquake. If we neglect the bending in the lithospheric plate, then the solution for the horizontal displacement as a function of time and space is a complementary error function (Elsasser 1969). Assuming the

parameter values h_1=80 km, h_2=200 km, Young's modulus 2.0×10^{12} dyne/cm^2, viscosity 10^{20} poise, and initial displacement on the edge 10 m, the resulting plate velocities at 400 and 1000 km away are given in figure 5.4.3. The transient velocity for the plate over viscous fluid model has a strong propagation effect. There is no instantaneous plate motion at any points other than at the source. The plate velocity reaches a maximum at a later time, then it decays to zero monotonically. This propagation effect of plate velocity does not exist in the viscoelastic models. The maximum adjustments in viscoelastic models happen right after the earthquake. The plate velocities are also much larger in the viscous fluid model than those in the viscoelastic model. There are two reasons for these differences: Viscous fluid cannot be deformed instantaneously by shearing, thus the plate velocity must be zero immediately after the event; the maximum plate velocity must occur later. In contrast, the viscoelastic models have instantaneous respone, and the maximum adjustments occur right after the event. This effect has also been pointed out by Savage and Prescott (1978a). The other reason is that dislocations are used to simulate the earthquakes in our viscoelastic models, while a step in displacement simulates the earthquake in the viscous fluid model. In general the effect of a dislocation decays with distance faster than a simple push or pull. This also

makes the plate velocities in the viscous fluid model larger. In the discussion of transient phenomena associated with an earthquake, the models assuming viscoelastic media and dislocation faults are more realistic than the simple viscous fluid model.

The thrust event causes horizontal tension along the fault but horizontal compression in the regions beyond the fault edges along the strike direction. The tensile stress may trigger the normal fault events seawards of the thrust region; the compressional stress may trigger the thrust fault events in the region along the strike direction. The migration of thrust fault events along subduction zones has been observed in Aleutian, Kurile Islands, Japan, and South America (Fedotov 1965, Mogi 1968, Kezlleher 1970, 1972). The magnitude of the compressional stress caused by the thrust fault earthquake increases with time; thus the triggered events may happen years after the triggering event. This is consistent with the observed migration of earthquakes in subduction zones.

Normal fault earthquakes triggered by thrust fault events have also been observed in subduction zones. A large normal fault event (m_b=7) occurred on March 30, 1965 beneath the Aleutian trench near Rat Island (Stauder 1968, Abe 1972). This event was considered to be triggered by the thrust fault event on February 4, 1965 located at about 100

km away towards the island (Abe 1972). Normal fault events were also triggered in the 1938 Shioya-oki swarm of large earthquakes in the southern part of Japan trench (Abe 1977b). In the Shioya-oki region, there had been no other earthquakes larger than magnitude 7.5 in historical time. A large earthquake of magnitude 7.4 occurred in May 1938; about 6 months later four earthquakes with magnitudes larger than 7 happened within 2 days. The fault mechanisms for these earthquakes were determined by Abe (1977) using seismic, tsunami and geodetic data. The first three events had shallow dipping thrust faults while the latter two had normal faults. The two normal fault events were located seawards of the three thrust fault events. The locations and occurence times suggested that the two normal fault events were triggered by the first three thrust fault events. Notice that near the source region, the tensile stress caused by a thrust fault event decays with time (figures 5.3.9 and 5.3.10); thus the triggered normal faulting event should happen soon after the thrust fault event. In contrast, the migration of thrust fault events along the strike direction may happen years after the triggering event, because the triggering stress increases with time in this case (figure 5.3.12).

The magnitude of the stress decreases rapidly with distance from the source. At 1000 km away, the magnitude of the stress is less than 2 bars. However, the stress at this

distance increases with time. For one event the physical effect is not significant. But the stress is long lasting and the cummulative effects due to many events may be significant.

Figure Captions - Chapter 5

Figure 5.2.1 The viscosity and fault of the three dimensional dip slip earthquake model in this chapter. (a) Cross sectional view of the plane (y=0) bisecting the fault. The fault has offset 10 m along the solid line segment and tapers off to zero at 80 km depth along the broken line segment. The fault dip is 30 degrees. The viscosity has a layered structure. The numbers with exponents are the viscosity values in poise for each region. (b) Projection of the fault on the the surface (z=0 plane). The fault intersects the surface at x=0 and y=-250 to 250 km. The fault has offset 10 m in the double hatched area and the offset tapers linearly in the single hatched area.

Figure 5.2.2 Top view of the finite element grid used in the three dimensional model. The finite element model uses half of the physical model. The plane y=0 is the symmetry plane bisecting the physical region. The grids for surfaces at lower depths are similar to this top surface except for some shift to accomodate the fault configuration.

Figure 5.3.1 The surface horizontal displacement along the symmetry plane (y=0). Curves 1 and 2 are for time= 0 and 25 years after the event. Positive values are in the positive X direction, i.e., toward ocean.

Figure 5.3.2 The surface horizontal displacement along the symmetry plane (y=0) vs. time at selected locations on the overiding plate side. Curves 1, 2, 3, 4, and 5 are for horizontal distances x= 0, -100, -400, -760, and -1000 km. Positive values are in positive X direction.

Figure 5.3.3 The surface horizontal displacement along the symmetry plane (y=0) vs. time at selected locations on the underthrusting plate side. Curves 1, 2, 3, 4, and 5 are for horizontal distances x= 0, 100, 400, 760, and 1000 km.

Figure 5.3.4 The surface horizontal velocity V_x along the symmetry plane (y=0) vs. time at selected locations on the overiding plate side. Curves 1, 2, 3, 4, and 5 are for horizontal distances x= 0, -100, -400, -760, and -1000 km.

Figure 5.3.5 The surface horizontal velocity V_x along the symmetry plane (y=0) vs. time at selected locations on the underthrusting plate side. Curves 1, 2, 3, 4, and 5 are for horizontal distances x= 0, 100, 400, 760, and 1000 km.

Figure 5.3.6 The surface horizontal velocity V_x along the line x=-400 km. The curves 1, 2, and 3 are at y= 0, 120, and 250 km.

Figure 5.3.7 The surface horizontal velocity V_x along the line x=-1000 km. The curves 1, 2, and 3 are at y= 0, 210, and 560 km.

Figure 5.3.8 The normal stress perpendicular to the fault strike (S_{xx}) at 20 km depth near the x axis. Curves 1 and 2 are for time = 0 and 25 years respectively. Positive stress indicates tension and negative stress indicates compression.

Figure 5.3.9 S_{xx} vs. time at selected locations near x axis at 20 km deep on the overiding plate side. Curves 1, 2, 3, 4, and 5 are for x = -60, -165, -385, -695, and -1175 km.

Figure 5.3.10 S_{xx} vs. time at selected locations near x axis at 20 km deep on the underthrusting plate side. Curves 1, 2, 3, 4, and 5 are at x = 10, 95, 225, 445 and 845 km.

Figure 5.3.11 S_{xx} vs. time at selected locations along the fault near the y axis (strike direction) at 20 km deep. The curves 1, 2, and 3 are at y = 25, 75, and 125 km.

Figure 5.3.12 S_{xx} vs. time at selected locations beyond the fault edge near the y axis (strike direction) at 20 km deep. The curves 4, 5, 6, and 7 are at y = 285, 380, 510, and 670 km.

Figure 5.4.1 Typical time dependent behavior of plate velocity of a two dimensional viscoelastic model. The model uses the finite element grid of figure 4.4.3 in chapter 4. The fault dip is 45 degrees. The fault slip is 10 m from surface to 40 km deep; it tapers off to zero at 80 km deep. The viscosity structure is similar to figure 5.3.1 except that the layer with viscosity 10^{20} poise is 80 km thick. Curves 1 and 2 are for 380 and 900 km away from the source.

Figure 5.4.2 The schematic diagram of the plate over viscous fluid model. An elastic plate simulates the lithopshere. A viscous fluid layer simulates the asthenosphere. A sudden horizontal displacement on the edge of the elastic plate simulates an earthquake.

Figure 5.4.3 The horizontal plate velocities for the model in figure 5.4.2. The model parameters are: Young's modulus in the lithosphere 2×10^{12} dyne/cm^2, viscosity in the asthenosphere 10^{20} poise, h_1 = 80 km, h_2 = 200 km, and the sudden displacement on the edge of the lithosphere 10 m. Curves 1 and 2 are for x = 400 km and 1000 km.

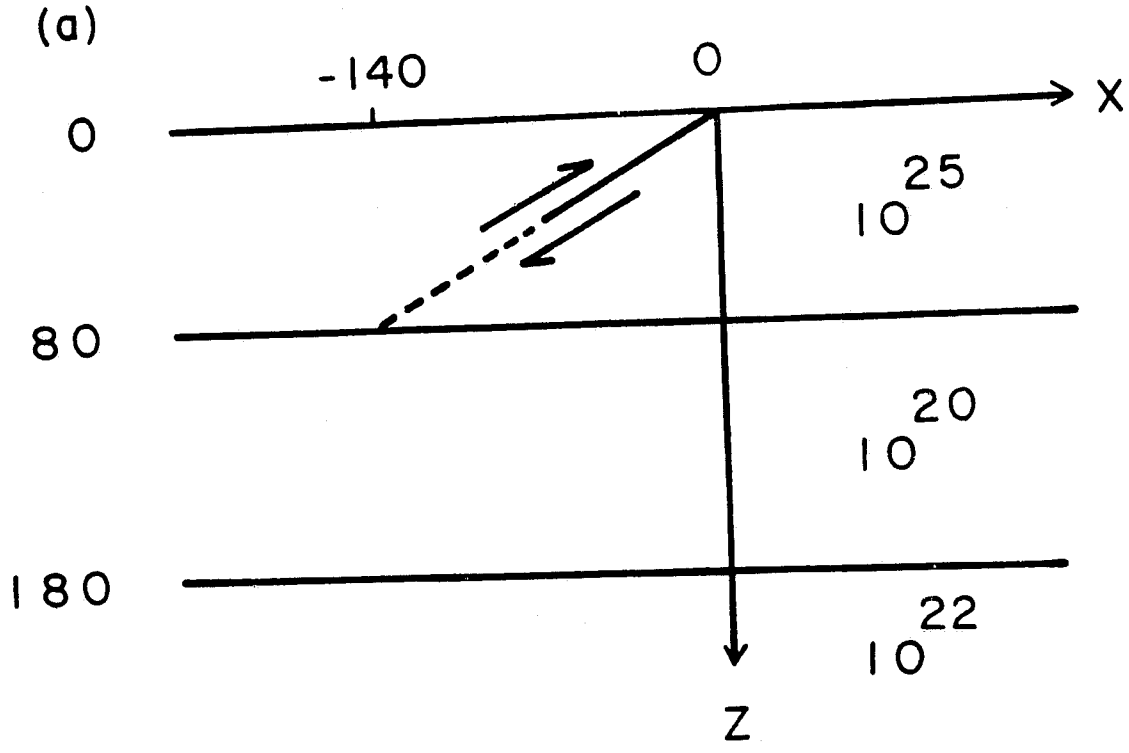

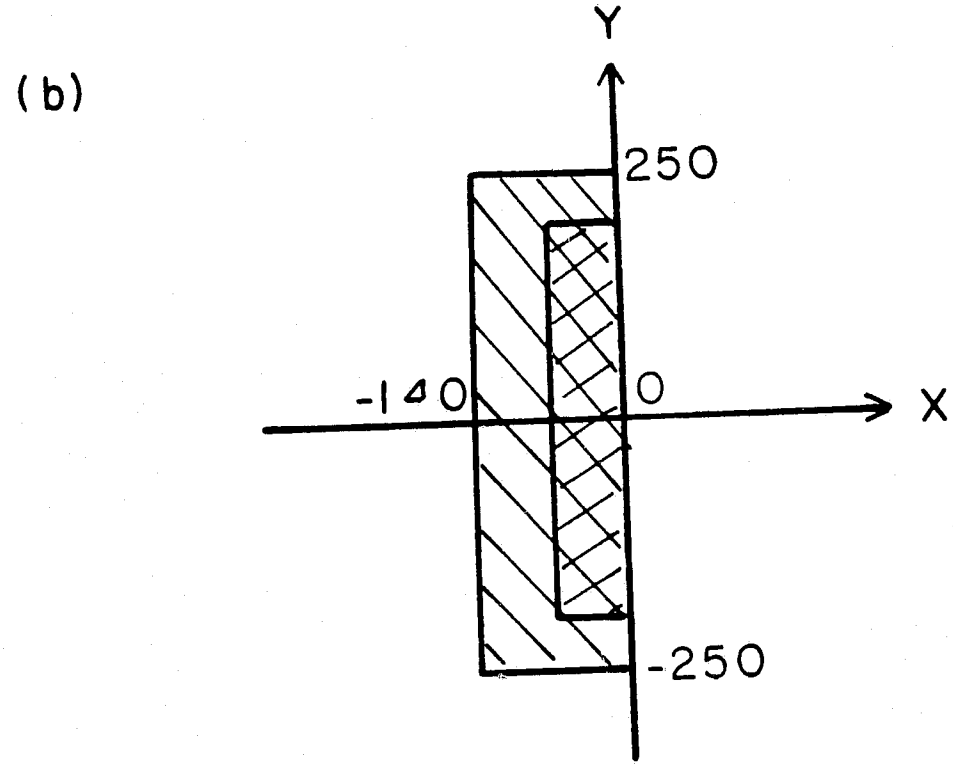

Fig 5.2.1

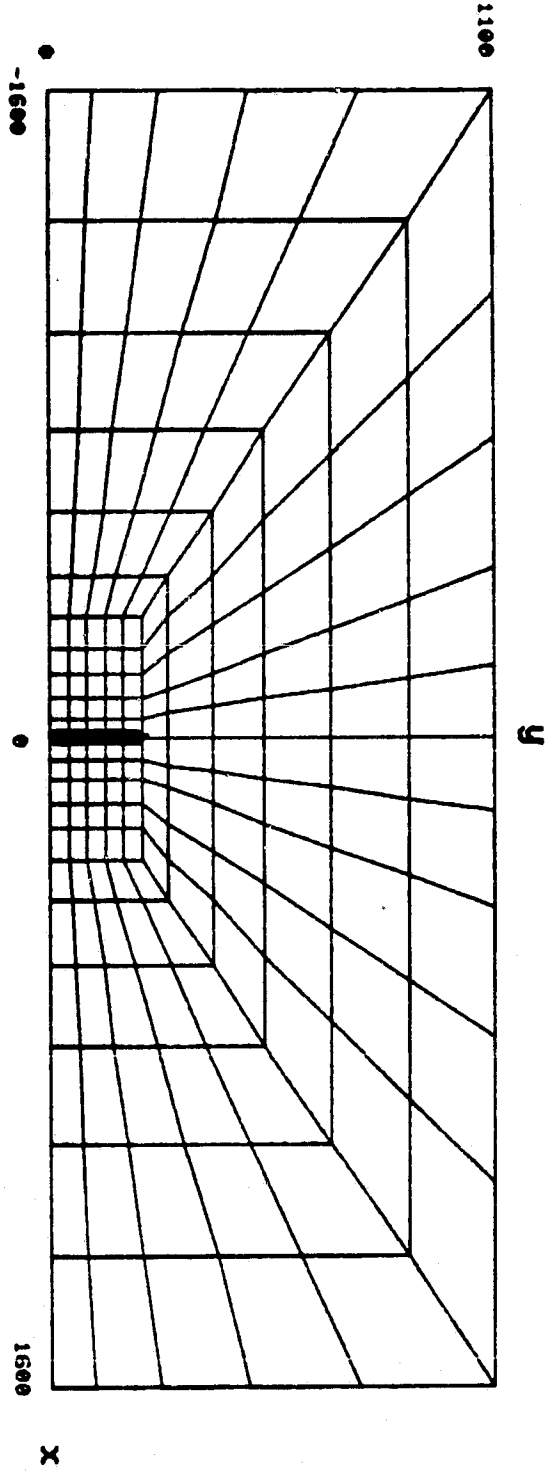

Fig 5.2.2

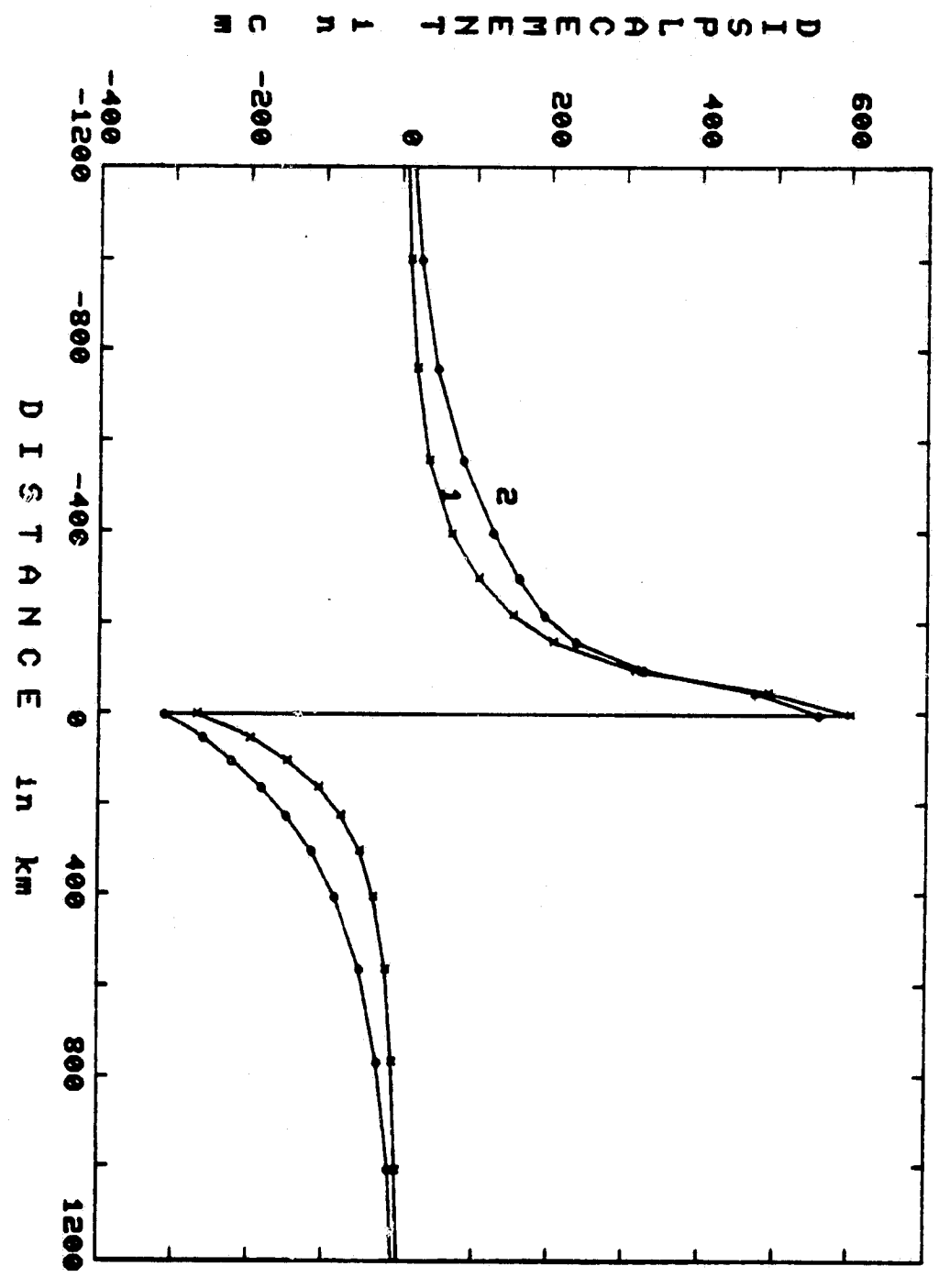
DISPLACEMENT in cm
-400
-200
0
200
400
600
-1200
-800
-400
0
400
800
1200
DISTANCE in km
1
2

Fig 5.3.1

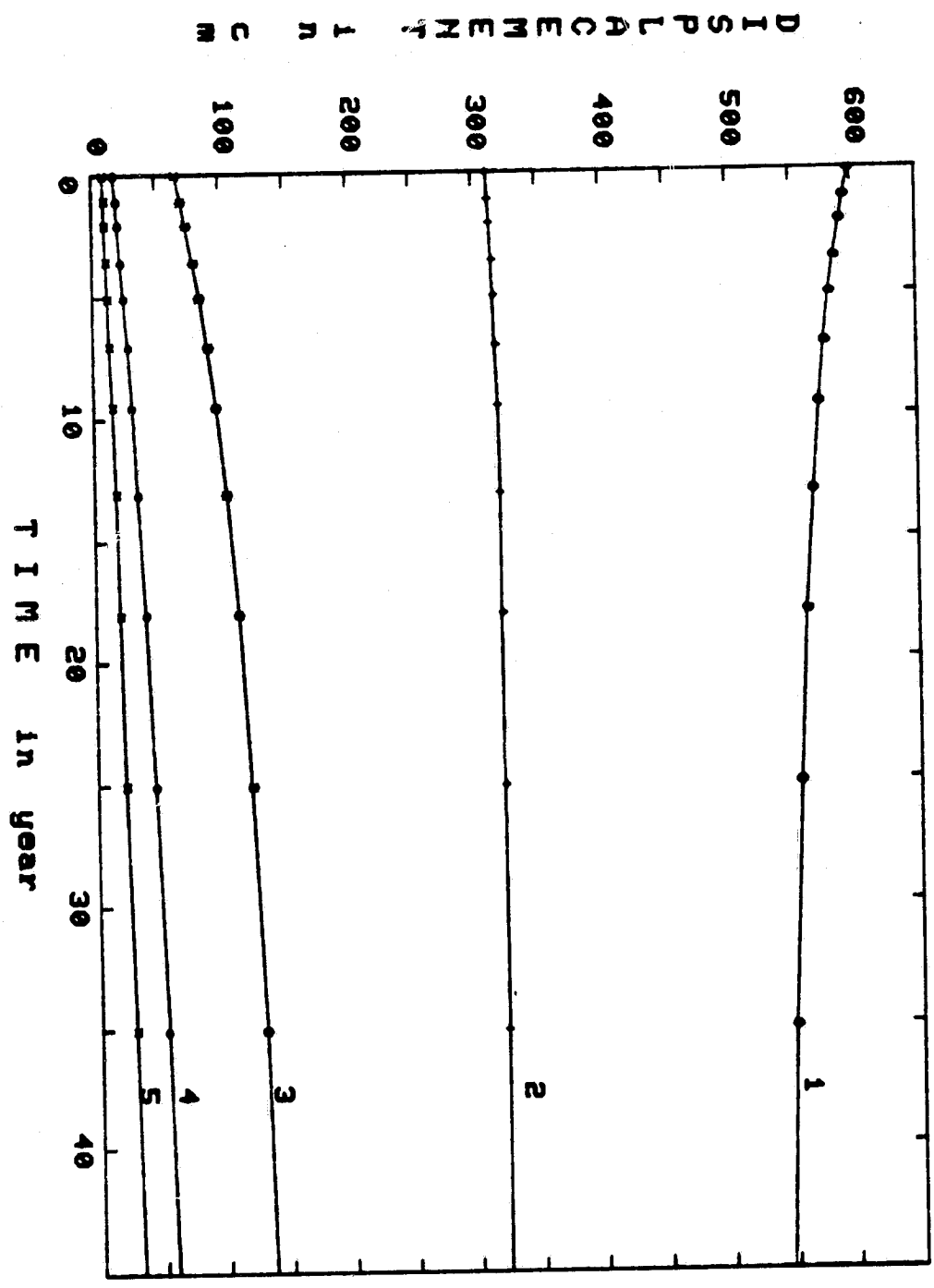
DISPLACEMENT in cm
0
100
200
300
400
500
600
TIME in year
0
10
20
30
40
1
2
3
4
5

Fig 5.3.2

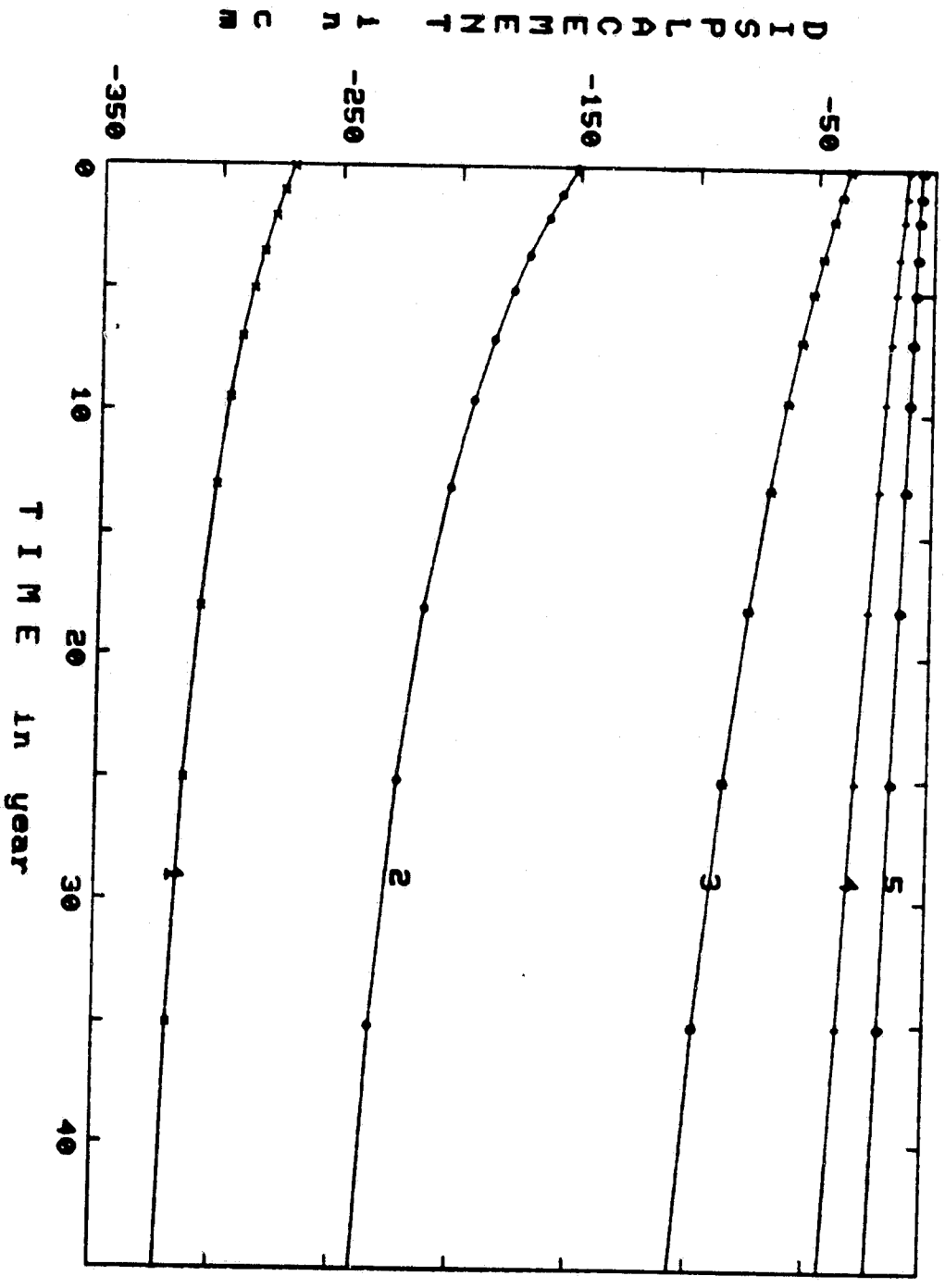
DISPLACEMENT in cm
-350
-250
-150
-50
0
10
20
30
40
TIME in year
1
2
3
4
5

Fig 5.3.3

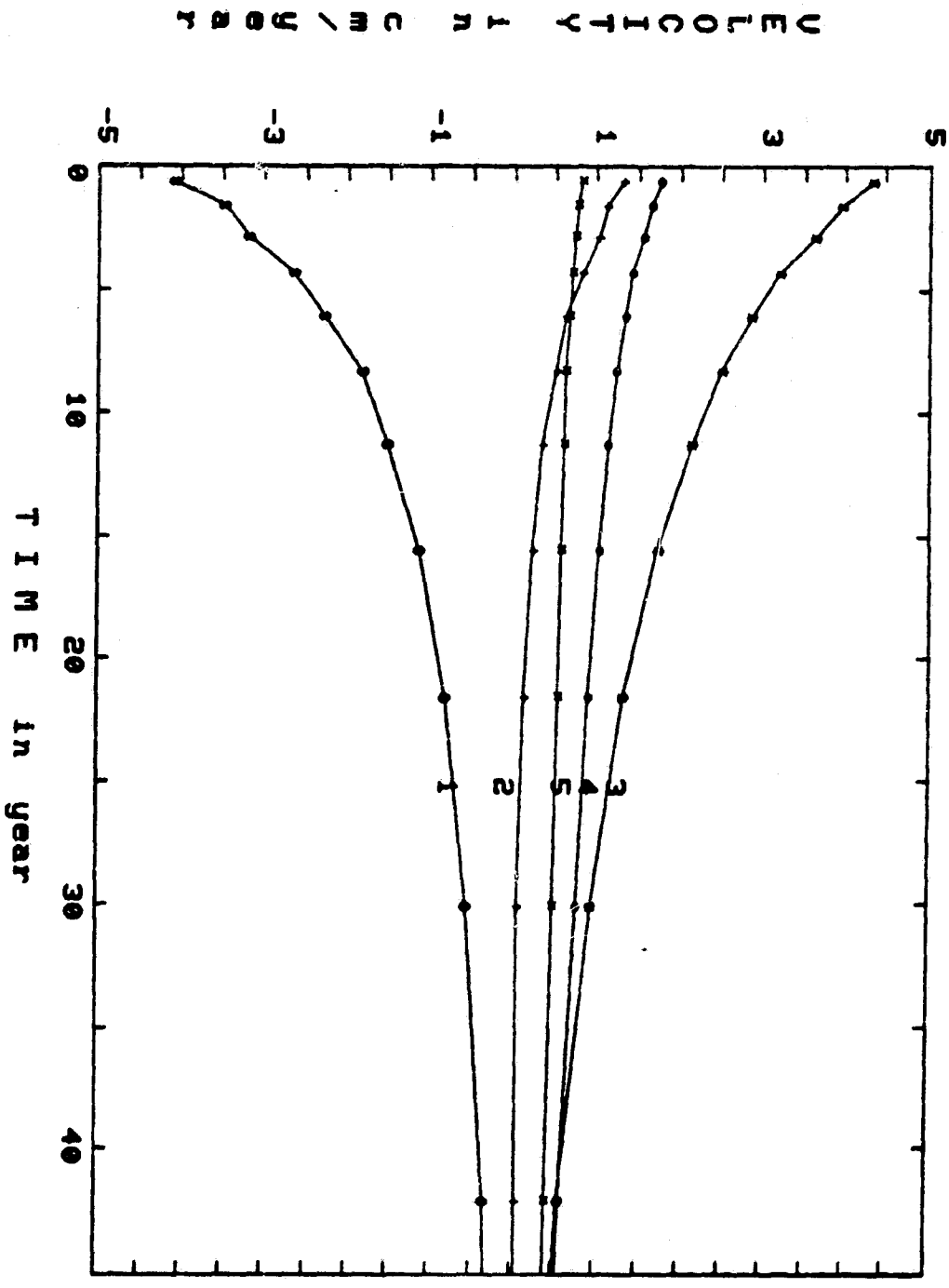

Fig 5.3.4

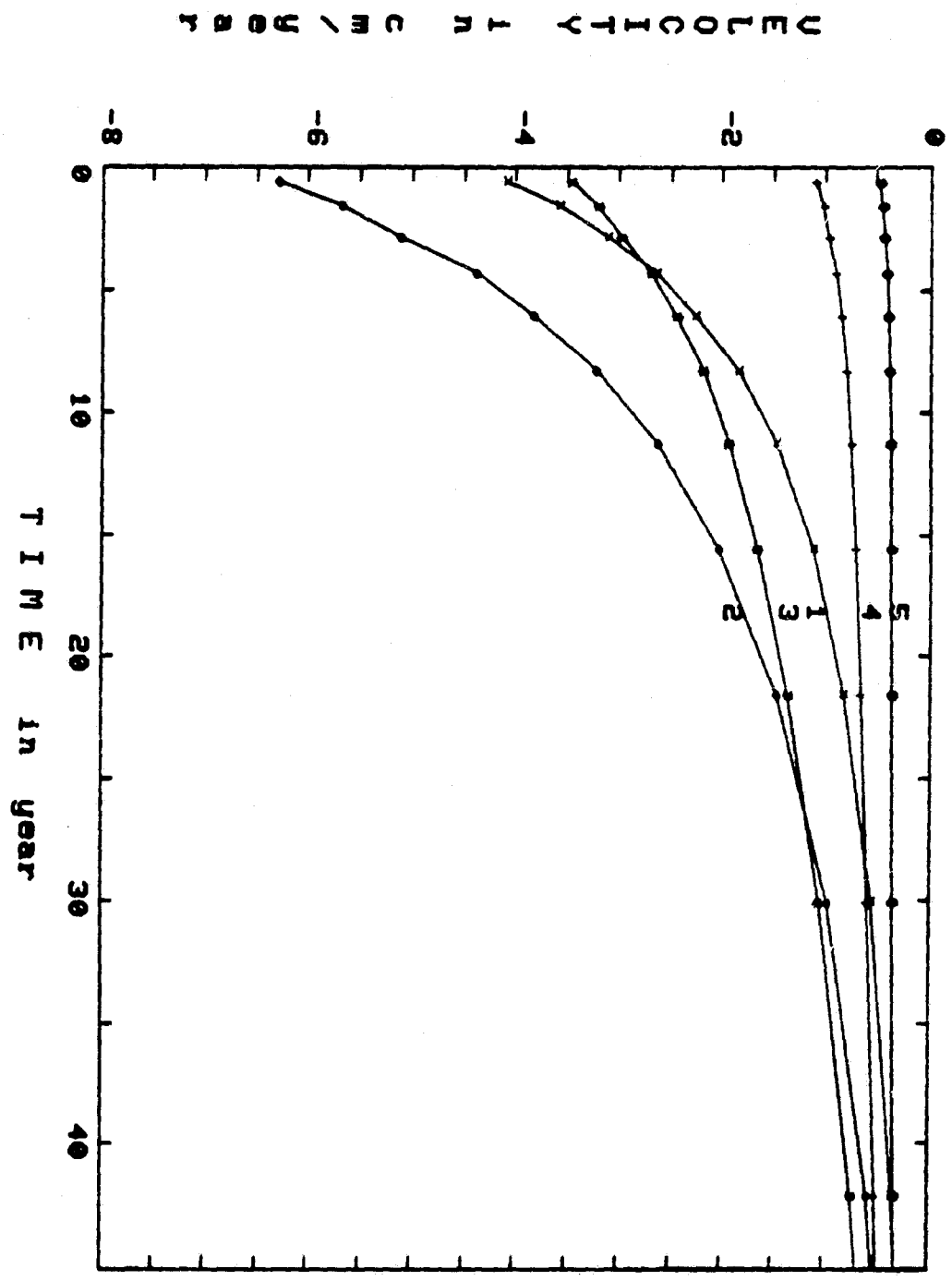

Fig 5.3.5

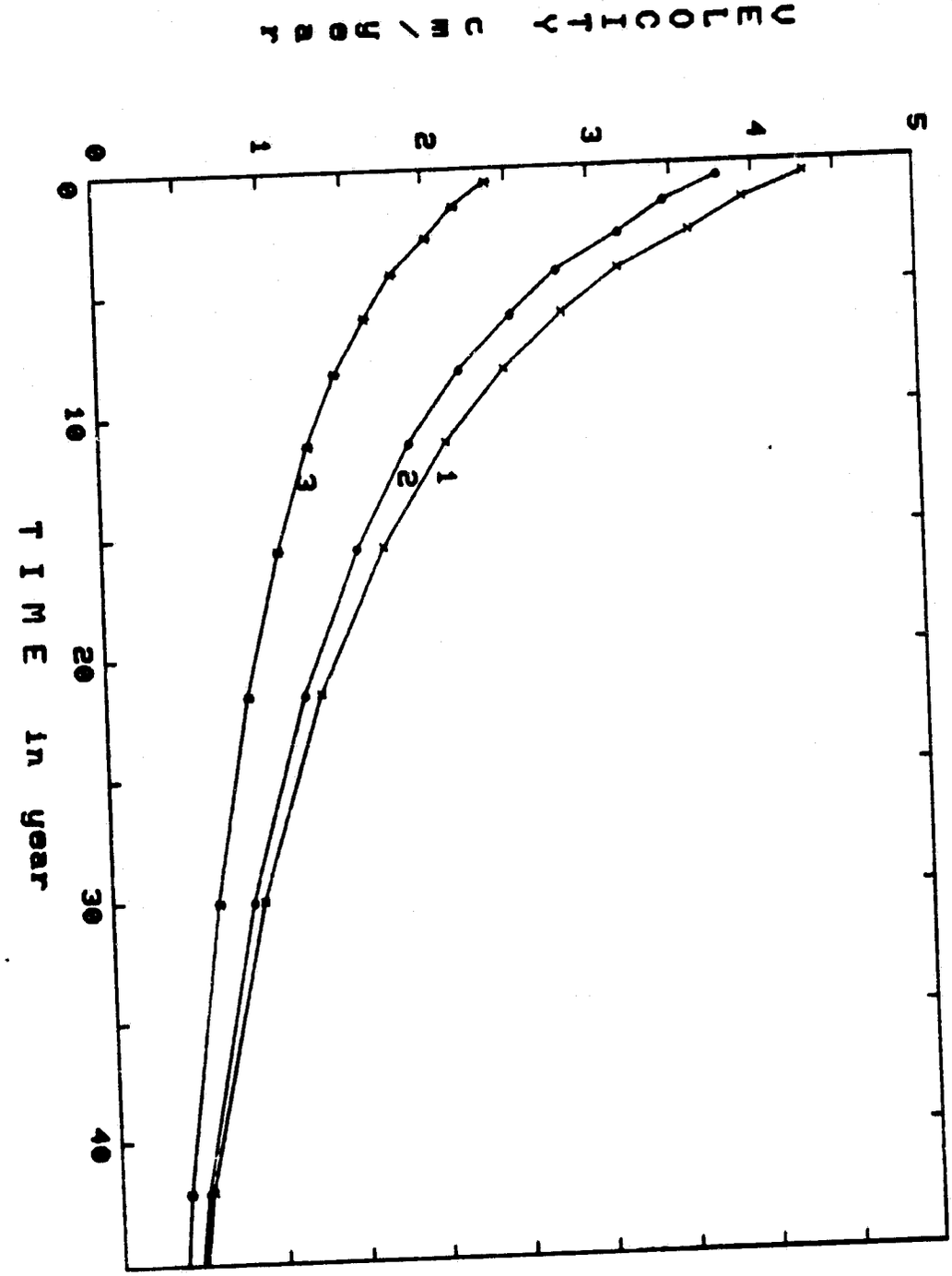

Fig 5.3.6

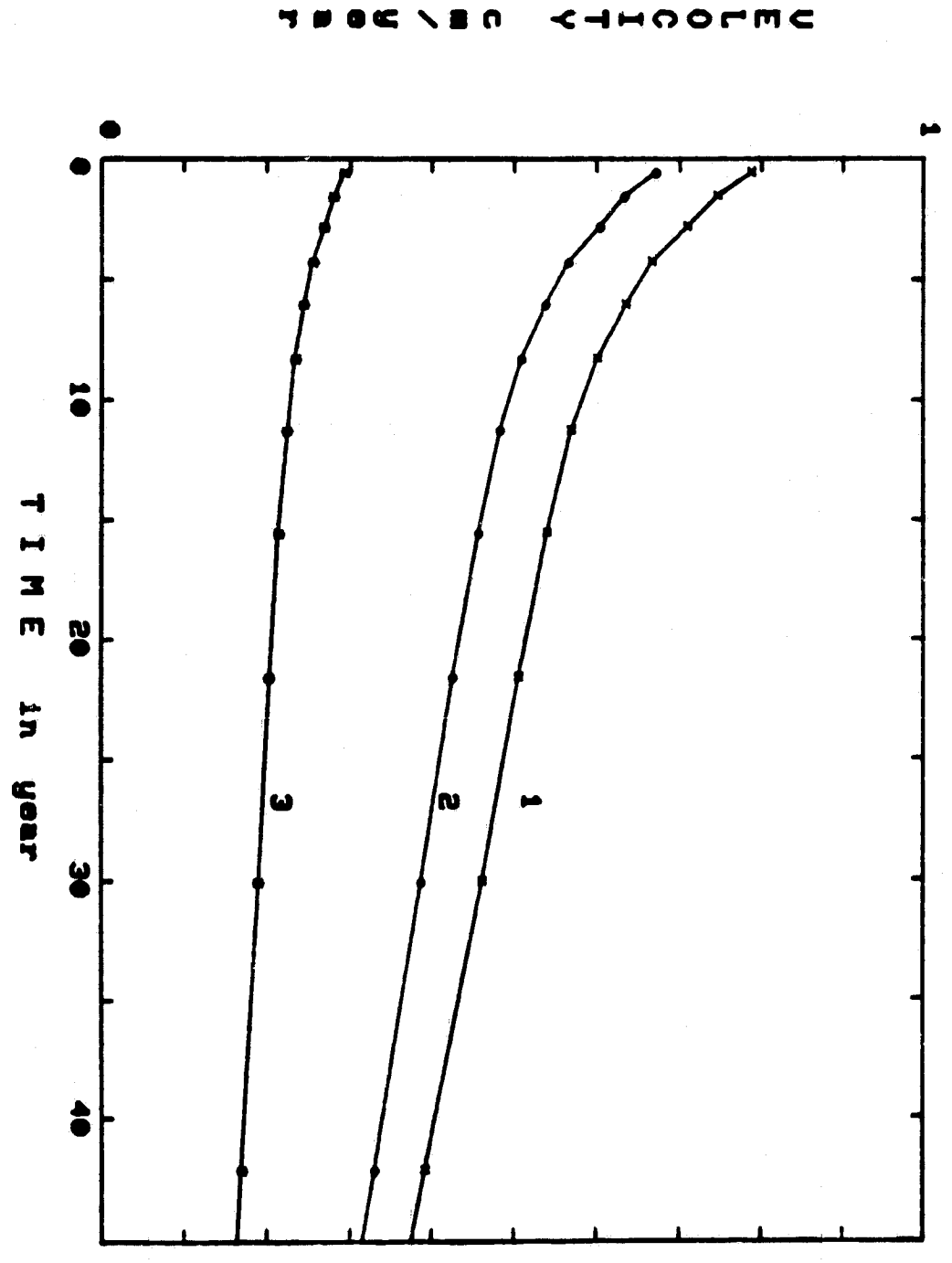

Fig 5.3.7

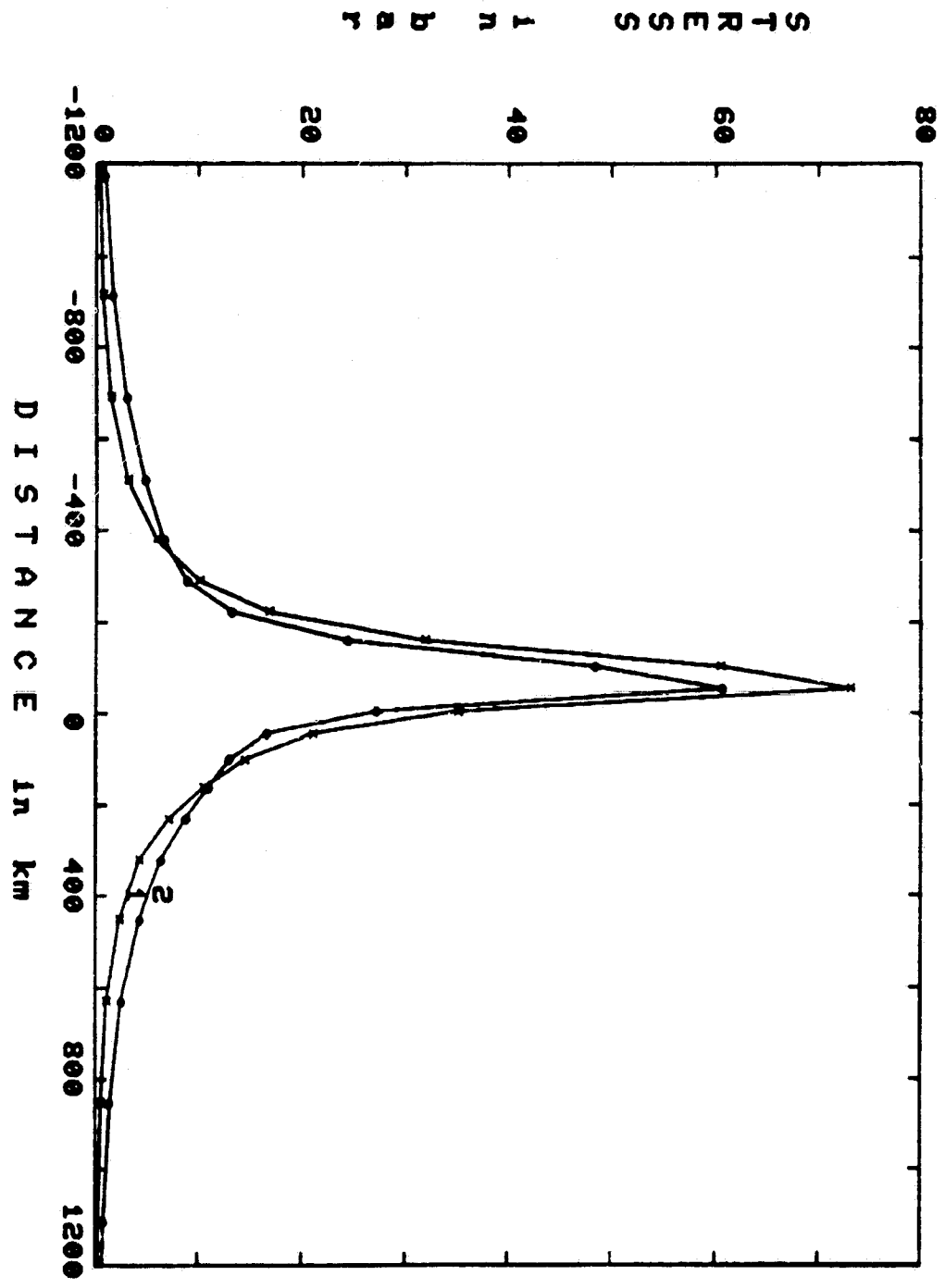
STRESSES in bars
0
20
40
60
80
-1200
-800
-400
0
400
800
1200
DISTANCE in km
2

Fig 5.3.8

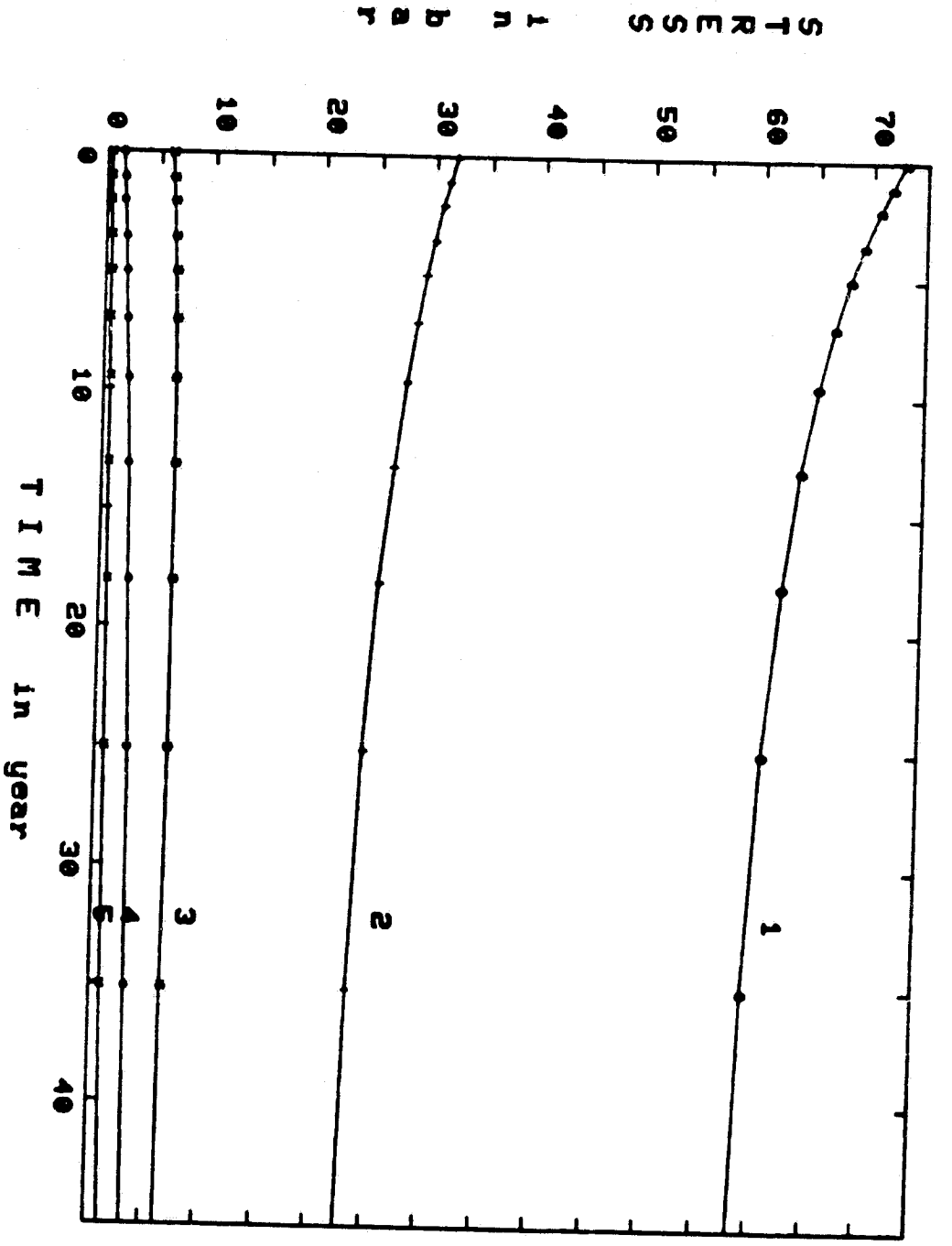
STRESS in bar
0
10
20
30
40
50
60
70
TIME in year
0
10
20
30
40
1
2
3
4
5

Fig 5.3.9

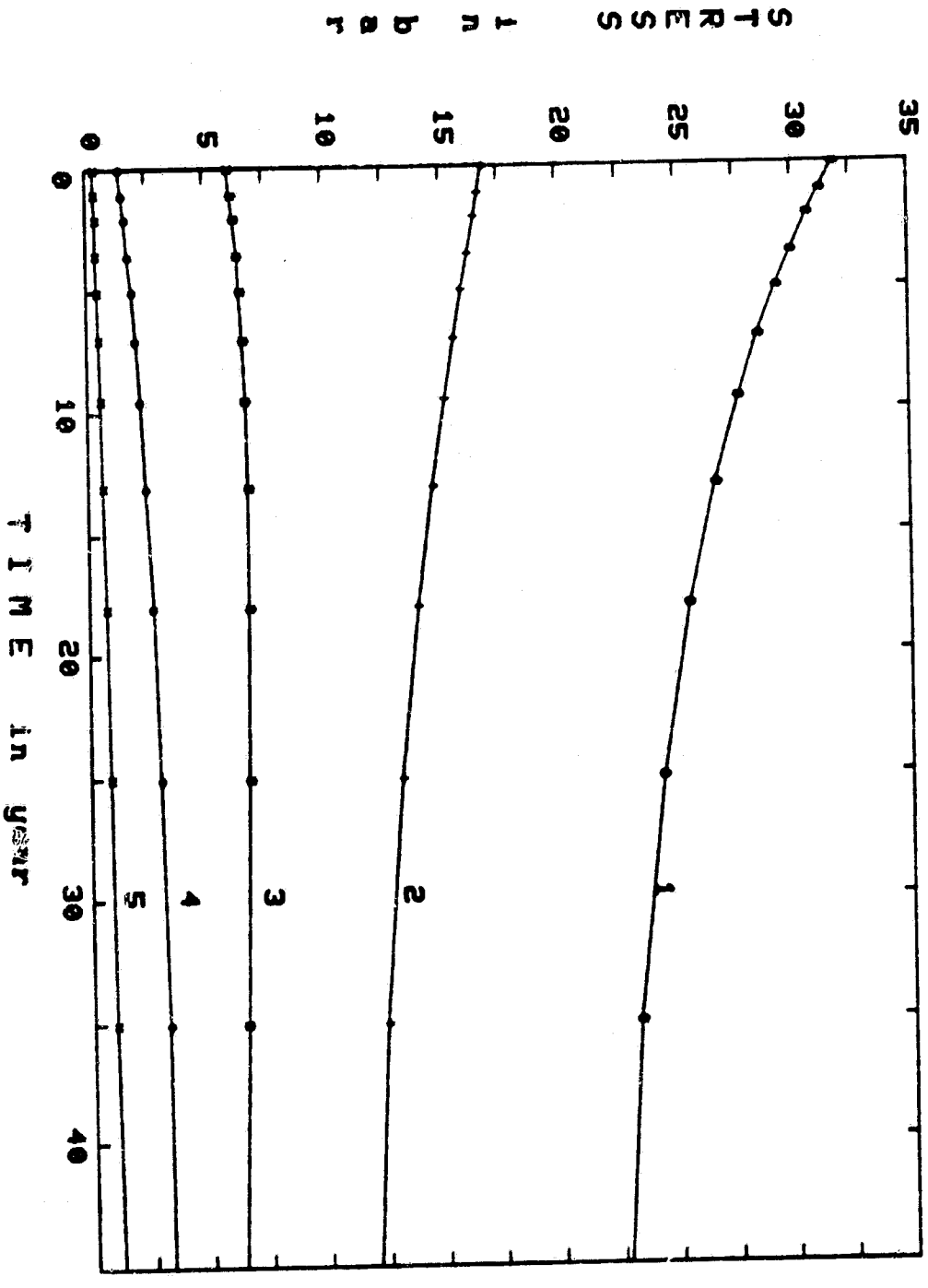
STRESS in bars
0
5
10
15
20
25
30
35
TIME in year
0
10
20
30
40
1
2
3
4
5

Fig 5.3.10

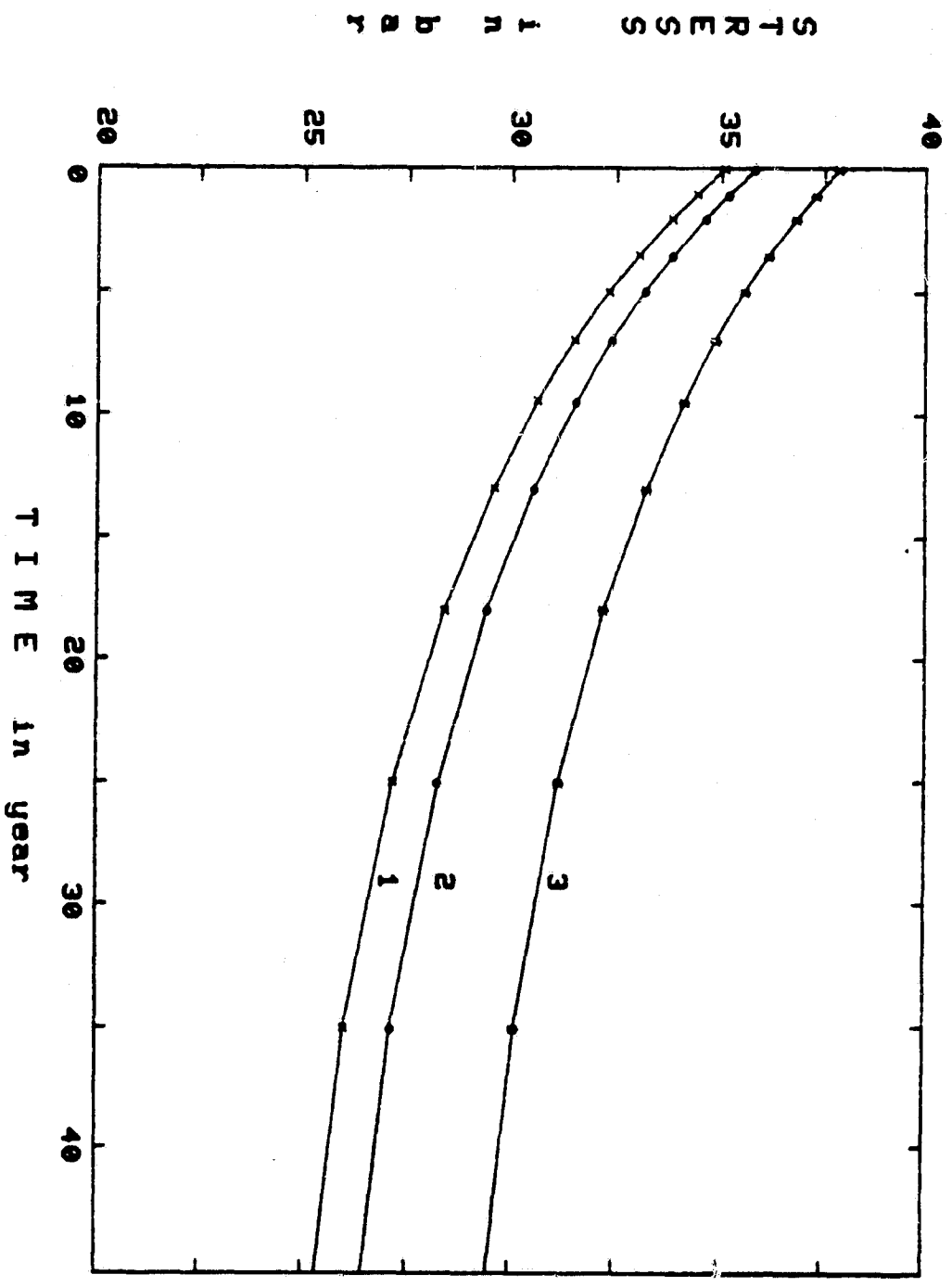

Fig 5.3.11

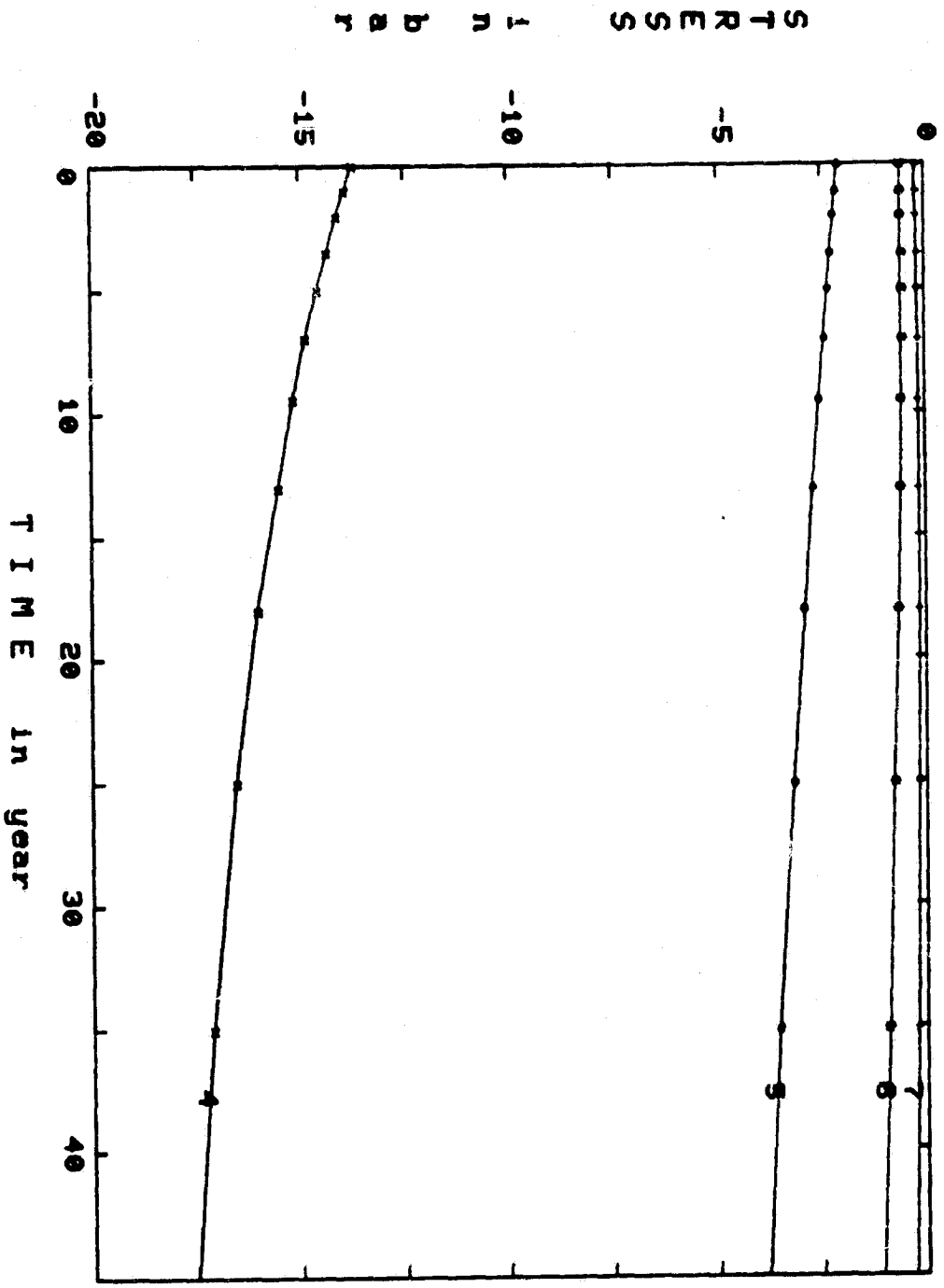

Fig 5.3.12

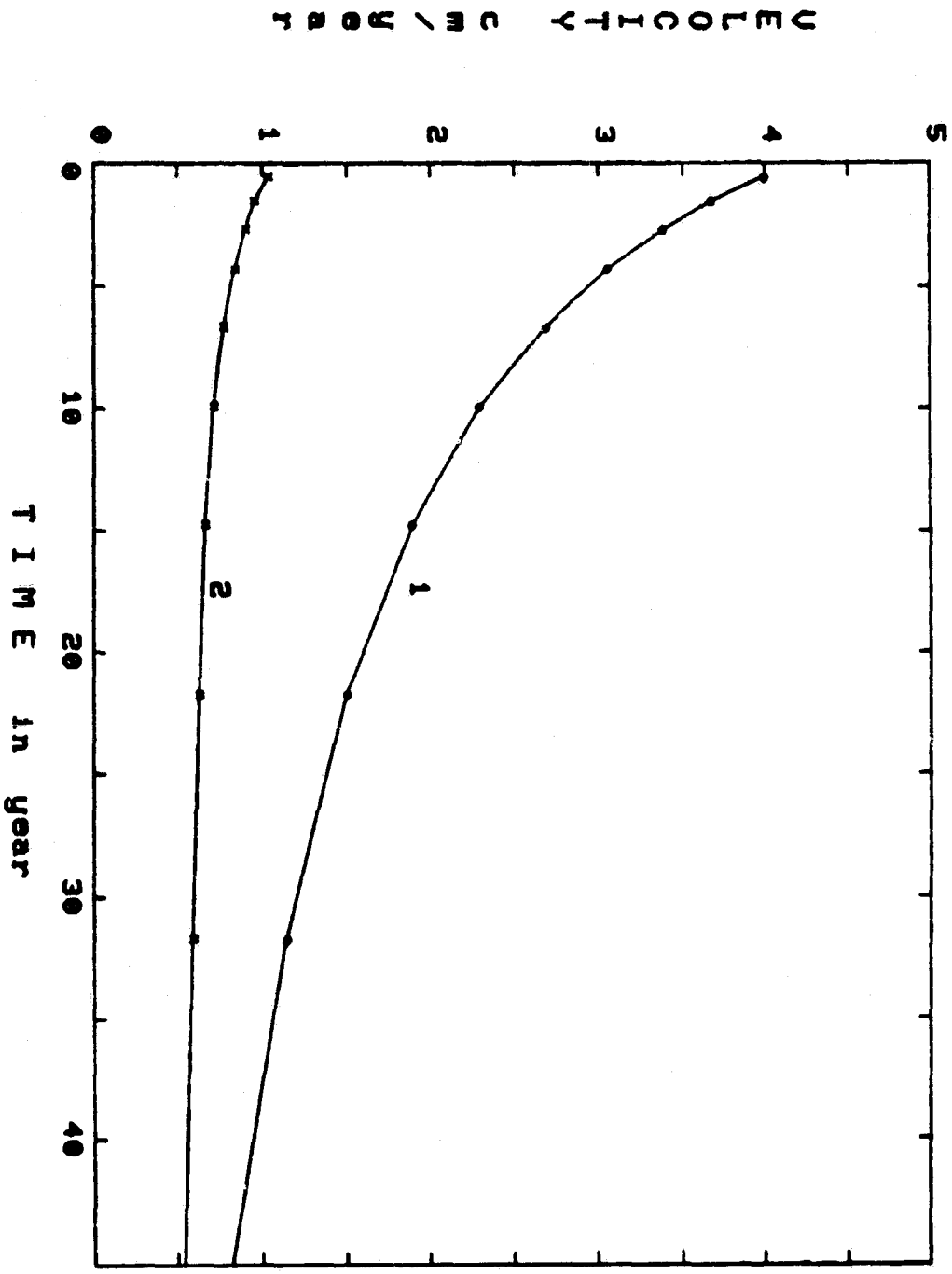

Fig 5.4.1

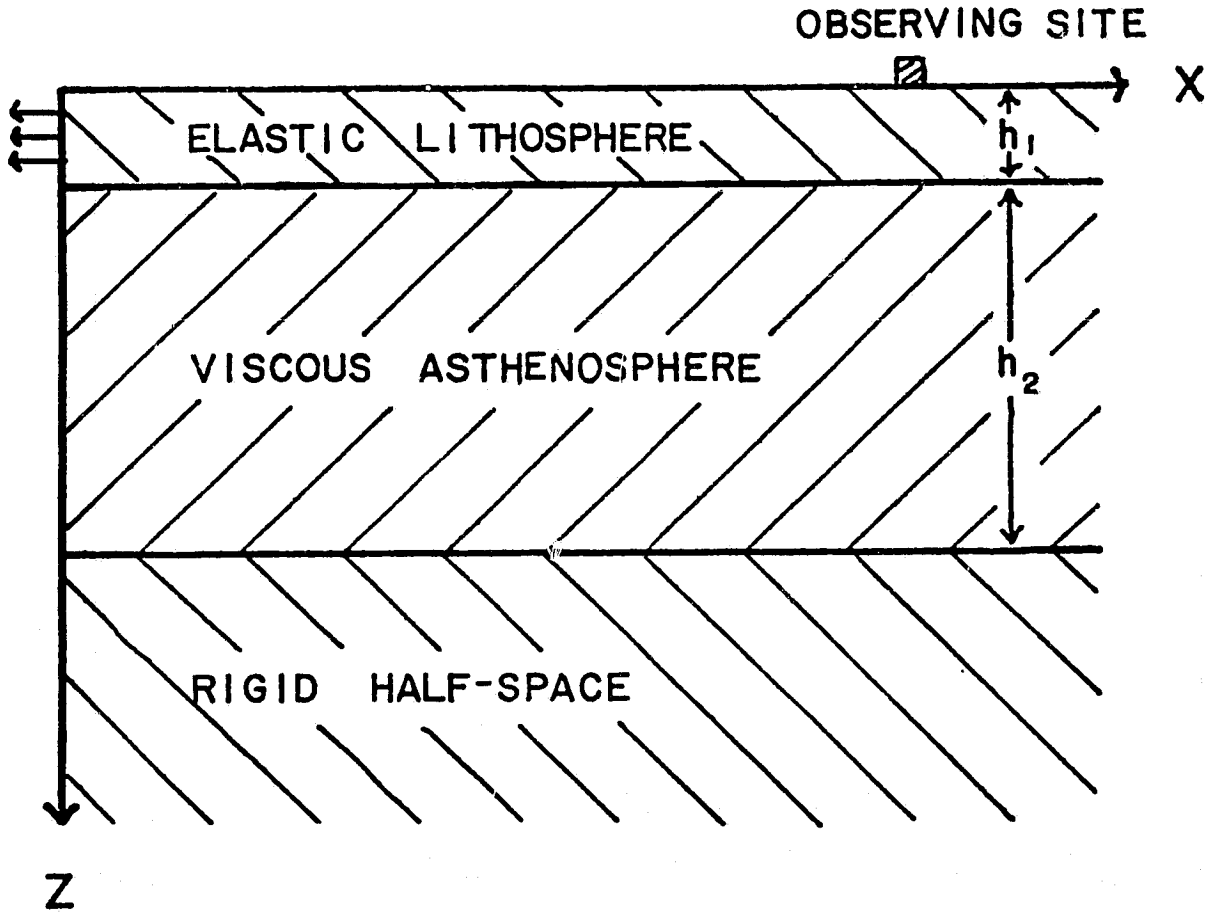
OBSERVING SITE
X
ELASTIC LITHOSPHERE
h_1
VISCOUS ASTHENOSPHERE
h_2
RIGID HALF-SPACE
Z

Fig 5.4.2

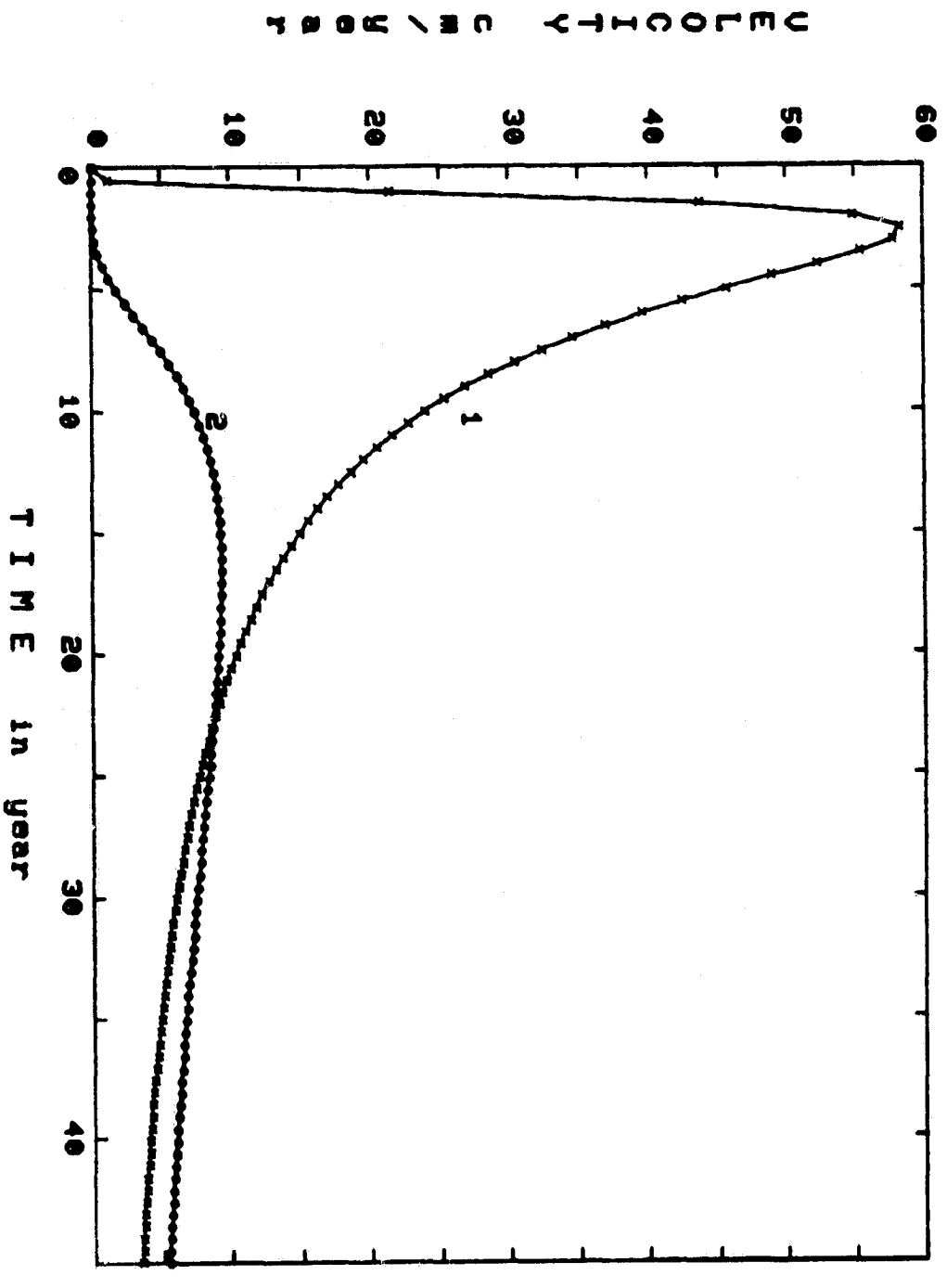

Fig 5.4.3

Chapter 6

Conclusions

This thesis is mainly concerned with the problem of time dependent deformation and stress diffusion associated with earthquakes. A time dependent finite element scheme incorporating frontal solution and time stepping procedure was implemented. The efficiency of the scheme allowed us to model large scale problems on a moderate size computer. We applied the finite element analysis to models of two and three dimensional thrust earthquakes and three dimensional strike slip earthquakes. The finite element procedure permited us to model the viscosity distribution realistically. The modelling indicated that variations in viscosity distribution often produce different time dependent deformation patterns. The distinctive patterns of the time dependent deformation associated with an earthquake can be used to infer the viscosity structure of the fault zone. Stress relaxation following an earthquake is probably related to the seismicity in the adjacent regions. The stress diffusion effects in the models are consistent with the migration and correlation of seismicity in both transform fault zones and subduction zones.

Models of three dimensional strike slip earthquakes indicated that lateral heterogeneities in viscosity across the fault zone can produce profound effects on the vertical deformation. If a low viscosity zone exists beneath the

fault zone, the increased viscosity away from the fault deters the material from moving away from the fault zone after the earthquake. This complicates the surface deformation. For example, the sudsiding region near fault for a layered model can become an uplift region with the laterally heterogeneous model. Thus the vertical deformation after a strike slip event, although smaller in magnitude than the horizontal deformation, is the most diagnostic information for the viscosity structure in a transform fault zone. The shear stress in the adjacent region along the strike direction increases with time due to the event. Therefore the possibility of earthquakes in the adjacent regions is enhanced in the years following the event. This stress diffusion may have caused the observed earthquake migration along the North Anatolian fault zone.

For the postseismic vertical displacement following thrust events in simple layered models, the area near the lower fault tip subsides continuously while the adjacent areas are uplifted. Increasing the viscosity with depth reduces the subsidence and increases the uplifts. The relaxation in the simple layered model cannot explain the postseismic uplift data following the 1964 Alaskan earthquake. Rather, certain models including a descending slab and a low viscosity wedge above the descending slab can reproduce the observed phenomenon. The descending slab acts as a guide for the induced viscous movement; it prevents the

material in the low viscosity wedge from going down and guides the movement sideways. The resulting deformation pattern in the downdip extension region of the earthquake fault is very similar to that of an aseismic slip, and the uplift data can be fit very well. These models, although still simple compared with the real world, probably contain the essential elements in a subduction zone. We believe that it is important to include these lateral variations of viscosity for modelling a subduction zone.

In three dimensional model of a thrust earthquake, it was found that a great earthquake could produce measurable disturbance of plate velocity at intermediate distances. Beyond 1000 km away, the perturbation of plate velocity becomes smaller than 1 cm/year. The transient plate velocity of a viscoelastic model differs substantially from that of a simple elastic plate over viscous fluid models.

A thrust fault earthquake causes horizontal compression in the adjacent regions along its strike direction. Therefore the possibility of another thrust earthquake in the adjacent region increases after the original event. This is consistent with the observation of the migration of great thrust events along subduction zones. The event causes horizontal tension in the adjacent regions along its dip direction; this is consistent with the observation of the normal fault events seawards of a thrust event.

With the available time dependent data today, often an observed phenomenon cannot be interpreted uniquely. However, the information on the time dependent deformation of the earth is being added at a rapid rate. There is no question that the study of time dependent behavior of the earth will provide significant new information on viscosity structure and earth dynamics.

Reference

Abe, K., Lithospheric normal faulting beneath the Aleution trench, Phys. Earth Planet. Interiors, 5, 190-198, 1972.

Abe, K., Re-examination of the fault model for the Niigata earthquake of 1964, J. Phys. Earth, 23, 349-366, 1975.

Abe, K., Some problems in the prediction of Nemuro-oki earthquake, J. Phys. Earth, 25, Suppl., S261-S271, 1977a.

Abe, K., Tectonic implications of the large Shioya-oki earthquake of 1938, Tectonophysics, 41, 269-289, 1977b.

Aki, K., Generation and propagation of G waves from the Niigata earthquake of June 16, 1964, Part 2: Estimation of earthquake moment, released energy and stress-strain drop from the G wave spectra,
Bull. Earthq. Res. Inst.,Tokyo Univ., 44, 73-88, 1966.

Adey, R.A. and C.A. Brebbia, Efficient method for solution of viscoelastic problems, ASME, EM 6, 1119-1127, 1973.

Agreen, R.W. and D.E. Smith, A simulation of San Andreas fault experiment, J. Geophys. Res., 79, 4413-4417, 1974.

Algermissen, S.T., Prince William Sound, Alaska earthquake of March 28, 1964 and aftershock sequence,
Geol. Soc. Amer. Spec. Pap., 82, 2, 1965.

Allen, C.R., Active faulting in northern Turkey, Contr. No. 1577, Div. Geol. Sci., Calif. Inst. Tech., 32p., 1969.

Anderson, D.L., Accelerated plate tectonics, Science, 187, 1077-1079, 1975.

Ando, M. Seismo-tectonics of the 1923 Kanto earthquake, J. Phys. Earth, 22, 263-277, 1974.

Ando, M., Source mechanisms and tectonic significance of historical earthquakes along Nankai Trough, Japan, Tectonophysics, 27, 119-140, 1975.

Andrew, D.J., and N.H. Sleep, Numerical modelling of tectonic flow behind island arcs,
Geophys. J. R. Astr. Soc., 38, 237-251, 1974.

Archuleta, R.J., and G.A. Frazier, Three dimensional numerical simulations of dynamic faulting in a halfsphere, Bull. Seism. Soc. Am., 68, 541-571, 1978.

Ashby, M.F. and R.A. Verall, Micromechanisms of flow and fracture, and their relevance to the rheology of the upper mantle, Phil. Trans. R. Soc. Lond., Ser.A, 288, 59-95, 1978.

Barazangi, M., W.Pennington and B.Isacks, Global study of seismic attenuation in the upper mantle behind island arcs using P waves, J. Geophys. Res., 80, 1079-1092, 1975.

Barker, T.G., Quasi-static motion near the San Andreas fault zone, Geophys. J. R. Astr. Soc., 45, 689-705, 1976.

Bender, P.L. and E.C. Silverberg, Present tectonic plate motions from lunar ranging, Tectonophysics, 29, 1-7, 1975.

Ben-Menahem, A., S.J. Singh and F. Soloman, Deformation of a spherical earth model by internal dislocations, Bull. Seismol. Soc. Amer., 59, 813-853, 1969.

Bird, P., Finite element modelling of lithosphere deformations: The Zagros Collision Orogeny, Tectonophysics, 509-538, 1978.

Bischke, R.E., A model of convergent plate margins based on the recent tectonics of Shikoku, Japan, J. Geophys. Res., 79, 4845-4857, 1974.

Bott, M.H.P. and D.S. Dean, Stress diffusion from plate boundaries, Nature, 243, 339-341, 1973.

Brace, W.F. and J.D. Byerlee, California earthquakes: Why only shallow focus?, Science, 168, 1573-1575, 1970.

Brown, R.L., A Dislocation Approach to plate Interaction, Ph.D. thesis, M.I.T., Cambridge, Mass. 1975.

Brown, L.D., R.E.Reilinger, S.R.Holdahl, and E.T.Balazs, Post seismic crustal uplift near Anchorage, Alaska, J. Geophys. Res., 82, 3369-3378, 1977.

Bucknam, R.C., G. plafker, and R.V. Sharp, Surface faulting and afterslip along the Motagua fault in Guatemalan, in Proc. Inter. Symp. on the Fec. 4th, 1976 Guatemalan Earthq. and the Reconstruction Process, Vol.1, 1978.

Budiansky, B. and J.C. Amazigo, Interaction of fault slip and lithosphere creep, J. Geophys. Res., 81, 4897-4900, 1976.

Burford, R.O., Continued slip on the Coyote Creek fault after the Borrego Moutain earthquake, in The Borrego Moutain Earthquake of April 9, 1968, U.S. Geol. Survey Prof. Paper 787, p. 105-111, 1972.

Byerlee, J.D., Frictional characteristics of granite under high confining pressure, J. Geophys. Res., 72, 3639-3648,

1967.

Byerlee, J.D. and R. Summers, Stable sliding proceeding stick-slip on fault surfaces in granite at high pressure, Pageoph, 113, 63, 1975.

Canitez, N. and M.N.Toksoz, Static and dynamic study of earthquake source mechanism: San Fernando earthquake, J. Geophys. Res., 77, 2583-2594, 1972.

Carter, N.L. and H.G. Ave'Lallemant, High temperature flow of dunite and peridotite, Geol. Soc. Amer. Bull., 81, 2181-2202, 1970.

Carter, N.L., Steady state flow of rocks, Rev. Geophys. Space Phys., 14, 301-360, 1976.

Cathles, L.M., The Viscosity of the Earth's Mantle, Princeton Univ. Press, 1975.

Chang, Y.C., The anomalous curstal uplift and aseismic slip before the Tangshan earthquake of 1976, preprint (in Chinese), 1980.

Chinnery, M.A. The deformation of the ground around surface faults, Bull. Seism. Soc. Am., 51, 355-372, 1961.

Chinnery, M.A.. The stress changes that accompany strike-slip faulting, Bull. Seism. Soc. Am., 53, 921-932, 1963.

Chinnery, M.A., Secondary faulting, I: theoretical aspects, Canadian J. Earth Sciences, 3, 163-174, 1966.

Chinnery, M.A. and T.E. Landers, Evidence for earthquake triggering stress, Nature, 258, 490-493, 1975.

Christensen, R.M., Theory of viscoelasticity., Academic Press, 1971.

Coates, R.J., T.A. Clark, C.C.Counselman,III, I.I. Sharpiro, H.F. Hinteregger, A.E. Rogers and A.R. Whitney, Very long baseline interferrometry for centimeter accuracy geodetic measurements, Teronophysics, 29, 9-18, 1975.

Cobbold, P.R., Finite element analysis of fold propagation-A problematic application., Tectonophysics, 38, 339-353, 1977.

Cohen, S.C., Postseismic viscoelastic surface deformation and stress, Part 1: Theoretical considerations, displacement and strain calculations, J. Geophys. Res., 85, 3131-3151, 1980a.

Cohen, S.C., Postseismic viscoelastic deformation and stress, Part 2: Stress theory and computation, dependence of displacement, strain and stress on fault parameters, J. Geophys. Res., 85, 3151-3158, 1980.

Cole, D.M., D.D. Kosloff, and J.B. Minster, A numerical boundary integral equation method for elastodynamics. I., Bull. Seism. Soc. Am., 68, 1331-1357, 1978.

Cook R.D., Concepts and applications of finite element analysis., John Wiley and Sons, 1974.

Coppersmith, K.J., T.H. Rogers and W.U. Savage, Ground cracks and afterslip observed following the 6 August 1979 earthquake at Coyote Lake, California, EOS, Trans. Am. Geophys. Un., 60, 890, 1979.

Counselman, C.C.,III, Very-Long-Baseline Interferometry techniques applied to problems of geodesy, geophysics, planetary science, astronomy, and general relativity, Proc. IEEE, 61, 1225-1230, 1973.

Cruse, T.A., Mathematical foundations of the boundary integral equation method in solid mechanics, Air Force Office of Scientific Research Technical Report AFOSR-TR-77-1002, 1977.

Curray, J.R., F.P.Shepard and H.H. Veeh, Late Quaternary sea level studies in Micronesia: Carmarsel expedition, Geol. Soc. Amer. Bull., 81, 1865-1880, 1970.

Dewey, J.W., Seismicity of Northern Anatolia, Bull. Seism. Soc. Am., 66, 843-868, 1976.

Dieterich, J.H., Sequence and mechanics of folding in the area of New Haven, Naugatuck, and Westport, Connecticut, Ph.D. Thesis, Yale University, 1969.

Dieterich, J.H., Time dependent friction as a possible mechanism for aftershocks, J. Geophys. Res., 77, 3771-3781, 1972.

Dieterich, J.H., Preseismic fault slip and earthquake prediction, J. Geophys. Res., 83, 3940-3947, 1978.

Dieterich, J.H., Modelling of rock friction, 1, Experimental results and constitute equations, J. Geophys. Res., 84, 2161-2168, 1979a.

Dieterich, J.H., Modelling of rock friction, 2, Simulation of preseismic slip, J. Geophys. Res., 84, 2169-2175, 1979b.

Elsasser, W.M., Convection and stress propagation in the upper mantle, in The Application of Modern physics to

Earth and Planetary Interiors, ed. S.K. Runcorn, 223-246, Wiley Interscience, 1969.

Fairbridge, R.W., Eustatic change in sea level, in Physics and Chemistry of the Earth, vol.4, Pergamon Press, 1961.

Fedotov, S.A., Regularities of the distribution of strong earthquakes in Kamchutka, the Kurile Islands and Northern Japan, (in Russian), Tr. Inst. Fiz. Zemli. Akad. Nauk, USSR, 36, 66-98, 1965.

Fitch, T.J. and C.H. Scholz, Mechanism of underthrusting in southwest Japan: A model of convergent plate interactions, J. Geophys. Res., 76, 7260-7292, 1971.

Flugge, W., viscoelasticity, Blaisdell Publishing Co., Waltham, Ma., 127pp, 1967.

Forsyth,D., and S. Uyeda, On the relative importance of the driving force of plate motion, Geophys. J. R. Astr. Soc., 43, 163-200, 1975.

Freund, L.B. and D.M. Barnett, A two dimensional analysis of surface deformation due to dip-slip faulting, Bull. Seism. Soc. Amer., 66, 667-675, 1976.

Fujii, Y., Phases and characteristics of seismic crustal movement with special reference to Japanese earthquakes, Bull. Geogr. Survey Inst., 23, 7-78, 1978.

Fujii, Y. and K. Nakane, Anomalous crustal strain prior to the 1923 Kanto, Japan Earthquake as deduced from analysis of old triangulation data, Pageoph, 117, 1301-1315, 1979.

Geological Survey of Japan, Quaternary tectonic movements in Konsen district, eastern Hokkaido, (in Japanese), Rep. Coord. Comm. Earthq. Pred., 11, 31-35, 1974.

Goetze, C., The mechanisms of creep in olivine, Phil. Trans. R. Soc. Lond., Ser. A, 288, 99-119, 1978.

Griggs, D.T., The sinking lithosphere and the focal mechanism of deep earthquakes, in Nature of the Solid Earth, 361-384, ed. E.C. Robertson, McGraw Hill, N.Y., 1972.

Gutenberg,B. and C.F.Richter, Seismicity of the earth, Princeton University Press, 1954

Haddon, R.A.W. and K.E. Bullen, An earth model incorporating free earth oscillation data, Phys. Earth Planet. Interiors, 2, 35-49, 1969.

Harada, T., Accumulation of data observed by the Geographical Survey Institute, J. Geod. Soc. Japan, 22, 228-234, 1976.

Hasabe, K., N. Fujii and S. Uyeda, Thermal process under island arc, Tectonophysics, 10, 335-355, 1970.

Haskell, N.A., Dispersion of surface waves on multilayered medium, Bull. Seism. Soc. Am., 43, 17-34, 1953.

Hastie, L.M. and J.C. Savage, A dislocation model for the Alaska earthquake, Bull. Seism. Soc. Am., 60, 1389-1392, 1970.

Hayashi, T., A study on the vertical movements on the earth's crust by means of the precise leveling, Bull. Geogr. Survey Inst., 15, 1-66, 1970

Hildebrand, F.B., finite difference equations and simulations, Prentice-Hall, N.J., 1968.

Ho, S.C. and A.T. Smith, Analytical solution to stress propagation in a two dimensional lithosphere, EOS, Trans. A. G. U., 60, 953, 1979.

Hsui, A.T. and M.N. Toksoz, The evolution of thermal structures beneath a subduction zone, Tectonophysics, 60, 43-60, 1979.

Huene, R., R.J. Malloy, G.G. Shor, and P. St.Amand, Geological structures in the aftershock region of the 1964 Alaskan earthquake, J. Geophys. Res., 72, 3649-3660, 1967.

Hughes, T.J.R. and R.L.Taylor, Unconditionally stable algorithsm for quasi-static elasto/visco-plastic finite element analysis, Comput. Struct., 8, 169-173, 1978.

Imamura, A., On the seismic activity of the Kanto district, Jap. J. Ast. Geophys., 5, 127-135, 1928a.

Imamura, A., On the tilting of the earth preceding the Kanto earthquake of 1923, Proc. Imp. Acad. Japan, 4, 148-150, 1928b.

Irons, B.M., A frontal solution program for finite element analysis, Int. J. Num. Meth. Engng., 2, 5-32, 1970.

Isacks, B. and P. Molnar, Distribution of stresses in the descending lithosphere from a global survey of focal mechanism solutions of mantle earthquakes, Rev. Geophys. Space Phys., 9, 103-174, 1971.

Isacks, B., J. Oliver and L.R. Sykes, Seismology and the new global tectonics, J. Geophys. Res., 73, 5855-5899, 1968.

Isacks,B.L. and M. Barazangi, Geometry of Benioff zones: lateral segmentation and downward bending of subducted lithosphere, in Island Arcs, Deep Sea Trenches and Back Arc Basins, ed. M.Talwani and W.C.Pittman III, A.G.U. Maurice Ewing series, 1, 99-114, 1977.

Jackson,D.D., W.B.Lee and C.C.Liu, Aseismic uplift in Southern California: an alternative interpretation, Science, 210, 534-536, 1980.

Javanovich, D.B., M.I. Husseini, and M.A. Chinnery, Elastic dislocations in a layered half space - I. Basic theory and numerical methods, Geophys. J. R. Astr. Soc., 39, 205-217, 1974a.

Javanovich, D.B., M.I. Husseini, and M.A. Chinnery, Elastic dislocations in a layered half space - II. The point source, Geophys. J. R. Astr. Soc., 39, 219-239, 1974b.

Jungels, P.H., and G.A. Frazier, Finite element analysis of the residual displacements for an earthquake rupture: Source parameters for the San Fernando Earthquake, J. Geophys. Res., 78, 5062-5083, 1973.

Kanamori, H., The Alaska earthquake of 1964: Radiation of long-period surface waves and source mechanism, J. Geophys. Res., 75, 5029-5040, 1970.

Kanamori,H. Great earthquakes at island arcs and the lithosphere, Tectonophysics, 12, 187-198, 1971a

Kanamori, H., Faulting of the great Kanto Earthquake of 1923 as revealed by seismological data, Bull. Earthq. Res. Inst., Tokyo Univ., 49, 13-18, 1971b.

Kanamori, H., Tectonic implications of the 1944 Tonankai and the 1946 Nankaido earthquakes, Phys. Earth Planet. Interiors, 5, 129-139, 1972a.

Kanamori, H., Relation between tectonic stress, great earthquakes and earthquake swarms, Tectonophysics, 14, 1-12, 1972b.

Kanamori, H., Mode of strain release associated with major earthquakes in Japan, Ann. Rev. Earth Planet. Sci., 1, 213-239, 1973.

Kasahara, K., Aseismic faulting following the 1973 Nemuro-oki earthquake, Hokkaido, Japan (a possibility),

Pageoph, 113, 127-139, 1975.

Kasahara, J., Crustal deformation associated with a fault estimated by the finite element method, Bull. Earthq. Res. Inst., Univ. Tokyo, 53, 339-357, 1978.

Kato,T., Crustal movements in the Tohoku district, Japan, during the period 1900-1975, and their tectonic implications, Tectonophysics, 60, 141-167, 1979

Kelleher, J., Space-time seismicity of the Alaska-Aleutian seismic zone, J. Geophys. Res., 75, 5754-5756, 1970.

Kelleher, J., Rupture zones of large South American earthquakes and some predictions, J. Geophys. Res., 77, 2087-2103, 1972.

King, C.Y., R.D. Nason and D. Tocher, Kinematics of fault creep, Phil. Trans. R. Soc. Lond., Ser.A., 274, 355-360, 1973.

Kohlstedt, D.L. and C. Goetze, Low stress high temperature creep of olivine single crystals, J. Geophys. Res., 79, 2045-2051, 1974.

Kosloff, D.D., Numerical models of crustal deformation, Ph.D. thesis, Calif. Inst. Tech., Pasadena, Ca, 1978.

Kusznir, N.J., and M.H.P.Bott, Stress concentration in the upper lithosphere caused by underlying visco-elastic creep, Tectonophysics, 43, 247-256, 1977.

Lachat, J.C. and J. Watson, Effective numerical treatment of boundary integral equations: a formulation for three dimensional elastostatics, Int. J. Num. Meth. Engng., 10, 991-1005, 1976

Lachenbruch, A.H. and J.H. Sass, Thermo-mechanical aspect of the San Andreas fault system, in Proc. Conf. Tectonic Problems of the San Andreas Fault System, ed. A.Nur and R.Kovach, Stanford University Publications in the Geological Sciences, 13, 192-214, 1973.

Lachenbruch, A.H. and J.H. Sass, Heat flow and stress in the San Andreas fault zone, EOS, Trans. Am. Geophys. Un., 60,955, 1979.

Lee, W.H.K., D.G. Herd, V. Cagnetti, W.H. Bakun and A. Rapport, A preliminary study of the Coyote Lake earthquake of August 6, 1979 and its Major aftershocks, preprint,. 1979.

Lehner, F.K., V. Li and J.R. Rice, stress relaxation in the

asthenosphere and rupture propagation along plate boundaries, EOS, Trans. Am. Geophys. Un., 60, 953, 1979.

Luo, H.Y., On the application of finite element method in geomechanics, (in Chinese), Scientia Geologica Sinica, 1, 81-100, 1974,

Lysmer, J and L.A. Drake, A finite element method for seismology, in Methods in Computational Physics, vol. 11, 181-216, Academic Press, N.Y., 1972

Maruyama, T., On the force equivalents of dynamical elastic dislocations with reference to earthquake mechanisms, Bull. Earthq. Res. Inst. Tokyo Univ., 41 ,467-486, 1963.

Maruyama, T., Statical elastic dislocation in an infinite and semi-infinite medium, Bull. Earthq. Res. Inst. Tokyo Univ., 42, 289-368, 1964.

Maruyama, T., On two-dimensional elastic dislocations in an infinite and semi-infinite medium, Bull. Earthq. Res. Inst. Tokyo Univ., 44, 811-872, 1966.

Mansinha, L. and D.E.Smylie, The displacement fields of inclined faults, Bull. Seism. Soc. Am., 61, 1433-1440, 1971.

Massonet, C.E., Numerical use of integral procedures, in Stress Analysis, ed. O.C.Zienkiewicz and G.S.Hollister, Wiley, 1965

Matsuda, T., Emperical rules on sense and rate of recent crustal movements, J. Geod. Soc. Japan, 22, 252-263, 1976.

McCowan, D.W., P.Glover and S.S.Alexander, A static and dynamic finite element analysis of the 1971 San Fernando, California, earthquake, Geophys. J. R. Astr. Soc., 48, 163-185, 1977.

McKenzie,D.P., Speculations on the consequences and causes of plate motions, Geophys. J. R. Astro. Soc., 18, 1-32, 1969.

Meade, B.K., Precise surveys of the Anchorage monitoring system, in The Prince William Sound,Alaska, Earthquake of 1964 and Aftershocks, vol.III, 113-118, U.S.C.G.S., Government printing office, Washington, D.C., 1969.

Melosh, H.J., Nonlinear stress propagation in the earth's upper mantle, J. Geophys. Res., 81, 5621-5632, 1976.

Melosh, H.J. and A. Raefsky, The dynamic origin of subduction zone topography, Geophys. J. R. Astr. Soc., 60, 333-354, 1978.

Melosh, H.J. and A. Raefsky, Surface deformation due to vertical dip-slip faulting in a non-Newtonian earth, EOS, Trans. Am. Geophys. Un., 60, 316, 1979.

Mikumo, T. and T. Miyatake, Earthquake sequence on a frictional fault model wth non-uniform strengths and relaxation times, Geophys. J. R. Astr. Soc., 59, 497-522, 1979.

Minear, J.W. and M.N.Toksoz, Thermal regime of a downgoing slab and new global tectonics, J. Geophys. Res., 75, 1397-1419, 1970.

Miyabi, N., Vertical earth movement in Nankai district, Bull. Geogr. Surv. Inst., 4, 1-14, 1955.

Mogi, K., Earthquakes and fractures, Tectonophysics, 5, 35-55, 1967.

Mogi, K., Migration of seismic activity, Bull. Earthq. Res. Inst. Tokyo Univ., 46, 53-74, 1968a.

Mogi, K., Sequential occurrence of recent great earthquakes, J. Phys. Earth, 16, 30-36, 1968b.

Mogi, K., some features of recent activity in and near Japan, 2, Actvity before and after great earthquakes, Bull. Earthq. Res. Inst. Tokyo Univ., 47, 395-417, 1969a.

Mogi, K., Relationship between the occurrence of great earthquakes and tectonic structures, Bull. Earthq. Res. Inst. Tokyo Univ., 47, 429-451, 1969b.

Mogi, K., Relationship between shallow and deep seismicty in the western Pacific region, Tectonophysics, 17, 1-22, 1973.

Molnar, P. and J.Oliver, Lateral Variations on attenuation in the upper mantle and discontinuities in the lithosphere, J. Geophys. Res., 74, 2648-2682, 1969.

Mura, T., The continuum theory of dislocations, in Advances in Materials Research, ed. H.Herman, vol.3, 1-108, Wiley, 1968.

Nagata, T., and A. Okada, Land deformation of the Muroto Point before and after the Nankai great earthquake on December 21, 1946, Bull. Earthq. Res. Inst. Tokyo Univ., 25, 85-89, 1947.

Nakamura,K., K.Kasahara and T.Matsuda, Tilting and uplifting of an island, Awashima, near the epicenter of the Niigata earthquake in 1964, J. Geod. Soc. Japan, 10, 172-179, 1964.

Nason, R.D., Fault creep and earthquakes on the San Andreas fault, Proc. Conf. on Tectonic Problems of the San Andreas Fault System, Stanford Univ. Publications in the Geological Sciences, 13, 275, -285, 1973.

Nason, R. and J. Weertman, A dislocation theory analysis of fault creep events, J. Geophys. Res., 78, 7745-7751, 1973.

Mendelson, A., Boundary integral methods in elasticity and plasticity, NASA technical notes, NASA TN D-7418, 1973

Neugebauer, H.J. and G.Breitmeyer, Dominant creep mechanism and the descending lithosphere, Geophys. J. R. Astr. Soc., 43, 873-895, 1975.

Neugebauer, H.J. and T. Spohn, Late stage development of mature Atlantic-type continental margins, Tectonophysics, 50, 275-305, 1978.

Niell, A.E., K.M. Ong, P.F. MacDoran, G.M. Resch, D.D. Morabito, E.S. Calflin and J.F. Dracup, Comparison of a radio interferometric differential baseline measurement with conventional geodesy, Tectonophysics, 52, 49-58, 1979.

Nur, A., and G. Mavko, Post-seismic viscoelastic rebound, Science, 183, 204-206, 1974. of the lower mantle,

Okada, A., On the mode of the vertical land deformation accompanying the great Nankaido earthquake 1946, Bull. Geogr. Surv. Inst., 2, 37-59, 1950.

Okada, A. and T. Nagata, Land deformation of the neighborhood of Muroto Point after the Nankaido great earthquake of 1946, Bull. Earthq. Res. Inst. Tokyo Univ., 31, 169-177, 1953.

Oliver, J. and B. Isacks, Deep earthquake zones, anomalous structures in the upper mantle and the lithosphere, J. Geophys. Res., 72, 4259-4275, 1967.

Orringer, O., FRAP (frontal analysis program), Aeroelastic and structures laboratory, M.I.T., Cambridge, Ma, 1974.

Parkin, E.J., Horizontal crustal movements determined from surveys after the Alaskan earthquake of 1964, in The Prince William Sound, Alaska Earthquake of 1964 and Aftershocks, Vol.III, 35-98, U.S.C.G.S., Washington D.C., 1969.

Parmentier, E.M., D.L. Turcotte and K.E. Torrance, Studies of finite amplitude non-Newtonian thermal convection with application to convection in the earth's mantle, J. Geophys. Res., 81, 1839-1846, 1976.

Parrish, D.K., A nonlinear finite-element fold model, Am. J. Sci., 273, 318-334, 1973.

Parrish, D.K., A.L.Krivz and N.L. Carter, Finite element folds of similar geometry, Tectonophysics, 32, 183-207, 1976.

Peltier, W.R. and J.T. Andrews, Glacial-isostatic adjustment-I. The forward problem, Geophys. J. R. Astr. Soc., 46, 605-646, 1976.

Peltier, W.R., Glacial-isostatic adjustment-II. The inverse problem, Geophys. J. R. Astr. Soc., 46, 669-705, 1976.

Plafker, G., Tectonics of the March 27, 1964 Alaska earthquake, U. S. Geol. Survey Prof. Pap., 543-I, 74 pp, 1969.

Plafker, G., Alaskan earthquake of 1964 and Chilean earthquake of 1960: Implications for arc tectonics, J. Geophys. Res., 77, 901-925,1972.

Press, F., Displacements, strains, and tilts at teleseimic distances, J. Geophys. Res., 70, 2395,-2412, 1965.

Press, F. and D.D. Jackson, Alaskan earthquake, 27 March 1964: Vertical extent of faulting and elastic strain energy release, Science, 147, 867-868, 1965.

Reid, H.F., Permanent displacements of the ground, in The California Earthquake of April 18, 1906, Report of the State Earthquake Investigation Commission, Carnegie Institution of Washington, Washington, D.C., 1910.

Richardson, R.M., Intraplate stress and the driving mechanism for plate tectonics, Ph.D. thesis, M.I.T., Cambridge, Ma 1978a.

Richardson, R.M., Finite element modeling of stress in the Nazca plate: driving forces and plate boundary earthquakes, Tectonophysics, 50, 223-248, 1978b.

Richardson R.M. and E.A.Bergman, Finite element modelling of the stress along the San Andreas fault, EOS, Trans. Am. Geophys. Un., 60, 953, 1979.

Richter, C.F., Elementary Seismology, Freeman and Cooper,

San Francisco, 1958.

Richtmeyer, R.D. and R.W. Morton, Difference Methods for Initial-value Problems, Wiley-Intersciences, N.Y., 1967.

Rosenman, M. and S.J. Singh, Quasi-static strain and tilts due to faulting in a viscoelastic half-space, Bull. Seismol. Soc. Amer., 63,1737-1752, 1973a.

Rosenman, M. and S.J. Singh, Stress relaxation in a semi-infinite viscoelastic earth model, Bull. Seismol. Soc. Amer., 63, 2145-2154, 1973b.

Rundle, J.B. and D.D. Jackson, A three-dimensional viscoelastic model of a strike-slip fault, Geophys. J. R. Astr. Soc., 49,575-591, 1977a.

Rundle, J.B. and D.D. Jackson, A kinematic viscoelastic model of the San francisco earthquake of 1906, Geophys. J. R. Astr. Soc., 50, 441-458, 1977b.

Rundle, J.B., Viscoelastic crustal deformation by finite, quasi-static sources, J. Geophys. Res., 83, 5937-5945, 1978.

Sato, R. Crustal deformation due to a dislocation in a multi-layered medium, J. Phys. Earth, 19, 31-46, 1971.

Sato, R. and M. Matsu'ura, Static deformation due to the fault spreading over several layers in a multi-layered medium, Part I: Displacement, J. Phys. Earth, 21, 227-249, 1973.

Savage, J.C. and L.M. Hastie, Surface deformation associated with dip slip faulting, J. Geophys. Res., 71, 4897-4904, 1966.

Savage, J.C., A theory of creep waves propagating along a transform fault, J. Geophys. Res., 76, 1954-1966, 1971.

Savage, J.C., Comment on 'An analysis of strain accumulation on a strike-slip fault', by D.L. Turcotte and D.A. Spence, J. Geophys. Res., 80, 4111-4114, 1975a.

Savage, J.C., A possible bias in the California State Geodimeter Data, J. Geophys. Res., 80, 4078-4088, 1975b.

Savage, J.C. and W.H. prescott, Comments on 'Nonlinear stress propagation in the earth's upper mantle', by H.J. Melosh, J. Geophys. Res., 83, 5005-5007, 1978a.

Savage, J.C. and W.H. prescott, Asthenosphere readjustment

and the earthquake cycle, J. Geophys. Res., 83, 3369-3376, 1978b.

Savage, J.C., Dislocation in seismology, in Dislocation Theory: A Treatise, ed. F.R.N. Nabarro, N. Holland, Amsterdam, 1979.

Schapery, R.A., Approximate methods of transform inversion for viscoelastic stress analysis, Proc. 4th U. S. Nat. Cong. of Appl. Mech., 1075-1085, 1961.

Schlue, J.W., Love wave propagating in three-dimensional structures using finite element techniques, Bull. Seimol. Soc. Am., 69, 319-328, 1979.

Scholz, C.H., M. Wyss and S.W. Smith, Displacement on seismic and aseismic slip on the San Andreas fault, J. Geophys. Res., 74, 2049-2069, 1969.

Scholz, C.H. and T.J. Fitch, Strain accumulation along the San Andreas fault, J. Geophys. Res., 74, 6649-6666, 1969.

Scholz, C.H., Crustal movement in tectonic areas, Tectonophysics, 14, 201-217, 1972.

Scholz, C.H., P. Molnar and T. Johnson, Detailed studies of frictional sliding of granite and implications for the earthquake mechanism, J. Geophys. Res., 77, 6392-6406, 1972.

Scholz, C.H. and T. Kato, The behavior of a convergent plate boundary: crustal deformation in the south Kanto district, Japan, J. Geophys. Res., 83, 783-797, 1978.

Schubert, G., D.A. Yuen and D.L. Turcotte, Role of phase transition in a dynamic mantle, Geophys. J. R. Astr. Soc., 42, 705-735, 1975.

Shimazaki, K., Pre-seismic crustal deformation caused by an underthrusting oceanic plate, in eastern Hokkaido, Japan, Phys. Earth Planet. Interiors, 8, 148-157, 1974a

Shimazaki, K., Nemuro-oki earthquake of June 17, 1973: a lithospheric rebound at the upper half of the interface, Phys. Earth Planet. Interiors, 9, 314-327, 1974b

Shimazaki, K., Intra-plate seismicity and inter-plate earthquakes: historical activity in southwest Japan, Tectonophysics, 33, 33-42, 1976.

Shimazaki, K., Correlation between intraplate seismicity and interplate earthquakes in Tohoku, Northwest Japan, Bull. Seism. Soc. Am., 68, 181-192, 1978.

Singh, S.J. and A.Ben-Menahem, Displacements and strain fields due to faulting in a sphere, Phys. Earth Planet. Interiors, 2, 77-87, 1969.

Singh, S.J., Static deformation of a multi-layered half space by internal sources, J. Geophys. Res., 75, 3257-3263, 1970.

Singh, S.J. and M. Rosenman, Quasi-static deformation of viscoelastic space by a displacement dislocation, Phys. Earth Planet. Interiors, 8, 87-101, 1974.

Slade, M.A., H.J. Melosh and A. Raefsky, Non-Newtonian post seismic motions: A source of Chandler wobble?, EOS, Trans. A. G. U., 60, 879, 1979.

Small, J.B. and C.C. Wharton, Vertical displacements determined by surveys after the Alaska earthquake of March 1964, in The Prince William Sound, Alaska Earthquake of 1964 and Aftershocks, vol.III, p.21-23, U.S.C.G.S., Government printing office, Washington, D.C., 1969.

Smith, A.T. and M.N. Toksoz, Stress distribution beneath island arcs, Geophys. J. R. Astr. Soc., 29, 289-318, 1972.

Smith, A.T., Time dependent strain accumulation and release at island arcs: Implications for the 1946 Nankaido earthquake, Ph.D. Thesis, M.I.T., Cambridge, Mass., 1974.

Smith, A.T., Models of time dependent deformations for strike-slip and thrust faults, EOS,Trans. A. G. U.,60, 953, 1979.

Smith, D.E., R. Kolenkiewicz, P.J. Dunn, and M.H. Torrence, The measurement of fault motion by satellite laser ranging, Tectonophysics, 52, 59-67, 1979.

Smith, W.D., The application of finite element analysis to body wave propagation problem, Geophys. J. R. Astr. Soc., 42, 747-768, 1975.

Smith, W.D. and B.A. Bolt, Rayleigh's principle in finite element calculations of seismic response, Geophys. J. R. Astr. Soc., 45, 647-655, 1976.

Solomon, S.C., N.H. Sleep, and R.M. Richardson, On the forces driving plate tectonics: inferences from absolute plate velocities and intraplate stress, Geophys. J. R. Astr. Soc., 42, 769-801, 1975.

Spence, D.A. and D.L. Turcotte, Viscoelastic relaxation of cyclic displacements on the San Andreas fault, Proc. R. Soc. Lond., Ser.A, 365, 121-144, 1979.

Stauder, W. and G.A. Bollinger, The focal mechanism of the Alaska earthquake of March 28, 1964, and of its aftershock sequences, J. Geophys. Res., 71, 5283-5296, 1966.

Stauder, W., Tensional character of earthquake foci beneath the Aleution trench with relation to sea-floor spreading, J. Geophys. Res., 73, 7693-7701, 1968.

Steketee, J.A., On Volterra's dislocations in a semi-infinite medium, Can. J. Phys., 36, 192-205, 1958a

Steketee, J.A., Some geophysical applications of the elastcity theory of dislocations, Can. J. Phys., 36, 192-205, 1958b.

Stocker, R.L. and M.F. Ashby, On the rheology of the upper mantle, Rev. Geophys. Space Phys., 11, 391-462, 1973.

Sydora, L.J., F.W. Jones and R.St.J. Lambert, Model calculation of the thermal fields of subducting lithospheric slabs and partial melting, Tectonophysics, 62, 233-249, 1980.

Sykes, L.R., Aftershock zones of great earthquakes, seismicity gaps and earthquake prediction for Alaska and Aleutions, J. Geophys. Res., 76, 8021-8041, 1971.

Tada, T., Crustal movement and fault motion associated with the 1973 Nemuro-oki earthquake, Bull. Geogr. Survey Inst., 20, 175-186, 1974.

Thatcher, W., Strain accumulation and release mechanism of the 1906 San Francisco earthquake, J. Geophys. Res., 80, 4862,4872, 1975a.

Thatcher, W., Strain accumulation on the nothern San andreus zone since 1906, J. Geophys. Res., 80, 4873-4880, 1975b.

Thatcher, W. and J.B. Rundle, A model for the earthquake cycle in underthrust zones, J. Geophys. Res., 84, 5540-5556, 1979.

Thatcher, W., Systematic inversion of geodetic data in Central California, J. Geophys. Res., 84, 2283-2295, 1979.

Toksoz, M.N., N.H.Sleep and A.T.Smith, Evolution of the downgoing lithosphere and the mechanisms of deep focus earthquakes, Geophys. J. R. Astr. Soc., 35, 285-310, 1973.

Toksoz, M.N. and P. Bird, Formation and evolution of marginal basins and continental plateau, in Island Arcs, Deep Sea Trenches and Back Arc Basins, Maurice Ewring Ser. 1, ed. M.Talwani and W.C. Pittman, A.G.U., Washington, D.C., p.379-393, 1977.

Toksoz, M.N. and A.T. Hsui, Numerical studies of back arc convection and the formation of marginal basins, Tectonophysics, 50, 177-196, 1978.

Toksoz, M.N., A.F. Shakal and A.J. Michael, Space-time migration of earthquakes along the North Anatolian fault zone and seismic gaps, Pageoph, 117, 1158-1170, 1979.

Tsuboi, C., Geophysical significance of the areal deformation of the base line rhombus at Mitaka, Proc. Imp. Acad., 6, 367-370, 1930.

Tsubokawa, I., Y. Ogawa, and T. Hayashi, Crustal movements before and after the Nilgata earthquake, J. Geod. Soc. Jap., 10, 165-171, 1964.

Turcotte, D.L. and E.R. Oxburgh, Convection in a mantle with variable physical properties, J. Geophys. Res., 74, 1458-1474, 1969.

Turcotte, D.L., K.E. Torrance and A.T. Hsui, Convection in the earth's mantle, in Methods of Computational physics 13, 431-453, 1973, ed. B.A. Bolt.

Turcotte, D.L., R.T. Clancy, D.A. Spence, and F.H. Kulhawy, Mechanisms for the accumulation and release of stress on the San Andreas fault, J. Geophys. Res., 84, 2273-2282, 1979.

Utsu, T., Anomalies in seismic velocity and attenuation associated with a deep earthquake zone, J. Fac. Sci, Hokkaido Univ., Ser.7, 1-25, 1967.

Utsu, T., Seismological evidence for anomalous structure of island arcs with special reference to the Japanese region, Rev. Geophys. Space Phys., 9, 838-899, 1971.

Utsu, T., Large earthquakes near Hokkaido and the expectancy of the occurrence of a large earthquake off Nemura, (in Japanese), Rep. Coord. Comm. Earthq. Pred., 7, 7-13, 1972.

Utsu, T., Space-time pattern of large earthquakes occuring off the Pacific coast of the Japanese Islands, J. Phys. Earth, 22, 325-342, 1974.

Utsu, T., Correlation between shallow earthquakes in Kanto region and intermediate earthquakes in Hida region, Central

Japan, J. Seismol. Soc. Japan II, 28, 303-311, 1975.

Uyeda, S. and V. Vacquier, Geothermal and geomagnetic data in and around the island arc of Japan, in, The crust and upper mantle of the Pacific area, ed. L. Knopoff, C. Drake and P.Hart, A.G.U. Monogr., 12, 349-366, 1968.

Uyeda, S., Some basic problems in the trench-arc-back arc system, in Island Arcs, Deep Sea Trenches and Back Arcs Basins, ed. M.Talwani and W.C.Pittman III., AGU Maurice Ewing series, 1, 1-14, 1977.

Van Wormer, J.D., J.Davies, and L.Gadney, Seismicity and plate tectonics in south central Alaska, Bull. Seism. Soc. Am., 64, 1467-1475, 1974.

Wahr, J. and M. Wyss, Interpretation of postseismic deformation with a viscoelastic relaxation model, J. Geophys. Res., 84, 6471-6477, 1980.

Walcott, R.J., Stucture of the earth from Glacio-Isostatic rebound, Annual Reviews of Earth and Planetary Sciences, 1, 15-37, 1973, ed. F.A. Dorath.

Watanabe, A., The Geomorphology of the coastal districts of the southern part of Shikoku Island and its bearing on the crustal deformations accompanying the great Nankai earthquakes, Bull. Geogr. Surv. Inst., 1, 37-72, 1948.

Watanabe, T., M.Langeseth and R.N. Anderson, Heat flow in back arc basins of the Western Pacific, in M.Talwani and W.C. Pitman III (ed), Island Arcs, Deep Sea Trenches and Back Arc Basins. Maurice Ewing Ser. Vol. 1. A.G.U., Washington D.C., pp 137-161, 1977.

Weertman, J., The creep strength of the earth's mantle, Rev. Geophy. Space Phys., 8, 145-168, 1970.

Weertman and J.R. Weertman, High temperature creep of rock and mantle viscosity, Annu. Rev. Earth Planet. Sci., 3, 293-315, 1975.

Weertman, J., Creep laws for the mantle of the earth, Phil. Trans. R. Soc. Lond., Ser. A, 288, 9-26, 1978.

Wempner, G., Finite difference via finite elements, in Proc. on the Computer Oriented Analysis of Shell Structures, 821-824, Air Force Flight Dynamics Laboratory, Wright-Patterson Air Force Base, Ohio, 1971.

Woidt, N.D. and H.J. Neugebauer, Finite element models of

density instabilities by means of bicubic spline interpolation, Phys. Earth Planet. Interiors, 21, 176-180, 1980.

Wood, M.D. and S.S.Allen, Recurrence of seismic migration along the central California segment of the San Andreas fault system, Nature, 244, 213-215, 1973

Yohiko Crustal Movements Observatory, Crustal movement in the Sado-Yahiko District, (in Japanese), Rep. Coord. Comm. Earthq. Pred., 9, 79-85, 1973.

Yamashina, K., A possible factor which trigger shallow intra-plate earthquakes, Phys. Earth Planet. Interiors, 18, 153-164, 1979.

Yamashita, T., Aftershock occurence due to viscoelastic stress recovery and an estimate of the tectonic stress field near the San Andreas fault system, Bull. Seism. Soc. Am., 69, 661-687, 1979.

Yoshii, T., A detailed cross section of the deep seismic zone beneath northeaster Honshu, Japan, Tectonophysics, 55, 349-360, 1979.

Yuen, D.A., L. Fleitout, G. Schubert and C. Froidevaux, Shear deformation zones along major transform faults and subducting slabs, Geophys. J. R. Astr. Soc., 54, 93-119, 1978.

Zandt, G., Study of three dimensional heterogeneity beneath seismic arrays in Central California and Yellowstone Wyoming, Ph.D. thesis, M.I.T., Cambridge, Mass., 1978.

Zienkiewicz, O.C. and I.C. Cormeau, Viscoplasticity-plasticity and creep and creep in elastic solids-a unified numerical solution approach, Int. J. Num. Meth. Engng., 8, 821-845, 1974.

Zienkiewicz, O.C., The finite element method, McGraw-Hill, London, 787 pp, 1977

Zienkiewicz, O.C., D.W.Kelly and P.Bettess, The coupling of the finite element method and boundary solution procedures, Int. J. Num. Meth. Engng., 11, 355-375, 1977.

END DATE

MAR. 25, 1981